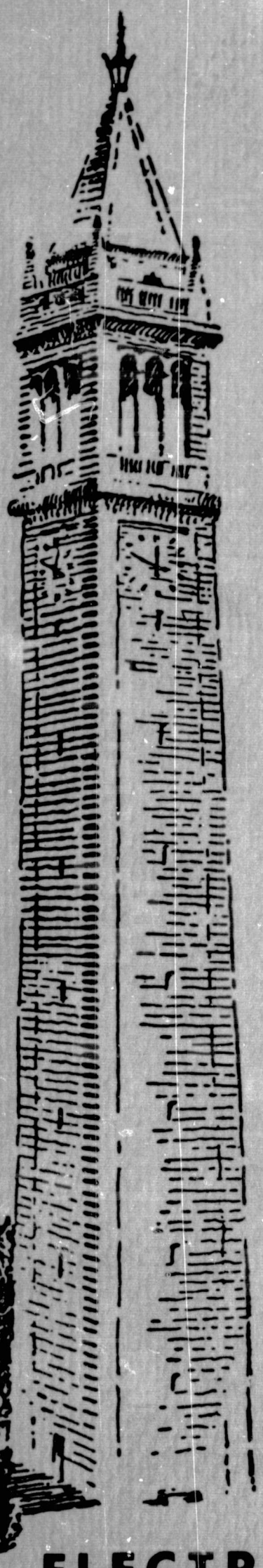

SEMIANNUAL PROGRESS REPORT No. 1

June 30, 1965

ELECTRONICS RESEARCH LABORATORY

UNIVERSITY OF CALIFORNIA

BERKELEY, CALIFORNIA

SEMIANNUAL PROGRESS REPORT
NO. 1

Prepared by
ELECTRONICS RESEARCH LABORATORY
Professor D. J. Angelakos
Acting Director

16 November 1964 through 30 June 1965

UNIVERSITY OF CALIFORNIA
BERKELEY, CALIFORNIA

BLANK PAGE

TABLE OF CONTENTS

I. INTRODUCTION

This, our first semiannual report, summarizes the progress of all research projects directly administered by the Electronics Research Laboratory (ERL) of the University of California, Berkeley. Previous consolidated progress reports were issued quarterly; the last was for the period ending 15 November 1964. In making the transition from quarterly to semiannual reports, it was necessary that this report cover the seven-and-a-half-month period of 16 November 1964 through 30 June 1965. Our next report will be for the period ending 31 December.

This report is in essentially the same format as past reports. In the next section, Personnel, the faculty, graduate research students, and ERL staff are listed. In the following section, Sponsored Support, we have listed the names of the sponsoring agencies, contract and grant numbers, project titles, and faculty investigators. From these two sections it can be seen that many faculty members act as faculty investigators in ERL research programs, thus helping with one of the principal aims of the laboratory, to integrate student and faculty research with the graduate curriculum of the Department of Electrical Engineering.

Under the title of each project reported on in Section III, Summary Progress Reports, we show the supporting agency, the contract or grant number, and the name of the graduate student and/or professor conducting the research. Graduate students are urged to participate in ERL research as an important and integral part of their work towards advanced degrees. Thus, the number of graduate students supported by research grants during this period has been substantial. A grant from the Joint Services Electronics Program (Departments of the Army, Navy, and Air Force), entitled "JSEP" for brevity, serves as the general core of support funding to assure that all ERL research is continuous, as well as to initiate and support new research.

Each research project has been evaluated on its own merit as well as on it place in the overall research program of both the Electronics Research Laboratory and the Department of Electrical Engineering. In Section III, we have arranged the summary research reports under the following seven areas of the engineering sciences.

A. BIOELECTRONICS

Research in bioelectronics encompasses areas that are involved in investigations of various aspects of life processes by means of either the analytical or experimental tools of electrical engineering. Molecular properties and control aspects of living systems form the basis; applications lead to various simulations of life processes as, for example, in aids to handicapped persons.

B. ELECTRON STREAMS AND INTERACTIONS

Within this area, research is devoted to studies of electron-optical properties of guns and focusing systems and interactions of electron streams with solids and with wave guiding systems. Sample topics include noise mechanisms in electron streams, traveling-wave interactions between streams and waves in ferrites and plasmas, electron-beam-probe studies in solids, etc.

C. PLASMAS

Research in plasmas is devoted primarily to the creation, containment, stability, and heating of high-temperature plasmas. Projects in progress include magnetic mirror compression and rotating plasma experiments. Other programs include low-temperature studies such as the properties of waves in plasmas, beam-plasma interactions, plasma-diode instabilities, and magnetohydrodynamic stability of alkali vapor plasmas in minimum $|B|$ field configurations.

D. QUANTUM AND OPTICAL ELECTRONICS

Research in this area comprises studies of generation, modulation, demodulation, focusing of coherent and photon-phonon interaction, etc.

E. RADIATION AND PROPAGATION

Radiation and propagation research comprises theoretical studies of problems in electromagnetism, frequency-independent antennas and structures, antennas in general, wave propagation through guides and through anisotropic media, and electromagnetic scattering.

F. SOLID-STATE ELECTRONICS

Research in solid-state electronics can be divided into two groups: (1) materials and mechanisms, and (2) semiconductor integrated circuits. Materials and mechanisms includes experimental and analytical work on phonon (elastic-wave) amplifiers, direct recombination radiation in semiconductors, studies of space-charge-limited currents in semiconductors and in thin-film active devices, etc. Semiconductor integrated circuits includes studies in optimal realization of multistable circuits, near-harmonic oscillators, low-pass and selective amplifiers, various transducer actions, measurements on solid-state devices using high-resolution scanning electron beams, etc.

G. SYSTEMS

Systems research includes a wide variety of interrelated disciplines such as circuit theory, information theory, statistical communication theory, nonlinear and optimal control, finite and discrete-time

systems, pattern recognition, and automata. The systems group maintains close coordination with the Departments of Statistics and Mathematics, and the Operations Research Center. Some typical projects in progress are: analysis and synthesis of linear multiple-loop feedback circuits, characterization and stability study of general nonlinear time-varying networks, generalization of the frequency domain stability criteria for nonlinear systems, coding theorems for discrete channels, sequential detection, signal selection, classification of threshold logic networks, etc.

The last section of this semiannual report, Publications, lists ERL technical reports and memoranda, technical talks presented by faculty and graduate students, and papers and journal articles -- all published between 16 November 1964 and 30 June 1965.

BLANK PAGE

II. PERSONNEL

Acting Director: Prof. D.J. Angelakos

Advisory Committee:

Prof. D.J. Angelakos
Prof. C.A. Desoer
Prof. T.E. Everhart
Prof. E.S. Kuh
Prof. A.W. Trivelpiece
Prof. J.R. Whinnery

Faculty:

N. Abramson
D.J. Angelakos
M. Aoki
A.R. Bergen
E.R. Berlekamp
C.K. Birdsall
P.R. Bryant
J.B. Cruz
C.F. Dalziel
C.A. Desoer
J.H. Eaton*
A.C. English
D.C. Evans
T.E. Everhart
C.E. Frank
I.T. Frisch
R. Gallagher
M.J. Gans
A. Gill
M.H. Graham
G. Hachtel
M.A. Harrison
A.M. Hopkin
T.C. Hu
H.D. Huskey
E.I. Jury
R. Kulikowski
E.S. Kuh
R.M. Lee
A.J. Lichtenberg
W.W. Lichtenberger
K.K. Mei
P.L. Morton
R.S. Muller
W.G. Oldham
R.F.W. Pease
D.O. Pederson
R.S. Pepper*
E. Polak
B. Raphael
G.A. Rigby
R. Riordan
V.H. Rumsey*
D.J. Sakrison
R.M. Saunders*
S.E. Schwarz
J. Siambis
S. Silver
J. Slagle
D.H. Sloan*
O.J.M. Smith
C. Süsskind
A.J. Thomasian
C.A. Tobias
I. Toda
A.W. Trivelpiece
G.L. Turin
T. Van Duzer
R. Van Slyke
P.O. Vogelhut
J. Wakabayashi
S. Wang
W.H. Wattenburg
D. Weiner
W.J. Welch
J.R. Whinnery
R.M. White
E. Wong
J.R. Woodyard
L.A. Zadeh
J.R. Singer*

Visiting Research Personnel:

J.W. Backus
N. Bloembergen
R. Rohrer

---

* On leave

Research Engineers:

G.A. Becker
F.D. Clapp
S.R. Pedersen

Programmers:

W. Groch
L.Workman

Graduate Research Students:

A. Al-Shalchi
M. Bamford
L. Barbosa
R. Biswas
G. Bodway
M. Breuer
A. Brodersen
D. Buhl
J. Byers
M. Canon
S. Chai
Y.T. Chan
C.C. Chang
C.L. Chang
P. Chang
T.Y. Chang
D. Chazan
C.T. Chen
J. Chen
G. Cheng
S. Cho
T. Cisco
W. Clark
J. Colvin
C. Cullum
N. DaCunha
D. Deuel
A. Dewey
M.T. El-Bardai
J. Fiebiger
H. Forsen
J. Frey
D. Frohman
T. Fujita
A. Gaw
J. Gibson
B. Gillet
B. Gluss
E. Greeneich
L. Gurley
H. Hall
B. Haskell
J. Hayes
C.W. Ho
R. Ho
W.W. Ho
D.A. Hodges
P. Hoff
P. Holmstrom
K. Howard
J.W. Hwan
O. Ibarra
E. Ippen
Y. Iwadare
R. Iwens
P. Jackson
J.P. Jacob
D. Johnstone
S. Joshi
P. Kaiser
D. Kajfez
H. Kawamoto
S. Kawamura
Y.L. Kuo
J. Kurzweil
A. Larsen
D. Layton
L. Lecoq
C.T. Lee
R.E. Lee
S.H. Lee
S. Lin
H. Lu
R. Lundgren
I. Mansoori
R. Mantena
J. Mataya
R. McAulay
S. Moaveni
M. Moberg
R. Mortensen
K. Mouthaan
J. Ogunlana
K. Oza
R. Pechacek
A. Pine
G. Poe
W. Quackenbush
R. Rao
A. Rault
M. Reid
A. Roederer
F. Romeo
S. Sankaran
A. Sasaki
J. Scharer
E. Schoen
M. Schwartz
L. Seidman
M. Selser
D.K. Sen
S. Sesnic
M. Shortall
D. Solimini
S. Sondov
J. Spector
S. Sugimoto
N. Sugino
C.J. Tan
V. Tarakci
G. Thomas
J. Tow
I. Traiger

Graduate Students:

C. Tseng
D. Tuma
C. Tung
V. Tyree
P. Varaiya
F. Voltmer
J. Wagner
S. Weinstein
J. Weisner
K. K. Wong
K. Y. Wong
O. Wood
G. Wrixon
Y. S. Yeh
V. Zaviantseff
Y. Zalcstein

Undergraduate Research Students:

D. Brownlee
J. Fan
J. Gray
J. Hong
L. Rickertson
H. Taylor

Technical and other Support Personnel:

L. Archibald
J. Benasso
G. Conklin
M. L. Conragan
P. Franke
L. Graziano
R. E. Humphrey
M. Link
D. McDaniel
F. Ofril
C. Solodyna
O. Westwick
P. Wilson

Business Office:

R. J. Gregory, Business Officer

J. Bernard
C. Holbrook
K. Karsberg
C. Klute
P. Rasmussen
D. Simpson
L. Torrance

Technical Publications Office:

K. L. Meraw, Editor
M. Bradley
C. Conti
M. Lynn
J. Rouiller
R. Sakamoto
N. Susta
M. Torigian
C. Whittle

BLANK

PAGE

III. SPONSORED SUPPORT

Sponsor and Contract/Grant No.	Project Title	Faculty Investigators
JSEP Grants AF-AFOSR-139-64 and 65	Basic Research Program Electronics (General Support)	Profs. D.J. Angelakos and J.R. Whinnery
AFOSR Grant AF-AFOSR-230-64	Program of Systems Research	Profs. A.R. Bergen and G.L. Turin
AFOSR Grant AF-AFOSR-639-65	Switching and Automata Theory	Profs. E.R. Berlekamp, A. Gill, and M. A. Harrison
AFOSR Grant AF-AFOSR-292-64	Study of Biocontrol Systems	Prof. E.I. Jury
AFOSR Grant AF-AFOSR-759-65	International Conference on Programming and Control	Profs. D.J. Angelakos, R. M. Oliver, G. Dantzig, and L. A. Zadeh
AFAL Contract AF33(615)-1078	Research in Electromagnetic Properties of Ionized Gases	Profs. A.W. Trivelpiece and C.K. Birdsall
AFAL Contract AF33(615)-2306	Research with Scanning Electron Beam Microscope	Prof. T. E. Everhart
AEC Contract AT(11-1)-34	Computer and Alkali Plasma Instability Experiments	Prof. C.K. Birdsall
AEL Contract DA-36-039AMC-02164(E)	Study of Crossed-Field Amplifiers	Profs. T. Van Duzer and J.R. Whinnery
AROD Contract DA-31-124-ARO-D-385	Field-Effect Device Studies	Prof. R.S. Muller
AROD Grant DA-ARO-D-31 124-G557	Research on Damping Mechanisms in Ferrimagnets	Prof. S. Wang
AROD Grant DA-ARO-D-31-124 G576	Proposal for Research in Discrete Information Processing	Profs. I. T. Frisch and E. Wong
AROD Grant DA-ARO-D-31-124-G678	Electronic Interaction with Surface and Bulk Elastic Waves	Prof. R.M. White

Sponsor and Contract/Grant No.	Project Title	
NASA Grant NSG-354(Suppl. 2)	Advanced Theoretical and Experimental Studies in Automatic Control and Information Systems	Profs. C.A. Desoer, E. Polak, D. Sakrison, and L. A. Zadeh
NSF Grant GK-392	Antenna Pattern Range Equipment	Prof. D.J. Angelakos
NSF Grant GK-0431	Propagation of Elastic Waves in Semiconductors	Prof. R.M. White
NSF Grant GK-457	Measurement of Low Absorbancies by Gas Lasers	Prof. J.R. Whinnery
NSF Grant GP-2203	Frequency Independent Antennas	Prof. D.J. Angelakos, K.K. Mei, and V.H. Rumsey
NSF Grant GP-2239	Research in High Energy Plasmas	Profs. A.J. Lichtenberg and A.W. Trivelpiece
NSF Grant GP-2413	System Theory	Profs. C.A. Desoer, A.J. Thomasian, and L.A. Zadeh
NSF Grant GP-2684	Active Circuits	Profs. C.A. Desoer, I.T. Frisch, and E.S. Kuh
NSF Grant GE-8234	Undergraduate Research Participation Program	Prof. W.J. Welch
ONR Contract Nonr-222(53)	Research In Information Theory	Prof. A.J. Thomasian
ONR Contract Nonr-222(57)	Research on Semiconductor Devices	Profs. D.J. Angelakos, C. Susskind, P.O. Vogelhut, and S. Wang
ONR Contract Nonr-3653(11)	Research in Some Applied Problems in Electromagnetism	Prof. D.J. Angelakos

LEGEND:

AEC - U.S. Atomic Energy Commission
AEL - U.S. Army Electronics Laboratory, Fort Monmonth, N.J.
AFAL - U.S. Air Force Avionics Laboratory, Wright Patterson AFB
AFOSR - U.S. Air Force Office of Scientific Research
AROD - U.S. Army Research Office, Durham, N.C.
JSEP - Joint Services Electronics Program (Depts. of the Army, Navy, and Air Force).
NASA - National Aeronautics and Space Administraction
NSF - National Science Foundation
ONR - Office of Naval Research

IV. SUMMARY PROGRESS REPORTS

Research projects conducted within the Electronics Research Laboratory in many cases overlap, however, for the purposes of administration and report writing, they are grouped into the following areas: bioelectronics, computer sciences, electron streams and interactions, plasmas, quantum and optical electronics, radiation and propagation, solid-state electronics, and systems.

Under the title of each research project reported on in this section, we have listed the name of the sponsor and, where applicable, the number of the contract or grant. The name of the researcher (professor or graduate student) and advisor concerned with the project are also given.

A. BIOELECTRONICS

Our research in bioelectronics can be classified in two major areas: molecular and organismic bioelectronics. Our efforts on the molecular level of organization of living systems are concentrated on the elucidation of charge-transfer mechanisms of proteins (both wet and dry) and on application of those results of actual protein systems. These molecular systems are studied with novel microwave techniques. Our past investigations were mainly concerned with the construction of sufficiently accurate instruments. Results are now forthcoming. Future studies will decide such questions as the importance of water for the functioning of enzyme systems and the possibility of deriving equivalent electrical networks for the representation of molecular systems.

On the level of organismic bioelectronics we aim to join forces with the investigators who are concerned with the control aspects of living organisms. Partially stimulated by our research into aids to handicapped persons we have initiated research into novel methods of transduction of neuronal action potentials that may be applicable to an "activity" analysis of whole nerve-fiber bundles. The latter effort is very new and no significant results can be reported as yet other than our previous involvement with isolated topics in biocontrol systems.

GENERAL BIOELECTRONICS

University of California Support
Professor C. Susskind

During the first half of 1965 two reports were published in the general area of bioengineering. The first was a survey concerned with electronic aids to the blind and the use of electronics in problems arising from sensory impairment [1] *. This survey pays particular attention to guidance for locomotion, fundamental considerations related to guidance and reading machines, research on various methods of sensory stimulation, and methods of aiding the blind to perform industrial tasks. An attempt was also made to survey the field of direct stimulation of the brain but relevant literature is not yet extensive.

The second publication comprises a chapter on bioengineering by C. Susskind in a recently published book [2]. The book is aimed primarily at young people on the brink of a career decision and does not divide the engineering profession into the classical disciplines. Much of the chapter is concerned with recent advances in bioelectronics.

PROTONIC SEMICONDUCTORS

ONR Contract Nonr-222(92)
S. Chai (Professors C. Susskind and P. O. Vogelhut)

A study of the activation energy of ice crystals with HF and NH_3 added was completed and the results were reported [3-4]. An abstract follows:

> The activation energies of ice with varying amounts of impurities added were investigated using sintered platinum electrodes. For both types of impurities a minimum in the activation energy was found at a concentration of 10^{-4} M. The experimental arrangement and possible reasons for the existence of a minimum in activation energy are discussed.

HALL EFFECT OF PROTEIN POWDER WITH ADSORBED WATER

ONR Contract Nonr-222(57)
S. Chai (Professors C. Susskind and P. O. Vogelhut)

The importance of structurally defined water to the surface of biological macromolecules, such as proteins and enzymes, is a first step in many biophysical and biochemical investigations of bond formation and energy transport systems. This research project is concerned

---

* References for this section are listed on page 16 .

with the role of water in protein. The structure of water around proteins is in general well defined due to extensive hydrogen bonding between water molecules and the various amino-acid residues of the polypeptide chain. As the polypeptide chain folds itself in a specific manner, the surface of the macromolecule may have a unique influence on the structure of the bound water, and thereby on its charge-transport properties.

Accurate measurements of the d-c conductivity of proteins as a function of adsorbed water show a time-independent current, which increases by a factor of 10^{12} as the relative humidity changes from zero to 100 per cent. This observation is interpreted to show the strong dependence of current on the amount of adsorbed water which changes the dielectric constant of protein.

Measurements of the dielectric constant of proteins, at microwave frequencies as a function of hydration, show that the adsorbed water increases the dielectric constant of the protein by lowering the activation energy to separate the charges due to the increase in the polarizability of the medium[6]. This increasing dielectric constant of protein with increasing water content may be regarded as responsible for the formation of ice-like structures on the surface of the protein since ice has a larger dielectric constant than water. Presumably the dielectric polarizability of the protein is caused by proton-jump in the hydrogen bonds which connect the water molecules with the vacant polar sites of a protein surface, thus allowing protein transfer along these hydrogen bonds.

The dielectric constant and conductivity, both functions of water of hydration, show two different rates of change. Thereby we define a critical hydration which indicates the change in the mechanism of dielectric polarization and conduction process of proteins. For proteins, the critical hydration is close to 0.24 g H_2O per gram of dry protein [6]. This phenomenon is interpreted as hydration layer formation which bounds tightly at the first layer and becomes loosely bound at the second and third layers. The critical hydration may be identified with the amount of adsorbed water required to complete the tightly bound primary hydration layer.

According to the above hypothesis, this experimentally determined value of critical hydration is a significant physical quantity which determines the amount of primary bound water in the system. It seems necessary to consider the sudden increase of conductivity at the critical hydration as related to the nature of the charge carriers. There has been considerable speculation about the nature of the charge carriers in proteins. Proteins are generally accepted as a semiconductor, which has activation energy of about 3 eV [5]. It has been speculated that the charge carriers are electrons or protons, but unless significant evidence is presented, no definite conclusion can be drawn.

Thus, we are concerned with the nature of the charge carriers of each state of distinguishable mechanisms as a function of critical hydration and shall correlate changes in bound water with charge-transport processes. The hypothesis, in view of the studied adsorption of water on protein, is that the dry proteins are electronic semiconductors

since there is no path for protons, and that in the wet state, proteins are both electronic and protonic.

In conclusion, we hope to show whether movements of protons on the surface of a protein molecule can interact with electrons in the protein in such a way as to produce conformational changes in the whole molecule.

To investigate the relative contributions of protons or electrons to conduction current, a new microwave measuring technique was developed. This technique is used to measure Faraday rotation (related to the Hall effect) as a function of hydration of the sample surface. The TE_{10} mode of x-band microwaves is excited in a rectangular wave guide, which is transferred into the circularly polarized TE_{11} mode of the circular guide by means of a smooth transition. This plane-polarized electromagnetic wave, propagating through a sample medium with a d-c magnetic field in the direction of propagation, slightly rotates the plane of polarization. This effect, explained by introducing a Hall-effect field into Maxwell's equations, was used to measure mobilities of charge carriers in semiconductors [7]. The technique has been refined and adapted in our laboratory in order to give an angle of resolution of approximately 10^{-4} degrees. The detection system uses a phase-lock amplifier and two opposite-polarity crystals at 90 degrees to each other.

The angle of rotation is expressed in the following relationship:

$$\theta = \sqrt{\frac{\epsilon_0}{\mu_0}}\ \frac{\sigma \mu B_t}{\sqrt{K}},$$

where $\sqrt{\frac{\epsilon_0}{\mu_0}}$ = impedance of free space,

σ = conductivity of the sample,

μ = mobility of its charge carriers,

B = magnetic field strength,

t = thickness of the sample, and

K = dielectric constant of the sample.

Since σ and K of the sample can be measured very accurately by a method developed in this laboratory [8], the only unspecified value is the mobility μ. The mobility measurement will not only determine the number of charge carriers but also define their type (proton or electron).

This experiment has the advantage of not requiring electrodes of any kind and can be used to determine mobilities in powdered samples such as proteins. The immediate result of this investigation will determine whether water aids materially in reactions by initiating protonic rearrangements leading to activated states or whether bound water indirectly influences reactions by changing the electronic and thereby steric configurations of protein molecules.

Progress during this period has been in the building and modification of equipment. A sample holder for controllable temperature and humidity was designed and built, and the detecting system was completed. Construction for refining the system is under way.

BOUND WATER OF ENZYMES

Department of the Navy ONR Contract Nonr-222(57)
K. Howard (Professor P.O. Vogelhut)

Knowledge of the nature of bound water in the microenvironment of enzymes could elucidate possible mechanisms for enzyme action. For a discussion of hypothesized electronic or protonic activity, see the preceding report, "Hall Effect of Protein Powder with Adsorbed Water." We are attempting to find the change between the dielectric constants of the bound water when the enzyme is in the inactive and active states. To do this a microwave apparatus is being used[8]. Two schemes are being worked on. One is to have the enzyme stationary with respect to the microwaves while the substrate passes through the cavity. The other is to have both the enzyme and the substrate in a mobile, liquid phase passing transverse to the direction of microwave propagation.

Biochemical assays have been modified for our purposes. By utilizing the light-absorbancy of a product in the visible and ultraviolet ranges, convenient assays can be made with a DB spectrophotometer. The lysine-p-nitroanilide (LPA) method for trypsin, developed by Erlanger et al.[9], has been adapted. The optimum pH at which the reaction could be run was determined as 8.65. The Michaelis constant for the reaction under our conditions was determined. Calibration of the optical density as a function of product concentration was made with a stock solution of p-nitroaniline; the range 97.5% transmission $= 1 \times 10^{-9}$ moles to 14.0% $= 1 \times 10^{-7}$ moles was within a hyperbolic curve. By varying the substrate concentration with the enzyme held constant, initial reaction curves were obtained on a strip-chart recorder. A convenient way of extrapolating the Michaelis constant, K_m, is to plot the inverse velocities of the initial reactions ($\frac{1}{v}$) against the corresponding inverse substrate concentrations ($\frac{1}{s}$). The ordinate intercept of this slope is V_{max} for the reaction of the enzyme with a particular substrate under defined conditions of temperature, pH, and ionic strength. The slope equals $\frac{K_m}{V_{max}}$, so the apparent K_m can be easily calculated (Lineweaver-Burk method)[10]. The K_m for the LPA assay under our conditions was found to be 0.752×10^{-3} M which agreed well with the K_m obtained by the originators of the assay (0.364×10^{-3} M). Determination of the actual dissociation constant was also started so that if this information is needed later it will be available.

The benzoyl arginine ethyl ester (BAEE) assay for trypsin has been modified. The product concentration was calibrated and again a hyperbolic curve was obtained. A sufficient number of reactions has not been run at this time to obtain the K_m. The actual dissociation constant of the reaction cannot be found easily because, after five minutes, the product appears to be inhibited.

Trypsin was made insoluble by combining it with a maleic anhydride-ethylene copolymer (EMA31 supplied by Monsanto Chemical Co.). This compound (IMET) was developed by Katchalski et al[11]. The nitrogen content of the IMET will be determined by the Kjeldahl method. The IMET will be packed into a microcapillary and the capillary placed in a wave guide. A successful packing method has been developed and measurements of dielectric constants are in progress.

REFERENCES

[1] P.G. Shrager and C. Susskind, "Electronics and the Blind," Advances in Electronics and Electron Physics, Vol. 20.

[2] The World of Engineering, John R. Whinnery, Ed., McGraw-Hill Book. Co., (1965).

[3] S.Y. Chai and P.O. Vogelhut, "The Activation Energy of d-c Electrical Conductivity of Ice Doped with HF and NH_3," Internal Tech. Memo M-103, Electronics Research Laboratory, University of California, Berkeley; October 19, 1964.

[4] S.Y. Chai and P.O. Vogelhut, "Activation Energy of Direct-Current Electrical Conductivity of Ice with HF and NH_3 Added," Science, Vol. 148, No. 3677, pp. 1595-1598, June 18, 1965.

[5] B. Rosenberg, "Electrical Conductivity of Proteins; II. Semiconduction in Crystalline Bovine Hemoglobin," J. Chem. Phys., Vol. 36, pp. 816-823 (1962).

[6] D. Rosen, "Dielectric Properties of Protein Powders with Adsorbed Water," Trans. Faraday Soc. Vol. 59, pp. 2178-2191 (1963).

[7] R.R. Rau and M.C. Caspari, "Faraday Effect in Germanium at Room Temperature," Phys. Rev. Vol. 100, pp. 632-639 (1955).

[8] P.O. Vogelhut, "Use of Microwave Technique for the Determination of Bound Water," Nature, Vol. 203, pp.1169-1170 (1964).

[9] B.F. Erlanger, N. Kokowsky and W. Cohen, "The Preparation and Properties of Two New Chromogenic Substrates of Trypsin," Arch. of Biochem. and Biophys., 95, 271-278 (1961).

[10] H. Lineweaver and D. Burk, "The Determination of Enzyme Dissociation Constants," J. Am. Chem. Soc., 56, 658-666 (1934).

[11] Y. Levin, E. Katchalski et al, "A Water-insoluble Polyanionic Derivative of Trypsin," Biochemistry, 3, 190501913 (1964).

B. ELECTRON STREAMS AND INTERACTIONS

Research in the area of electron streams has been concerned with beam control, crossed-field tube dynamics, and noise studies, notably in connection with crossed-field amplifiers. A novel device for controling a high-intensity electron beam, developed in an earlier contract period, has undergone final tests. A statistical theory for the smooth-bore magnetron has been completed and presented. Noise studies have been carried out in the course of several projects, and a method for synthesizing electron-gun designs of the Kino type has been developed. The research effort has been relatively intensive during this semiannual period, with several of the projects coming to or near completion.

NONINTERCEPTING CONTROL OF HIGH-INTENSITY ELECTRON BEAM

JSEP Grants AF-AFOSR-139-64 & 65
Professor C. Süsskind

Final tests have been completed on a nonintercepting control electrode for a high-intensity thermionic cathode (the "pierced" cathode), in which metal pins insulated from the cathode project through apertures in the cathode surface; a negative voltage applied to the pins serves to cut off emission from the cathode without intercepting much of the emission current (U.S. Patent 2,975, 317, C. Süsskind). The tests were performed at Litton Industries, San Carlos, California, where a high-voltage pulser was made available. The principle was shown to be a valid one and good control characteristics were obtained, although further improvement could doubtless be achieved by modifying the exact configuration.

At present, the control pins are oriented parallel to the axis of a spherical-cup cathode, so that those near the edge are at a greater angle with the normal to the cathode surface than those near the center and may project into the path of some of the emitted electrons. Orienting the pins everywhere along the normal to the cathode surface would represent a considerable improvement in that respect.

The proposed method also represents a possibility of designing modulation characteristics (i.e., the variation of emission current with control voltage) according to an arbitrary prescription. No attempt was made to do so in the present case, but the characteristics differ from those obtained with ordinary grids and in fact resemble the variable mu (remote-cutoff) characteristics of some tetrodes.

The main objective of the project was to provide a method of controling high-intensity cathodes with a reduction in control voltage and power below that necessary in a diode arrangement, in which the high-voltage anode itself must be switched.

STATISTICAL THEORY FOR THE SMOOTH-BORE MAGNETRON

AEL Contract DA-36-039AMC-02164 (E)
K. Mouthaan (Professor C. Süsskind)

The objective of this research is to obtain a theoretical description of the characteristics of the cut-off smooth-bore magnetron. This goal has been achieved, and the final report is being prepared. A paper entitled "New Statistical Theory for the Smooth-Bore Magnetron," by K. Mouthaan and C. Süsskind, was presented at The Institute of Electrical and Electronics Engineers' Annual Conference on Electron Device Research, in Urbana, Illinois, June 23 - 25, 1965. An outline of the theory and the comparison of theoretical and experimental results were given. A summary of the paper follows.

In research carried on at the University of California, crossed-field interaction was studied in large smooth-bore magnetrons (interaction areas of the order of 0.5 m^2 at multimegawatt pulsed beam powers). As in earlier experiments performed by Jepsen and Muller (J. Appl. Phys. 22:1196, 1951), it was found that large currents are drawn by the anode under heavy "cut-off" conditions. Furthermore, rf fields were found to be present in the beam even though there was no rf structure. It was found that these time-dependent fields are of a randomly fluctuating character, with frequency components throughout the microwave range and electric-field amplitudes as high as several per cent of the impressed electric field. The experimental results led us to the realization that electron motion in the smooth-bore magnetron must be described by means of one of the transport equations of statistical mechanics; and that electron transport across the magnetic field is caused by randomly fluctuating fields (rather than by thermal motion). A new theory has been developed on that basis. It is assumed (as often proposed by previous investigators) that the randomly fluctuating fields result from the slipping-stream instability (diocotron effect). A detailed consideration of the random motion of electrons in fluctuating fields with the frequency spectrum of the slipping-stream instability shows that the appropriate transport equation is the diffusion equation. The components of the diffusion tensor transverse to the magnetic field are proportional to the square of the impressed electric field and inversely proportional to the cube of the magnetic field, with the constant of proportionality expressed in terms of the growth rate of the slipping-stream

instability. The essential assumption is that electron drift energy is converted into gyration energy at a rate equal to the time rate of change of the square of the fluctuating field quantities, as obtained from the analysis of the slipping-stream instability.

The theoretical and experimental results for the space-charge density, the electric field, the anode current, and the circulating current were compared in the last ERL quarterly progress report. The agreement between theory and experiment is excellent, especially for the anode current.

An account of the derivation of the diffusion tensor will soon appear in The Physics of Fluids; a paper on the new statistical theory for the smooth-bore magnetron is also being prepared.

NOISE-FIGURE STUDIES ON FORWARD-WAVE CROSSED-FIELD AMPLIFIER

AEL Contract DA-36-039AMC-02164(E)
A. Sasaki (Professor T. Van Duzer)

The aim of this work is to develop understanding of the noise characteristics of forward-wave crossed-field amplifiers to a sufficient degree to permit appreaciable noise-figure reductions. The normal-mode approach will be used in the study of noise transducing schemes.

It is well-known that the general noise-figure theory which was developed by Haus and Robinson [1], [2] and uses the normal mode amplitudes, can be applied to the microwave beam amplifier where the beam wave carries real ac power (positive or negative kinetic power) as in an O-type amplifier. The theory cannot be applied to the amplifier where the beam wave does not carry real ac power, as in the crossed-field amplifier. The theory is extended to obtain the minimum noise-figure expression for the crossed-field amplifier. The procedure of the analysis is based on the normal-mode amplitudes and the coupled-mode equations developed by Sasaki and Van Duzer [3].

---

[1] H.A. Haus and F.N. Robinson, "The minimum noise figure of microwave beam amplifiers," Proc. of IRE, Vol. 43, July 1955, pp. 981 - 991.

[2] F.N.H. Robinson and H.A. Haus, "Analysis of noise in electron beams," J. Electronics, Vol. 1, Jan. 1956, pp. 373 - 384.

[3] A. Sasaki and T. Van Duzer, "Coupled-mode analysis of interactions in crossed fields," (to be published).

The kinetic power carried by an electron beam, the dc velocity of which is assumed to be much less than the velocity of light, is given by [4]

$$P = \frac{1}{2} \mathrm{Re}(U_L I_L^* + U_T I_T^* + \phi I_L^*), \tag{1}$$

where Re and * indicate the real part and the complex conjugate, respectively, U is the kinetic potential, I is the ac current, the subscripts L and T represent the direction along the beam path and the direction transverse to the beam path, respectively. Equation 1 can be written in the matrix form, introducing the matrix R,

$$P = \frac{1}{4} w^{\dagger} R w, \tag{2}$$

where $\dagger$ represents the Hermitian conjugate,

$$w = \begin{pmatrix} U_T \\ U_L \\ I_L \\ I_T \end{pmatrix} \quad \text{and} \quad R = \begin{pmatrix} 0 & 0 & 0 & 1 \\ 0 & 0 & 1 & 0 \\ 0 & 1 & 0 & \frac{j}{K_b} \\ 1 & 0 & \frac{-j}{K_b} & 0 \end{pmatrix} \tag{3}$$

and K_b has units of admittance and is given by

$$K_b = \frac{\eta \omega (-\sigma_0)}{\omega_c v_0} \tag{4}$$

for the beam in crossed fields [3], where η is the absolute value of the ratio of electron charge to mass, σ_0 is the dc charge density multiplied by the beam thickness, v_0 is the dc velocity of the beam, ω_c is the angular cyclotron frequency. The terms $\pm \frac{j}{K_b}$ appear in the matrix R for the crossed-field amplifier in forming the product of the ac potential ϕ and the ac current I_L. They do not appear in R for such an amplifier where there is no kinetic power due to the ac potential ϕ as in an O-type amplifier.

The kinetic potential and the ac current at the different places along the beam in a linear, lossless region can be related by the matrix M;

$$w_b = M w_a, \tag{5}$$

where w_b is the vector of the kinetic potential and the ac current at the place b and w_a is at the place a. We may have the conservation of kinetic power in a linear, lossless region,

$$w_b^{\dagger} R w_b = w_a^{\dagger} R w_a. \tag{6}$$

---

[4] H. A. Haus and D. L. Bobroff, "Small signal power theorem for electron beams," J. Appl. Phys., Vol. 28, June 1957, pp. 694-704.

Using Eqs. 5 and 6, we obtain the matrix equation which holds in any linear, lossless region,

$$M^{\dagger} = R\, M^{-1} R^{-1}, \tag{7}$$

which is the same form as given for the O-type amplifier. Now, we introduce the self-power density spectrum (SPDS) and the cross-power density spectrum (CPDS) of noise defined as

$$\left.\begin{aligned} \Phi_T &= \frac{\overline{\frac{1}{2} U_T(\omega)^2}}{4\pi \Delta f}, \qquad \Phi_L = \frac{\overline{\frac{1}{2} U_L(\omega)^2}}{4\pi \Delta f} \\ \Psi_T &= \frac{\overline{\frac{1}{2} I_T(\omega)^2}}{4\pi \Delta f}, \qquad \Psi_L = \frac{\overline{\frac{1}{2} I_L(\omega)^2}}{4\pi \Delta f} \end{aligned}\right\} \tag{8}$$

and

$$\left.\begin{aligned} \theta_1 &= \frac{\overline{\frac{1}{2} U_T(\omega)\, U_L(\omega)^*}}{4\pi \Delta f}, \qquad \theta_2 = \frac{\overline{\frac{1}{2} U_T(\omega)\, I_T(\omega)^*}}{4\pi \Delta f} \\ \theta_3 &= \frac{\overline{\frac{1}{2} U_T(\omega)\, I_L(\omega)^*}}{4\pi \Delta f}, \qquad \theta_4 = \frac{\overline{\frac{1}{2} U_L(\omega)\, I_T(\omega)^*}}{4\pi \Delta f} \\ \theta_5 &= \frac{\overline{\frac{1}{2} U_L(\omega)\, I_L(\omega)^*}}{4\pi \Delta f}, \qquad \theta_6 = \frac{\overline{\frac{1}{2} I_L(\omega)\, I_T(\omega)^*}}{4\pi \Delta f} \end{aligned}\right\} \tag{9}$$

where the bar represents the mean-squared value and Δf is the bandwidth of the amplifier. The CPDS is complex, written as

$$\theta_n = \Pi_n + j\Lambda_n . \tag{10}$$

To express Eq. 5 in terms of SPDS and CPDS, we use the matrix W whose elements are SPDS and CPDS;

$$W = \lim_{T \to \infty} \frac{\pi}{2T} \overline{w(\omega)\, w(\omega)^{\dagger}}, \tag{11}$$

where the bar represents the ensemble average for the time interval T. The ensemble average and the mean-squared average are related by

$$\lim_{T\to\infty} \overline{\frac{\pi}{T} X(\omega)X(\omega)^*} = \frac{\overline{X(\omega)^2}}{4\pi\Delta f} , \tag{12}$$

where $x(\omega)$ is any noise fluctuation of a Fourier component at the angular frequency ω. Using Eq. 7, we obtain the useful matrix equation:

$$M^{-1} W_b R M = W_a R. \tag{13}$$

This is a similarity transformation of the matrix WR, so the trace and determinant of WR are invariant, which means those quantities are invariant through the linear, lossless region. The trace of the matrix WR is

$$\frac{1}{2}\,\text{trace}\,(WR) = \Pi_2 + \Pi_5 + \frac{\Lambda 6}{K_b} , \tag{14}$$

which represents the kinetic power of the electron beam due to the noise fluctuations and corresponds to the parameter Π in an O-type amplifier. It is zero in the case of zero correlation between noise fluctuations. The determinant of the matrix WR is, for simplicity, given in the case of zero correlation.

$$\det(WR) = S_i^4 = \Psi_L \Psi_T \Phi_L \Phi_T \text{ (zero correlation assumed)}, \tag{15}$$

which is equivalent to the parameter S in an O-type amplifier.

There is another useful relation for the interaction region in terms of normal-mode amplitudes (Fig. 1).

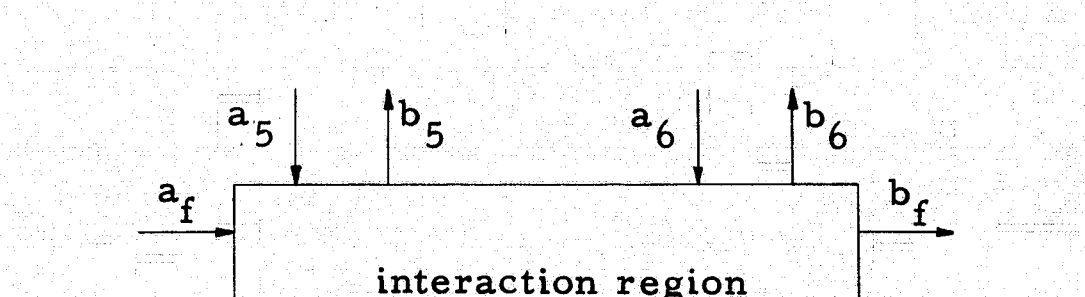

Fig. 1. Model for the analysis of the interaction region.

The ac power carried by the beam waves and the circuit waves is given by

$$P = a^{\dagger} pa \ , \tag{16}$$

where

$$a = \begin{bmatrix} a_f \\ a_s \\ a_g \\ a_d \\ a_5 \\ a_6 \end{bmatrix} \quad \text{and parity matrix} \quad p = \begin{bmatrix} 1 & 0 & 0 & 0 & 0 & 0 \\ 0 & -1 & 0 & 0 & 0 & 0 \\ 0 & 0 & 0 & j & 0 & 0 \\ 0 & 0 & -j & 0 & 0 & 0 \\ 0 & 0 & 0 & 0 & 1 & 0 \\ 0 & 0 & 0 & 0 & 0 & 1 \end{bmatrix} \tag{17}$$

In an amplifier, such as an O-type amplifier, where each wave carries real ac power, the parity matrix has only non-zero elements (+1 or -1) on the diagonal. However, the parity matrix p for the crossed-field amplifier is no longer diagonal, because each space-charge wave (the growing or the decaying wave) does not carry real ac power, but real ac power can be carried by the growing and decaying waves in the cross-product of ac potential ϕ of one and the ac current I_L of the other [3], [5] since both propagate with the same phase velocity. The normal mode amplitudes at the point b can be expressed by the linear combination of the normal mode amplitudes at point a,

$$b = Ga \ , \tag{18}$$

where G is the gain matrix. The conservation of the ac power gives the equality:

$$b^{\dagger} pb = a^{\dagger} pa \ . \tag{19}$$

Using Eqs. 18 and 19, we obtain

$$G^{\dagger} pG = p \text{ and } GpG^{\dagger} = p \ , \tag{20}$$

which hold for any linear amplifier of crossed fields.

We use the beam model in which the reference plane near the cathode is followed by a drift region where the dc velocity of the beam is much larger than the magnitude of the fluctuations of velocity. This is not a restriction on the generality of our results as far as we use the invariant noise parameters of the linear, lossless region. It must be

---

[5] S. Saito, Electromagnetic Theory for Electron Beam, Ohm Press, Tokyo, Jan. 1960, pp. 141 - 173.

mentioned that the dioctron effect does not prevent the drift region from being represented by a linear, lossless transducer [3], [5]. From Eq. 18, we obtain the normal mode amplitude b_6 of the circuit wave at the output plane. Taking the absolute squared value $|b_6|^2$ which can be considered the noise output, we obtain the noise-figure expression, following the definition of the noise figure.

$$NF = 1 + \frac{4\pi}{kT} \frac{1}{|G_{65}|^2} \left\{ |G_{6g}|^2 e^{2\beta_s d} A_{gg} + |G_{6d}|^2 e^{-2\beta_s d} A_{dd} + (G_{6g}^* G_{6d}^* A_{gd} + G_{6g}^* G_{6d} A_{gd}^*) \right\} \qquad (21)$$

where we assumed synchronization of phase velocity between the circuit wave and the space-charge waves and impedance matching to the output circuit. Here the gain term G_{6g} is defined as

$$G_{6g} = \left. \frac{b_6}{a_g} \right|_{a_f = a_s = a_g = a_d = a_5 = 0} ,$$

and the SPDS of normal mode amplitude of the growing space-charge wave is defined by

$$A_{gg} = \frac{\overline{a_g(\omega) a_g(\omega)^*}}{4\pi \Delta f} ,$$

and the other terms follow the same definition, d is the length of the drift region, k is Boltzmann's constant, and T is room temperature. In the coming period, the minimization of Eq. 21 subjected to the invariance of the parameter S_i (Eq. 15) will be calculated to obtain the minimum noise-figure expression for the crossed-field amplifier.

CATHODE REGION STUDIES

AEL Contract DA-36-039AMC-02164(E)
R. Y. C. Ho (Prof. T. VanDuzer)

The aim of this work is to construct a relatively simple space-charge feedback model to study the noise phenomena under space-charge-limited conditions in both long and short guns as a two-dimensional problem, from the viewpoint of potential minimum instability.

The procedure of the study may be roughly divided into two steps; (1) the perturbation of space charge causes the potential minimum perturbation; and (2) the perturbation of potential minimum causes the perturbation of space charge.

The effect of the space charge on potential minimum perturbation

is studied by modeling the electron stream with four discrete sheet beams of a particular shape since the actual electron trajectories are complicated by the crossed magnetic field. That is, for each pair of initial velocities, there is a trajectory which is different from the others. With the assumed trajectories of the electron streams and by using line-charge model the perturbation of the electric field at the cathode can be calculated, and hence the perturbation of the potential minimum.

It was reported that in the presence of a crossed magnetic field, the beam current density is the integral of the velocity distribution function over the region beyond the critical initial velocity curve in velocity space. Furthermore, the curve of critical initial velocity is a straight line which intersects with the abscissa and is a function of potential minimum parameters and magnetic field. Thus, when the minimum potential is perturbed by a small value, the curve for critical initial velocity and hence the beam current density should be perturbed correspondingly.

The space-charge shot-noise factor was calculated as a function of the crossed magnetic field strength for the case with anode potential, V_a, of 454 volts; beam current density, J, of 2000 amp/m^2; and the same space-charge-limited condition, namely, $V_m = -0.12$ volts, $X_m = 0.81\,10^{-5}$ m, as shown in Fig. 1.

Figure 1 shows that the shot-noise factor β^2 is almost the same as that of an ordinary diode if the crossed magnetic field is smaller than 200 gauss but the shot-noise factor increases rapidly when the magnetic field is larger than 200 gauss; however, if $B > 400$ gauss, β^2 will again increase rather slowly. Furthermore, the shot-noise factors β^2 for all the magnetic-field values that we considered are less than unity, that is, the temperature-limited shot noise is smoothed by the space-charge. Thus, we may conclude that for the space-charge feedback model based on d-c analysis with fixed trajectories, sheet beam flow for each current generator at the cathode and parabolic potential distribution near the cathode shows no possibility of instability caused by space-charge feeback.

In continuing this work we will consider the β-electron termination on the cathode. We note that the β-electrons are those electrons which pass through the first critical plane. The β-electron termination model may be constructed by modeling the electron beam with more sheet streams which are functions of initial velocities, the crossed magnetic field value, and the space-charge-limited condition.

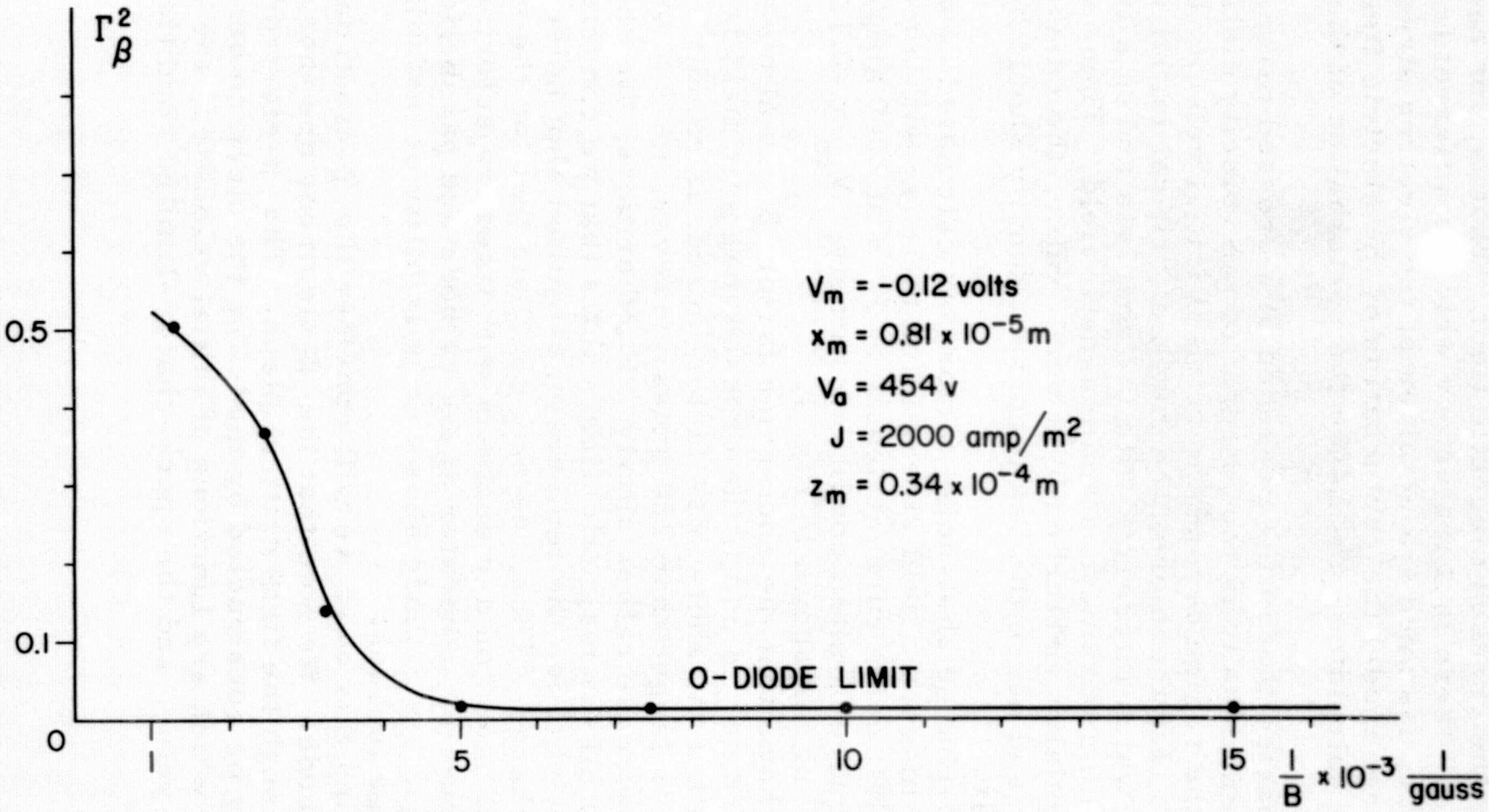

Fig. 1. Space-charge shot-noise factor vs magnetic field.

BACKWARD-WAVE NOISE FIGURE STUDIES

AEL Contract DA-36-039AMC-02164(E)
N. Mantena (Prof. T. Van Duzer)

The objective of this project is to identify and reduce excess noise in crossed-field amplifiers. This report deals with the theoretical justification of the experimental results presented in the previous quarterly reports.

Following Hutter's five-wave analysis [1], the amplitude and phase factors of all the five waves resulting from the interaction between the circuit wave and the beam space-charge waves can be determined. These are given from the following set of linear equations:

$$\begin{pmatrix} E_{1zt} \\ \sigma_{1t} \\ y_{1t} \\ v_{1yt} \\ v_{1zt} \end{pmatrix} = \begin{pmatrix} \alpha_{11} & \alpha_{12} & \alpha_{13} & \alpha_{14} & \alpha_{15} \\ \alpha_{21} & \alpha_{22} & \alpha_{23} & \alpha_{24} & \alpha_{25} \\ \alpha_{31} & \alpha_{32} & \alpha_{33} & \alpha_{34} & \alpha_{35} \\ \alpha_{41} & \alpha_{42} & \alpha_{43} & \alpha_{44} & \alpha_{45} \\ \alpha_{51} & \alpha_{52} & \alpha_{53} & \alpha_{54} & \alpha_{55} \end{pmatrix} \begin{pmatrix} E_1 \\ E_2 \\ E_3 \\ E_4 \\ E_5 \end{pmatrix} \qquad (1)$$

where E_{1z} is the longitudinal component of the circuit electric field; σ_1, y_1, v_{1y}, and v_{1z} are, respectively, the fluctuations in the surface-charge density, the transverse beam position, and the two velocity components at the interaction entrance plane; "t" refers to the total quantities; $E_i \mid_{i=1 \text{ to } 5}$ are the amplitudes of the modified circuit wave, the two modified beam space-charge waves, and the two cyclotron waves at the circuit plane of the interaction input plane; α_{ij} are complicated functions of Gould's parameters g, d, b, D, S. The incremental propagation constants δ_i are defined below.

For the modified circuit and space-charge waves

$$\beta_i = \frac{\omega}{u_0}(1 + jD\delta_i), \qquad i = 1 \text{ to } 3, \qquad (2)$$

and for the cyclotron waves,

$$\beta_4 = \frac{(\omega + \omega_c)}{u_0}(1 + jD_4\delta_4), \qquad (3)$$

$$\beta_5 = \frac{\omega - \omega_c}{u_0}(1 + jD_5\delta_5),$$

---

[1] R. G. E. Hutter, Beam and Wave Electronics in Microwave Tubes, D. Van Nostrand Co., Inc., Princeton, N. J. (1960).

δ_1, δ_2, and δ_3 are determined from the determinantal equation

$$(\delta + jb \pm d)(\delta^2 + j\,2gS\delta - S^2) = \pm\,\delta\,, \tag{4}$$

where the upper and lower signs refer to the circuit forward and backward wave interactions; δ_4 and δ_5 have been determined to be

$$\delta_4 = j\left[\frac{e^{-(\beta_e+\beta_m)(a-d)}}{\sinh(\beta_e+\beta_m)(a+d)} - \frac{D_4 S_4}{2}\,\frac{\beta_e+\beta_m}{\beta_m}\right]\cdot\ S_4$$

$$\text{and}\qquad \delta_5 = -j\left[\frac{e^{-(\beta_e-\beta_m)(a-d)}}{\sinh(\beta_e-\beta_m)(a+d)} - \frac{D_5 S_5}{2}\,\frac{\beta_e-\beta_m}{\beta_m}\right]\cdot\ S_5\,, \tag{5}$$

where $\beta_e = \frac{\omega}{u_0}$, $\beta_m = \frac{\omega_c}{u_0}$, and a, d are the distances of the beam from the sole and circuit planes; D_4, S_4, and D_5, S_5 are just like Gould's D, S but evaluated for the slow and fast cyclotron wave phase constants, $(\beta_e + \beta_m)$ and $(\beta_e - \beta_m)$. In deriving Eqs. 1, 4, and 5, the assumptions $D << 1$, $D\delta_i << 1$ and $DS << 1$ have been made.

Using the parameters resulting from the experimental conditions and inverting Eq. 1 with the help of an IBM 7094, we found that the cyclotron wave amplitudes due to the circuit electric field E_{1zt} are at the most 10^{-8} times the amplitude of the growing, decaying, or constant wave. Similarly the cyclotron wave amplitude due to the beam noise quantities σ_{1t}, y_{1t}, v_{1yt}, and v_{1zt} were also found to be negligible as compared to the amplitudes of the growing, decaying, and constant wave amplitudes. Therefore, the results clearly show that the cyclotron waves, with phase velocities far different from the electron-beam velocity, do not appear either in the interaction process or the noise analysis. It is thus seen that the three waves with phase velocity near the electron-beam velocity are the most important in the interaction and noise analyses. The amplitudes of these waves as a function of normalized beam distance from the sole plate for the usual experimental conditions are shown in Fig. 1. It is interesting to note that the relative growing wave excitation follows the theoretical expression $\frac{1}{2(1+S^2)}$ in accordance with Wightman's results [2].

---

[2] B.A. Wightman, "An Investigation of the Magnetron Amplifier," Stanford Univ. Electronics Lab., T.R. No. 52 (February, 1959).

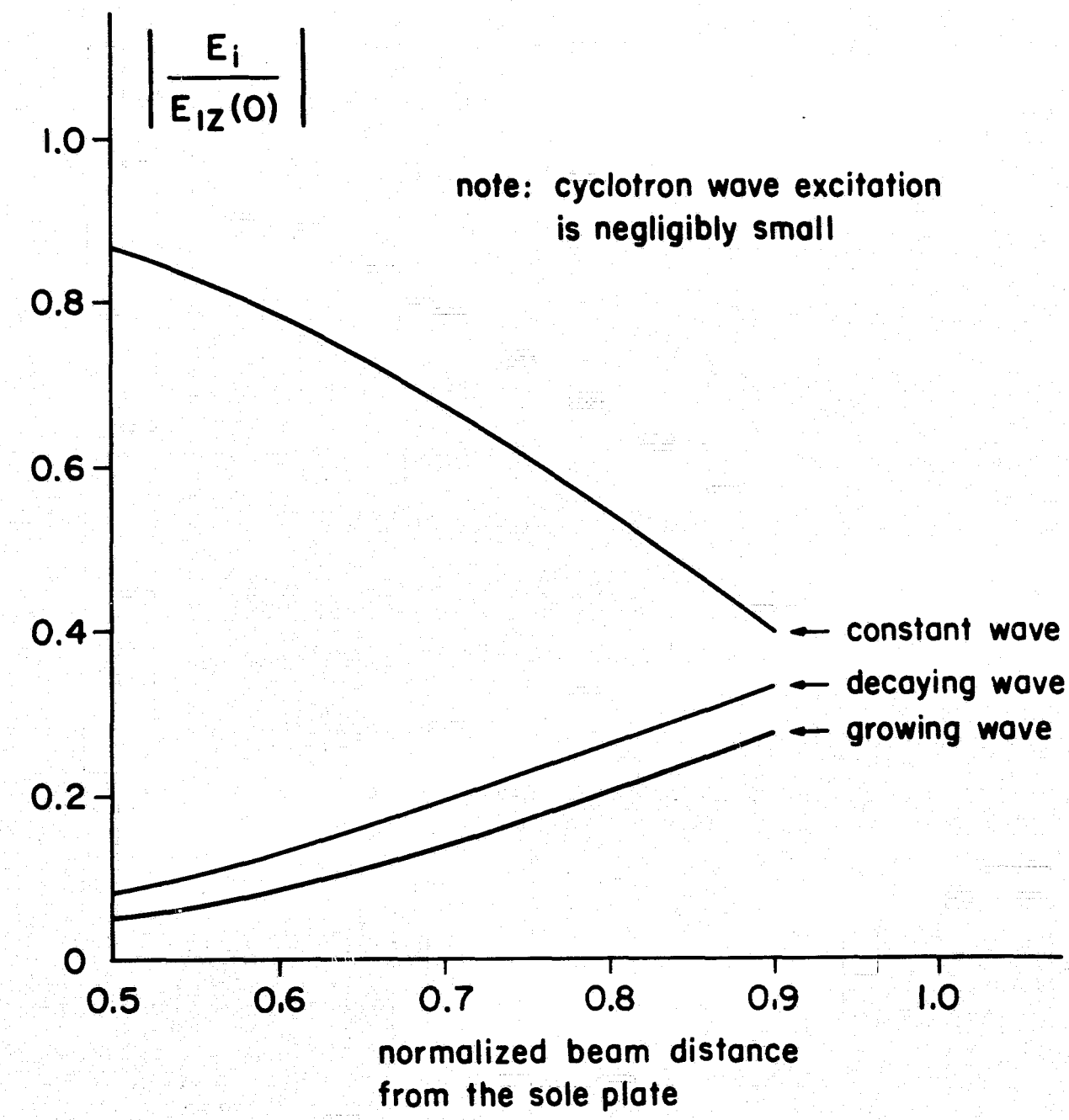

Fig. 1. Wave excitation as a function of normalized beam distance, (for V_0= 790 volts, I_0= 130.5ma, f = 1.51Gc, B_0= 232 Gauss & K_0 = 7.2 Ω).

1. Noise Figure of Forward- and Backward-Wave Amplifiers

The noise figure of either forward- or backward-wave amplifiers is expressed in terms of the mean square values of σ_1, y_1, v_{1y} mean values of cross correlation among them. It is found that the terms involving v_{1y} and v_1 make very slight contributions to the noise figure. In terms of other quantities, the noise figure F can be written as:

$$F = 1 + P_{11}\,\overline{\sigma_1^2(0)} + P_{12}\,\overline{y_1^2(0)} + P_{13}\,\overline{\mathrm{Re}\{\sigma_1(0)\,y_1^*(0)\}} + P_{14}\,\overline{\mathrm{Im}\{\sigma_1(0)\,y_1^*(0)\}}, \tag{6}$$

where (0) refers to the entrance plane of the interaction region; P_{11}, P_{12}, and P_{14} are complicated functions of Gould's parameters, frequency, and beam position in the interaction region. Van Duzer's model [3] has been used to determine

$\overline{\sigma_1^2(0)}$, $\overline{y_1^2(0)}$, $\overline{\mathrm{Re}\{\sigma_1(0)\,y_1^*(0)\}}$ and $\overline{\mathrm{Im}\{\sigma_1(0)\,y_1^*(0)\}}$ starting from velocity, beam position and shot current fluctuations at the potential minimum plane, assuming zero cross correlation among them. Calculations show that the beam position fluctuations contribute most to the noise figure. For a beam (normalized) position of 0.5, the forward wave amplifier noise figure calculated from Eq. 6 is 31.24 db as compared with the experimental value of 27.2 db.

Our estimate of noise figure variation (Fig. 2) with normalized beam distance shows good qualitative agreement with experiment. By including diocotron gain change with beam position in the drift region preceding the interaction space, this qualitative agreement is greatly improved. In view of many approximations made in the gun region and drift space analyses, the quantitative agreement with experiment seems to be satisfactory. The noise figure calculations will be made for the backward wave amplifier then compared with the experimental results.

2. Space Charge Smoothing in Crossed-Field Amplifiers

Since the beam position fluctuations appear to be dominant in determining the noise figure, it seems logical to investigate whether the beam position fluctuations are smoothed by the space-charge loading of the cathode. Following Van Duzer's [3] analysis, position fluctuations have been derived assuming a smoothing factor Γ^2 for the shot current. It was found that the position fluctuations contain the same smoothing factor. This finding agrees very well with the theoretical justification for space-charge smoothing obtained previously [4]. However, the reasons for larger reduction of noise figure in the BWA (about 5 db at f= 860 Mc) as compared to 3.1 db at 1510 Mc. in the FWA will be investigated and

---

[3] T. Van Duzer, "Noise figure calculations for crossed-field forward-wave amplifiers," IEEE Trans. on Electron Devices, Vol. ED-10, No. 6, Nov. 1963

[4] N.R. Mantena and T. Van Duzer, "Crossed-field backward-wave amplifier noise figure studies," J. Electronics and Control, Vol. 17, No. 5, p. 497, Nov. 1964.

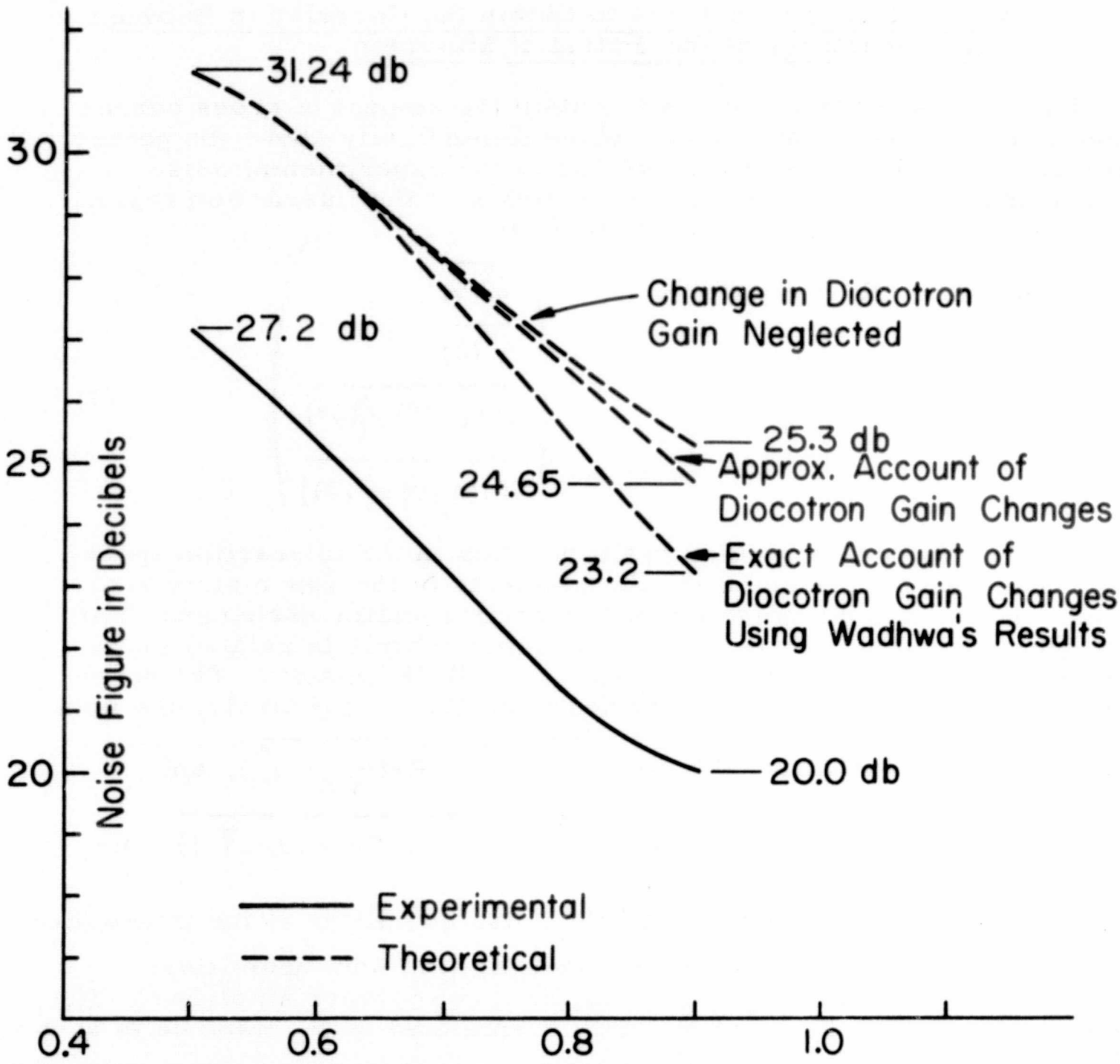

Fig. 2. Normalized beam distance a/(a + d)

related to the potential minimum parameter, namely, the ratio of the frequency of operation to the plasma frequency at the potential minimum.

3. Matrix Inversion Scheme to Obtain the Correlation Between Noise Quantities at the Potential Minimum

The purpose of this work is to obtain the amount of cross correlation among noise quantities at a plane immediately above the potential minimum. For this, we make use of the experimental noise figures and theoretical noise figure analysis of the interaction region as shown below. We can rewrite Eq. 6 as

$$F_i - 1 = (P_{i1}\, P_{i2}\, P_{i3}\, P_{i4}) \begin{pmatrix} \overline{\sigma_1^2(0)} \\ \overline{y_1^2(0)} \\ \overline{\mathrm{Re}\{\sigma_1(0)\, y_1^*(0)\}} \\ \overline{\mathrm{Im}\{\sigma_1(0)\, y_1^*(0)\}} \end{pmatrix} \tag{7}$$

where i refers to a particular beam position in the interaction space. If the beam position is changed, the elements of the row matrix also change and the column noise quantity matrix remains unchanged. For four beam positions, the (4 x 1) noise figure matrix is related to the (4 x 1) noise quantity matrix through a (4 x 4) "P" matrix. The noise quantity matrix can be easily obtained from Eq. 7. Similarly, the noise quantities at the potential minimum $\overline{v_{ym}^2}$, $\overline{y_m^2}$, $\overline{\mathrm{Re}(v_{ym} \cdot y_m^*)}$, and $\overline{\mathrm{Im}(v_{ym} \cdot y_m^*)}$ are linearly related to $\overline{\sigma_1^2(0)}$, $\overline{y_1^2(0)}$, $\overline{\mathrm{Re}\{\sigma_1(0)\, y_1^*(0)\}}$, and $\overline{\mathrm{Im}\{\sigma_1(0)\, y_1^*(0)\}}$. Having determined the noise quantities at the interaction input plane, we can now obtain the potential minimum quantities.

This analysis is being applied to the forward wave amplifier. The variation of P_{i1}, P_{i2}, P_{i3}, and P_{i4} with normalized beam distance is shown in Fig. 3 and these elements will be used to obtain the potential quantities. It is hoped that the small discrepency in the theoretical and experimental noise figure will be explained by finite noise correlation at the potential minimum which so far has been assumed to be zero.

Finally, the low noise figures [4, 5] recently reported will be explained by using our theory and some general criteria for very low noise operation will be established and reported in the final report that is being written on this project.

---

[5] R. P. Wadhwa and T. Van Duzer, "A 3.5 db Noise-Figure, S-Band, Medium Power, Forward-Wave, Injected-Beam Crossed-Field Amplifier, Proc. IEEE (correspondence), Vol. 53, April 1965, pp. 425-426.

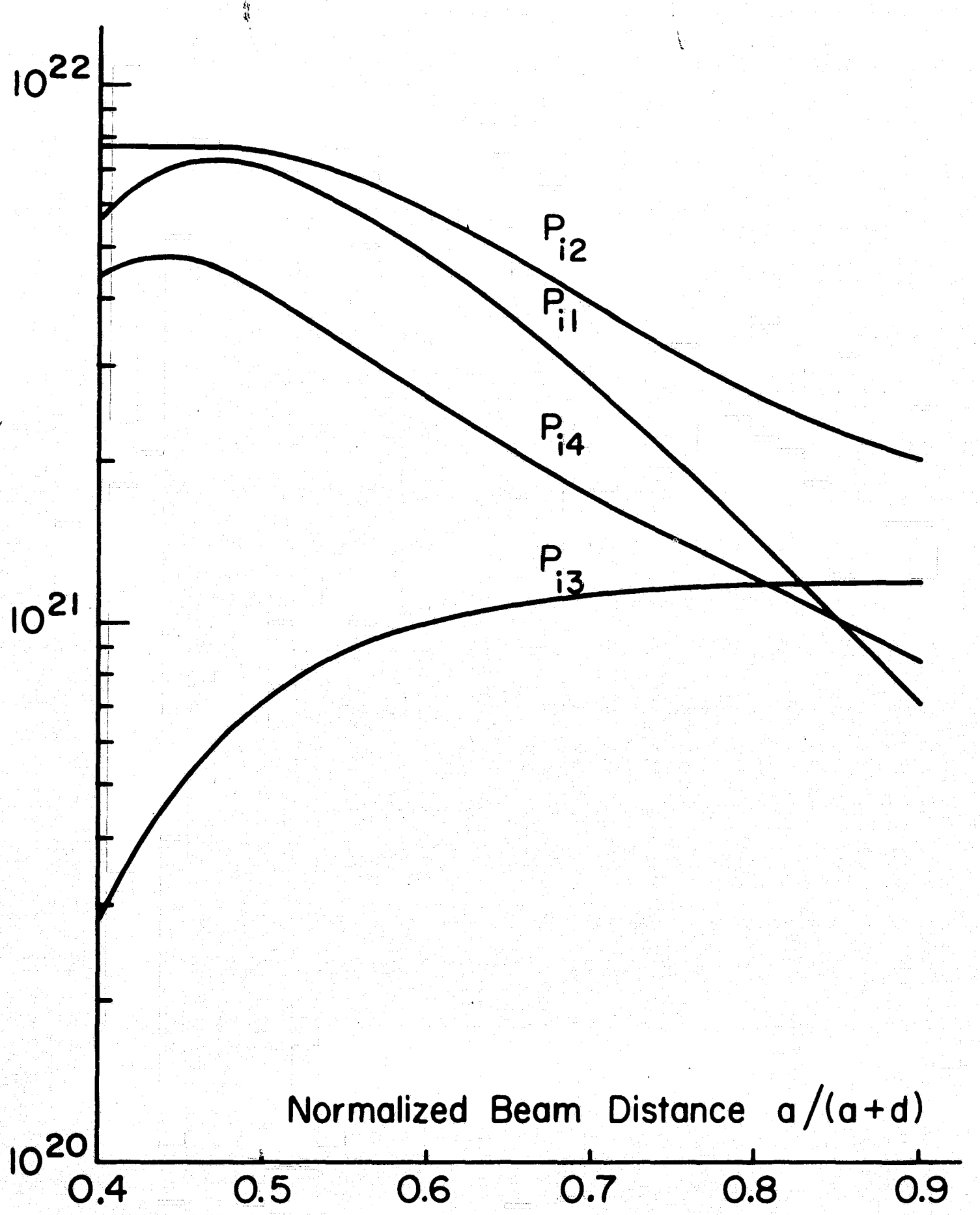

Fig. 3. Matrix elements $P_{i1}, P_{i2}, P_{i3}, P_{i4}$ as a function of beam normalized distance from the sole plate.

SHIELDED-GUN LOW-NOISE AMPLIFIER

AEL Contract DA-36-039 AMC-02164(E)
R.A. Rao (Prof. T. VanDuzer)

The objective of this project is to design a low noise shielded-gun amplifier and measure its noise characteristics.

As part of the project, a method for synthesizing crossed-field electron guns has been developed. An electron beam which has the characteristics of Kino short-gun flow near the cathode and Brillouin flow characteristics in the drift region has been synthesized. The reason for selecting this particular beam was that early experiments showed that crossed-field amplifiers with the Kino short-gun had better noise characteristics than with other types of guns. This is believed to be the result of better beam formation in the Kino short-gun. Hence, it is useful to design an electron gun having the desirable features of the Kino short-gun but without some of its shortcomings. Ideally, one would like to have a crossed-field Brillouin flow in the interaction region with the electrons drifting along parallel and rectilinear paths perpendicular to the d-c electric and magnetic fields. For Brillouin flow, the charge density is constant across the beam and is related to the magnetic field by the relation $\omega_p = \omega_c$. In Kino flow, the trajectories are not parallel near the exit plane of the gun. Hence, when the beam is injected into the interaction region, the trajectories cross over and the beam becomes non-laminar. Furthermore, the charge density at the exit plane of the Kino gun is not equal to the desired Brillouin value. Our objective is to obtain smooth matching between Kino flow and Brillouin flow. For this purpose the first-order paraxial-ray equation was used. The paraxial-ray equation is

$$2\phi_0 r'' + \phi_0' r' + (\phi_0'' + 4k_0^2\phi_0 - 2k_0 b\sqrt{2\eta\phi_0} + \eta b^2)\, r = \frac{\pm I}{2\epsilon_0 w\sqrt{2\eta\phi_0}} \qquad (1)$$

where η = magnitude of the charge-to-mass ratio of an electron,

ϵ_0 = permittivity of free space,

b = uniform magnetic field perpendicular to the plane of the axial trajectory,

I = total current in the beam,

k_0 = curvature of the axis,

w = length of the cathode along the magnetic field,

r = half thickness of the beam, and

ϕ_0 = potential along the axis.

The primes indicate differentiation with respect to the arc length along the axis. Figure 1 shows the geometry used for the paraxial-ray equation. The first-order paraxial-ray equation is consistent with Kino

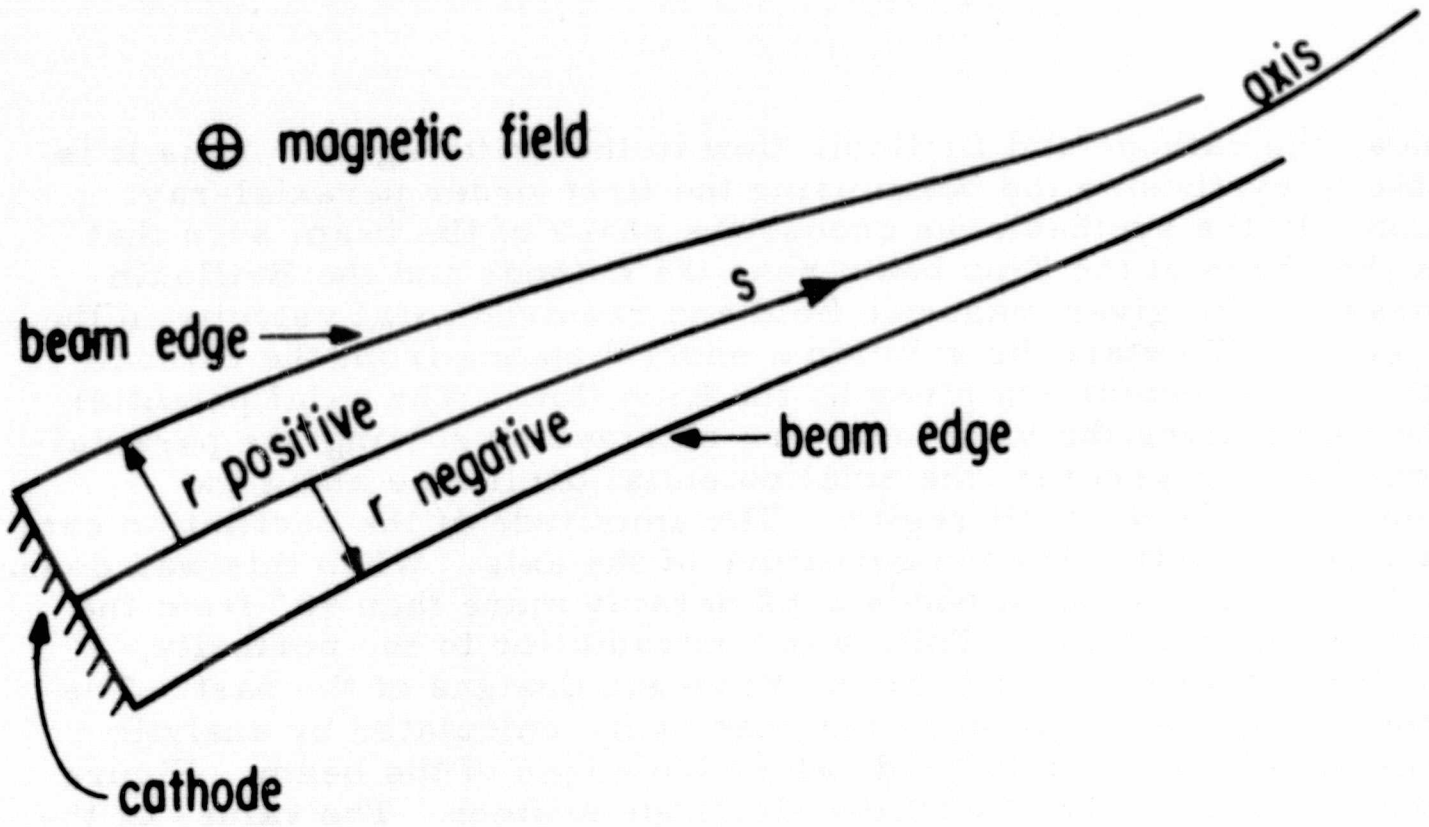

Fig. 1. Geometry for the paraxial ray equation.

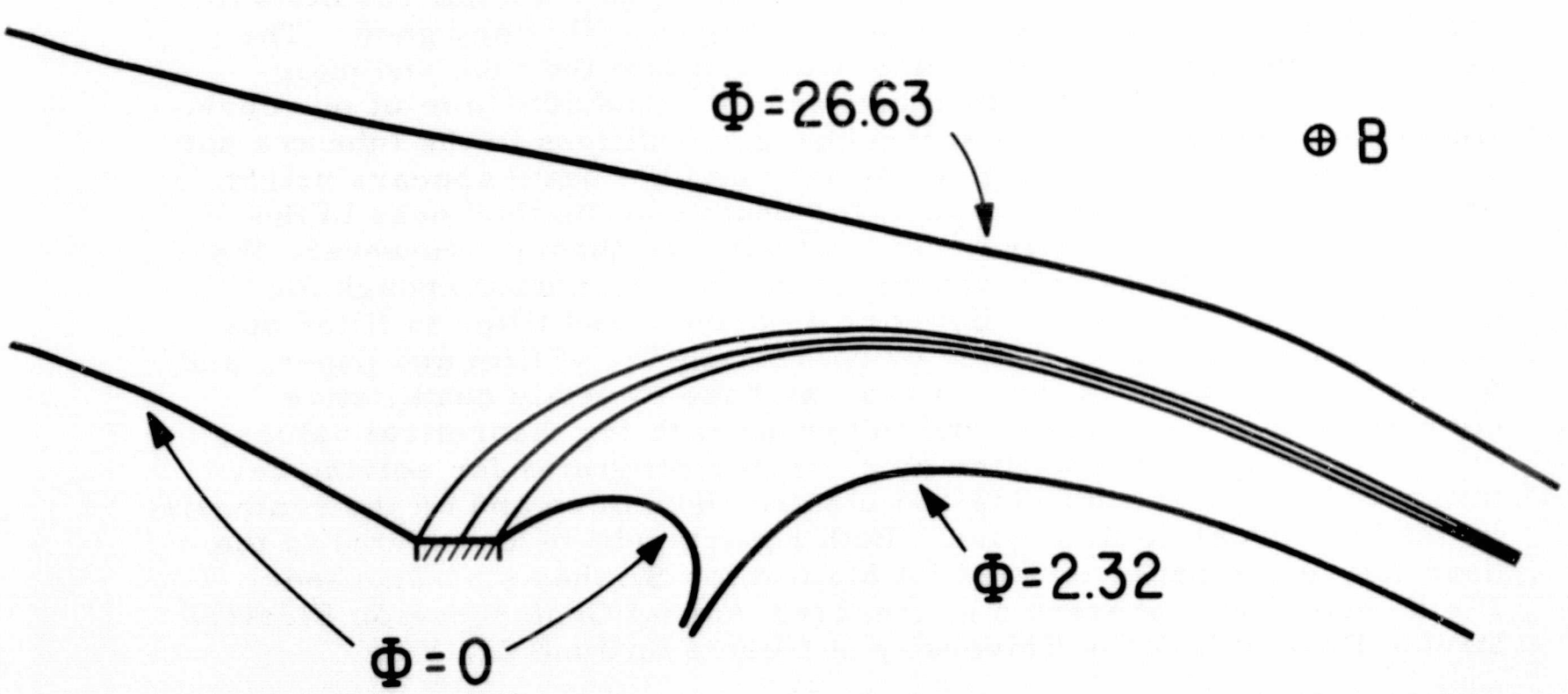

Fig. 2. Electrodes for newly synthesized beam.

flow near the cathode and Brillouin flow in the drift region. Thus it is possible to synthesize the beam using the first-order paraxial-ray equation. In the synthesis we choose the shape of the beam such that it has the shape of the Kino beam near the cathode and the Brillouin thickness for the given magnetic field and required axial velocity in the drift region. We start the solution a short distance from the cathode with the initial conditions given by the Kino flow. The axial potential and the fields along the beam edge are obtained by solving the paraxial-ray equation. In general, the axial potential oscillates about the Brillouin value in the drift region. The amplitude of the oscillation can be reduced by controlling the curvature of the axis. When this was done, it was found that the beam bends considerably more than 90° from the cathode to the exit plane. This is in contradiction to the normally used values of less than 90° for the Kino-gun designs of the past. The electrodes required to produce the beam were calculated by analytic continuation of the electric fields along the edges of the beam. Figure 2 shows the electron beam and the electrode system. The values of the potential indicated in the figure are normalized values.

The electron gun described above was fabricated and tested. Figure 3 shows a photograph of the experimental tube. The tube has an ion pump to control the pressure inside the tube and a palladium leak through which hydrogen gas may be introduced into the tube to observe the beam. The transverse focusing electrodes are made of glass and coated with a transparent conductive coating so that the beam may be viewed through them. Table 1 compares the experimental results with the theoretical values. The agreement is generally very good The beam was observed by introducing hydrogen into the tube and maintaining the pressure in the tube between 10^{-6} and 10^{-5} mm of mercury. Under these conditions, the space-charge conditions in the tube are not altered much from the design conditions and the beam appears bright enough for viewing. The shape of the beam and the thickness in the drift region appear to be in agreement with the theory. However, the quality of the pictures obtained so far has not been good enough for quantitative comparisons. By using a narrow band filter to filter out the light from the hot cathode, by correct choice of film and paper, and by careful alignment of the camera, we hope to obtain quantitative comparisons of beam shape and thickness with the theoretical values.

Reports are being written on computer programs for solving certain problems in static fields and electron dynamics and on the synthesis method for crossed-field guns. Both reports will be completed in the near future. A paper entitled "A Method for Synthesis of Crossed-Field Guns," was presented at the 23rd Annual Conference on Electron Device Research at the University of Illinois on June 25, 1965.

Future Plans: The design of the shielded-gun tube will be continued, and the characteristics of the electron beam in the gun will be measured.

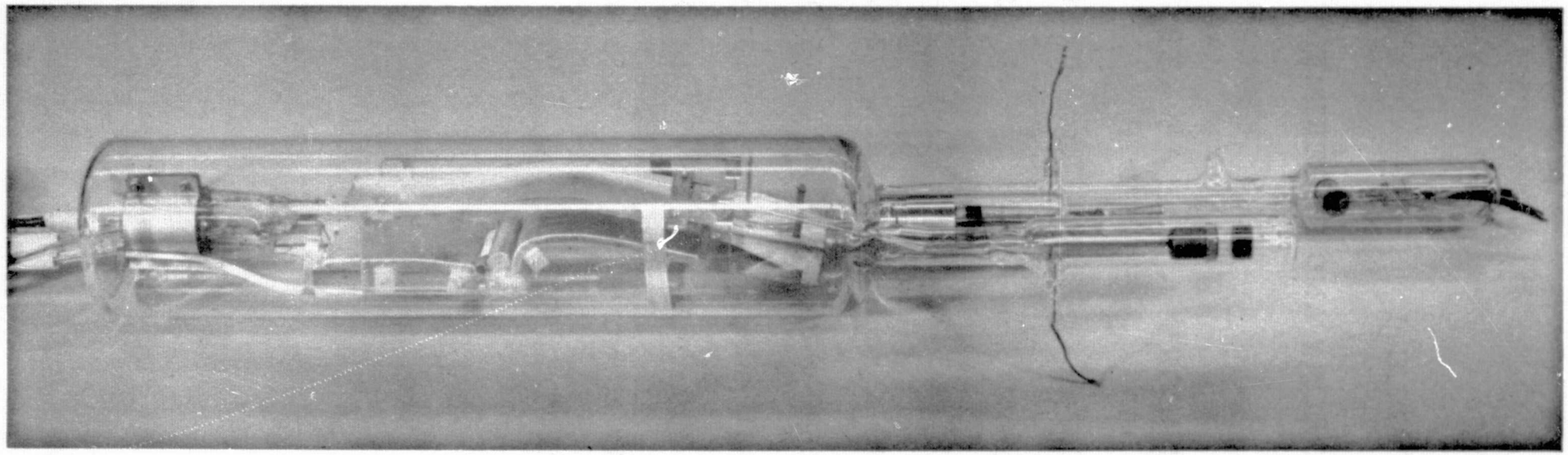

Fig. 3. The experimental tube.

TABLE I

COMPARISON OF THEORY AND EXPERIMENT

PARAMETERS	THEORY	EXPERIMENT
Cathode width	0. 2 in.	0. 2 in.
Cathode width	infinite	1. 5 in.
Brillouin thickness	0. 0363 in.	-
Magnetic field	70. 5 gauss	72 gauss (± 2%)
Anode potential	1500 volts	1500 volts (± 2%)
Cole potential	131 volts	131 volts (± 2%)
Circuit potential	1500 volts	1450 volts (± 2%)
Cathode current	47. 2 ma	52. 0 ma (± 2%)
Transmission to collector	100%	99%

C. PLASMAS

Plasma research in ERL and the Electrical Engineering Department is concerned primarily with the problems of high-temperature plasmas; however, during this period a new project to study low-temperature plasmas was initiated.

The high-temperature plasma research is concerned with the problems of creating, containing, heating, and measuring the physical and electromagnetic properties of ionized gases.

The two main experiments on high-temperature plasmas utilize the same 0.25 MJ capacitor energy storage system on a time-sharing basis. This capacitor bank has been in operation for more than two years and, except for normal electronic failures, has functioned satisfactorily.

The first experiment is a single-stage magnetic mirror compression experiment that produces a $10^{12}/cm^3$ hot-electron plasma which has a temperature of 40 keV at 30 kG magnetic field. The plasma is stable and lasts for more than 15 msec. At double the magnetic field, the electron temperature is doubled to 80 keV, but at this higher temperature the plasma becomes unstable and is lost after 1.5 msec. The properties of this plasma have been studied with such diagnostic techniques as spectroscopy of the x-ray Bremsstrahlung, spectroscopy of x rays produced by end-loss electrons striking targets, probes of visible radiation, microwave radiation, and synchrotron radiation. The synchrotron radiation measurements have confirmed many features of the theory of radiation from a hot, tenuous, magnetically confined plasma.

The plasma produced in this experiment will be investigated by other diagnostic methods in order to gain a better understanding of its properties. In particular, it is the purpose of these studies to explain the stability of the plasma in a supposedly theoretically unstable magnetic field configuration and then to explain the mechanism of the instability that occurs at the higher magnetic fields during periods when the plasma is unstable. A recently acquired image-converter camera will be used to "photograph" the plasma by taking a picture of the end-loss flux of hot electrons striking an aluminum-coated (10 keV layer) phosphor-coated quartz flat. This system will be capable of detecting macroscopic motion of the contained plasma.

Electron-cyclotron heating, experiments to measure the electron distribution function, laser scattering from the hot electrons, a hydromagnetically stable coil configuration, and a data acquisition system are being worked on.

The second experiment making use of the capacitor bank is a two-stage magnetic mirror compression experiment in which the plasma is created by $\underline{E} \times \underline{B}$ breakdown in the first stage. The first stage is a coaxial region that has a radial electric field (~ 5 kV/cm) and an axial magnetic field (~20 kG) into which a predetermined amount of D_2 gas is admitted by a fast-puff valve. An avalanche breakdown occurs and produces a plasma that has both bulk rotation about the chamber axis and a superimposed gyromotion. The energies in bulk rotation and gyromotion are comparable and for typical operating conditions are about 2. keV. The density of the rotating plasma donut is about $10^{14}/cm^3$. The objective of this project is to stop the bulk rotation of this plasma by shorting out the electric field between the inner and outer conductor and then to transfer adiabatically the plasma along the vacuum chamber to the second-stage region which has no center conducting rod. In the second stage, the magnetic field can be increased to as much as 100 kG, which would increase the plasma temperature by a factor of 2 to 4.

The low-temperature plasma research that was started during this period involves the study of plasma stability of alkali metal vapor plasmas. There will be a new facility in the program of plasma research which will seek to gain information about stability problems in high-temperature plasmas by operating in a regime where the significant plasma parameters can be scaled from high-temperature situations. Much of the effort during this period has been devoted to the construction of the basic experiment.

In addition to these experiments there are related experimental and theoretical studies including computer models of plasmas, wave plasma interaction, and hydromagnetically stable coil designs.

HOT-ELECTRON EXPERIMENT (BME-I)

AFAL Contract AF-33(615)-1075;NSF GP2239
J. Colvin, R.A. Pecachek, S. Sesnic, and D. Tuma,
(Profs. A.J. Lichtenberg and A.W. Trivelpiece)

This experiment was operated many times during this period. Initial experiments on scattering of light from a laser beam by the hot electron plasma, studies of the synchrotron radiation, heating of the plasma by electron cyclotron waves, x-ray energy analysis, energy analysis of electrons escaping from the magnetic mirror region and a plasma camera were carried out. The experiment produced a satisfactory hot electron plasma, except for a brief period of difficulty with the plasma source.

HOT-ION PLASMA (BME-II)

NSF Grant GP2239
H.K. Forsen and V. Zaviantseff (Prof. A.W. Trivelpiece)

During the first half of this period this experiment (Fig. 1) was operated and studies on the transfer and trapping problems were carried out. An energy spectrum of the ions that escape from the second stage was made with an electrostatic energy analyzer. The results of this study are shown in Fig. 2. A spectrum of the impurity radiation in the visible and vacuum ultraviolet was also obtained. This is shown in Fig. 3. During the second half of this period, a report of the work was written and the experiment was not operated. An abstract of this report follows:

> A two stage magnetic mirror compression experiment was constructed to investigate a rotating plasma as a clean, high-temperature plasma source. Kilovolt deuterons are created in the crossed electric and magnetic fields of the first stage and are transferred or injected into the second stage. The purity and trapping of the plasma is limited by electrode effects.
>
> Ionization takes place in the coaxial system which has a radial electric field of $7 \cdot 10^5$ V/m and an axial magnetic field of 11 to 20 kG. The 10^{17} particles are injected into the field region by a fast-acting valve in the central anode. Particles ionized in these $\vec{E} \times \vec{B}$ fields have equal energy in the gyromotion and in the drift motion. If the electric field is turned off, the drift energy is removed but the energy of gyromotion remains. The plasma is in contact with the electrodes, therefore high mass impurities are liberated from the electrodes and contaminate the plasma. Measurements are made on the plasma to determine energy density, ion energy distribution, electron temperature, impurity content, and neutron flux.
>
> To transfer the plasma out of the first stage to the second stage, two methods are used: One involves sequentially energizing the first-stage magnetic field coils to move the plasma into the second-stage mirror field; the other involves ionization in a gradient field which directly injects the plasma into the second stage. In the process of transfer, the plasma leaks out of the first stage. The escaping deuterons are given additional axial acceleration by the fringing electric field at the tip of the anode which extends through the first stage and ends between the two stages. This tip acceleration made trapping by the available fields and rise times impractical.

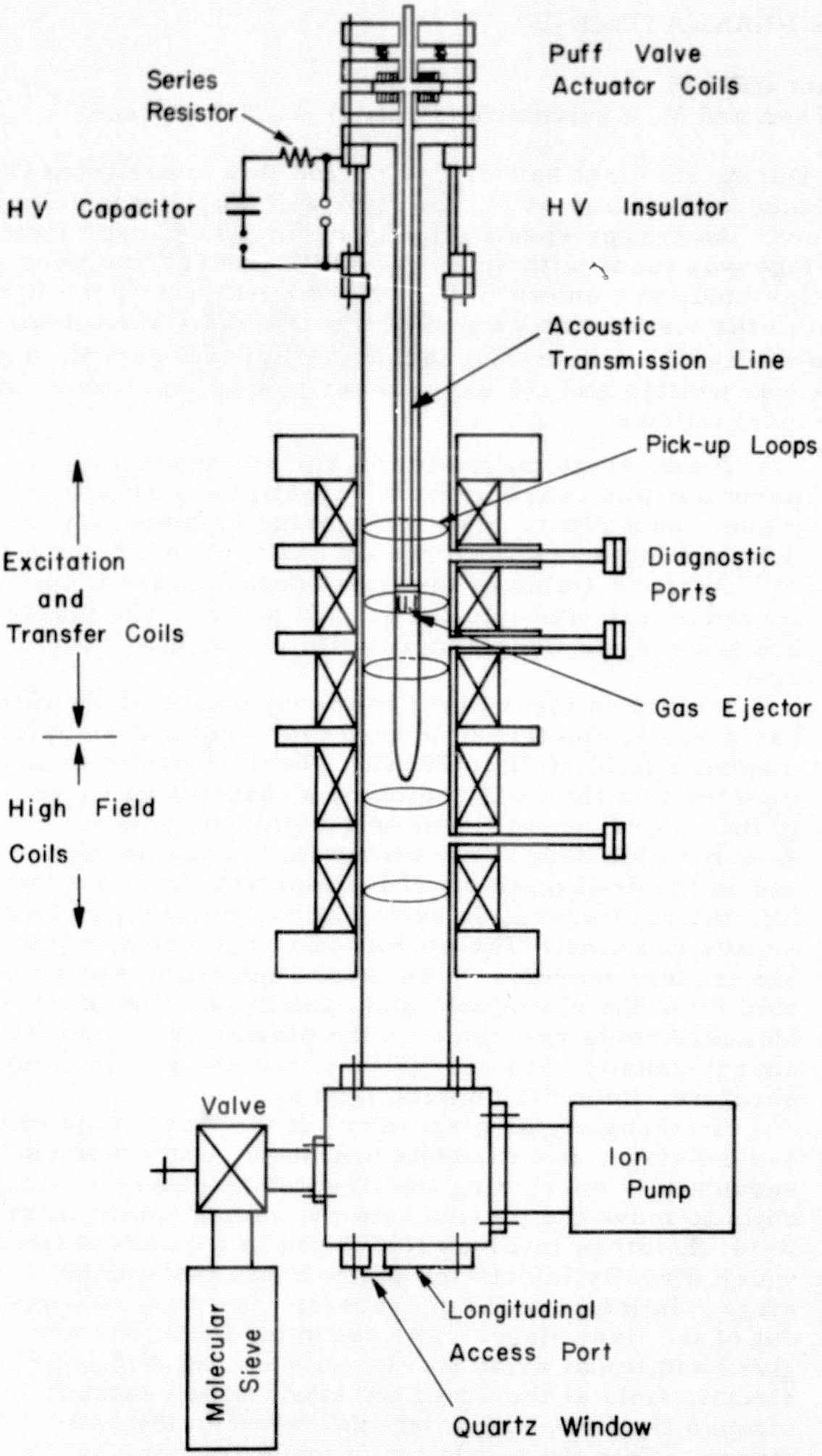

Fig. 1. Diagram of the two-stage experiment.

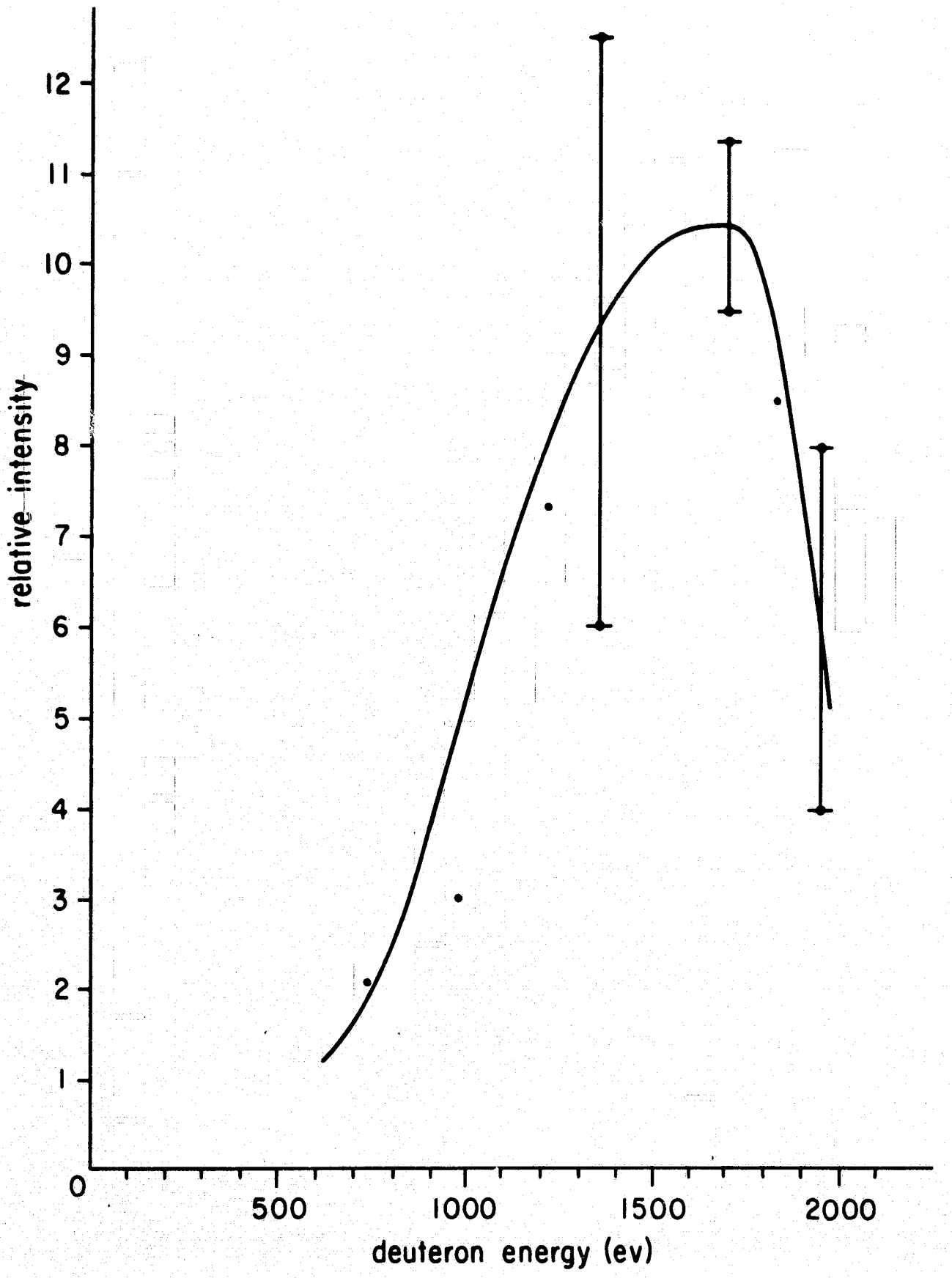

Fig. 2. Plot of the peak signal from the energy analyzer as a function of the energy accepted by the analyzer. Error flags represent extremes of several shots.

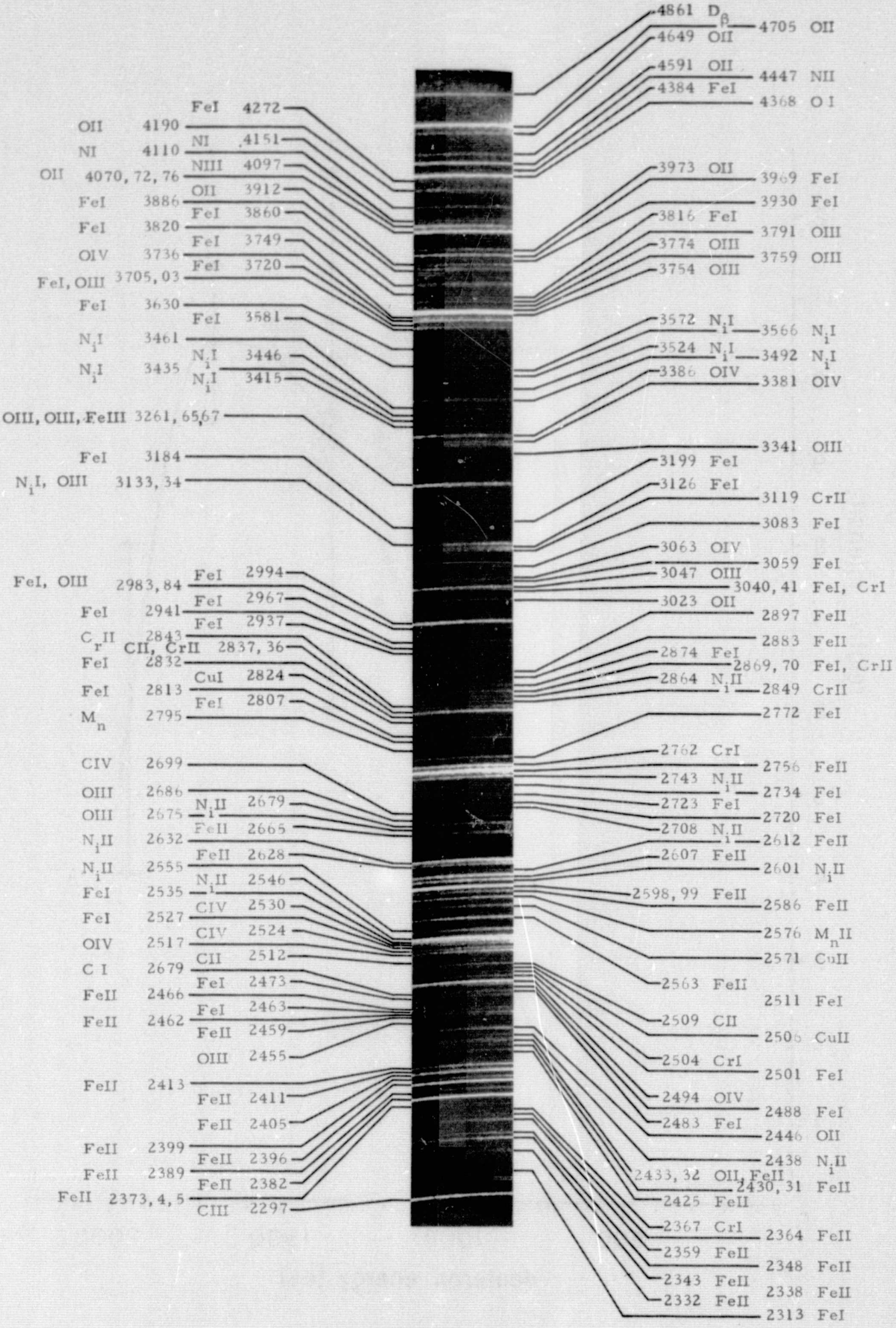

Fig. 2. Expanded view of identified impurity spectrum.

SYNCHROTRON RADIATION MEASUREMENTS

NSF Grant GP-2239
S. Sesnic (Professor A.J. Lichtenberg)

In order to make absolute measurements of synchrotron radiation it is necessary to calibrate the spectrometer-detector system with a source having known characteristics, e.g., a blackbody with known parameters (temperature, radiating area, solid angle, frequency bandwidth). The system response to the synchrotron radiation can then be compared with the system response to the blackbody radiation.

To insure that the radiation of the calibration source is the same as that of the blackbody, three cavities were built in different form and with different wall materials. All three cavities -- two, sooted, cast iron cavities and one glass cavity -- were held at the same temperature (480°K ± 10°) and had the same radiation area and solid angle. One of the cast iron cavities was conical, the other was cylindrical with a small hole at the center of its circular base. The glass cavity was conical. All three cavities showed essentially the same radiation over the whole wavelength region, i.e., between $\lambda = 2$ and 0.2 mm. The experimental results shown in Fig. 1 were obtained with an InSb-photoconductive detector and echelette grating spectrometer. The responsivity of the InSb detector drops very rapidly with frequency; therefore, below $\lambda = 0.2$ mm the curves show a sharp cutoff. Above a wavelength of 2 mm the blackbody radiation also fell below the detectable level. Up to $\lambda = 1$ mm, both (conical and cylindrical) cast iron blackbodies showed almost the same radiation pattern, but above $\lambda = 1$ mm the detected signal of the conical cavity began to differ very sharply from that of the cylindrical cavity, which showed stronger radiation. Evidently at these low frequencies a conical metal-walled cavity does not radiate as a blackbody. This was confirmed when another conical cavity of identical form but with glass wall material was built. The new blackbody had the same radiation pattern as the cylindrical cavity, which confirmed the fact that between 1 and 2 mm the cylindrical and glass-walled cavities acted as blackbodies, but the conical metal-walled cavity ceased to act as a blackbody above 1 mm. Although not indicated in Fig. 1, for wavelengths smaller than 1 mm the radiation pattern from the glass-walled cavity followed closely the radiation pattern of the cylindrical and conical blackbodies. The reason that the glass-walled conical cavity is still a blackbody in the wavelength region between 1 and 2 mm and the metal conical cavity, though of the same form, is not, is that reflectivity (90 to 95%) of the sooted cast iron is higher than the reflectivity of the glass (20%). These reflectivity measurements were performed in the same wavelength region (0.2 to 2 mm) and were found to be rather constant. The four separate curves in Fig. 1 represent four main gratings with slightly overlapping frequency regions.

The blackbody signals were very low; the lowest detectable signal was about 0.5×10^{-9} V. This required very long recorder integration times (of the order of 10 min.), which would require too much

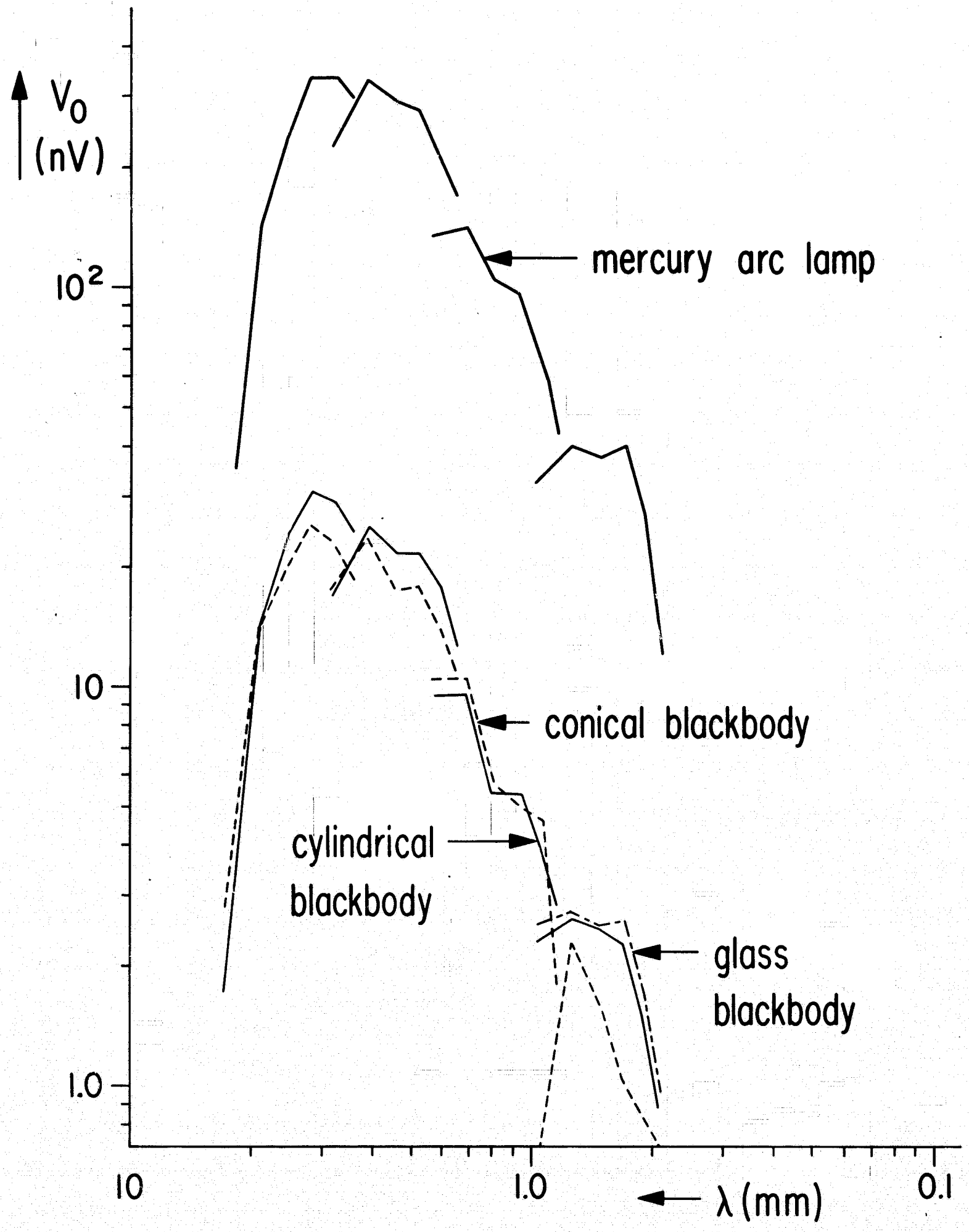

Fig. 1. Detector output voltage for blackbodies and mercury arc lamp.

time to be spent on calibration during synchrotron radiation measurements. The objective was to calibrate a source which radiated more strongly than a blackbody; after the source was calibrated it could then be used as a secondary standard. In Fig. 1 the top curve represents the detected signal from a mercury arc lamp (UA-2, General Electric) used as a radiation source. The radiation is about 15 times stronger than the radiation from the blackbody. Using these data and comparing them to the blackbody signal we computed the equivalent blackbody temperature of the mercury arc lamp as a function of the wavelength (Fig. 2). The points represent an average of two to four measurements with error bars indicating the rms deviation. The points without error bars represent single measurements. After the mercury arc lamp is calibrated it can be used as a secondary standard for absolute calibration of the synchrotron radiation.

To find the best filtering combination, extensive measurements were performed to calibrate various components of the spectrometer, mainly different types of filters.

In Fig. 3, the filtering characteristics of the grating filters (echelette grating) as a function of λ/d are given where λ is the wavelength and d is the grating constant. The various curves represent characteristics of different filter gratings with different grating constants. The filtering coefficient F is found by taking the ratio between the signal with the filter and signal obtained when the filter was replaced by a plain mirror. But in case of the signal with plain mirror, the filtering was inadequate and the main grating transmitted a strong second harmonic (second order). This tended to overestimate the normalizing signal and underestimate the filtering factor, F. The effect is stronger at the long wavelength end of a main grating because the filtering is weaker there. On the other hand, main grating distribution of the second harmonic into second order is rather sharply peaked in the neighborhood of the inblaze wavelength. Therefore the contribution of the second harmonic to the normalization signal is strongest somewhere in the middle of the main grating region. This makes the filtering curve appear to sag, as shown on some of the curves of Fig. 3. To reject partly the second harmonic, we used NaCl filters, whose filtering characteristics were also measured. Results are shown in Fig. 4, where it can be seen that the filtering of the NaCl filters is rather slow and cannot eliminate the second harmonic. Nevertheless, by comparing the measurements of the same echelette filter with and without NaCl filters one can see that the dips in the filtering curve are smaller with the extra filters. To obtain the true filtering curve, the higher harmonics should be completely filtered out. This would show the envelope of the measured curves as the true filtering curve.

In the last quarterly report it was reported that filtering of the filter gratings in the divering beam is stronger than filtering in the converging beam; however, new measurements with more echelette filters do not confirm this. The cause for this disagreement was due to an additional, very shallow, and difficult to observe, second groove on the broad facelets of the echelette filter used only in the converging beam

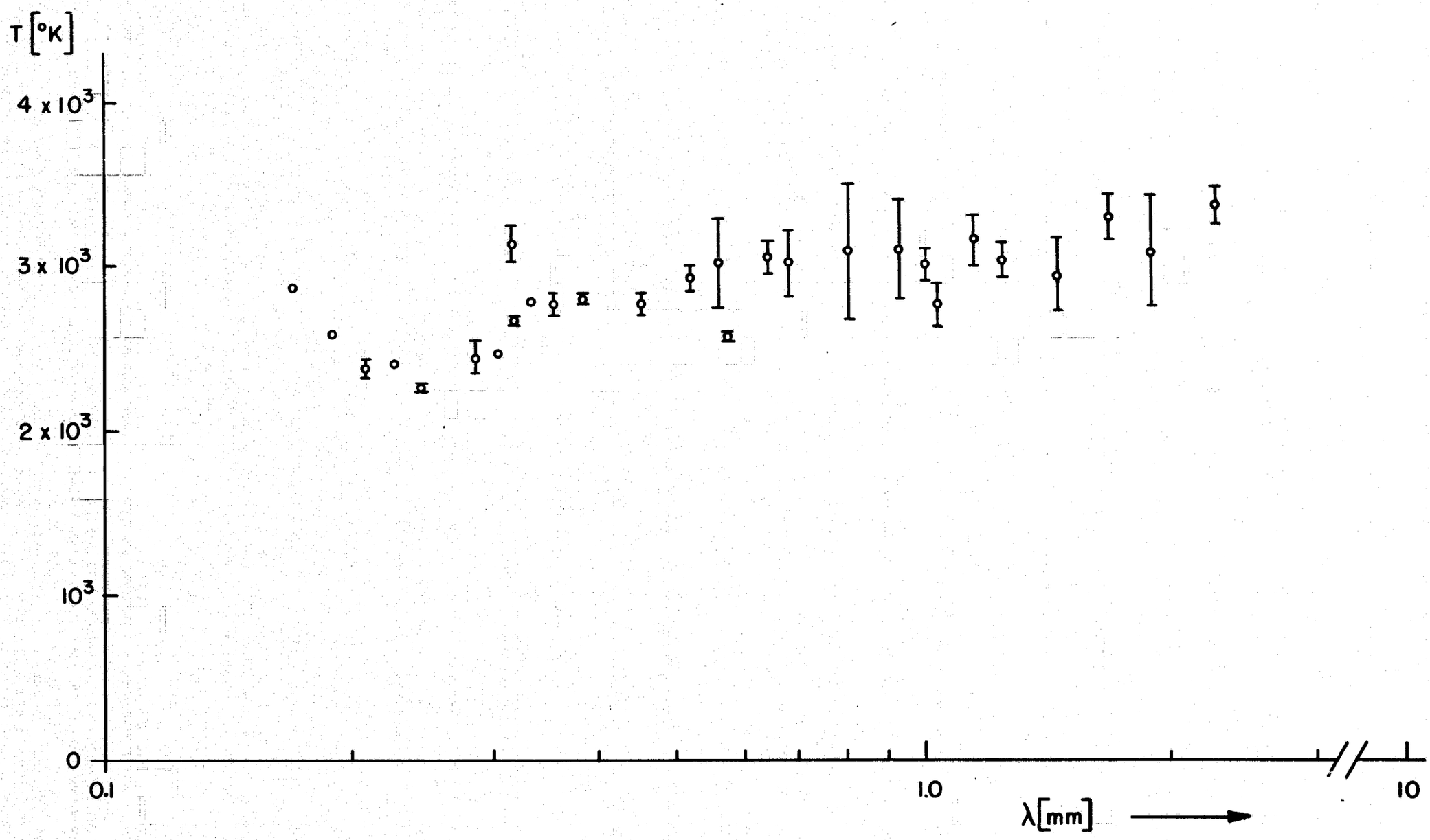

Fig. 2. Equivalent blackbody temperature of mercury arc lamp as a function of wavelength.

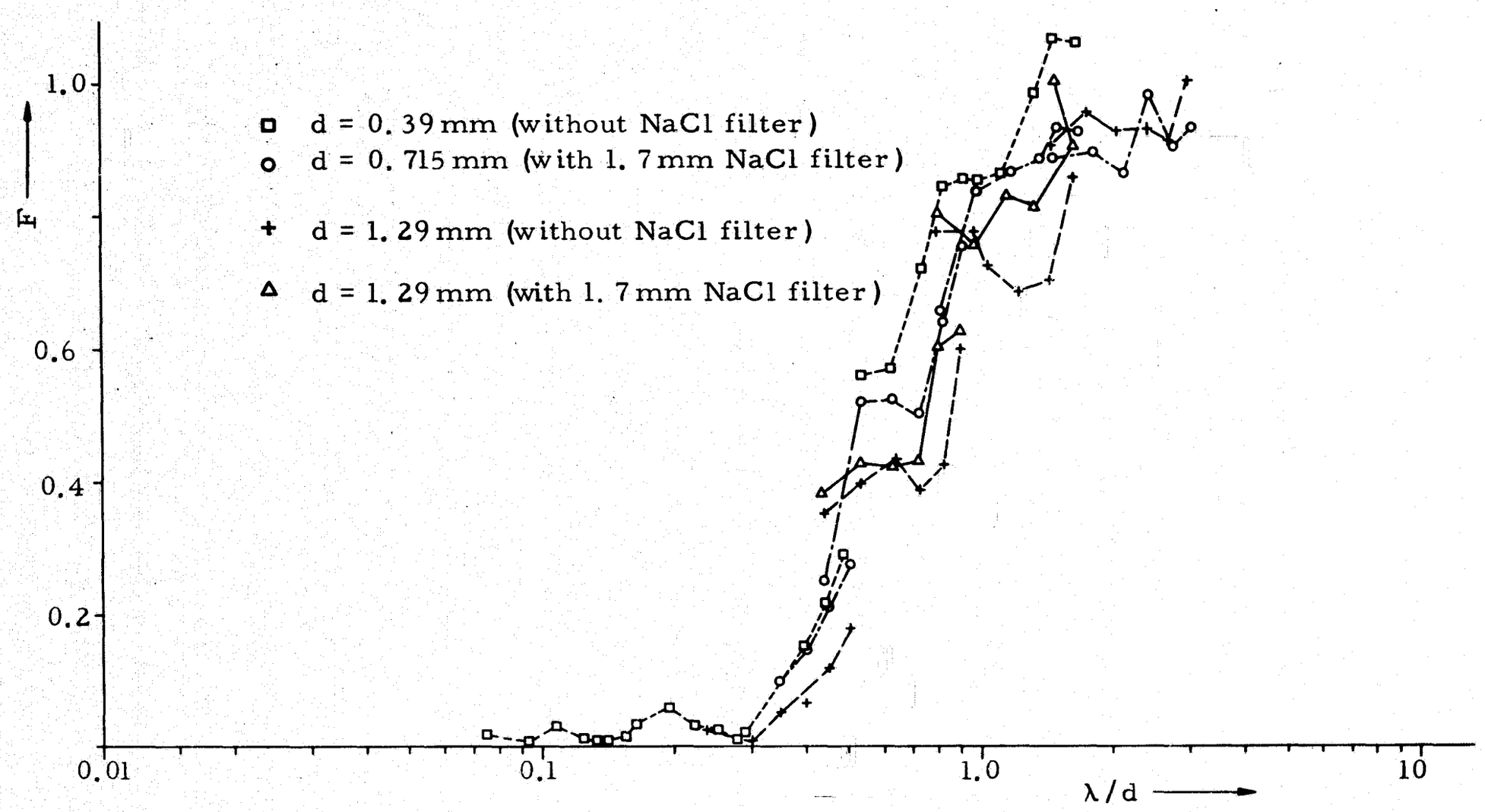

Fig. 3. Filtering characteristics of the echelette filters with different grating constant, d.

This caused the echelette filter to shift its filtering characteristics by one octave. It was mistakenly concluded that filtering in the diverging beam was weaker.

The filtering with an echelette filter spreads over 2-3 octaves. To improve this we decided to investigate wire mesh filters [1, 2] and actually replaced one of the two echelette filters with a wire mest filter. The measured filtering characteristics of various mesh filters is shown in Fig. 5 as a function of λ/d, where λ is the wavelength and d is the distance between the axes of the two neighbouring wires. The filtering is spread slightly over more than an octave, and compared to the echelette filter the wire mesh filter is more effective. Here a strong second harmonic appears again and, associated with it, the filtering curve is lowered. The content of the second harmonic is more pronounced here than in the case of the eschelette filter measurements. The reason is that for the echelette filter measurements wire mesh filters were used as a second filter, and filtered more effectively with only one filter than the single grating filter. Also, the filtering curves were more distorted for the rougher mesh because of the larger content of the higher harmonics. The true filtering curve is again represented by the envelope of the measured curves.

The longer wavelengths are not filtered by filter gratings, NaCl transmission filter, and wire mesh reflection filter. Only the main grating "filters" the longer wavelengths by scattering them into zero-order. The main grating is usually near the exit slit and some of the long wavelength radiation could then be scattered into the exit slit. Therefore it is important also to filter out the long wavelength radiation, particularly in case of the synchrotron radiation, where most of the radiation for a magnetic field of 50 kG is between 1 and 4 mm. This means that, when we are measuring, say, around 0.2 mm, where the synchrotron radiation is very small and the detector responsivity is low, the long wavelength-scattered signal could be larger than the original 0.2 mm signal. The use of a wire mesh as a transmission filter to attenuate the longer wavelengths has also been considered. Unfortunately the wire mesh filter does not have an adequate high pass characteristic but resonantly transmits over approximately a half octave from a lowest frequency a little above cutoff. The transmission was measured and the results for three different meshes are given in Fig. 6. The relative bandwidth, defined by 3db points on transmission characteristic, is equal to 0.4. The transmission of the longer wavelengths is very sharply cut off. The transmission characteristic of the wire mesh filters is too narrow to be used over one octave. But by using two of the wire meshes with properly displaced transmission characteristics and replacing them during the measurement over one octave, it would be possible to achieve very strong attenuation for the long wavelength signals.

---

[1] Renk and Genzel, Applied Optics, 1, p. 643 (1962).

[2] Mitsuishi et al.: Japan. J. Appl. Phys., 2, p. 574 (1963).

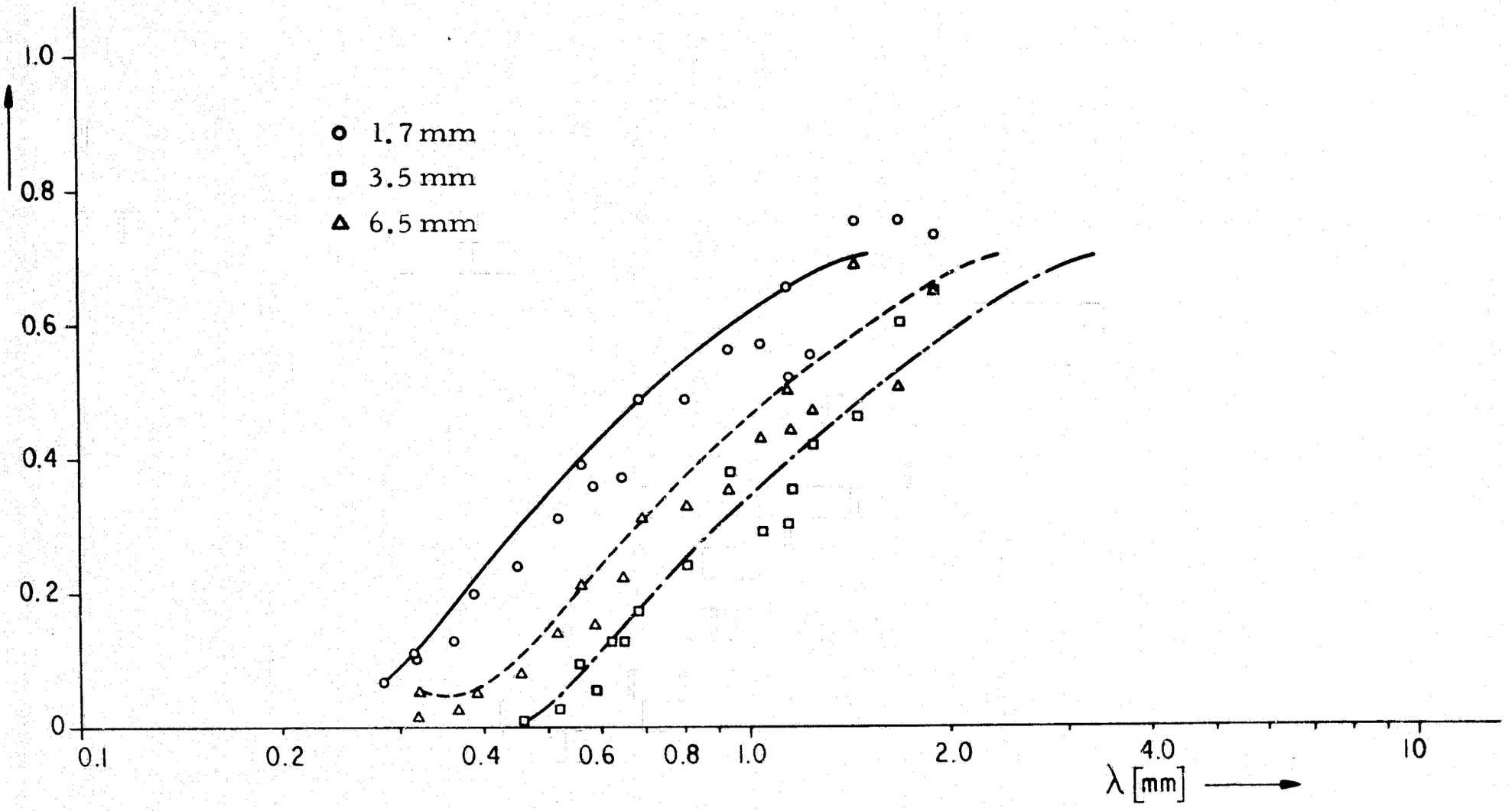

Fig. 4. Filtering characteristics of NaCl crystals of various thicknesses.

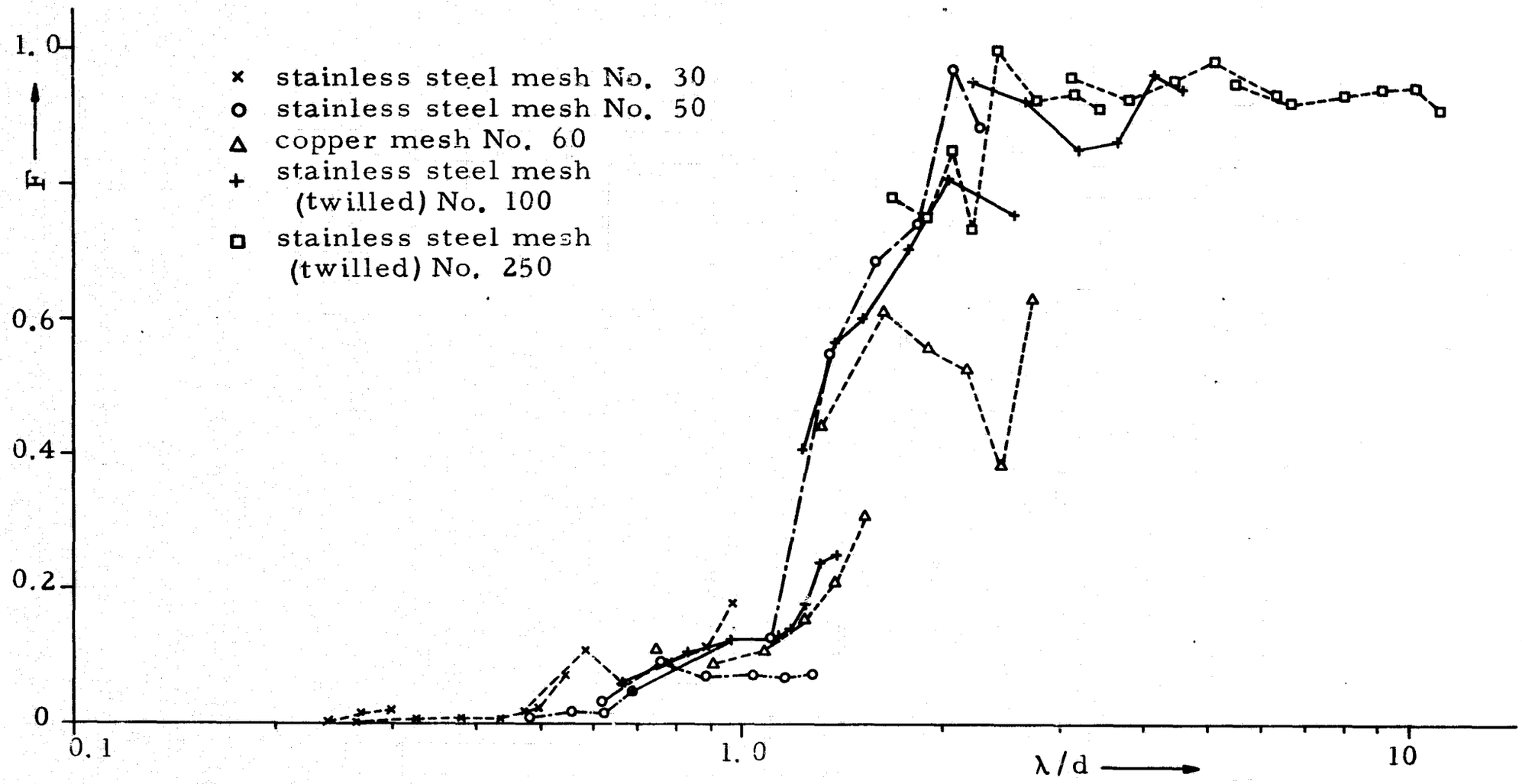

Fig. 5. Filter characteristics of the wire meshes of different mesh constant.

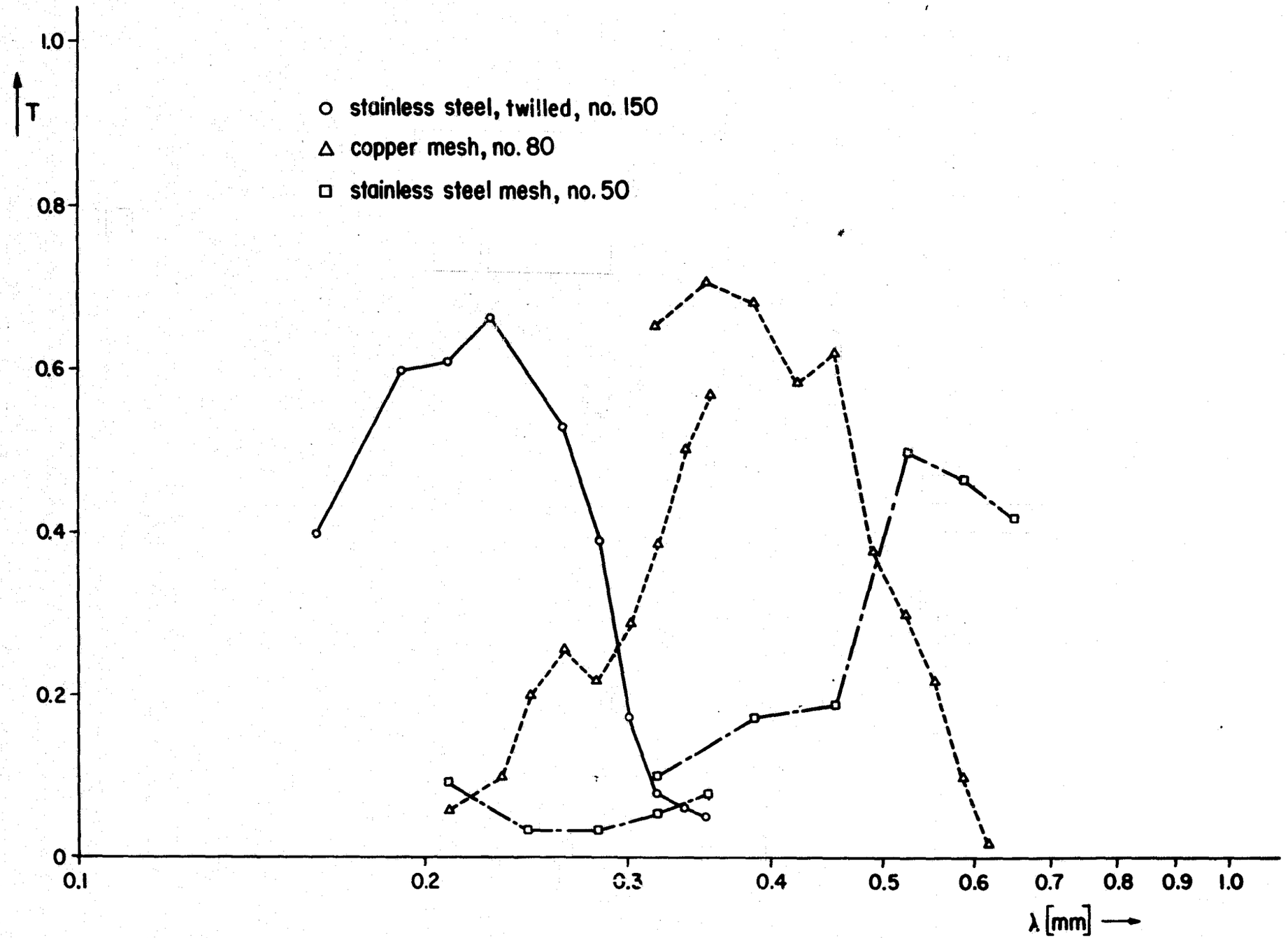

Fig. 6. Transmission characteristics of three different wire meshes.

PLASMA DIAGNOSTICS USING A LASER

AFAL Contract AR33(615)-1078
R.E. Pechacek (Prof. A.W. Trivelpiece)

Early during this period we made our first attempt to measure the radiation scattered from a giant pulsed laser beam by electrons in the mirror machine plasma. No scattered photons were detected, but occasionally and unpredictably an abrupt change was observed in the rate or loss of electrons along the machine axis, when the laser was fired. This effect was not observed in a subsequent experiment. The optics of the experiment were then rebuilt to permit enough angular displacement of the laser beam and detector optics to insure that we could focus on a plasma that was removed from the center of the vacuum chamber. At the same time ground planes and double shielding was incorporated in the detector circuitry to reduce pickup from the 30 kV Kerr-cell pulse. The circuitry for multiple Q-switching the laser was also completed and tested. It is now possible to generate four giant pulses during the 1.6 msec that the laser pump fires.

Using the new optics and a dummy mirror-machine vacuum chamber, we calibrated the sensitivity of the detector using nitrogen, and also reduced the wall-scattered light to an equivalent 10^{15} electrons cm^{-3}. The optics were then installed in the mirror machine, using a filter to eliminate the wall-scattered light at 6943Å and pass doppler shifted light between 6000 Å and 3800 Å. The system sensitivity was such that 10^{12} electrons cm^{-3}, between 50 and 100 keV in temperature would yield 5 detected photons. This would have easily been observable above the plasma luminosity. However, no photons were detected.

The laser and detector optics were aligned on the center line of the vacuum chamber, which may be several millimeters from the centerline of the magnet. It is conceivable that, since the cross section of the laser beam is about 1 mm and the detector observes about 1 mm on the chamber axis, we have missed the plasma. It is also possible that the plasma is not dense enough. We are presently modifying the detector optics and intend to use a more sensitive photomultiplier tube. This improvement will increase the detectors sensitivity by a factor of 25.

ELECTRON CYCLOTRON HEATING

AFAL Contract AF33(615)-1078
D. Tuma (Prof. A.J. Lichtenberg)

As reported in the previous quarterly report, an experiment is being performed to heat the electrons of the BMEI plasma by rf power propagated parallel to the magnetic field. A 3-cm magnetron with a 0.5-μsec, 250-kW rf pulse has been used but no definite results of electron heating were obtained. However, in our experimental work, the density of the plasma is such that the plasma frequency is about

10^{10} cps (corresponding to 3 cm wavelength). It is belived that the rf pulse from the magnetron, having about the same frequency as the plasma, does not penetrate appreciably into the plasma but is rather reflected, so that little interaction between the plasma electrons and the rf pulse occurs.

Dandl et al., working on electron cyclotron heating in a mirror machine at Oak Ridge, have reported substantial heating, of the order of 100 keV [1]. The rf power, supplied by a 3 cm, 50 kW, cw klystron, is radiated perpendicular to the mirror magnetic field into a cavity to which neutral gas is continuously fed. The rf field ionizes the neutral gas and then heats it up during the whole containment time. Our electron cyclotron heating experiment differes from the Oak Ridge experiment, in that we are heating an already hot ionized plasma along the magnetic field, and that the pulse duration, 0.5 to 2 μsec, is a few orders of magnitude shorter than a collision time. Seidl has predicted theoretically that no substantial electron cyclotron heating in the mirror machine is possible on the single, non-relativistic particle picture unless randomness, such as collisions, is instroduced into the heating mechanism [2]. Trivelpiece, and Piliya and Frenkel suggest that the reflection of the electrons from the mirrors is in itself a randomizing mechanism [3, 4]. Seidl's results, however, are based on certain assumptions that do not hold true in the BMEI because they apply to non-relativistic electrons, many larmor radii away from the axis of a mirror machine in which the three adiabatic invariants are conserved, interacting with an electric field whose amplitude is small enough so that the relative change in the electron energy during one longitudinal oscillation is small. In the BMEI, most of the electrons are within a few larmor radii from the axis of the mirror machine, they are relativistic, and the electric field used for electron cyclotron heating is quite high.

To circumvent some of the assumptions of Seidl, a different approach was used to calculate the effect of rf pulses on a single electron in a mirror machine geometry. As a first step, a calculation has been made of the heating by rf power of a non-relativistic electron in a magnetic field which has a constant value plus a sinusoidally time varying part to simulate the effect of an electron oscillating in a mirror magnetic field. The electron then performs a two-dimensional motion in a

$$B_z = B_0 (1 + a \sin w_1 t) \qquad 0 < a < 1$$

---

[1] R.A. Dandl, et al., Nuclear Fussion, 4, 344, (1964).

[2] M. Seidl, Plasma Physics, 6, 597 (1964).

[3] Consolidated Quarterly Progress Report on Plasma Research, 1 January - 31 March 1965.

[4] A.D. Piliya and V. Frankel, Soviet Phys.-Tech. Phys. 9, 1356, (1965).

and electric field

$$E_x = E_0 \sin w_2 t ,$$

where

$$a = \frac{R-1}{R+1} \qquad R \text{ is the mirror ration.}$$

One can then obtain an analytic solution for the energy of the electron in this case which is rather complicated and will be omitted here. It is found that the electron energy both increases and decreases on a short time basis, but over the time of a complete longitudinal oscillation in the mirror magnetic field the trend is towards increasing energy. Fig. 1 shows two plots of the velocity variation over approximately two longitudinal periods. In one plot the electric field frequency is equal to the cyclotron frequency of the electron at two positions in the mirror and the velocity increases on the average, while in the second the electric field frequency is never in resonance with the electron and there is no energy gain. Fig. 2 is a smoothed out plot for the electron velocity as a function of time for different initial phases with respect to the electric field. The initial velocity and field values have been reduced from that of Fig. 1 in order that the particles energy remain essentially non-relativistic. It should be noted that the relative change of the electron velocity per longitudinal oscillation is quite substantial. These calculations will be further refined to take into account that the mirror points of the electron move towards the center of the machine as the electron energy perpendicular to the magnetic field increases.

Another approach is to determine the cyclotron radiation emissivity from a plasma in a mirror machine in which the electrons have a two-dimensional Maxwellian distribution function at each point in space. By using the principle of detailed balance [5], the absorptivity of the plasma can be determined as a function of frequency. However, the absorption coefficient obtained in this way does not reduce properly at $\omega = \omega_0$ to no absorption which we know to be true from physical considerations. This inconsistency is being investigated further. One can approximately deduce the absorption coefficient at a frequency ω by using the simpler expression of Kirchoff's Law:

where $\frac{\eta(\omega)}{\alpha(\omega)} = BB(\omega) = \frac{\omega^2 k T}{8\pi^3 c^2}$,

BB = blackbody,

$\mu(\omega)$ = emission of plasma at frequency ω, and

$\alpha(\omega)$ = adsorption coefficient of plasma at frequency ω.

Although this relation is strictly valid only for an isotropic plasma, it gives an approximate value of the absorption coefficient for our case. Using the expression of Beard and Baker for the emission from a two-dimensional Maxwellian plasma[6], and applying for the case $\theta = 0$, one gets

---

[5] B.A. Trubnikov and V.B. Yakubov, Plasma Physics (J. Nucl. Energy, Part C) 5, 7, (1963).

[6] D.B. Beard and J.C. Baker, Phys. Fluids, 4, 611, (1961).

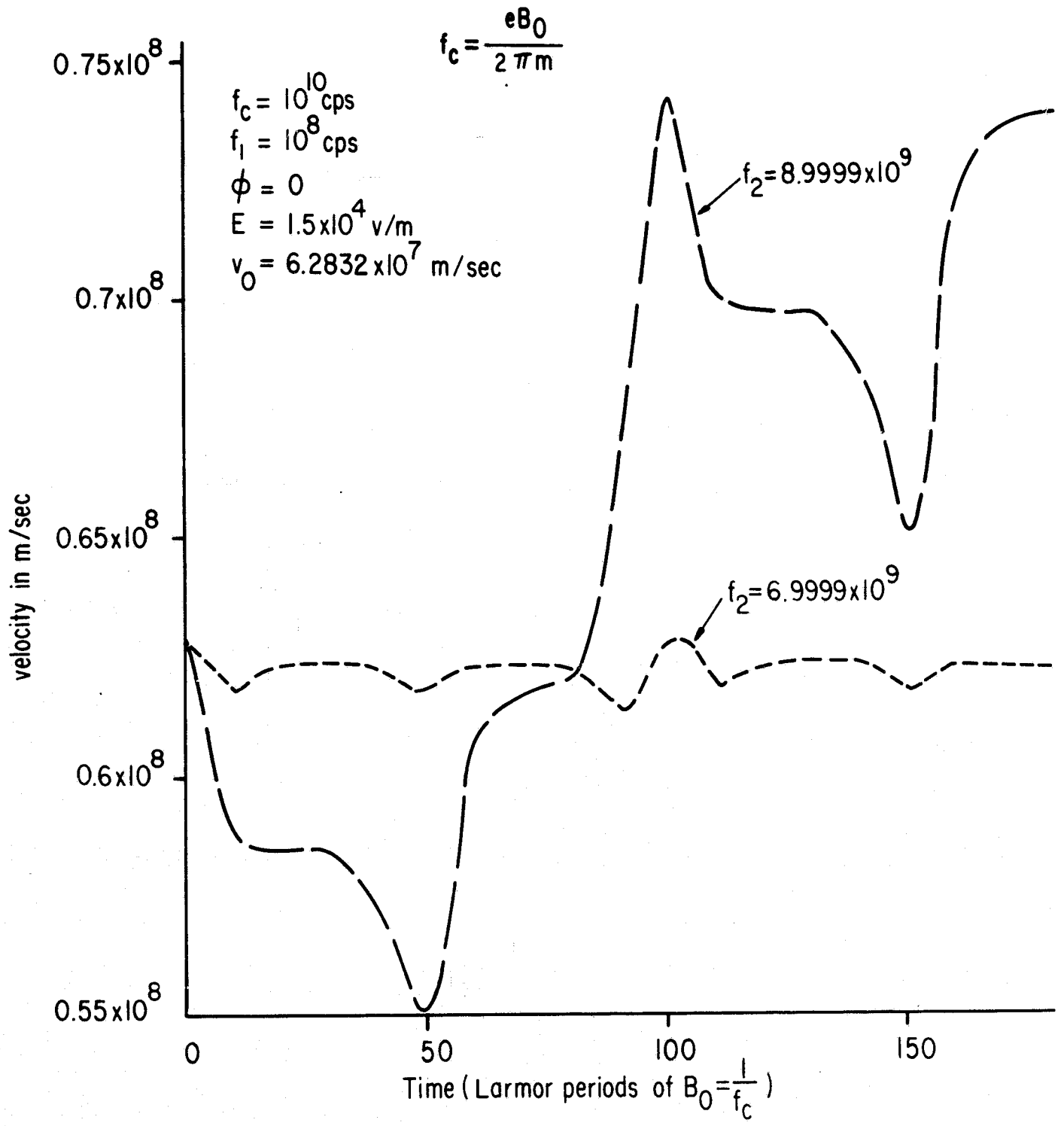

Fig. 1. A plot of the velocity of the electron perpendicular to the magnetic field as a function of time for two electric field frequencies.

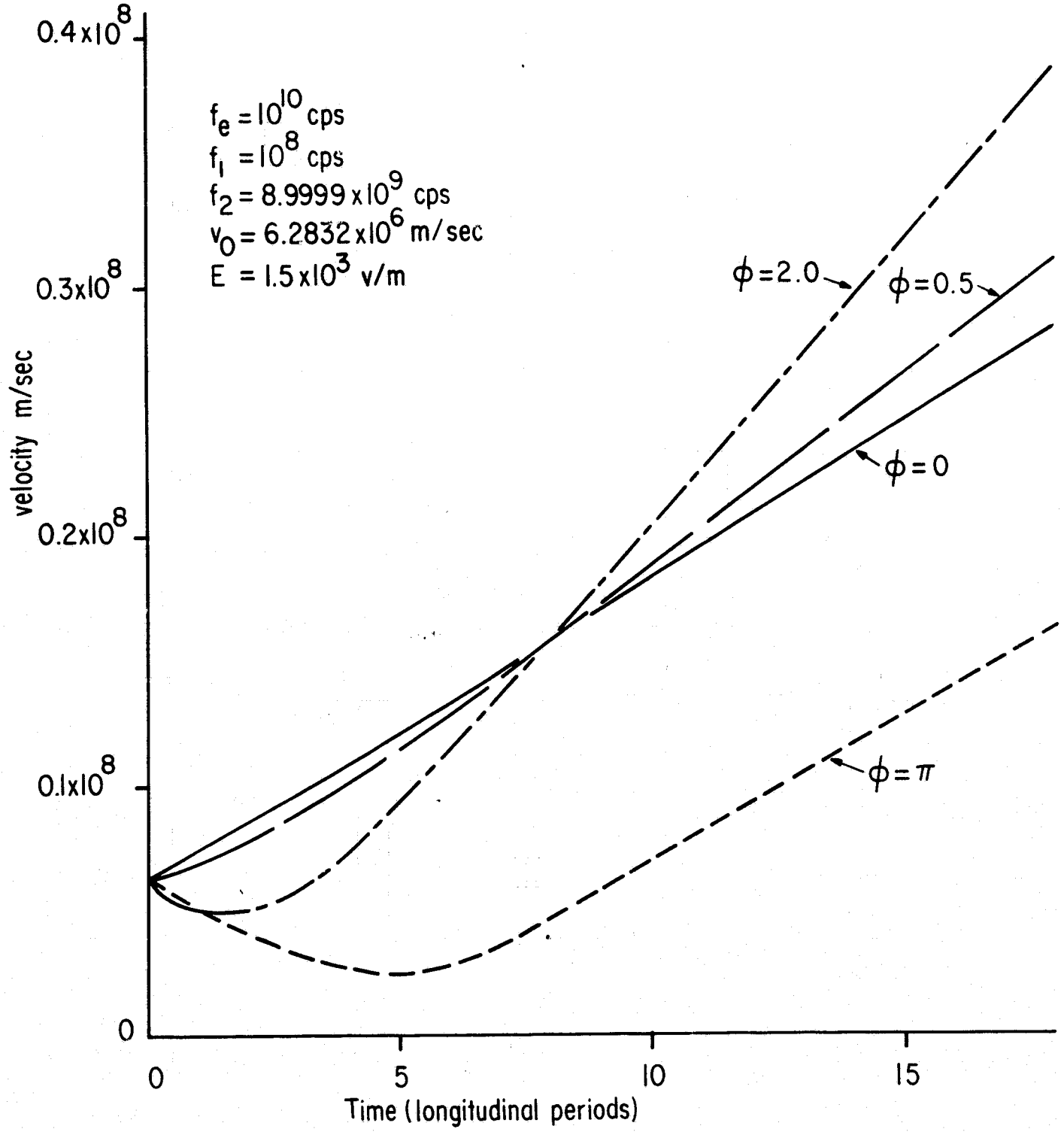

Fig. 2. A plot of the velocity of the electron perpendicular to the magnetic field as a function of time for different initial phases between electric field and electron.

$$\eta_{\theta=0}(w,z) = 2.87 \times 10^{-63} C_p(z) \frac{\omega_0^2(z)}{\omega} e^{-\mu(z)\frac{\omega_0(z)}{\omega}} \left[1 - \left(\frac{\omega}{\omega_0(z)}\right)^2\right],$$

where

$$C_p(z) = \frac{\mu(z)e^{\mu(z)}}{2\pi\left(1+\frac{1}{\mu(z)}\right)(mc)^2}, \quad \mu(z) = \frac{mc^2}{kT}, \quad \omega_0 = \frac{eB}{mc}.$$

The z-dependence arises due to the dependence of the cyclotron frequency and temperature on the poistion along the axis of the mirror machine. This expression is integrated over z taking into account the area of the plasma as a function of z. One obtains for the total radiation from the mirror machine parallel to the magnetic field,

$$\eta_T(\omega,\theta = 0) = A(0)\, NL \int_0^1 \eta_{\theta=0}(\omega, z) \frac{B(0)}{B(z)}\, dz,$$

where A(0) is the area of the plasma at the center of the machine, B(0) is the magnetic field at the center of the machine, N is the density of the plasma which is assumed constant, and L is the distance from the mirror to the midplane. The integration was carried out numerically and the results plotted in Fig. 3. Taking the case of $\omega = 2.5 \times 10^{11}$ rad/sec and kT = 20 keV, the blackbody radiation is BB = 7.2×10^{-9} ergs/$_{cm^2\text{-sec}}$ while for 10^{11} electrons in BMEI the radiation is 1.6×10^{-9} ergs/$_{sec}$ parallel to the magnetic field, from the approximately 1-cm^2 surface area parallel to the magnetic field. The plasma absorption coefficient at $\omega = 2.5 \times 10^{11}$ rad/sec, obtained from Kirchoff's Law, is therefore

$$\alpha \approx \frac{1.6}{7.2} \approx 0.22 .$$

One expects substantial absorption of the rf power by the plasma with the above calculated absorption coefficient, provided the dielectric constant of the plasma at this frequency is very near unity, so that the rf field penetrates it.

A numerical calculation is now in progress to solve the exact equations of motion of a relativistic electron in a mirror machine with an incident plane electromagnetic wave. Such a calculation should more conclusively determine whether a single electron can be heated in a mirror machine. The single electron picture for the interaction of the rf power with the plasma electrons is valid if the rf frequency is much higher than the plasma frequency, for then the index of refraction of the plasma is unity and the rf fields would therefore penetrate into the interior.

An 8-mm magnetron delivering 150-kW, 2-μsec pulses will be used next to heat the plasma electrons. It is hoped that because of its higher frequency and larger energy output than that of the 3-cm magnetron, electron cyclotron heating will be effective.

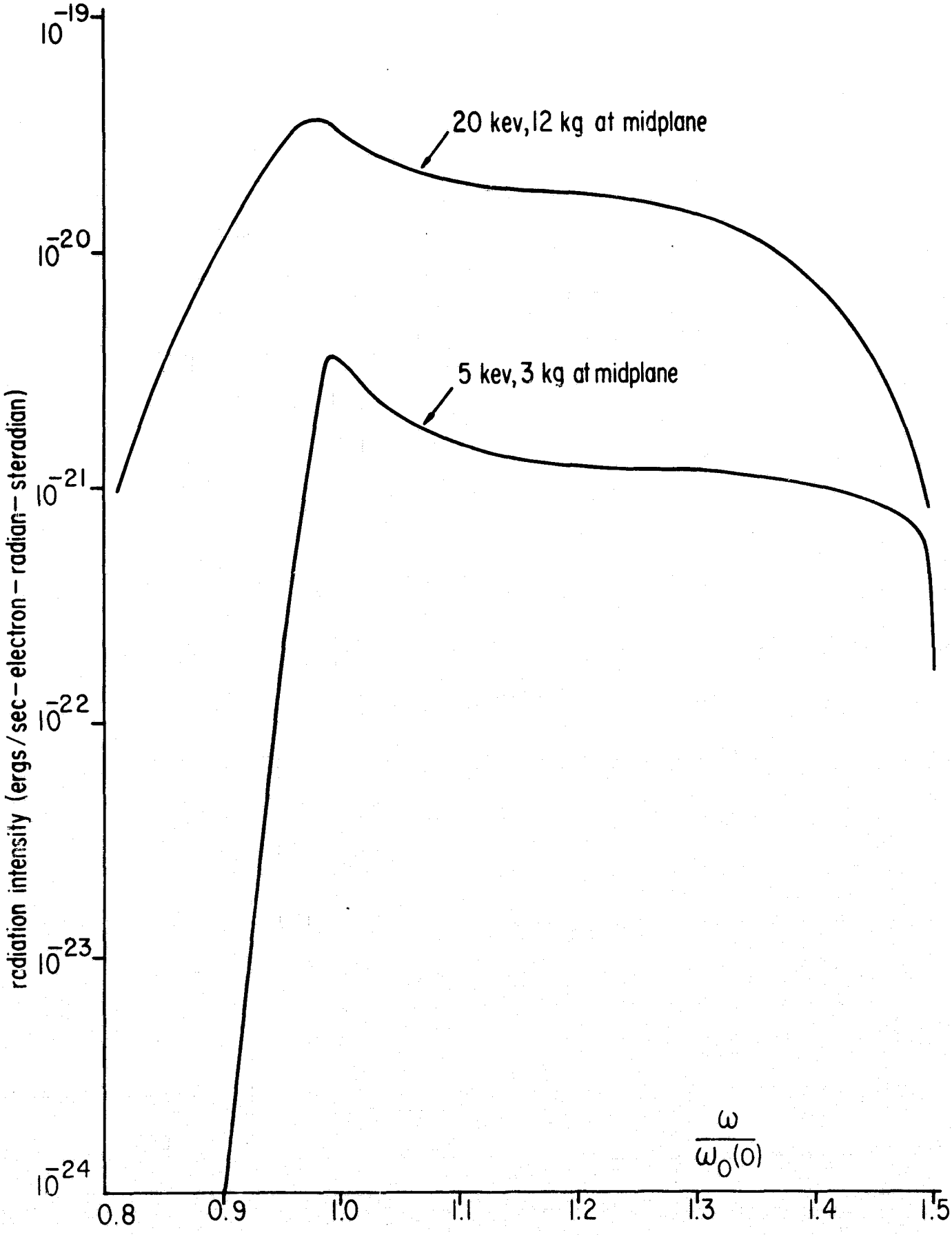

Fig. 3. A plot of the radiation intensity parallel to the magnetic field as a function of frequency that is normalized to the cyclotron frequency at the midplane of the mirror machine. The mirror ratio is 1.5.

ELECTRON VELOCITY ANALYZER

AFAL Contract AF33(615)-1078
J. Colvin (Prof. Trivelpiece)

The analyzer will be used to measure the velocity distribution of the end loss of the magnetic mirror machine. It uses crossed E and B fields to allow electrons with a narrow spread of velocities around $v_0 = E/B$ to pass undeflected to a Lucite scintillation crystal. The light output of the crystal is coupled to a 7244 photomultiplier tube, and the resulting pulse is observed on an oscilloscope and can be photographed.

Electrons from 20 to 100 keV (0.8 to 1.6 x 10^8 m/sec) will be measured by varying the electric field. It was decided that the electrode voltage should be limited to 3000 VDC, so the maximum electric field obtainable if 3 x 10^6 V/m with 1 mm electrode spacing. For 100 keV electrons the magnetic induction required is then 180 gauss. An electromagnet was built with a mild steel core and 2000 turns to give 180 gauss at 200 ma coil current. The velocity spread in the detected beam with these field strengths was calculated as $\pm$ 5% at 20 keV, increasing to $\pm$ 10% at 100 keV.

The scintillation crystal and photomultiplier tube were calibrated using the 0.663 MeV gamma rays from Cs^{137}. With 2000 V on the dynodes, the average output pulse height for four measurements was 0.26 $\pm$ 0.05 mV/keV lost in the crystal. This is unaffected by the electromagnet's field. The analyzer was checked for leaks, and the leaks were sealed. It is now ready to take measurements.

PLASMA INSTABILITY EXPERIMENTS

JSEP Grants AF-AFOSR-139-64865
T.Y. Chang, J. Mataya (Prof. C.K. Birdsall)

The general idea for these experiments was outlined in ERL Technical Memorandum M-72. Parts of the experiment have been described in detail in previous progress reports. The PIE facility is nearly ready for assembly of all of the parts purchased or fabricated separately: vacuum pumps and gauges, main chamber, oven and collimator, hot plate, plasma camera, pulse coil and pulser, d-c coils, heat exchanger, interlock system, d-c coil and hot plate supply and the usual electronic instrumentation.

The pulse coil with shielding rings was designed using the MAFCO computer code, assuming d-c behavior similar to pulsed. The coil and rings have been made and inductance has been checked very close to the calculated value.

The coil pulser-crowbar supply is 70% assembled. Completion was delayed because of late delivery of relays. However, preliminary firings with coil and rings have been made, showing roughly 1.5 msec L/R decay time, which is more than adequate for the experiment.

The d-c coils, 9 in. ID, 6 in. long modules, have been on hand for some time.

The heat exchanger (50kW) is 95% complete and has been partially tested. Input and output manifolds for as many as four coils are complete.

Several interlock systems have been designed and parts are ordered.

For the vacuum system, the fore and diffusion pumps, pneumatic valve and cold trap are on hand. The manifold has been made and leak checked and is satisfactory. The main chamber is 60% complete.

The stand to support the coils, chamber, and pumps has been completed for some time.

The d-c coil and hot plate supplies are piped into the room from generators in the basement.

A hot plate was tested sometime ago. The surface temperature reached 2000°K as expected. But, the operation was unsatisfactory in that the temperature could not be maintained as the filament current was reduced. A new hot plate has been designed and the fabrication is about 40% complete.

STABILITY OF PLASMAS IN MIRROR-TYPE CONFIGURATIONS

JSEP Grants AF-AFOSR-139-64865

T.Y. Chang (Prof. C.K. Birdsall)

The energy principle for the stability of a plasma in static equilibrium was extended to include rotating equilibria in two-dimensional problems by demanding the total energy of an isolated system to be a local minimum with respect to all possible perturbations.* The principle is a direct result of Liapunov's general theory on stability problems. By expressing the total energy completely in terms of constants of motion, namely, the potential on conducting boundaries, the total cannonical angular momentum, the total number of electrons and ions, and moments of N_i with respect to $\frac{N_i}{B}$, we were able to obtain expressions giving the possible plasma equilibria which satisfy the above energy principle for stability. It was found that the angular velocity of all such equilibria is either very small or nearly uniform over the entire plasma cross section. Since the above energy principle is a sufficient but not necessary condition for stability, it is not conclusive whether all rotating equilibria must necessarily have a nearly uniform angular velocity to be stable. It appears that the last problem can only be answered by a normal mode analysis, which has now been carried out.

---

*Reported in ERL Consolidated Quarterly Progress Report and Plasma Research, 1 January - 31 March 1965, Report No. 112, Contract No. AF-33(615)-1078; pp. 18-20.

For the normal-mode analysis, we began by considering mirror-machine plasmas. A simplified, three-dimensional model was first developed. It consists of a uniform magnet field in z direction and a conservative potential for each species:

$$\Psi_j(r, z) = \Psi_{jr}(r) + \Psi_{jz}(z) \ .$$

Where Ψ_{jr} simulates the diamagnetic and curvature forces, while Ψ_{jz} represents the mirror forces. Their functional forms and values are such that both the longitudinal and azimuthal drift periods in the model correspond to those in the actual system. Next, a set of fundamental equations for a guiding center gas in such a system was derived. The equation of motion was obtained from a collisionless kinetic equation in an eight-dimensional phase space whose seventh and eighth dimensions are the gyroradius and the rate of change of gyroradius. Differential equations relating the guiding center densities to the particle densities and the effective potential seen by the guiding center gas to the actual potential were derived. These equations are correct to all orders in $\rho\nabla$, where ρ denotes the gyroradius. Our fundamental equations are, therefore, valid for all modes with $\omega << \omega_{ci}$ and with any wavelength.

A general equilibrium solution to the fundamental equations was obtained. The electric potential and the electron densities have the following forms:

$$\phi_0(r, z) = A_r \, r^2 + A_z \, \Psi_z(z) \ ,$$

$$N_{e0}(r, z) = R(r) \exp\left[\left(\frac{eA_z}{kT_{e0}} - \frac{1}{B_0} \right) \Psi_z(z) \right] ,$$

where A_r, A_z are arbitrary constants, and $R(r)$ is an arbitrary function of r. The general solution contains neutral, isothermal, and isobaric solutions in particular. It also contains a well-confined solution in which $T_{i\,\|}(z)$ vanishes only at the mirror points.

The first equilibrium state considered for normal mode analysis was a high density one ($\omega_{pi} >> \omega_{ci}$) for which the Poisson's equation was replaced by quazi-neutrality condition and in which

$$R(r) \approx \left[1 - \left(\frac{r}{r_p} \right)^{\ell} \right]^{1/2} \qquad 0 \leq r \leq r_p$$

$$= 0 \qquad r_p < r \ .$$

Only flute modes are considered. All first-order quantities except densities are independent of z. All density perturbations depend on z

in the same way as the equilibrium densities do. A complete set of eigenfunctions was obtained. In terms of the electric potential they are

$$\phi_{mn} = A_{mn}\, n!\; r^m\, P_n^{(\frac{2m}{\ell},\, \frac{1}{2})}[1 - 2\,(\frac{r}{r_p})^{\ell}]\; \exp[\, im\varphi - i\omega_{mn} t\,]$$

$$0 \le r \le r_p$$

$$= A_{mn}\, \frac{\Gamma(\frac{1}{2})}{\Gamma(\frac{1}{2} - n)}\quad \frac{r_p^{2m}\; r_w^{2m}}{r_w^{2m} - r_p^{2m}}\,[\,\frac{1}{r^m} - \frac{r^m}{r_w^{2m}}\,]\; \exp(\,im\varphi - i\omega_{mn} t\,),$$

$$r_p \le r \le r_w$$

where $P_n^{(\alpha,\beta)}(x)$ is a Jacobi-polynomial, and r_w is the radius of the conducting boundary. The corresponding characteristic frequencies are given by

$$\omega_{mn} = (m + \frac{1}{\lambda_{mn}})\; W_{i0} + \frac{1}{2}\, m\,(1 - \frac{1}{\lambda_{mn}^2})(W_{e0} - W_{i0})$$

$$\pm \left\{[\,\frac{1}{\lambda_{mn}}\, W_{i0} + \frac{1}{2} m (1 - \frac{1}{\lambda_{mn}^2})(W_{e0} - W_{i0})\,]^2 + \frac{1}{\lambda_{mn}}\, m\omega_{ci}(W_{e0} - W_{i0})\right\}^{1/2}$$

where W_{e0} and W_{i0} denote the electron and ion angular drift velocities in equilibrium. The eigenvalues λ_{mn} are given by

$$-\lambda_{mn} = 1 + \frac{2n\ell}{m}\,(n + \frac{1}{2} + \frac{2m}{\ell}).$$

It is seen that $n = 0$ modes are the most unstable modes. These modes which are excited solely by surface charges at the plasma-vacuum interface are characteristic of all equilibrium states with a sharp plasma boundary.

The above eigenmodes obtained from linearized analysis in Eurelian coordinates represent rippling of the plasma in azimuthal direction. The first-order nonlinear effects which give the actual flute growth has also been calculated.

The case of a plasma without a sharp boundary, including the effect of finite gyroradius, to the lowest order, and the case of a low density plasma ($\omega_{pi} << \omega_{ci}$) are being studied using a Gaussian-type density distribution. The eigenfunctions are in the form of confluent hypergeometric functions and the eigenvalues are related to the zeros of these functions.

The limiting case of very short wavelength ($\rho \nabla \to \infty$) was also considered. The related modes are pure electron oscillations transverse to the magnetic field. The eigenfunctions are in the form of Bessel functions. The phase velocity is directly related to the electron diamagnetic drift velocity. These drift modes are known to become unstable when the conductivity is finite and $k_{\parallel} \neq 0$. These instabilities will be considered further.

COMPUTER MODEL FOR NONLINEAR INVESTIGATION OF PLASMA INTERCHANGE INSTABILITY

AFAL Contract AF33(615)-1078
J. Byers (Prof. C. K. Birdsall)

The main problem encountered in this effort is numerical instability of finite difference equations which are analogs of the equation $\frac{\partial u}{\partial t} = F(u,t)$. Part of the concept of stability can be understood as a simple cumulative addition of a single time-step truncation error. Truncation error is defined by a Taylor series expansion of the finite difference analog of $\frac{\partial u}{\partial t}$. To some degree, all finite difference schemes are subject to cumulative error ("instability") of this type. However, the manner of cumulative addition can make this effect acceptable in one scheme and unacceptable in another even though both schemes are of the same order of accuracy. For example, the leapfrog scheme, $\frac{u^1 - u^{-1}}{2\Delta t} = F^\circ$, which has a truncation error $\sim \frac{\Delta t^3}{3} \frac{\partial^3 u}{\partial t^3}$, will reproduce the amplitude of an oscillating solution exactly with the cumulative error appearing entirely in an acceleration of phase; whereas, an Adams-Bashforth scheme, $\frac{u^1 - u^0}{\Delta t} = \frac{3}{2} F^0 - \frac{1}{2} F^{-1}$, which has a truncation error $\sim \frac{5}{6} \Delta t^3 \frac{\partial^3 u}{\partial t^3}$, results in a phase error approximately twice that of the leapfrog scheme but also causes a slow growth in the amplitude of the oscillation, which for long time observation can be unacceptable. Also, a leapfrog-correction scheme, an iterative procedure with truncation error $-\frac{\Delta t^3}{12} \frac{\partial^3 u}{\partial t^3}$, results in almost negligible phase errors but causes a slow damping of the amplitude which again can be unacceptable. While this type of cumulative error can be effectively reduced by reducing the time step, this is not a totally acceptable solution. A scheme which produces only moderate errors in phase and no errors in amplitude would be desirable. As previously noted, the leapfrog scheme satisfies this requirement but is unfortunately subject to computational instability of a more dangerous type. To obtain a composite scheme which has the desirable qualities of the leapfrog scheme and is not subject to the second

type of computational instability, we are testing methods which alternate two or more different schemes. The process can be loosely described as a partial cancellation of the truncation error of one scheme with an error of opposite sign due to the "second half" of the composite scheme. The actual process is more subtle, however, as the net effect cannot be judged simply by examining the separate parts alone. For example, since the leapfrog scheme causes no amplification, one might expect that an alternation of these two schemes would cause a slow growth of the amplitude -- in fact, a slow damping occurs. The reason for this is easily understood if a careful analysis is made, but this obviously makes the synthesis of a good composite scheme much more difficult than the simple procedure of alternating two schemes which have errors of opposite sign.

The second type of computational instability is confined to a class of finite difference operators of higher order than the corresponding continuous operator. For example, all finite difference operators which use more than two levels in approximating the first order continuous operator $\frac{\partial u}{\partial t}$ are of higher order and consequently introduce extraneous "computational modes." Some of these schemes -- for example the leapfrog -- can cause the computational mode to grow and thus swamp the physical mode. The leapfrog analog of the equation $\frac{\partial u}{\partial t} = -\omega u$ does yield a physical mode which damps exponentially at a rate closely approaching that of the analytic solution, but it also produces an exponentially growing computational mode which of course soon renders the numerical solution useless. Lilly gives other examples where the leapfrog is unstable [1]. Our equations are subject to a strong computational instability of this type when the leapfrog scheme is used. Fortunately, many schemes -- e.g., The Adams-Bashforth and several iterative methods -- strongly damp the computational mode. Damping of the computational mode then is another requirement on any composite scheme we devise.

1. Composite finite difference schemes

Three basic finite difference schemes were used in devising composite schemes: Leapfrog (Lf), Adams-Bashforth (AB), both described above, and the Heun (H), an iterative procedure defined as $u^* - u^0 = \Delta t\, F^0$ and $u^1 - u^0 = \frac{\Delta t}{2}(F^0 + F^*)$. In addition, Lfc and ABc will indicate iterative proceudres with a tentative value u^* obtained by either Lf or AB as defined above and then corrected by averaging the slopes just as in the 2nd half of H.

Several composite schemes were tested with respect to the

---

[1] D.K. Lilly, "On the Computational Stability of Numerical Solutions of Time Dependent Non-Linear Geophysical Fluid Dynamics Problems," Monthly Weather Review, 93, January 1965, p.11.

equation $\frac{\partial u}{\partial t} = i\omega u$. Both Lf and Lfc as well as several other inferior schemes were tested with respect to this equation by Kurihara [2]. He suggested that the damping produced by Lfc might be reduced by using it only intermittently with Lf. We show here that this will not necessarily yield less damping and that the synthesis of a good composite scheme requires greater care.

To obtain the solution of a finite difference equation we ask for the amplification factor or matrix as defined in Richtmyer [3]. The solution of $u(n\Delta t)$ is represented as $U^n = \lambda^n U^0$, where λ is the amplification factor of the finite difference procedure. Thus for Lf where we have $U^1 - U^{-1} = 2ibU^0 (b = \omega \Delta t)$ the characteristic equation is $\lambda - \frac{1}{\lambda} = 2ib$

or $\lambda = ib \pm \sqrt{-b^2 + 1}$

and $\lambda +$ corresponds to the physical mode and $\lambda -$ corresponds to an extraneous computational mode. Note that $|\lambda \pm|^2 = 1$ if $b^2 \leq 1$. The extraneous computational mode will be discussed in III. When dealing with composite schemes it is more convenient to use a matrix formulation described by Richtmyer [3]. Now, the amplification factor of the composite scheme cannot be simply the product of the individual eigenvalues, but the amplification matrix for the composite scheme is simply the product of the individual matrices, and the evaluation of the composite eigenvalue then proceeds as usual. .

Table I is a summary of the properties of several composite schemes obtained by various alternations of the single schemes. The amplification $\frac{U^n}{U^0}$ of the finite difference operator is expressed in the form Re, and we desire a solution as close as possible to the analytic amplification $\frac{U(n\Delta t)}{U(0)} = e^{inb}$. As noted in the introduction and as shown in Table I, Lf is the closest approximation to this ideal, but it must be rejected on grounds to be discussed in 2.. Comparison of the various schemes for a single operation is not feasible so we arbitrarily chose $\omega T = 50$ for a convenient comparison point at which $|R|^2$ is given for several values of $B = \omega \Delta t$. Phase errors are not shown as they appear to be tolerable and of comparable order of magnitude for all of the schemes of Table I. As can be seen, the last four schemes listed, Numbers 22 - 25, are the best and any of them are adequate for values of $\omega \Delta t$ as large as 0.3 radians if ωT is not too large. Better composite schemes can probably be devised if it becomes necessary to observe an oscillatory solution for a very large number of cycles. Using a scheme

[2] Y. Kurihara, "On the Use of Implicit and Iterative Methods for the Time Integration of the Wave Equation," Monthly Weather Review, 93, January 1965, p. 33.

[3] R.D. Richtmyer, Difference Methods for Initial Value Problems, Interscience, New York, 1957.

Table I

A list of various composite schemes compared with respect to the solution of the equation $\frac{\partial u}{\partial t} = i\omega u$. Any individual scheme yields an amplification $\frac{U^n}{U^o} = Re^{i\theta}$, whereas the analytic solution amplification is $\frac{U(n\Delta t)}{U^o} = 1.0xe^{in\omega\Delta t}$. $|R|^2$ at $\omega T = 50$ ($\approx$ 8 cycles) is given for several values of $\omega\Delta t$.

Description of scheme		Number of single schemes used	$\|R\|^2$ at $\omega T = 50$ for $\omega\Delta t =$		
			0.1	0.2	0.3
1	Lf	1	1.000	1.000	1.000
2	AB	1	1.025	1.24	2.25
3	H	1	1.012	1.12	1.45
4	Lfc	1	0.975	0.83	0.57
5	ABc	1	0.975	0.82	0.54
6	Lf-AB	2	0.977	0.85	0.65
7	Lf-Lfc	2	1.026	1.24	2.11
8	AB-ABc	2	1.012	1.09	1.30
9	Lf-ABc	2	1.025	1.20	1.73
10	AF-H	2	1.025	1.23	2.03
11	Lf-Lf-AB	3	1.025	1.21	1.68
12	Lf-Lf-Lf-AB	4	0.979	0.90	0.86
13	Lf-Lf-Lf-Lf-AB	5	1.023	1.12	1.02
14	Lf-Lf-Lf-Lf-Lf-AB	6	0.982	0.95	1.12
15	Lf-AB-AB-AB	4	1.006	1.05	1.20
16	Lf-Lf-AB-AB-AB	5	1.025	1.22	1.97
17	Lf-AB-AB-AB-AB	5	1.010	1.09	1.36
18	Lf-Lf-AB-AB-AB-AB	6	1.025	1.23	1.50
19	Lf-Lf-AB-AB	4	1.025	1.22	1.91
20	Lf-AB-Lf-AB-AB	5	0.990	0.93	0.82
21	Lf-AB-AB-H-Lf	5	1.025	1.20	1.73
22	Lf-H	2	1.0002	1.008	1.063
23	Lf-AB-AB	3	0.9996	0.990	0.946
24	Lf-AB-AB-Lf-H	5	0.997	0.984	0.978
25	AB-Lf-AB-Lf-H	5	1.00004	1.002	1.021

which slightly amplifies such as No. 25, say for the first ten cycles and then a scheme which slightly damps such as No. 24 for the next ten cycles etc., may also be feasible.

We have tried several of the schemes of Table I(1, 2, 4, 5, 6, 13, 23, 24) in our program when the linear analysis predicts a simple oscillating solution. No. 1 and 13 were unstable as will be discussed in 2. The other schemes were stable and in all these cases the predictions of Table I were well confirmed. (Actually, we tried most of these schemes before attempting the analysis -- the relatively large damping and amplification led us to the analysis).

2. Instability due to computational mode

A short description of part of the detail of our model is necessary at this point. We are employing a 2-fluid model consisting of a fluid of ion-quiding centers and a fluid of electron-guiding centers moving in two-dimensional motion perpendicular to a strong uniform magnetic field $B = B_0 a_z$. Both fluids move with a $v_E = E \times B/B^2$ drift velocity where $E = -\nabla\phi$ and $\nabla^2\phi = -\frac{(n_i - n_e)e}{\epsilon_0}$.

The difference in ion and electron densities is caused by small additional drifts which are the gravitational drift $v_g = \frac{M}{e}\frac{g \times B}{B^2}$ and the polarization drift $v_p = \frac{M}{eB^2}\frac{dE}{dt}$. We ignore both of these drifts for the electrons due to the large mass difference. The main source of difficulty is the $\frac{\partial}{\partial t}$ part of $\frac{d}{dt}$ in v_p so we will assume $\frac{dE}{dt} = \frac{\partial}{\partial t}E$ and will also ignore the v_g in the present discussion. $|v_E|$ is $>>$ $|v_p|$ and we can say $n_i \approx n_e = n$ so that our two-fluid model implicitly solves the following equation for the time rate of change of charge density, $\rho = e(n_i - n_e)$:

$$\frac{\partial \rho}{\partial t} = -\nabla \cdot \left(\frac{nM}{B^2}\frac{\partial E}{\partial t}\right)$$

or

$$\frac{\partial}{\partial t}\nabla^2\phi = -\frac{nm}{\epsilon_0 B^2}\frac{\partial}{\partial t}\nabla^2\phi - \frac{m}{\epsilon_0 B^2}\frac{\partial}{\partial t}(\nabla\phi)\cdot\nabla n \qquad (1)$$

Remember that in our two-fluid model we do not explicitly solve this equation so that we cannot combine the first term on the r.h.s. with the l.h.s.

Restricting the spatial coordinates to one dimension for simplicity we replace $\nabla\phi$ by $\frac{\phi_{j+1} - \phi_{j-1}}{2\Delta x}$ and $\nabla^2\phi$ by $\frac{\phi_{j+1} - 2\phi_j + \phi_{j-1}}{\Delta x^2}$.

If ϕ is represented by a finite Fourier series $\phi = \sum_k \phi_k e^{ikj\,\Delta x}$, equation (1) becomes

$$\frac{\partial}{\partial t}\,\phi_k = -\frac{nm}{\epsilon_0 B^2}\,\frac{\partial}{\partial t}\,\phi_k + \frac{\nabla nm}{\epsilon_0 B^2}\,\frac{n\Delta x}{n}\,\frac{i}{4}\,\frac{\sin(k\Delta x)}{\sin^2\frac{(k\Delta x)}{2}}\,\frac{\partial}{\partial t}\,\phi_k$$

$$\frac{\partial}{\partial t}\,\phi_k = -A\,\frac{\partial}{\partial t}\,\phi_k + iB\,\frac{\partial}{\partial t}\,\phi_k \qquad (2)$$

On the r.h. s. we can use only present and past information so that in the Lf scheme this takes the form

$$\phi_k^1 - \phi_k^{-1} = -2A\,(\phi_k^0 - \phi_k^{-1}) + 2iB\,(\phi_k^0 - \phi_k^{-1})$$

which yields

$$|\lambda -|^2 = 1 + 4A + 4A^2 + 4B^2$$

Since $A = \frac{nm}{\epsilon_0 B^2}$ is always > 0, $|\lambda -|$ is always > 1 and hence the computational mode becomes unconditionally unstable in the Lf scheme. A similar analysis shows that any scheme of Table 1 not dominated by Lf is stable for A of the order $\lesssim 1$. An Lf dominated scheme such as number 14 is unstable unless A becomes extremely small.

Thus, with certain restrictions on A a composite scheme which is stable with respect to the polarization term can be devised. This is not an entirely satisfactory situation however, as we would like to be able to have A range over values from $<<1$ to $>>1$. We can remove this restriction if we go to a 1 fluid model where we follow 1 fluid of density $n = n_i = n_e$ with v_E drifts only and calculate the charge separation using v_g and v_p. (This requires $v_E >> v_g$, which is usually the case when $A \gtrsim 1$). Equation 1 (corrected of course for the terms left out in the previous discussion) in this model is solved explicity so we can combine terms changing equation 2 to

$$\frac{\partial}{\partial t}\,\phi_k = \frac{iB}{\left(1+\frac{nm}{\epsilon_0 B^2}\right)}\,\frac{\partial}{\partial t}\,\phi_k = iB'\,\frac{\partial}{\partial t}\,\phi_k \qquad (3)$$

The stability condition for the AB scheme is now that B' be of the order $\lesssim \frac{1}{2}$ and is satisfied whatever the value of $\frac{nm}{\epsilon_0 B^2}$. This behavior is typical of most of the schemes of Table I. Lf is still unstable of course (although not as strongly), but the Lf dominated composite schemes may not be. For example, number 14 is marginally stable when $B' \approx .25$.

The computational mode behavior of those schemes of Table I which we have tried (1, 2, 4, 5, 6, 13, 23, 24) agrees very well with the foregoing analysis. There is evidence that the long range nature of the electrostatic field allows the stability condition to be violated in part of the region if it is satisfied sufficiently strongly elsewhere. Thus in scheme number 6 the stability analysis yields $\frac{nm}{\epsilon_0 B^2} = \frac{1}{3}$ as the condition of marginal stability, but the numerical solution with $\frac{n_{max} m}{\epsilon_0 B^2} = 0.5$ was perfectly stable (n varies from 0 up to n_{max}). In many systems this behavior does not occur, i.e., stability conditions must be satisfied everywhere [3].

3. Summary

We have succeeded in devising several composite schemes which reproduce oscillating solutions very well even for relatively large values of $\omega \Delta t$ and which are stable with respect to computational modes. The stability conditions require certain restrictions and changes in the model but the restrictions and changes appear to impose no essential limitation on our original concept.

More details on the above analysis are reported in ERL Consolidated Quarterly Progress Report on Plasma Research, 1 April - 30 June 1965, Contract No. AF-33(615)-1078.

DAMPING AND INSTABILITIES OF CYCLOTRON WAVES IN A PLASMA

AFAL Contract AF33(615)-1078
J.E. Scharer (Prof. A.W. Trivelpiece)

The purpose of this work is to study the damping and instabilities of transverse electromagnetic waves in a plasma resulting from anisotropy in velocity space of the plasma particles and to discuss their role in experimental applications.

The stability of ion cyclotron waves in an ion-electron plasma with anisotropic Maxwellian distribution functions has been studied during this report period. The dispersion relation for these left-hand circularly polarized waves is

$$\omega^2 = k^2 c^2 - \sum_{j=i,e} \omega_{pj}^2 \left[\frac{\omega}{k\alpha_{zj}} Z(\phi_j) + (\theta_j - 1)(1 + \phi_j Z(\phi_j)) \right],$$

where the sum is over the ions and electrons, and where

ω_{cj} = cyclotron frequency and carries the sign of the charge of the particle,

ω_{pj} = plasma frequency,

$\alpha_{\perp j}$ = thermal velocity of the particles perpendicular to the magnetic field,

α_{zj} = thermal velocity of the particles along the magnetic field,

$$\theta_j = \left(\frac{\alpha_{\perp j}}{\alpha_{zj}}\right)^2 ,$$

$$Z(\phi_j) = \frac{1}{\pi^{1/2}} \Longrightarrow \int_{-\infty}^{\infty} \frac{e^{-t^2}}{(t - \phi_j)}\, dt \quad \text{(plasma dispersion integral)}$$

$$\phi_j = \frac{\omega - \omega_{cj}}{k\alpha_{zj}} .$$

The general solution yields a complex frequency for a real value of the wave number. A positive imaginary part of the frequency corresponds to an instability and growth of the wave with time, and a negative imaginary part of the frequency corresponds to stability and damping of the wave with time. The general solution of the dispersion relation requires machine computation and is very lengthy for all ranges of the parameters. To simplify the dispersion relation, we consider cases in which the electron argument, ϕ_e, is much larger than unity.

The asymptotic form for the plasma dispersion function can be used and the dispersion relation is

$$\omega^2 = k^2c^2 - \omega_{pi}^2\left[\frac{\omega}{k\alpha_{zi}} Z(\phi_i) + (\theta_i - 1)(1 + \phi_i Z(\phi))\right] + \omega_{pe}^2\left[\frac{\omega}{\omega - \omega_{ce}} - \frac{(\theta_e - 1)}{2}\left(\frac{k\alpha_{ze}}{\omega - \omega_{ce}}\right)^2\right].$$

A technique for determining whether the wave grows or damps with time results in a much simpler relation. The threshold of instability is defined as the point where the imaginary part of the frequency changes from a negative to a positive value as the wave number is continuously varied. At this point, the frequency is purely real. Utilizing this condition, the solution of the imaginary part of the dispersion relation is

$$\omega_r = \frac{(\theta_i - 1)}{\theta_i}\, \omega_{ci} .$$

All waves with the real part of the frequency above this value are damped, and all waves with the real part of the frequency below this value grow.

Assuming equal densities of ions and electrons and taking advantage of the fact that $\omega_{ci} << \omega_{ce}$, we substitute the above relation

into the real part of the dispersion relation and obtain the threshold equation in terms of the parameters.

$$U_{pi}^2\left(1 - \frac{1}{\theta_i - 1} + \frac{1}{2}\left(\frac{\theta_e - 1}{\theta_i - 1}\right)\frac{M}{m}\left(\frac{k\alpha_{ze}}{\omega_{ce}}\right)^2\right) = \frac{\beta_i^{-2}}{\theta_i - 1} - (\theta_i - 1)\left(\frac{U_{ci}}{\theta_i}\right)^2 ,$$

where

$$U_{pi} = \frac{\omega_{pi}}{k\alpha_{zi}} ,$$

$$\beta_i = \frac{\alpha_{zi}}{c}$$

and

$$U_{ci} = \frac{\omega_{ci}}{k\alpha_{zi}} .$$

If the electrons can be considered as an isotropic neutralizing background in the neighborhood of the ion cyclotron frequency, the last two terms on the left-hand side of the threshold equation are negligible. The dashed lines in Fig. 1 represent the threshold of instability as the ion thermal anisotropy is varied. The wave-plasma conditions represented by the points inside the curves are stable; those points outside the curve are unstable. As the thermal anisotropy is increased, the stable region of the plane decreases. If we consider a case in which the wavelength is fixed and only the density and magnetic field are varied, we see that the wave becomes unstable as the density and magnetic field increased above the critical values given by the threshold curve for a given anisotropy. Alternatively, if we consider all parameters fixed, except for the wavelength, we see that there is a critical wavelength above which the wave is unstable due to the temperature anisotropy.

If a cold or isotropic thermal electron distribution is included in the analysis, it has a stabilizing effect on the waves, as shown by the solid curves in Fig. 1. For a given ion thermal anisotropy, the waves are stable up to higher plasma densities than without the influence of the electrons. Alternatively, for a fixed density and magnetic field, the critical wavelength, above which the wave is unstable, is increased.

The effect of electron anisotropy on the ion cyclotron wave is shown in Fig. 2. The dotted curve shows the threshold of instability for ions with an immobile neutralizing background of electrons. For $\theta_e > 1$, the waves are unstable for sufficiently small values of the magnetic field. Thus the electron thermal anisotropy has a very profound destabilizing effect on the ion cyclotron wave. For $\theta_e < 1$, the wave is stable for all densities for sufficiently small values of the magnetic field.

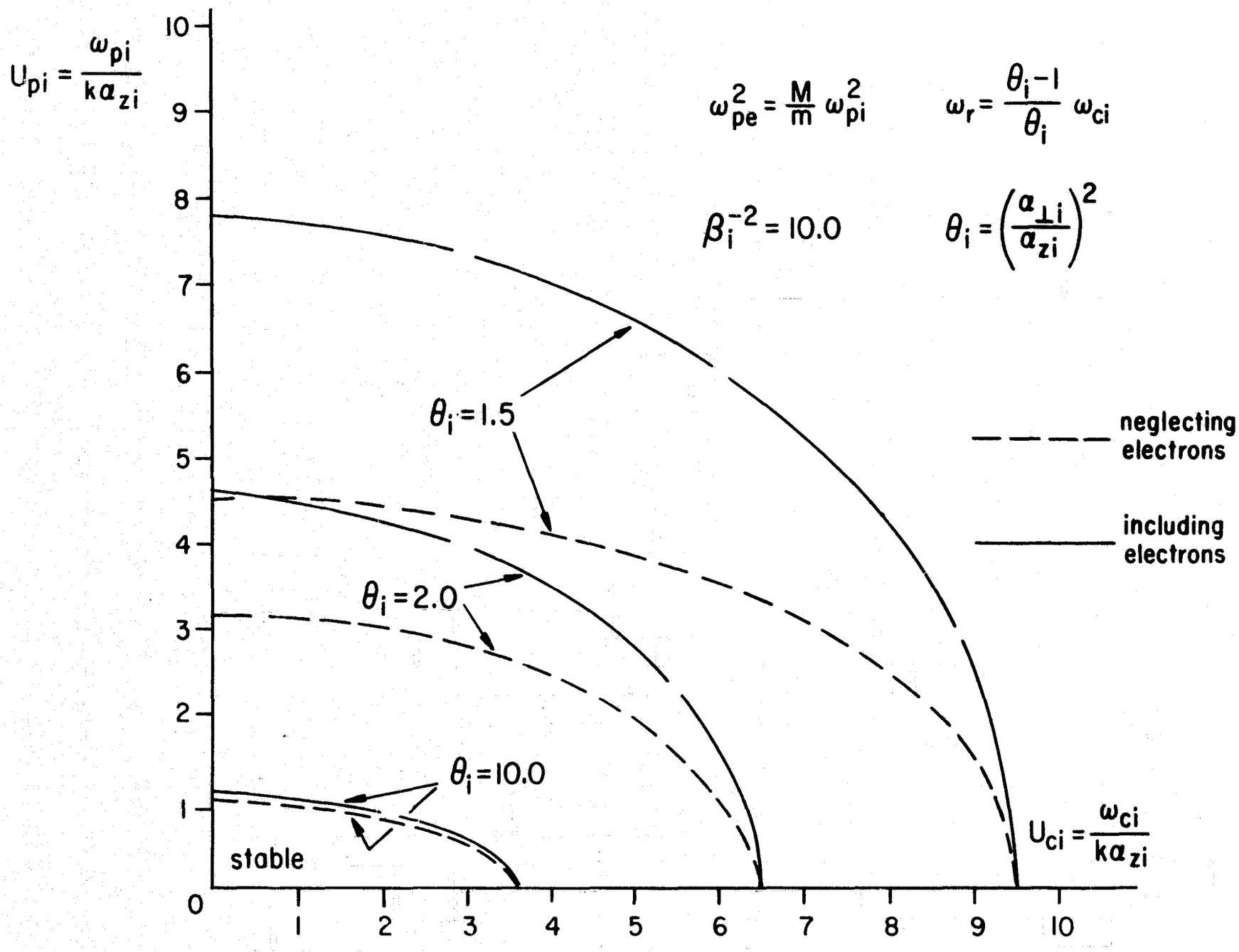

Fig. 1. Threshold of instability for ion cyclotron waves.

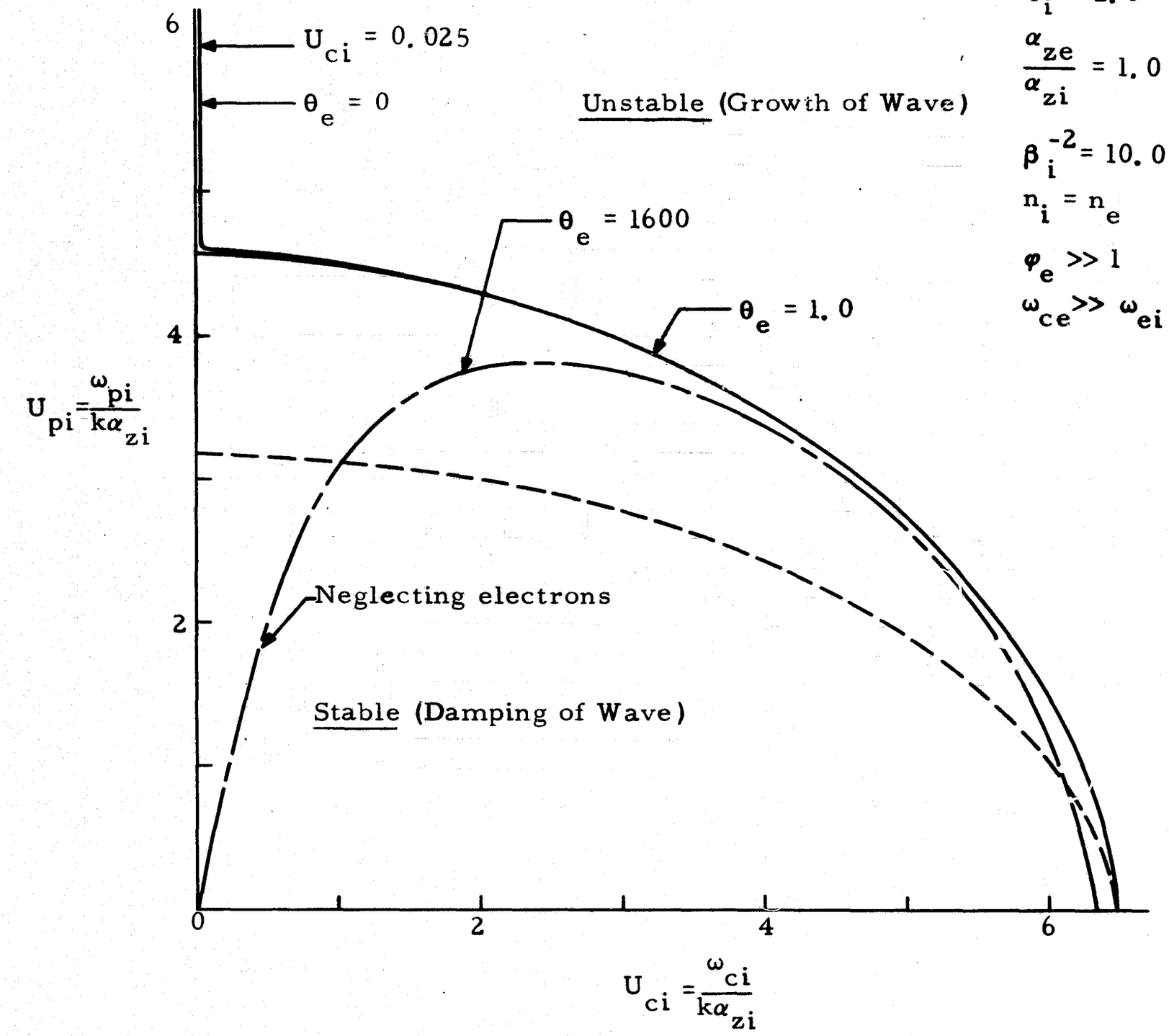

Fig. 2. Threshold of instability for ion cyclotron waves.

DESIGN OF WEAKLY STABILIZED MIRROR MACHINE OF THE MIRROR-QUADRUPOLE TYPE

AFAL Contract AF33(615)-1078
Professors J.G. Siambis and A.W. Trivelpiece

A method of designing coils for a mirror-quadrupole cusp-type magnetic field has been developed. The coils are essentially a current sheet enclosing a specified flux surface with nearly straight field lines. Plasma contained in such a field configuration is theoretically stable against the hydromagnetic interchange instability. Since the field lines are nearly straight, the velocity space instabilities can be studied in such a configuration.

The criteria for the design of the field and the coils, together with several aspects of the construction of such a machine, were presented [1]. The analytical investigation of the containment properties of the elliptical coil array has proceeded in two steps:

(a) A code for computing the magnetic field, and hence the mirror ratio, on the axis of the coil array was written and tested. For the particular choice of elliptical array being used, it has been found that the exact mirror ratio on axis is less than that predicted by simple and elementary concepts on flux tubes. See Fig. 1.

(b) A code for computing the magnetic field, field lines, surfaces of adiabatic motion, and integral 1/B for the elliptical coil array was also written and is being tested. The fact that the mirror ratio on the axis of the array is less than that predicted from elementary concepts, leads to the conclusion that this magnetic field configuration should be stable against the hydromagnetic interchange instability. This code will provide exact information on the stable containment properties and capabilities of an arbitrary elliptical coil array.

The experimental investigation of the containment properties of the elliptical coil array has also proceeded in two steps:

(a) A Lucite model (to scale) of the flux tube enclosed by the coil array has been constructed. On the outer surface of the model, thin copper wire has been wound with the shape of the elliptical coils. The array has been energized with 60 cycle power, and measurements of the magnetic field on the axis of the array have been performed. The mirror ratios measured are shown in Fig. 1. The measured values agree satisfactorily with those computed numerically from the code (a).

(b) A section of the actual pulsed elliptical coil assembly has been constructed. It is composed of four turns with the same internal elliptical shape and external circular size. Each coil turn is composed of two segments so that the turns can be assembled on a prefabricated liner. The purpose of this assembly is to test the mechanical strength

---

[1] ERL Consolidated Quarterly Progress Report on Plasma Research, 1 January - 31 March, 1965.

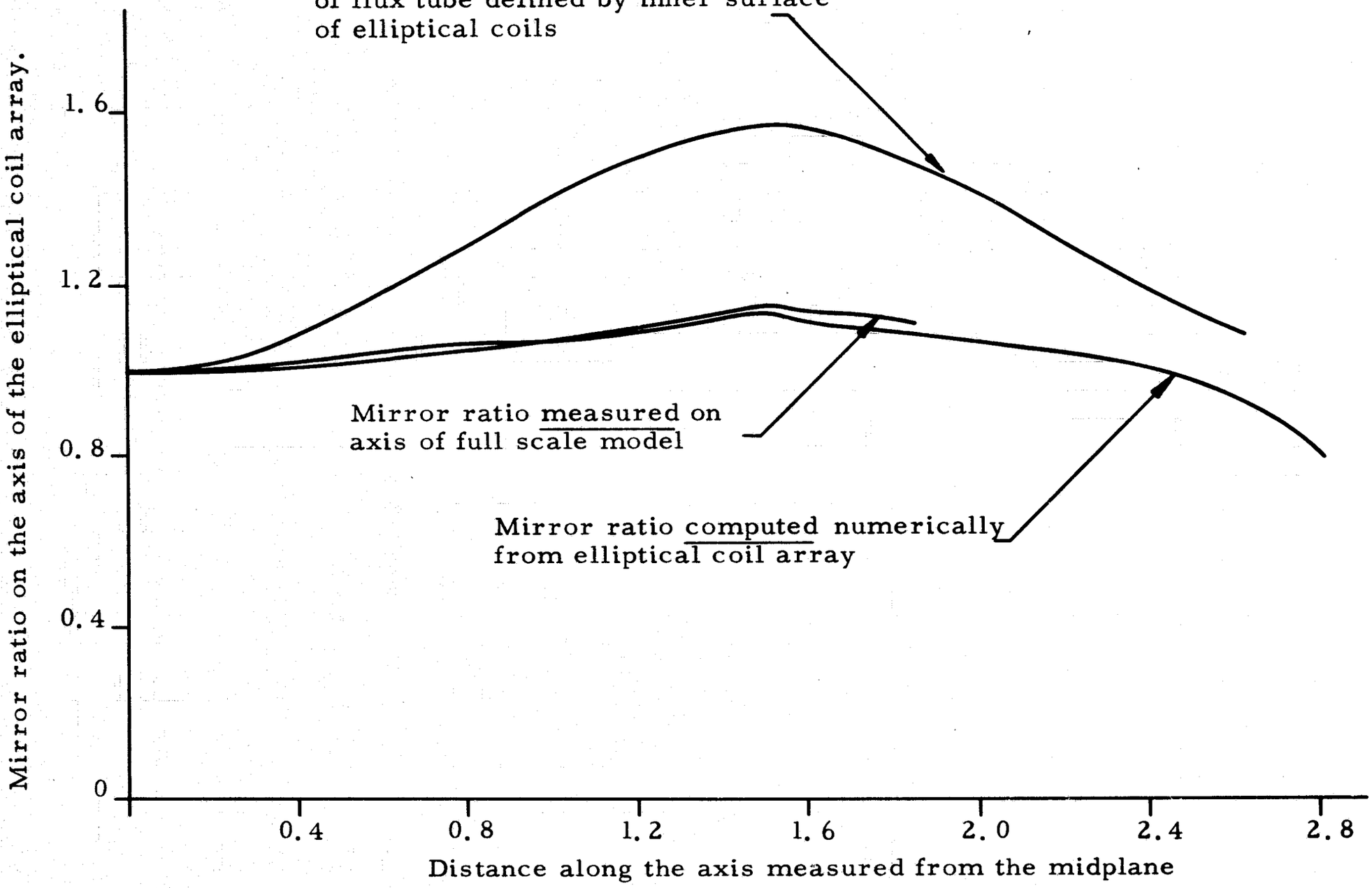

Fig. 1. Comparison of theoretical and experimental results.

of the elliptical turns and determine the amount of axial precompression that the coil assembly will require in order to be held together both electrically and mechanically. Also the effects of the variable magnetic pressure on the liner can be determined.

The work reported here concludes the preliminary studies related to the many problems of the construction of the machine.

NONLINEAR INTERACTION OF AN ELECTRON WITH AN E-M WAVE

NSF Grant GP-2239
J. Spector, (Prof. A.W. Trivelpiece)

The motion of electrons in electromagnetic waves is being studied under relativistic conditions. Possible applications being considered are the acceleration of electrons to high energies, and the generation of high-frequency radiation from the harmonies of the motion.

The case of a single free electron in a plane monochromatic linearly polarized wave has been studied extensively. It has been shown that the radiation reaction force on the electron is negligible for all reasonable value of field intensity, and can be ignored. If the field is sufficiently strong, the motion is highly non-linear. The motion transverse to the direction of wave propagation is made up of all of the odd harmonics of the primary frequency, while the motion parallel to the wave propagation contains all of the even harmonics. Thus, the electron radiates at all of these frequencies. The amplitude of the harmonics decrease with increasing frequency, but the ratio of the harmonic amplitude to the fundamental increases as the field strength increases.

RF ION SOURCE FOR AN ION ENERGY ANALYZER

NSF Grant GP-2239
V. Zaviantseff (Prof. A.W. Trivelpiece)

The purpose of this research is to develop an ion source in order to calibrate the electrostatic ion energy analyzer used on the rotating plasma experiment. The ion analyzer is modeled after the type used by H. Eubank [1] and constructed by H.K. Forsen.

The plan of this project is to

1. Design an rf discharge system capable of delivering an ion beam to the electrostatic ion energy analyzer.

---

[1] H.P. Eubank and T.D. Wilkerson, "An Ion Energy Analyzer for Plasma Measurements," Princeton University, Princeton, New Jersey, May 1962.

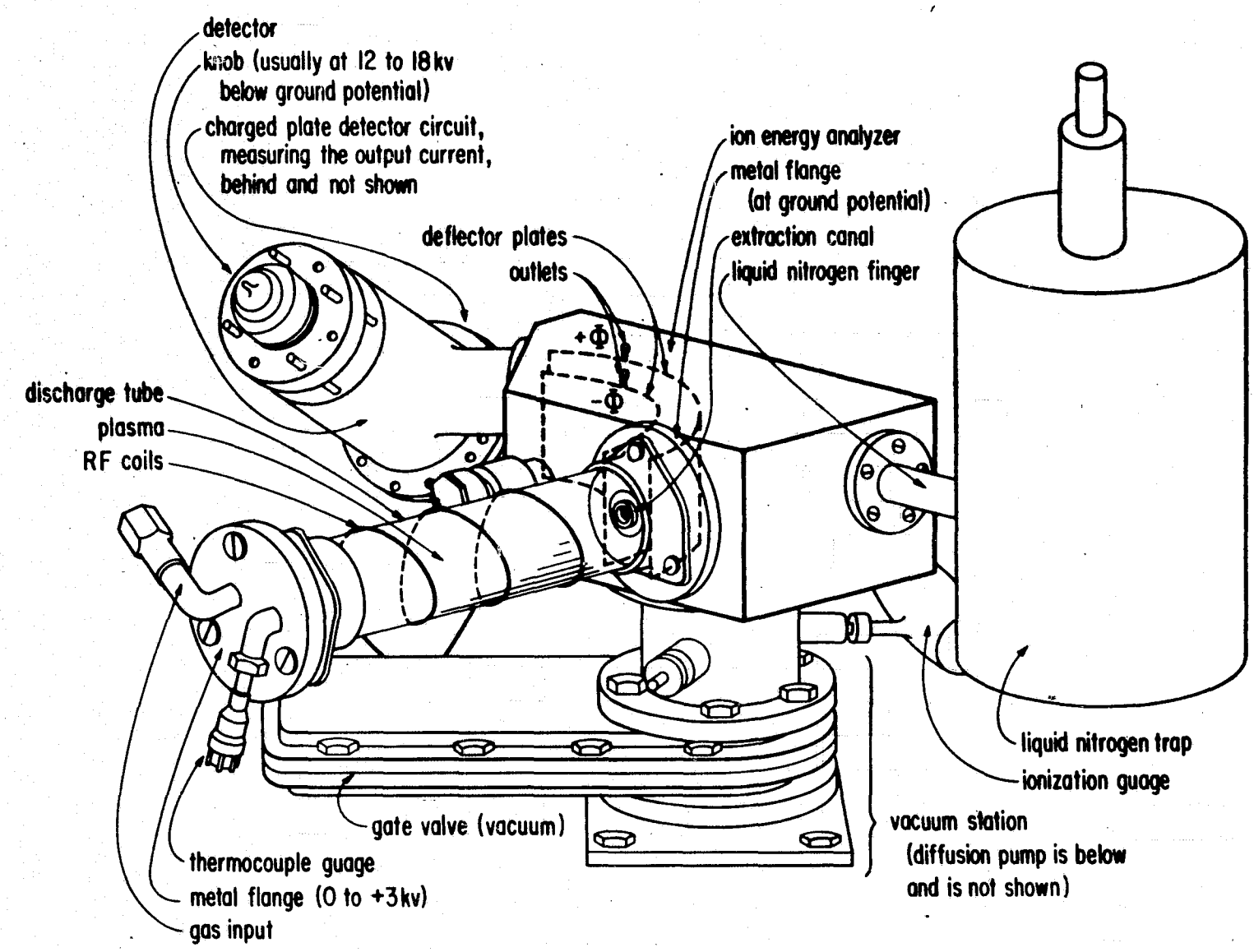

Fig. 1. R. F. ion source for Ion Energy Analyzer.

2. Modify the ion energy analyzer as follows:

   (a) Design an optimum canal geometry for the extraction and transmission of an ion beam [2 - 3] from the discharge tube to the analyzer, and

   (b) Design a liquid nitrogen cold trap, whose purpose will be to freeze all the hydrocarbons and water vapor in the electrostatic analyzer;

3. Design a detector capable of measuring the ion current after its passage through the analyzer; the following possibilities exist:

   (a) A charged-plate detector [4],

   (b) A Faraday cup [4],

   (c) A photosensitive screen.

The system including items 1, 2, (a) and (b), 3, (a) above has been put into operation. This project required building a new vacuum pumping station [5] which has been constructed.

Figure 1 shows the rf ion energy source for ion energy analyzer. The detector appearing in the background has a charged plate circuit (shown later). The pumping station is below the system shown on Fig. 1.

The whole system may be subdivided into two parts:

1. The rf ion source is in a Pyrex cylinder. It includes the following subsidiary parts:

   (a) Continuous supply of gas into the discharge tube. Nitrogen is used in the present experiment,

   (b) A thermocouple gauge;

   (c) An rf source: A Viking Challenger transmitter is being used. Its output A.C. RMS voltage is 50 V over the band (from 16 to 80 meters).

2. The analyzer-detector system includes

   (a) The electrostatic energy analyzer with two parallel de-

---

[2] P.C. Thonemann, "The Production of Intense Ion Beams," Progress in Nuclear Physics, Vol. 3, pp. 219-234, Pergammon Press, Ltd., London (1953).

[3] R.A. Coombe, "A Laboratory Ion Source Facility," Int. J. Elect. Eng., Vol. 2, pp. 415-423, Pergammon Press, Ltd., London (1965).

[4] K.S. Lion, Instrumentation in Scientific Research, pp. 216-218, McGraw-Hill Book Company, Inc. (1949).

[5] S. Dushmann, Scientific Foundations of Vacuum Technique, 2nd Edition, John Wiley and Sons, Inc., New York (1962).

flector plates bent into 127°. The analysis of this angle is described by A. L. Hughes and V. Rojansky [6]. The inner deflector plate is kept at a negative potential and the outer at a positive potential with respect to ground.

(b) The extraction canal and the rectangular exit slit are maintained at the ground potential.

(c) The detector includes:

(i) A high voltage knob which is a source of secondary electrons

(ii) A charged-plate circuit as follows:

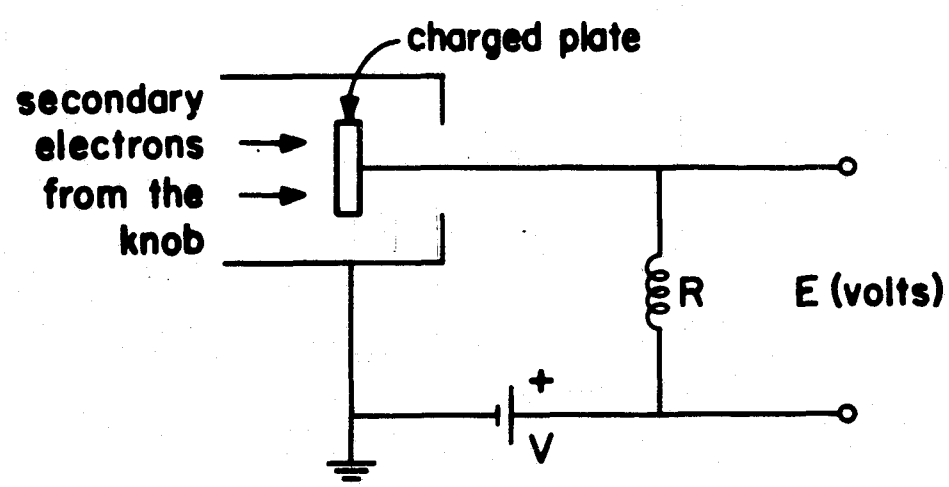

Performance of the system

The condition for a sustained rf discharge may be expressed through an inequality:

$$tv_e > \lambda ,$$

where $t = \frac{1}{f}$ and f = radio frequency in c.p.s.,

v = velocity of electrons which initiate ionization

λ = mean free path of the gas molecules.

The pressure in the discharge tube required to start ionization at rf = 20 Mc/sec, and assuming 50 volt RMS output from the transmitter is found to be almost one micron Hg. This has been verified experimentally.

Under the present conditions the extracted current is 0.16 μa at the pressure of one micron Hg in the discharge and rf = 20 Mc/sec. The current goes down to 0.06 μa at 20 microns Hg pressure. The extracting potential has been varied from 500-2000 V.

[6] A.L. Hughes and V. Rojansky, On the Analysis of Electronic Velocities by Electrostatic Means," Phys. Rev., Vol. 34, pp. 284-295 (1929).

Note: the current was normalized to the peak current in each case.

Pressure in the discharge: 1 micron Hg.
Pressure in the analyzer: 5×10^{-5} Torr.
Radio frequency: 20 Mc/sec.

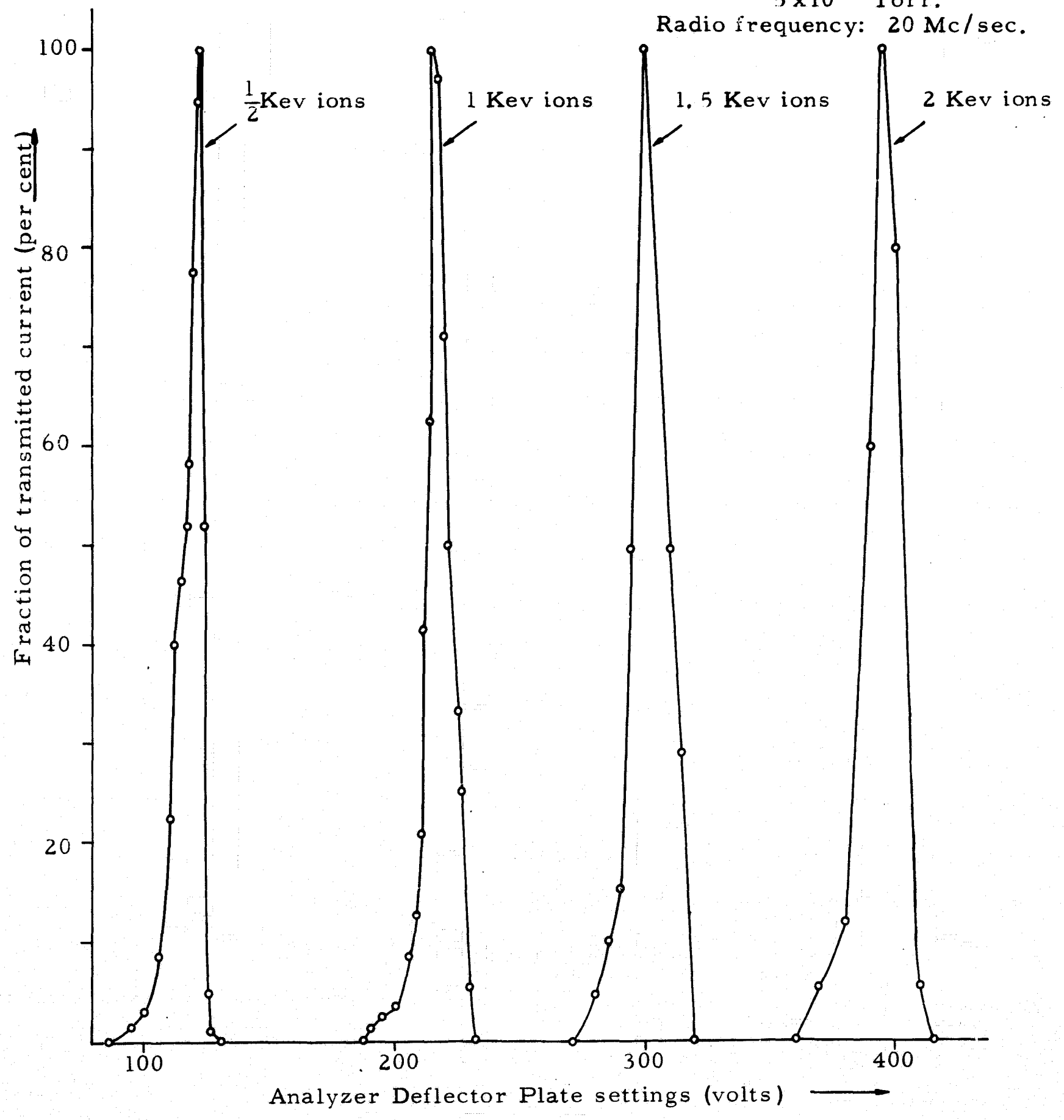

Fig. 2. Current transmitted by the Ion Energy Analyzer at various ion energies.

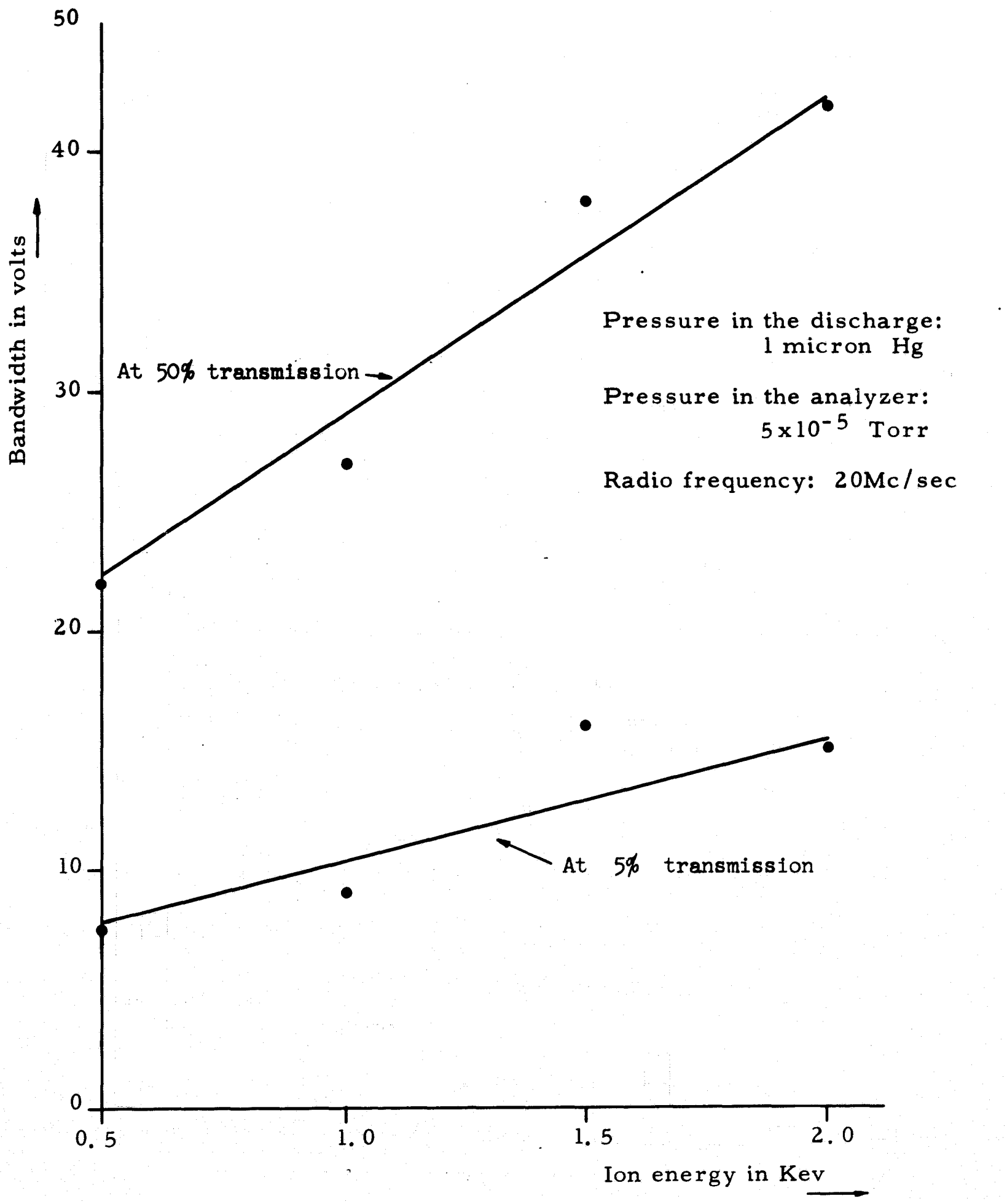

Fig. 3. Bandwidth of the ion energy analyzer as a function of ion energy.

With the optimum conditions of ionization in the discharge: rf = 20 Mc/sec, pressure = 1μ Hg, it has been possible to verify the property of the ion energy analyzer, that the bandwidth of the analyzer varies linearly with ion energy. The results are shown in Fig. 2 and 3.

INSTABILITIES OF CENTRIFUGAL-ELECTROSTATIC-FOCUSED (CEF) FLOW

AFAL Contract AF33(615)-1078
R. Lundgren (Prof. C.K. Birdsall)

In this project, the stability of a thin, hollow electron (or ion) stream subjected to axially asymmetric perturbations was investigated. The stream rotates in a radial electric field of such magnitude that the centrifugal and radial space-charge forces are balanced by the electrical force. It is well-known that stable orbits occur for a single particle or for thick streams (e.g., Harris flow) subjected to axially symmetric perturbations.

The thin stream model was first analyzed linearly in two dimensions (r, θ) and found to be unstable with an exponential time growth dependent on the aximuthal wave-number, n, as $\sqrt{n^2 + n - 1/2}$; for $n = 0$, there are radial oscillations with the well-known angular period $\sqrt{2\pi}$. As the coaxial walls were brought closer to the stream, the growth at small n first vanished, then reappeared at large values as a stream-image charge instability occurred. The physical mechanism of growth was examined in detail, especially in comparison with the dual, magnetically focused, model of Kyhl-Webster-Pierce. If axial motion were allowed, permitting axial escape from the aximuthal bunching, the growth rate is reduced and vanishes for small n as the axial wavelength approaches the stream circumference. With a model of charged rods, the large-amplitude growth region was examined, by numerical integration. The numerical method was checked in accuracy against the results of a single-rod small-amplitude analysis. The starting points of the non-linear calculations were small density perturbations for $n = 5, 15$, and 30. Exponential growth in time of the stream thickness occurred for about one or two stream revolutions, then quickly limited, went a much slower or zero growth rate. The end results was a shearing, but non-laminar, thick stream, apparently quite stable, with no loss of particles to the walls.

An experimental tube, constructed prior to the analysis, did not show any of the growths discussed, presumably because the stream was too thick radially and too free to move axially.

An ERL report on this project will be published in the near future.

INSTABILITIES OF FINITE-LENGTH ELECTRON-STREAM SYSTEMS

University of California Support
J. Frey (Prof. C.K. Birdsall)

The objective of this project was to study the behavior of electron streams injected into infinite diodes and cylindrical drift tubes with short-circuited gridded ends. Positive ions neutralized the average space charge of the stream, and solutions were obtained for both mobile and fixed ions. A large axial magnetic field confined the particles to one-dimensional motion. The effect of elastic collisions between stream particles and background neutrals was also considered.

The approach was to use a small-signal analysis with all lowest mode waves available to satisfy the boundary and initial conditions. A solution in terms of the complex frequency of the system was found as a function of input current. With infinitely-massive positive ions, the imaginary part of this frequency became negative at a current called I_{max}, indicating growth of small perturbations with time; the magnitude of I_{max} was related to the diode spacing or the ratio of tube radius to length, and could be stated in terms of perveance. At I_{max}, there was a sinusoidal standing wave of the axial electric field along the tube or diode. Values of I_{max} for various ratios of tube radius to length were determined; for the diode, exact solutions were obtained for growth and damping constants in alternating regions of stability and instability that correspond to increasing numbers of nodes in the standing wave.

If the background ions were allowed to move, instability would not occur. The larger the ratio of ion mass to electron mass, the more closely the imaginary part of the frequency approached zero; so that for large ratios, stability was marginal. Collisions enhanced the stability of the system, increasing I_{max} for systems with stationary ions and reducing the growth constant for any unstable input current.

The energy balances and wave-propagation properties of the systems considered were outlined. The instability is shown to arise primarily due to effects at the exit grid, possibly leading to an avalanching of electrons returned from this grid.

An ERL report on this project will be published in the near future.

BLANK PAGE

D. QUANTUM AND OPTICAL ELECTRONICS

Our research in quantum and optical electronics includes work with gas and ion lasers, semiconductor lasers, Raman lasers and other nonlinear phenomena, and the deflection of optical beams. With the visiting appointment of Professor Bloembergen to the laboratory, the work on nonlinear optics has been particularly emphasized during this period.

The specific projects in nonlinear optics include theoretical studies of interaction between light waves and spin waves or plasma waves; amplifier techniques for Raman laser studies; and the measurement of real and imaginary parts of nonlinear susceptibilities. A technique for inducing Raman oscillation at unconventional frequencies has been developed, which raises further problems in the behavior of Raman oscillators. A new study of the high-speed detailed structure of Ruby laser emissions has been initiated.

The work in semiconductor lasers now stresses modulation of these by acoustic waves excited to vary the band gap.

The gas laser work includes the study of microwave discharges in helium-neon lasers and the use of lasers for measuring low absorbencies in liquids. The gas laser is also used to produce the beam for the optical deflection experiment. A useful coaxial form of the He-Ne laser has been developed during this period, and several models were built for use in the experiments. Argon ion lasers have also been built and have successfully operated both pulsed and continuously.

STUDIES IN NONLINEAR OPTICS

JSEP Grant AF-AFOSR 139-65
Prof. N. Bloembergen (Visiting professor, 1964-1965, on leave from Harvard University)

The interaction between light waves and spin waves and between light waves and plasma waves has been treated in the same manner as the interaction between light waves and acoustical waves (Brillouin effect) and between light waves and optical phonons (Raman effect). This work, done in collaboration with Dr. Y. R. Shen of the Physics Department at Berkeley, was described at the Physics of Quantum Electronics Conference held in San Juan (P. R.) on June 28-30. A brief report will appear in the proceedings of this conference. A manuscript, describing the optical nonlinearities of a plasma, has been prepared for publication in The Physical Review. The second

harmonic generation of light from a plasma boundary is discussed in terms of a self-consistent field dielectric constant. The importance of a surface term, proportional to the discontinuity in the normal component of the electric field at the boundary, is pointed out. It is shown, however, that the experimentally observed second harmonic generation from metallic silver, silicon, and germanium is probably not a plasma effect but is caused by the bound electrons of ion cores or atoms at the surface. The stimulated Raman effect in a plasma follows naturally in the next higher approximation and may be expressed in terms of a Raman susceptibility, which is many orders of magnitude smaller than that of ordinary liquids. Another manuscript, dealing with the interaction of photons and magnons, is in preparation and will also be submitted to The Physical Review.

The anisotropy of the Raman susceptibility tensor has been investigated theoretically. The three nonlinear tensor elements are related to the spontaneous Raman scattering cross section and its depolarization factor. An experimental investigation was carried out in collaboration with P. Lallemand at Harvard University. A Raman amplifier technique has been developed for reliable measurements of the gain constants. This technique was described in the May 15, 1965, issue of Applied Physics Letters. The technique has been used to measure the Raman gain of benzene for different combinations of laser and stokes polarizations. The Raman gain has also been measured in benzene mixtures. These results have been reported at the Physics of Quantum Electronics Conference mentioned above. The paper will appear in the proceedings of this conference under the title, "Light Waves with Exponential Gain."

A method has been suggested for measuring the real and imaginary part of the nonlinear susceptibility for second harmonic generation in nonlinear media. So far, only the absolute value of this susceptibility has been determined. This proposal has led to a successful experiment which is described in a joint paper by R.K. Chang, J. Ducuing, and N. Bloembergen, Phys. Rev. Letters, 15, 6 (1965).

MODIFIED RAMAN LASERS

JSEP Grant AF-AFOSR-139-65
A. Pine and Professor S.E. Schwarz

The objectives of this experiment are: (1) to develop Raman-type laser oscillators operating on Raman lines which are not the most intense in normal Raman effect, and (2) to use this as a technique to obtain information about feedback effects in Raman oscillators.

The first technique to be tried was that of adding a dye to the liquid Raman laser medium. This dye was to reduce the Raman gain at the normal Raman laser frequency, allowing oscillation on another Raman transition, normally having less gain, to take place. This technique was unsuccessful because of the difficulty of finding a suitable dye with the needed selective filter properties in the range

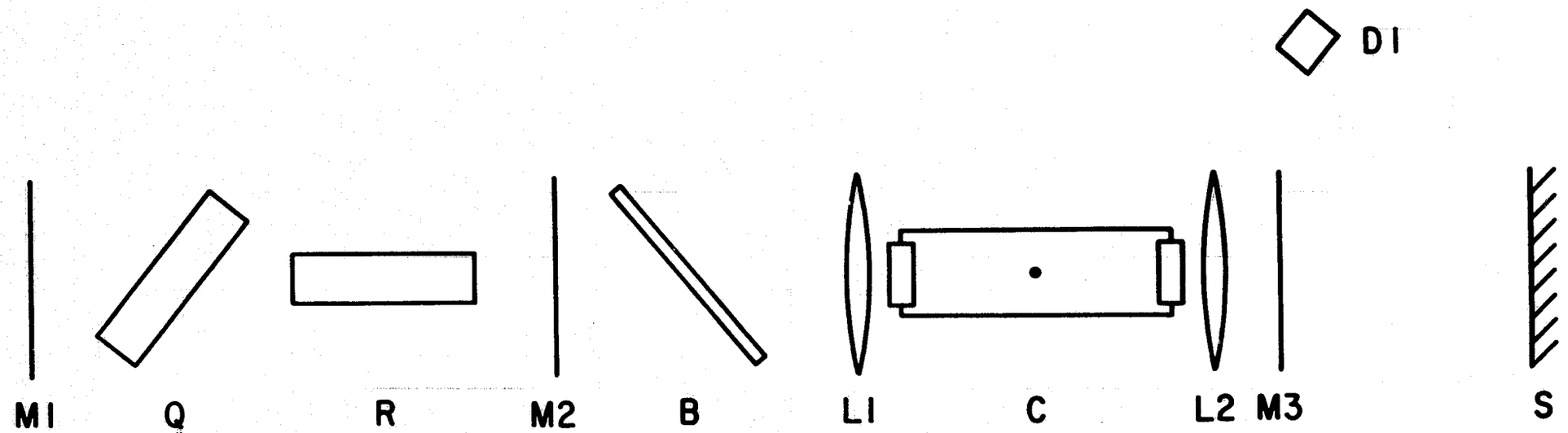

Fig. 1. Experimental arrangement. M1, M2, M3, dielectric mirrors; Q, cryptocyanine Q-spoiler; R, ruby rod; B, beam splitter; L1, L2, lenses, 10 cm focal length; C, cell containing cyclohexane, 10 cm long; S, diffuse scatterer; D1, D2, diodes (directed at S), equipped with spectral filters.

7000 - 9000 Å. Those which were found have rather broad absorption spectra, causing them to absorb some of the ruby laser pump power. Thus it seems likely that the dyes are being "bleached" and consequently are made inoperative. However, the negative result of this experiment also suggests that the per-pass gain in the Raman cell is rather high, possibly greater than the minimum of 10^3 imposed by the low (about 10^{-3}) feedback in the oscillator. This would make it difficult to provide sufficient dye absorption to discourage the principal mode of oscillation.

This situation can be corrected by reducing the per-pass gain of the oscillator to the point where moderate amounts of frequency discrimination will be sufficient. In any saturable oscillator the gain will automatically be reduced as the feedback is increased. Hence the feedback in our Raman oscillator was increased by adding a resonator external to the Raman cell (Fig. 1). In order to drive the oscillator strongly into the gain saturation region, a confocal resonator is used (lenses L_1 and L_2 in conjunction with mirrors M_2 and M_3). With this configuration it was possible to generate laser action on the 801 cm^{-1} Raman line of cyclohexane, which normally exhibits laser action only at 2852 cm^{-1}. The output of the Raman oscillator as a function of cavity alignment is shown in Fig. 2. (When the cavity is misaligned by more than 15 milliradians, only the normal strokes frequency 5, is seen.) When the cavity is aligned, S_2 appears and S_1 is strongly reduced in intensity. The effects are observed most strongly when the feedback of the reflectors is stronger at S_2 than at S_1. S_2 is also produced weakly and erratically when the feedback is present but not in its favor, which indicates that the laser pump is not being drastically depleted by the presence of S_1. Occasionally some S_2 is observed even when M_3 is absent, but only when M_1 and M_2 favor S_1; some reflection mechanism within the Raman liquid -- such as Brillouin scattering -- may be providing feedback.

The reduction in the strength of S_1 is interesting and unexpected. It is possible that it is due to deterioration of the ruby laser output because of distorted feedback into the ruby from M_3. However, it may also possibly be due to a local field effect inside the Raman liquid, in which the susceptibility for S_1 is disturbed by the excitations of S_2. Possibly it is due to other competition effects. Checks of some of these possibilities are being planned.

HIGH-SPEED STRUCTURE OF RUBY LASER EMISSIONS

JSEP Grant AF-AFOSR-139-65
A Pine & Professor S. E. Schwarz

Various experiments have given indirect indications that the output of ruby lasers is much more complex than is commonly believed. This complexity may involve spatial and temporal fine structure having extremely rapid time variations ($< 10^{-10}$ second), so that it is not observable with conventional techniques. An experimental search for fine structure has been initiated. The approach is essentially one of constructing auto and mutual correlation functions using techniques of nonlinear optics.

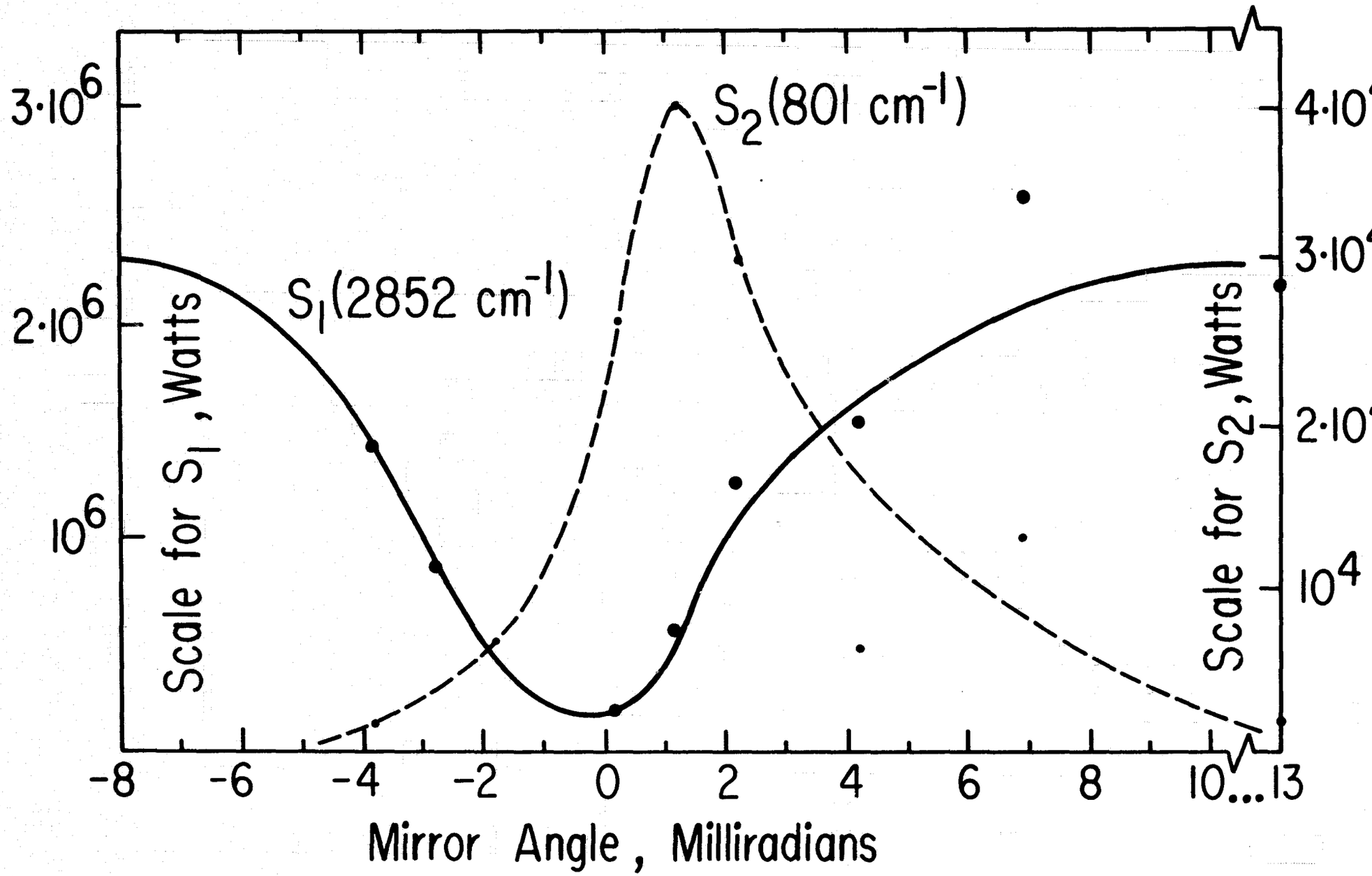

Fig. 2. Production of power at normal (2852 cm^{-1}) and abnormal (801 cm^{-1}) Raman frequencies as a function of cavity alignment.

INVESTIGATION OF MODULATION SCHEMES FOR SEMICONDUCTOR LASERS

AROD Grant DA-ARO-D-31-124-G557
C.C. Tseng (Professor S. Wang)

In the second scheme proposed in the last report, we mentioned that one end of an x-cut quartz rod will be mounted with a diode while the other end is to be placed in a resonant cavity. A longitudinal ultrasonic wave excited by the electric field of the cavity will propagate along the rod and into the diode. The stress wave into the diode will cause the change in energy band gap. Taking the GaAs diode, for example, the energy gap will change, approximately following the relation

$$E(ev) = h\nu = 1.48 + 1/3(1.1 \times 10^{-5})\ P\ (bars) \quad ev$$

Therefore, the spectrum of the emission before lasing will shift accordingly. In case of lasing, a dynamic interaction between laser modes and the ultrasonic wave must be considered. The effect of deformation potential on the optical transition must also occur. Some analysis has been done for the latter. The effect of uniaxial stress on the matrix element of optical transition between bands is described in the following.

The Schroedinger equation for the cell periodic function $u_K(r)$ can be represented in one electron approximation as

$$(H^0 + H_{k\cdot p} + H_{L\cdot s} + H_e)\, u_K = \lambda_i\, U_K \qquad \lambda_i = E_i - \frac{\hbar^2 k^2}{2m} ,$$

where $H_{kp} = \hbar/m\ \bar{k}\cdot\bar{p}$ is the $k\cdot p$ perturbation Hamiltonian[1].

$$H_{Ls} = (\hbar/4m^2c^2)\ \frac{1}{r}\ \frac{dv}{dr}\ \ L\cdot\sigma \equiv \xi(r)\ L\cdot\sigma$$

is the spin orbital coupling Hamiltonian, where L and σ are orbital and spin angular momentum operators.

$$H_e = D_d^c\ (e_{xx} + e_{yy} + e_{zz}) \qquad \text{for conduction band}$$

$$= D_d^v(e_{xx} + e_{yy} + e_{zz}) + 2/3\ D_u \sum_i [\ (J_i^2 - 1/3\ J^2)e_{ii}]$$

$$+ 2/3\ D_u' \sum_{i\neq j} \{(J_iJ_j)\}\ e_{ij} \quad \text{for valence band,}$$

---

[1] E.O. Kane, J. Phys. Chem. Solid 1 p. 249-261 (1957).

where i and j = x, y, z. H_e's are the strain Hamiltonians [2], [3] for conduction and valence bands. D_d^c is the deformation potential for conduction band and D_d^v for valence band. D_u is the deformation potential for stress applied along <100> direction while D_u' is for <111> direction.

In the present analysis the following approximations are made. We assume that central field approximation is still valid under stress, only the first order perturbation is taken into account, linear k term [1] in valence band is ignored, the k dependent spin orbital interaction [1] term is neglected, stress is applied only along 001 direction, stress and direction of quantization are taken in z direction. Under the last assumption the strain Hamiltonian becomes [2]

$$H_e = D_d^v(2s_{12} + s_{11})\,T + 2/3\,D_v(s_{11} - s_{12})\,T(J_z^2 - 1/3\,J^2)$$

$$\equiv \epsilon_1^v + \epsilon_2(J_z^2 - 1/3\,J^2) \text{ for valence band, and}$$

$$H_e = D_d^c(2s_{12} + s_{11})\,T \equiv \epsilon_1^c \text{ for conduction band,}$$

where s_{11}, s_{12} are elastic compliances, T the stress and J is total angular momentum operator.

If we choose the following set of orthonormal functions as basis [4]

$$iU_s(1/2,1/2) = iS\sigma, \qquad iU_s(1/2,-1/2) = iS\beta,$$

$$U_p(3/4,3/2) = \frac{-1}{\sqrt{2}}(X+iY)\sigma, \qquad U_p(3/2,-3/2) = \frac{1}{\sqrt{2}}(X-iY)\beta,$$

$$U_p(3/2,1/2) = \frac{1}{\sqrt{6}}(2Z\sigma - (X+iY)\beta), \qquad U_p(3/2,-1/2) = \frac{1}{\sqrt{6}}[(X-iY)\sigma + 2Z\beta],$$

$$U_p(1/2,1/2) = \frac{1}{\sqrt{3}}[Z\sigma + (X+iY)\beta], \qquad U_p(1/2,-1/2) = \frac{1}{\sqrt{3}}[(X-iY)\sigma - Z\beta],$$

where the first numerical value in the parenthesis is the value of J while the second is the value of Jz, which is the projection of J on Z axis. We obtain a secular equation in a form of

---

[2] J. C. Hensel and G. Feher, Phys. Rev. 129 p. 1041(1963).

[3] W. H. Kleiner and L. M. Roth, Phys. Rev. Letters 2 334(1959).

[4] J. M. Luttinger and W. Kohn, Phys. Rev. 97 869(1955).

$$\begin{bmatrix} H & 0 \\ 0 & H \end{bmatrix}$$

where

$$H=\begin{bmatrix} E_s+\epsilon_1^c-\lambda_i & 0 & \sqrt{2/3}k\rho & \frac{1}{\sqrt{3}}k\rho \\ 0 & E_\rho+1/3\Delta+\epsilon_1^v+\epsilon_2-\lambda_i & 0 & 0 \\ \sqrt{2/3}k\rho & 0 & E_\rho+1/3\Delta+\epsilon_1^v-\lambda_i & 0 \\ \frac{1}{\sqrt{3}}k\rho & 0 & 0 & E_\rho-2/3\Delta+\epsilon_1^v-\lambda_i \end{bmatrix}$$

where

$$\rho = -i\frac{\hbar}{m}\langle s \mid p_z \mid Z\rangle ,$$

$$\Delta = 3/2 \int \xi(r)\, U_i^*\, U_i\, d_r^3 ,$$

E_s and E_p are the eigen values of unperturbed Hamiltonian H^0. For simplicity we can choose the energy reference as zero at the top of the valence band. Then

$$E_\rho = -\Delta/3 - \epsilon_1^v - \epsilon_2 ,$$

$$E_s = E_g - \epsilon_1^c ,$$

where E_g is the energy gap of the stressed semiconductor. This energy gap can be measured experimentally. The secular equation becomes

$$H = \begin{bmatrix} E_G-\lambda_i & 0 & \sqrt{2/3}k\rho & \frac{1}{\sqrt{3}}k\rho \\ 0 & -\lambda_i & 0 & 0 \\ \sqrt{2/3}k\rho & 0 & -2\epsilon_2-\lambda_i & 0 \\ \frac{1}{\sqrt{3}}k\rho & 0 & 0 & -\Delta-\epsilon_2-\lambda_i \end{bmatrix}$$

where

$$\lambda_i = E_i - \frac{\hbar^2 k^2}{2m} , \qquad i = c,\ v_1,\ v_2,\ v_3 .$$

The eigen values are found to be

$$E_c = E_g + \frac{\hbar^2 k^2}{2m} + \frac{\{E_g + 2/3(\Delta + 2\epsilon_2)\}}{(E_g + 2\epsilon_2)(E_g + \Delta + \epsilon_2)} k^2 \rho^2, \quad \text{conduction band,}$$

$$E_{v_1} = \frac{\hbar^2 k^2}{2m} , \quad \text{heavy mass valence band,}$$

$$E_{v_2} = -2\epsilon_2 + \frac{\hbar^2 k^2}{2m} - \frac{2}{3(E_g + 2\epsilon_2)} k^2 \rho^2 , \quad \text{light mass valence band,}$$

$$E_{v_3} = -\Delta - \epsilon_2 + \frac{\hbar^2 k^2}{2m} - \frac{1}{3(E_g + \Delta + \epsilon_2)} k^2 \rho^2 , \quad \text{split off valence band.}$$

In the above equations if we put the stress term equal to zero we obtain the stress free values as found by Kane [1]. The doubly degenerate wave functions which result from the diagonalization of the Hamiltonian may be written

$$U_{i\alpha} = a_i [iS\alpha] + c_i \frac{1}{\sqrt{6}} [2Z\alpha - (X + iY)\beta] + d_i \frac{1}{\sqrt{3}} [Z\alpha + (X + iY)\beta] ,$$

$$U_{i\beta} = a_i [iS\beta] + c_i \frac{1}{\sqrt{6}} [(X - iY)\alpha + 2Z\beta] + d_i \frac{1}{\sqrt{3}} [-(X - iY)\alpha + Z\beta] ,$$

$i = E_c, E_{v_2}, E_{v_3}$, i.e., index denotes conduction band, light mass band, and split-off band, respectively;

$$U_{v_1\alpha} = \frac{-1}{\sqrt{2}} (X + iY)\alpha ,$$

$$U_{v_2\beta} = \frac{1}{\sqrt{2}} (X - iY)\beta ,$$

for heavy mass band,

where

$$a_i = \frac{(2\epsilon_2+\lambda_i)(\Delta+\epsilon_2+\lambda_i)}{N} ,$$

$$c_i = \frac{\sqrt{2/3}\,k\rho(\Delta+\epsilon_2+\lambda_i)}{N} ,$$

$$d_i = \frac{\frac{1}{\sqrt{3}}k\rho(2\epsilon_2+\lambda_i}{N} ,$$

and λ_i is the root of the secular equation.

N is the normalization factor of the wave functions.
The matrix element of optical transition between conduction band and the jth valence band is found as

$$|M_{c-j}|^2 = 4/3\left(\frac{m}{\hbar}\rho\right)^2 \left\{\left[a_c\left(\sqrt{2}\ c_j + d_j\right) + a_j\left(\sqrt{2}\ c_c + d_c\right)\right]^2 + 2\left[a_c\left(\frac{c_j}{\sqrt{2}} - d_j\right) + a_j\left(\frac{c_c}{\sqrt{2}} - d_c\right)\right]^2\right\}$$

Second-order perturbation terms for valence bands and the transition between conduction band and acceptor level will be considered in the next report.

LOSS MEASUREMENT OF MATERIALS AT LIGHT FREQUENCIES USING INTERACTION ON A LASER MODE

JSEP Grants AF-AFOSR-139-64 65
D. Solimini (Prof. J.R. Whinnery)

The absorbancy of highly transparent materials, for which photometric techniques are inapplicable, can be measured by taking advantage of the thermal-lens effect. It has been observed that when some liquids or solids are inserted in the cavity of a gas laser, a divergent lens is produced inside the material because of the absorption of the laser beam [1] .

Since this lens modifies the shape of the laser beam, measurement of the diameter of the beam, with the sample inserted in the cavity and the laser oscillating in the dominant (Gaussian) mode, allows

---

[1] J.P. Gordon, R.C.C. Leite, R.S. Moore, S.P.S. Porto and J.R. Whinnery: "Long Transients Effects in Lasers with Inserted Liquid Samples" J. Appl. Phys., 36 , 3 (1965).

the focal length of the lens to be calculated. The focal length is related to the local heating in the medium. Thus, in turn, the absorbency can be calculated knowing the refraction index, its derivative with respect to the temperature, and the thermal conductivity of the material.

The experimental setup used here is fundamentally the same as that used by Leite, Moore, and Whinnery [2]. The laser is a He-Ne gas laser oscillating in the red in the fundamental mode. A phototube with S-1 response and a hole diameter of 25μ scans the beam and from the nearly Gaussian diagram of power vs position, the spot-size can be determined.

The purpose of the present work is to measure absorbencies of several liquids at the 6328 Å of the He-Ne laser. The materials were chosen with the aim of studying the effect on the absorption of : a) increasing the number of cycles in aromatic compounds (absorbencies of benzene, naphthalene, anthracene, phenanthrene, chrysene, and pyrene will be measured); b) substituting a hydrogen atom in aromatic compounds by other groups as in toluene, tetraline, ethynilbenezene, phenol, etc; c) conjugation in polyenes as in diphenylmethane and benzophenone. The absorbency of several other rather common liquids will also be measured. These liquids include water, carbon disulphide, and carbon tetrachloride, lowest-order alcohols and ethers, some cycloalkanes and liquid alkanes.

The refractive indexes at the red line of the He-Ne laser have been calculated from published data for the materials to be studied; the derivatives of the refractive indexes were also calculated. The precision of data is in general quite good; however, for the thermal conductivity, the precision is seldom better than 5%. The experimental setup has been checked for determining how much the various components affect the precision of the measurements (curvature of the mirrors, strains and irregularities in the laser windows yielding non-uniform beams, and linearity of the detecting system). The presence of oscillations in the high-gain infrared lines has also been checked. The absorbencies of 10^{-2}, 10^{-3}, and 10^{-4} molar solutions of chromium sulfate in water were measured by standard photometric techniques and were found to be respectively 4.6×10^{-1}, 5.5×10^{-2}, and 8×10^{-3} cm^{-1} at 630 mμ. The 10^{-4} molar solution was measured with the thermal lens technique and yielded an absorbency of 4.6×10^{-3} cm^{-1}. Recognizing that scattering losses are included in the photometric measurement and that the lowest concentration was in a range of poor accuracy for photometric methods, this check seems very good.

---

[2] R.C.C. Leite, R.S. Moore and J. R. Whinnery, "Low Absorption Measurements by Means of the Thermal Lens Effect Using an He-Ne Laser," Appl. Phys. Letters, 5, 141 (1964).

ELECTRO-OPTIC LIGHT BEAM DEFLECTION

University of California Support
E. Ippen (Prof. J.R. Whinnery)

A study is being conducted of barium titanate and its properties applicable to light modulation and deflection. Barium titanate ($BaTiO_3$) was chosen for early experiments because it is available and its crystal properties are documented. It is representative of a class of crystals known as the perovskite oxides (ABO_3 with pseudo-cubic structure). Members of this class of crystals exhibiting ferroelectricity are known to have extremely large dielectric constants in the vicinity of the Curie temperature. Furthermore, as a consequence of this anamalous dielectric behavior these crystals have large electro-optic coefficients in the same region. Cubic structure above the Curie temperature precludes a linear electro-optic effect in these materials, but enhanced linear effects become possible with the help of d-c biasing. Lack of an optic axis also relaxes some of the conditions on beam direction and parallelism that are imposed when uniaxial crystals such as KDP are used. Recently, there has been new interest in the perovskites because of the development of single-crystal compounds such as KTN ($KTa_xNb_{1-x}O_3$ with $x = 0.65$). The compound KTN has the advantage of having pronounced nonlinearities at room temperature, whereas $BaTiO_3$ must be heated to about 130 °C.

Crystal platelets were obtained from I.P. Kaminow of Bell Laboratories. They were grown by the Remeika technique and are characteristically yellow. Initial cutting and polishing difficulties have been more or less overcome. Prisms with various apex angles have been cut then polished on edge to microscopic smoothness. Aluminum electrodes are deposited on the large, parallel faces; a thick layer of air-drying silver paint protects the electrodes from scratching.

A small oven was constructed to heat the electro-optic prisms above the Curie point. Thermocouple measurements indicate that temperature is stabilized to within 1°C for long periods of time. Crystal temperature relative to the Curie point has been most effectively monitored by means of P vs E curves displayed on an oscilloscope by a Sawyer-Tower circuit. Characteristic, single and double hysterisis curves are observed and vary markedly with temperature in this region.

The same 60-cycle voltage used for the P-E curves has been used to deflect a laser beam (6328Å) passing through the prism. With light polarization parallel to the applied field, deflections on the order of 0.5 to 1.0° have been observed. This corresponds to a change in the index of refraction of about 2×10^{-3}.

Development of the prism deflector will be continued. One problem has been that the crystal cracks under applied voltage, presumably because of nonuniformities in the crystal. As this and other problems are overcome, however, greater deflection angles and more rapid deflection will be possible. At the same time the possible application of $BaTiO_3$ and other perovskites to different deflection and modulation schemes will be investigated.

EFFECT OF MICROWAVE DISCHARGES UPON GAS LASERS

JSEP Grant AF-AFOSR-139-65
W. Clark (Prof. J.R. Whinnery)

To study the possibility of using microwaves to pump a laser, a detailed investigation has been undertaken of the pumping and excitation mechanism in He-Ne. In the initial experiment it is planned that the effect of a He-Ne microwave-induced plasma upon the operation of a He-Ne laser be studied. This will be accomplished by placing a microwave circular cylindrical cavity, with a tube containing He-Ne oriented along its axis, within the optical cavity of the laser and in series with the laser tube. All equipment necessary for the experiment has been obtained and work is now concentrated on optimum matching of the cavity.

Initially the microwave source frequency will be in the 0.95 to 1.5 Gc range since continuous-wave (cw) magnetron in that range is available, but it may prove necessary to experiment at different frequencies to examine the effects of the microwave excitation on the interesting range of He-Ne mixtures. Modes in the present cavity can be excited to establish the gas plasma via large transverse or longitudinal fields on the axis.

Because of the output power limitations of practically obtainable microwave cw sources it may be necessary to initiate pulsed operation. Based upon the work of MacDonald and Brown [1] the necessary axial fields for breakdown for He-Ne mixtures of the pressures used need to be in the range of 500-1000 v/cm. With these values, the present 200-w magnetron will barely provide the necessary power for the cavity (19.5 cm length, 8.5 cm radius) now being used.

This study has been undertaken in the belief that if the microwave source is near the plasma or cyclotron frequency of the gasses, then efficient pumping and a possibility of modulation may be realized. Also, since detailed analytic theories of high frequency discharges in gases have been formulated [1-4], it is expected that microwave pumping will similarly allow more exact theories of the pumping mechanism of lasers. Still other effects related to the interaction of light and microwave discharges may be expected.

---

[1] A.D. MacDonald, S.C. Brown, Phys. Rev. 75:411 (1949)

[2] S.C. Brown, Basic Data of Plasma Physics, MIT Press-Wiley Chapter 15; 1959.

[3] H. Margenau, Phys. Rev. 73:297 (1948)

[4] S.C. Brown, A.O. MacDonald, Phys. Rev. 76:1629 (1949)

BLANK PAGE

E. RADIATION AND PROPAGATION

Research in this area has been directed mainly towards the frequency-independent and log-periodic antennas. These antennas typically have low directivity, however several new designs have been evolved which indicate significant improvements in directivity. The antennas are being developed mainly through experimental programs. Also, several theoretical investigations, based on the integral equation formulation for thin-wire antennas, are contributing to the program. One investigation, based on the thin-wire formulation, considers a dipole immersed in a compressible plasma.

Other experimental and theoretical programs are concerned with various types of antennas: circularly polarized antennas, frequency scanning antenna arrays, optical antenna arrays, antennas in dissipative media, and a semi-infinite Yagi array.

HIGH-GAIN, LOG-PERIODIC ANTENNAS

NSF Grant GP-2203
S. H. Lin, Y. S. Yeh (Prof. K. K. Mei)

The objective of this research project is to increase the gain of a log-periodic antenna.

This project has made a significant advance since last November. The first model with a split-feed system* has been replaced with a serpent feed array (Fig. 1). The disadvantage of the split-feed system was that the transmission line had to traverse several elbows and junctions before it reached dipole, hence the design was very critical to imperfections in fabrication. The typical radiation patterns of the serpent-feed arrays (Figs. 2 and 3correspond to 4-element and 8-element arrays. These arrays give the same radiation patterns over the bandwidth designed for, thus proving the frequency-independent nature of the design.

The input VSWR of the serpent array is about 2.2 or less and the side-lobe level is about 13 db. The experimental work of the last two quarters has confirmed our concept of high-gain broad-band antennas. In the next six months, the research will be extended to reduce the VSWR and the side-lobe level and also explore the possibility of building very large arrays. The size of the antenna that can be investigated at present is limited by the capacity of available etching facility. A new fabrication technique involving the use of copper tape has been investigated and appears very promising.

---

*ERL Consolidated Quarterly Progress Report No. 15, August 16 - November 15, 1964; p. V-6.

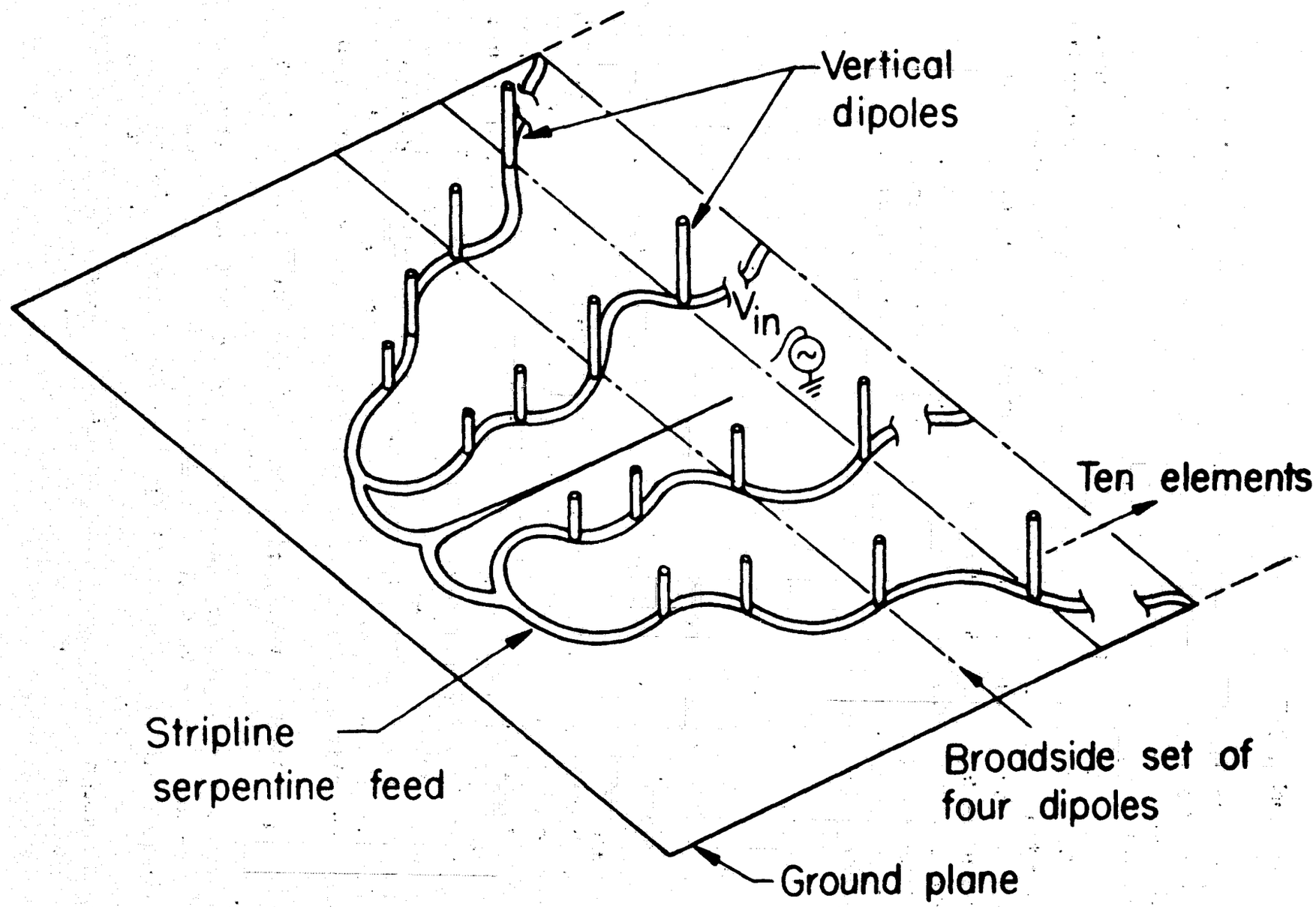

Fig. 1. A perspective view of a serpent array.

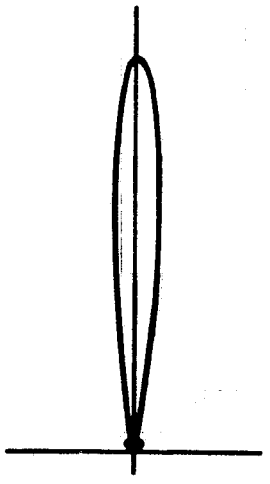

Fig. 2. H-plane power pattern of a four-element log-periodic array.

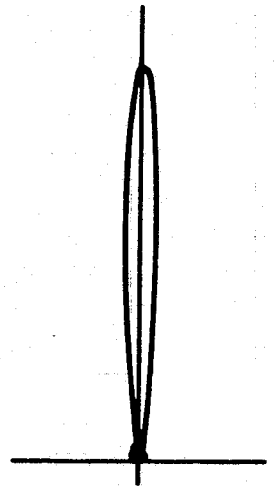

Fig. 3. H-plane power pattern of an eight-element log-periodic array.

COPLANAR LOG-PERIODIC ARRAYS

NSF Grant GP-2203
S. H. Lee (Prof. K. K. Mei)

The objective of this project is to extend the ideas of log-periodic arrays to obtain three-dimensional pencil-beam radiation patterns. This can be done by stacking coplanar log-periodic arrays in the third dimension.

The first step in this project is to investigate the behavior of coplanar log-periodic arrays. Coplanar log-periodic arrays have almost the same design parameters as other log-periodic arrays being investigated in the Electronics Research Laboratory, except that all of the radiating elements of the coplanar arrays lie on the same plane of the transmission line systems, which may have undesirable effects on the radiation. A preliminary design shown in Fig. 1 is intended to use parts of the transmission system as directors to the radiators. Thus far, the experimental results show great promise. A typical radiation pattern of a coplanar array is shown in Fig. 2. To see the scattering effect of the transmission system on radiation, dummy transmission lines were added. The transmission system did not disturb the radiation as seriously as had been expected.

The first experimental model has many imperfections because of poor fabrication techniques. A new model is being constructed for further investigation. When a dependable coplanar log-periodic array is obtained, a pencil-beam frequency-independent antenna will be built.

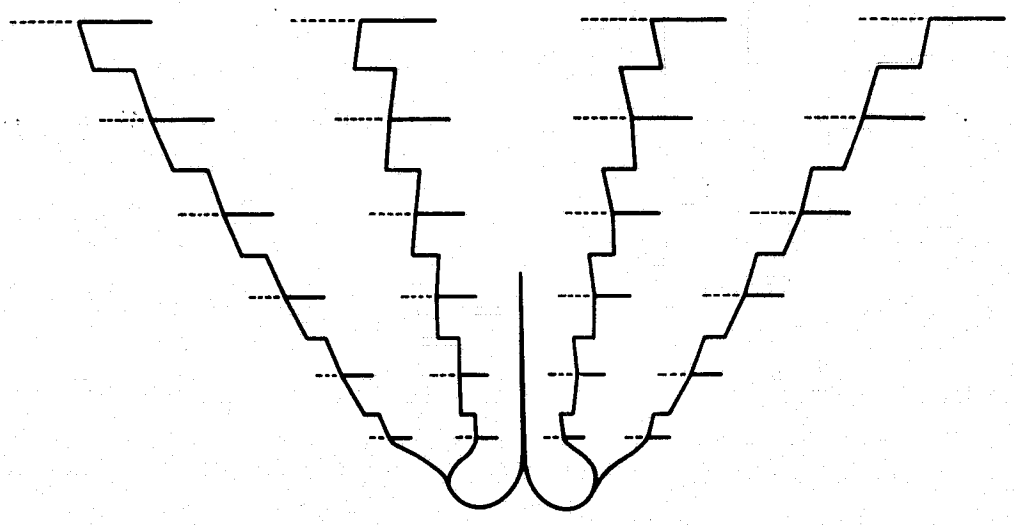

Fig. 1. A four-element coplanar log-periodic array.

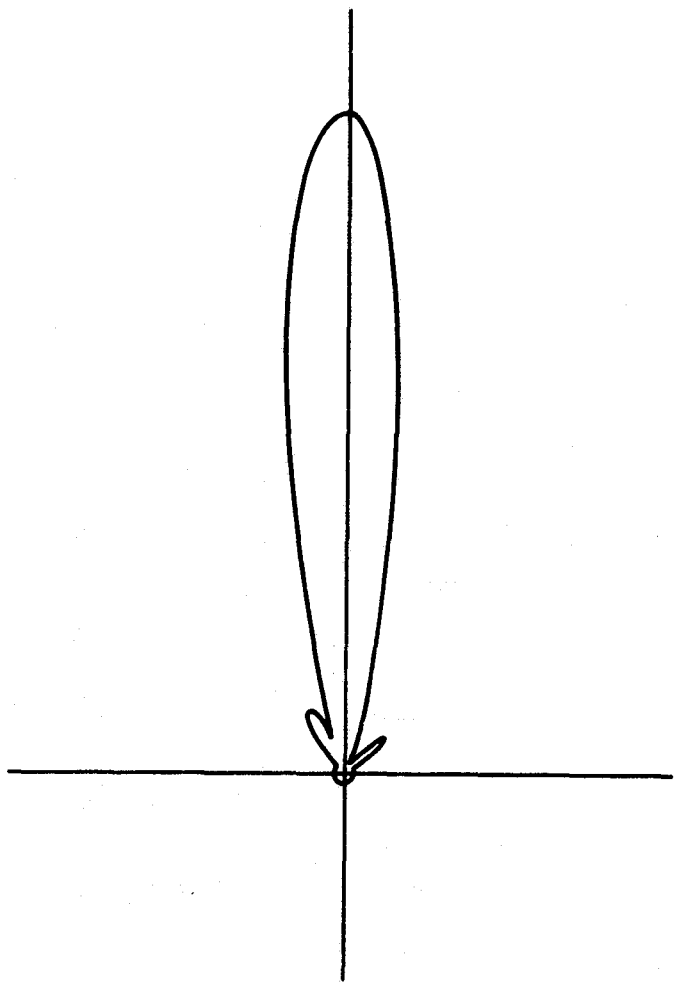

Fig. 2. Typical radiation pattern of a four-element coplanar log-periodic array.

LOG-PERIODIC, CAVITY-BACKED SLOT ARRAY

JSEP Grant AF-AFOSR-139-65
A. Roederer (Prof. M. J. Gans)

The purpose of this study is to realize a frequency-independent slot array, comparable to the dipole arrays which have been successfully developed and experimented with by the Electronics Research Laboratory. The first step has been to investigate the performance of a single cavity-backed slot.

The antenna is fed by a strip line running across the slot above a thin sheet of dielectric; the displacement current due to the interruption of the line excites the cavity, and the slot produces backfire, vertically polarized, radiation. This type of feeding is being investigated in order to incorporate the cavity-backed slots into a high-gain log-periodic "snake array;" the feeding technique is the unique feature of this study.

Several measurements (insertion loss, radiation pattern, and input impedance) have been performed on the single cavity, and the results have been compared with results from similar measurements on the dual half-wave dipole. Other measurements are being made to

complete the determination of the element of the future cavity-backed slot log-periodic array.

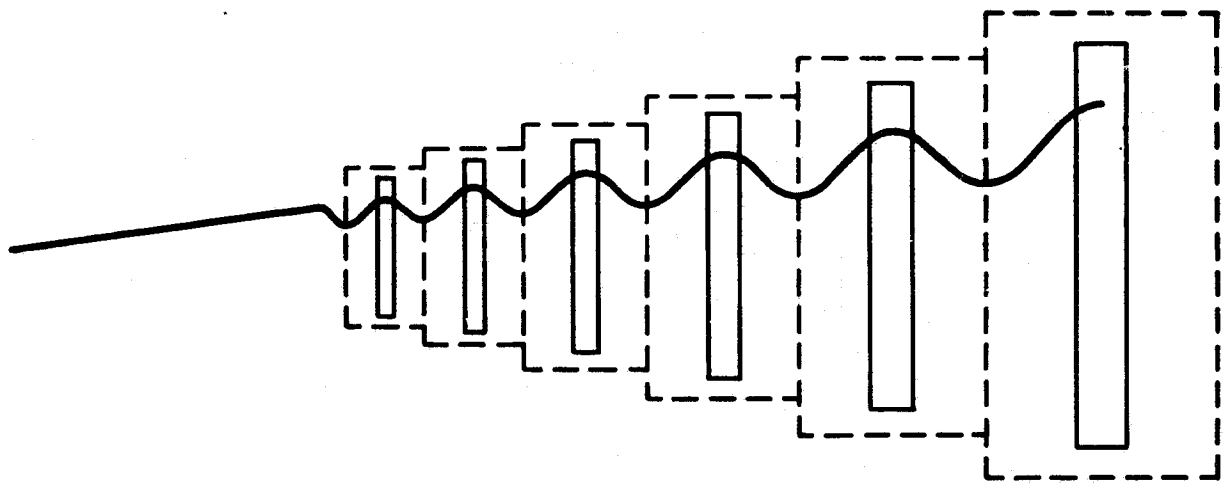

"Snake Array"

STUDY OF FREQUENCY-INDEPENDENT ANTENNAS

NSF Grant GP-2203
P. Kaiser (Prof. V. H. Rumsey)

1. The unidirectional log-spiral antenna

As a result of investigations of high-gain frequency-independent antennas,* a new type of unidirectional log-spiral antenna has been developed.

It was proved that truncation can not be obtained with the straight continuous spiral antenna.* On the other hand, the frequency-independent behavior of the plane log-spiral antenna is well-known. By changing the inclination of the sidesheets of the straight spiral, the effectiveness of truncation can be varied: The size of the active region will be determined by this effect. Hence, it is possible to choose a small half-power beamwidth through small inclination and vice versa. To obtain unidirectional radiation, the cone angle ψ has to be small so that no power is radiated in this direction.

The investigated structure (Fig. 1) had an expansion ratio of 1.5, the minimum and maximum diameters were 5 mm and 50 cm, respectively. The angle of inclination α was 30 and the cone angle $\psi = 30°$. The signal was detected by a small diode placed across the center of the spiral. The antenna can be fed by placing a transmission line on the back of the sheets.

The resulting radiation patterns were frequency-independent in the investigated range (1.8 to 9.5 Gc), unidirectional (front-to-back

*Annual Report on Frequency Independent Antennas, ERL Report No. 65-9, March 29, 1965.

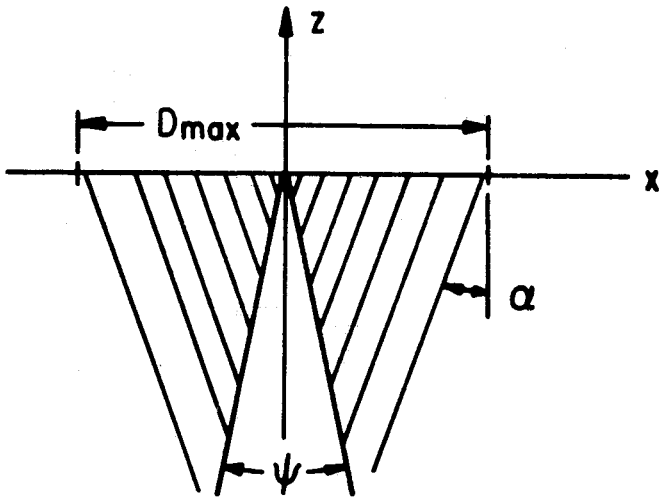

Fig. 1.

ratio larger than 20 db), and had very good circular polarization (mostly lower than axial ratio of 1.1). The half-power beamwidth had characteristic values of 60 , however, maximum values of 130 could be observed. The variations within one period were comparatively small. Repeating patterns are shown in Fig. 2.

The discussed model can be compared with the conical spiral antenna. However, because of its special construction it offers new possibilities, for example, complete elimination of back-radiation and excellent circular polarization.

2. Investigation of a log-periodic helical array

The possibility of obtaining high gain frequency-independent radiation in the broadside direction from a log-periodic helical array (Fig. 3) was investigated. The application of this feature would be the radial assembly of many such arrays, which would give a unidirectional, high gain, frequency-independent antenna.

Until now, a working model of a frequency-independent broadside array has not been found. Theoretical considerations with the k-β diagram point out the difficulties involved. The helix, as a single element of a frequency-independent array, is itself a periodic structure with frequency dependency of radiation pattern and input impedance. In order to use the axial mode of radiation it is necessary to eliminate the radiation of those elements in front of the region in which axial radiation occurs. This led to the development of special filter circuits with the strip-line technique.

A bandpass filter in the form of closed-loop resonance coupling to the single helices was unsuccessful. The resonance and the predetermination of the active region let most of the energy go through the structure without being radiated. Direct coupling of the helices with various loads of the transmission line (changing the impedances of the transmission line) gave good attenuation (approx. 30 db and more) with low VSWR. However, all elements of the structure contributed to the

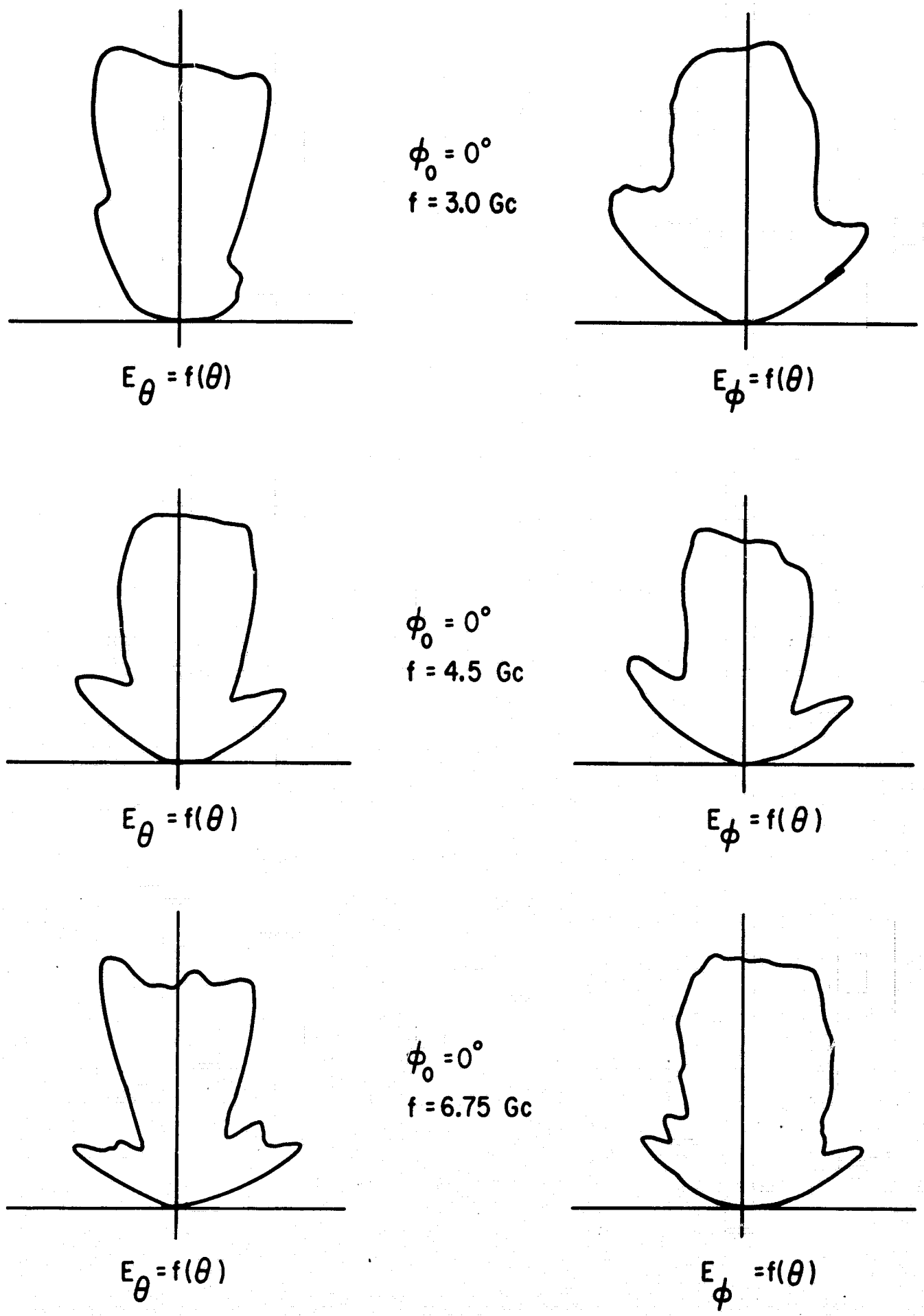

Fig. 2. Repeating patterns of the unidirectional inwardly inclined log-spiral antenna.

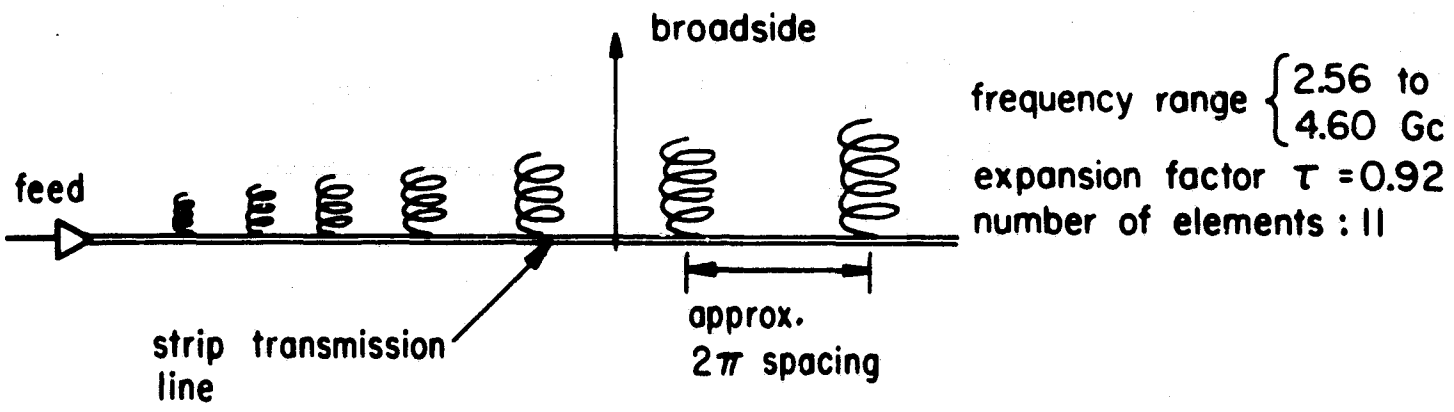

Fig. 3.

radiation and no well-defined active region could be observed.

A capacitive coupling, constructed with two closely-spaced (one quarter of a wavelength) stubs -- one connected to the transmission line, the other to the helix -- was supposed to suppress radiation from elements before the desired active region. Measurements of the VSWR showed that most of the energy was reflected. This could be expected where the stubs were not loaded sufficiently by the helix. The stubs acted as short circuits which were transformed through the transmission line and caused the reflections.

Further experimental and theoretical investigations will be performed to check the realizability of this type of antenna. A special feature of this antenna is that it offers the possibility of adjusting the phase of the single elements of a circular array by merely turning the helices around their axes.

CALCULATION OF CURRENT DISTRIBUTION ON EQUIANGULAR SPIRAL ANTENNA

NSF Grant GP-2203
Y. S. Yeh (Prof. K. K. Mei)

As reported previously,* a computer program for current distribution on the equiangular planar spiral antenna was completed. Efforts were made to interpret the calculated current distribution in terms of modes with different attenuation and propagation constants, or, if possible, the modes which have varying propagation constants dependent upon the radius of curvature of the spiral arm, but as yet no conclusion has been drawn.

A computer program for a conical spiral antenna was completed. The geometry of the conical antenna is defined by the projection of a planar spiral $\rho = \pm ie^{a\phi}$ upon a cone with angle $\theta = \theta_0$, (Fig. 1).

---

*ERL Consolidated Quarterly Progress Report No. 15, August 16 - November 15, 1964.

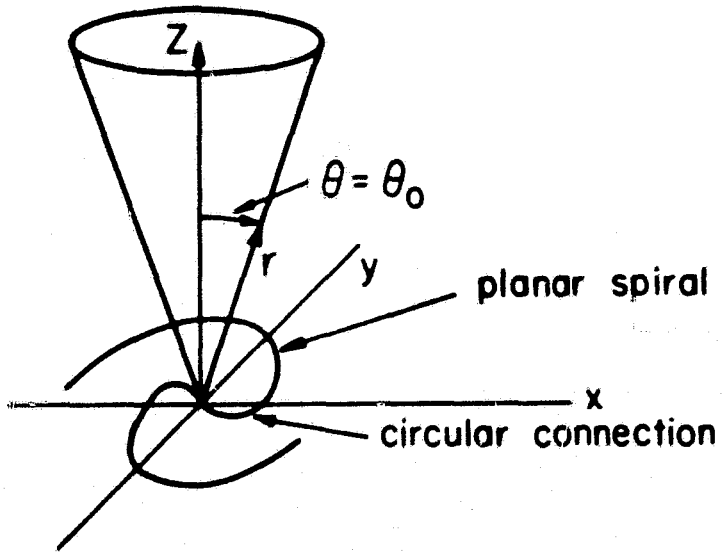

In spherical coordinates :

$$r = \frac{c'}{\sin\theta} e^{a\phi} = C e^{a\phi}$$

$$\theta = \theta_0$$

Testing this program by the extreme case of $\theta_0 = 90°$ gives exactly the same results as obtained with a previous planar program. This indicates that both programs are correct.

A series of runs have been made for antennas of the same length but with different cone angles. The results indicate that as the input impedance decreases, the cone angle θ_0 decreases. The attenuation of current becomes more rapid with tighter spirals.

A typical example of the current distribution on the conical spiral antenna is shown in Fig. 2. The input impedance is 166-j70 ohms. The current distribution is almost constant in the first λ. From 1λ to 2.5λ, current decays rapidly. This indicates the presence of an active region on the conical antenna. The current becomes extremely small from 2.5λ and above, which justifies the truncation of the antenna and also the frequency-independent behavior. The phase plot of this current distribution has also been investigated. As theoretically predicted, the results show a fast wave in the active region.

LOG-PERIODIC ANTENNAS

NSF Grant GP-2203
S. H. Lee (Prof. K. K. Mei)

The computer program based on the integral equation

$$\int I(s')\,\Pi(s,s')\,ds' = B\cos ks - j\frac{V}{2Z_0}\sin ks$$

$$\Pi(s,s') = G(s,s')\,\hat{s}\cdot\hat{s}$$

$$- \int_0^s \left[\frac{\partial G}{\partial \xi}\,\hat{\xi}\cdot\hat{s}' + \frac{\partial G}{\partial s'} + G\frac{\partial(\hat{\xi}\cdot\hat{s}')}{\partial \xi}\right]\cos k(s-\xi)\,d\xi$$

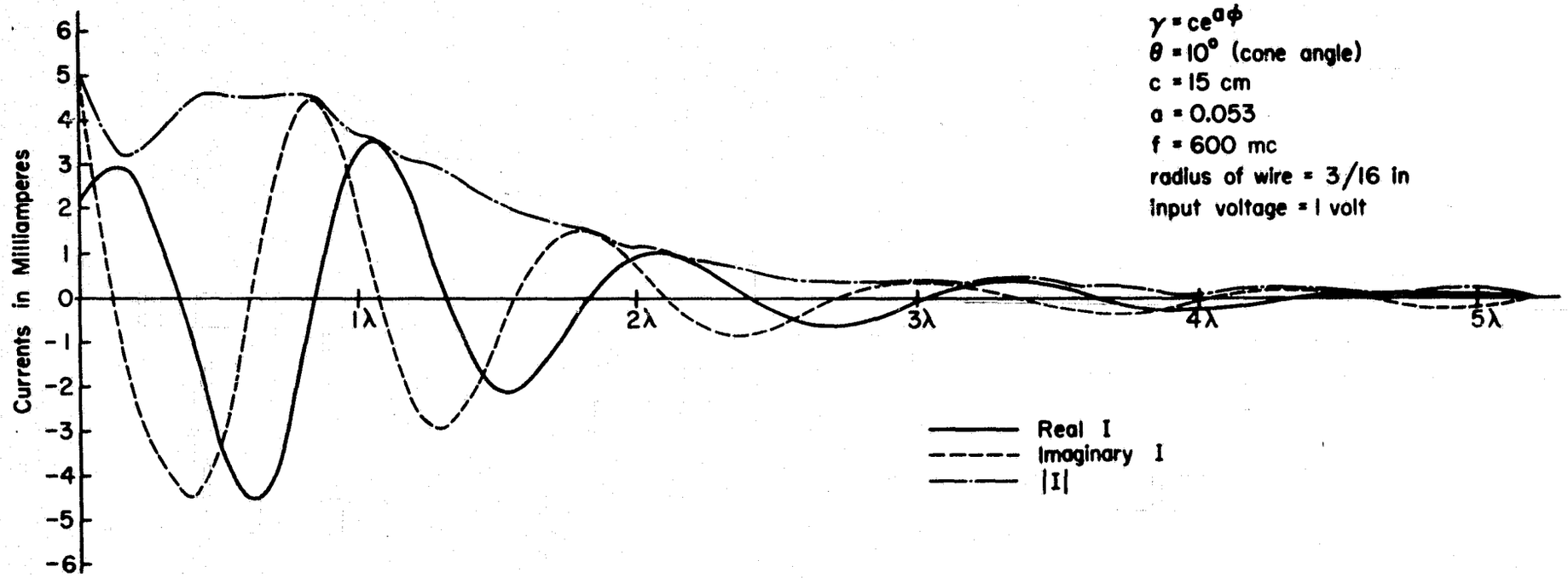

Fig. 2. Current distribution on the conical spiral antenna.

for a symmetrical zig-zag log-periodic dipole has been revised. This revised program provides more accurate current distribution on the antenna, and great saving in computer time. More accurate current distribution is obtained by carrying out the numerical integration

$$\int_0^s \left[\frac{\partial G}{\partial \xi}\,\hat{\xi}\cdot\hat{s}' + \frac{\partial G}{\partial s'}\right] \cos k\,(s-\xi)\,d\xi$$

carefully because the integrand varies very rapidly as $\xi \rightarrow s'$ when s' is near a bend. Computer time for the same antenna is saved by more than 50% by reorganizing the program.

Modification of the above-mentioned computer program for a V-shaped, zig-zag, log-periodic dipole is nearly completed.

We shall soon be able to start a systematic calculation of not only current distribution on the antenna but also its input impedance and radiation patterns, and to make direct comparisons between our results from theoretical calculation and the experimental measurements obtained by Bell, Elfving, and Franks. *

In the next six months we shall investigate the feasibility of applying Floquet's theorem to the current distribution on a uniformly zig-zag antenna.

INTEGRAL EQUATION FORMULATION OF A DIPOLE IN A COMPRESSIBLE PLASMA

JSEP Grant AF-AFOSR-139-65
S. H. Lin (Prof. K. K. Mei)

The objective of this project is to investigate the current distribution on a dipole antenna when immersed in a compressible plasma.

The current distribution on a dipole antenna in a cold or non-compressible antenna can be easily obtained by conventional techniques. When the plasma is warm or compressible, an acoustic wave will be coupled to the electromagnetic wave. This acoustic wave is known as the plasma wave, whose presence considerably modifies the solutions to Maxwell's equation.

The integral equation of the current distribution has been derived:

$$\mu \int_L J(z')\,\Pi\,(z,z')\,dz' = C' \cos k\,z + D \sin k|z|\ ,$$

---

* R. L. Bell, C. T. Efving, and R. E. Frank, "Logarithmically periodic antenna," IRE Trans. Antenna & Propagation, Vol. AP-8, pp. 559-567, November 1960.

where

$$\Pi(z, z') = G(z, z') - \left(\frac{\omega_p^2}{\omega^2}\right) G_p(z, z')$$

$$+ k\left(\frac{\omega_p^2}{\omega^2}\right)\int_0^z G_p(\zeta, z') \sin k(z - \zeta)\, d\zeta$$

where K = Boltmann's constant,

e = = electron charge,

m = electron mass,

T = absolute temperature,

n_0 = plasma density,

ω_p = plasma frequency $= \sqrt{\frac{n_0 e^2}{\epsilon_0 m}}$

$v_0 = \sqrt{3KT/m}$,

$\epsilon_r = \left(1 - \frac{\omega_p^2}{\omega^2}\right)$,

$k = \frac{\omega}{c}\sqrt{\epsilon_r}$,

$k_p = \frac{\omega}{v_0}\sqrt{\epsilon_r}$,

$$G(z, z') = \frac{e^{-jk|\bar{z} - \bar{z}'|}}{4\pi|\bar{z} - \bar{z}'|} ,$$

and

$$G_p(z, z') = \frac{e^{-jkp|\bar{z} - \bar{z}}}{4\pi\ |\bar{z} - \bar{z}'|} .$$

Since $v_0 < c$, we have $k_p >> k$; therefore, numerical solution to the integral equation is, at present, only practical for electrically short antennas. Preliminary calculations show that if the antenna is 1/2000 of an electrical wavelength long 1 plasma wavelength long, the presence of the plasma may raise the radiation resistance by 10^6. This indicates that at VLF the plasma wave dominates the radiation of a

small antenna. This project is expected to reveal many unknown facts in plasma radiation. It is hoped that our calculation will greatly facilitate the technique of plasma diagnosis.

SOURCES FOR CIRCULAR POLARIZATION

NSF Grant GP-2203
D. Kajfez (Prof. D. J. Angelakos)

The investigation of sources of circularly polarized waves * is being continued. Besides its possible use as a source for testing circularly-polarized antennas, a source of circularly polarized electromagnetic wave is a useful building block for certain electromagnetic field devices.

If, as in Fig. 1, two identical dipole antennas are immersed in the field of a circularly polarized wave and one dipole is rotated by the angle ϕ_d with respect to the other dipole, then the phase difference of the received signals on the output terminals of both dipoles is equal to the ϕ_d. This phase difference depends only on the physical angle ϕ_d and not on frequency. Furthermore, if the source antenna is rotated

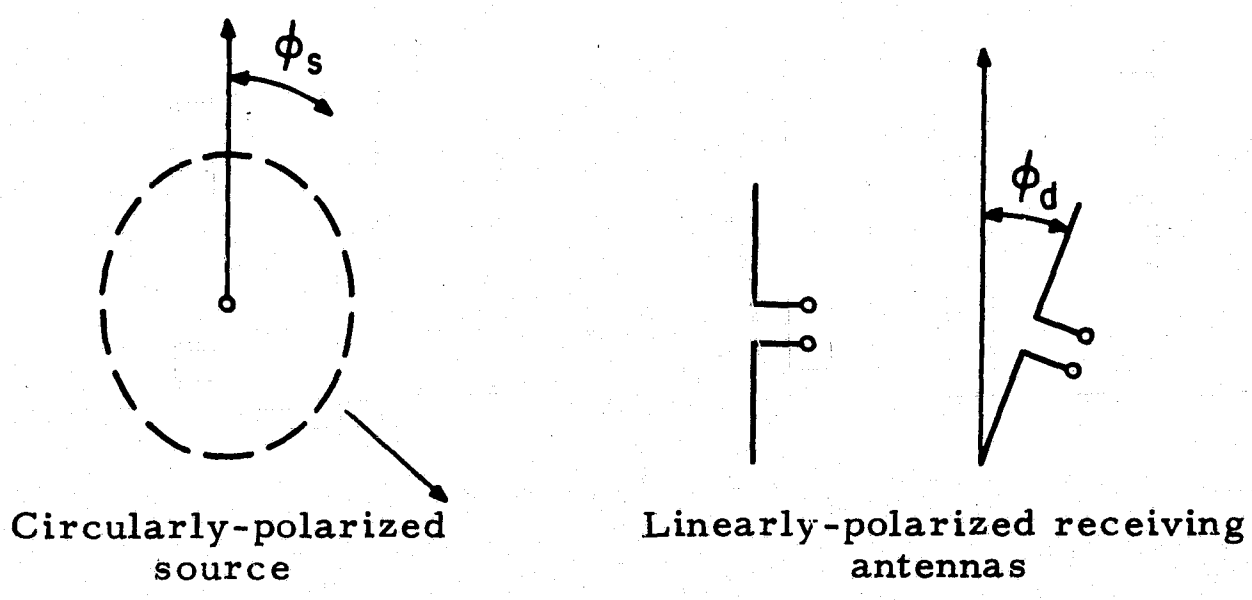

Fig. 1. Frequency-independent phase shifter.

*ERL Annual Report on Research in Frequency Independent Antennas, Report No. 65-9, March 29, 1965.

by an angle ϕ_s, both received signals are shifted in phase by the same angle ϕ_s, their phase difference still remaining ϕ_d. The arrangement of Fig. 1 clearly indicates the possibility of constructing a frequency-independent phase shifter, which offers an absolute phase calibration.

If the source produces a slightly elliptically polarized, rather than purely circularly polarized, wave, a phase error is introduced. To estimate this error, the elliptically polarized field is decomposed in two circularly-polarized fields, denoted E_L (left hand) and E_R (right hand), as shown in Fig. 2.

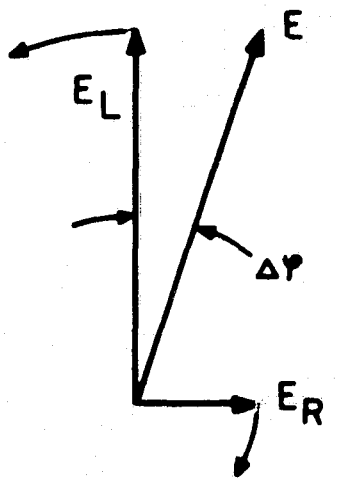

Fig. 2. Evaluation of phase error.

The greatest deviation, $\Delta\phi$, of the resulting field E is given by

$$\Delta\phi \approx \frac{E_R}{E_L} , \tag{1}$$

which represents the phase error of the phase shifter of Fig. 1. If one admits a phase error of two degrees, the axial ratio (abbreviated AR) of the wave produced by a circularly polarized source should be

$$AR = \frac{1 + \frac{E_R}{E_L}}{1 - \frac{E_R}{E_L}} \leq 1.07.$$

Another possible application of a circularly polarized source is represented in Fig. 3. Two circularly polarized sources are spaced apart by distance d and mechanically rotated with respect to each other through angle ϕ. The resulting radiation pattern of the right-hand, circularly polarized wave will be tilted by angle θ, given by

$$\sin\theta = \frac{\lambda\phi}{2\pi d} . \tag{2}$$

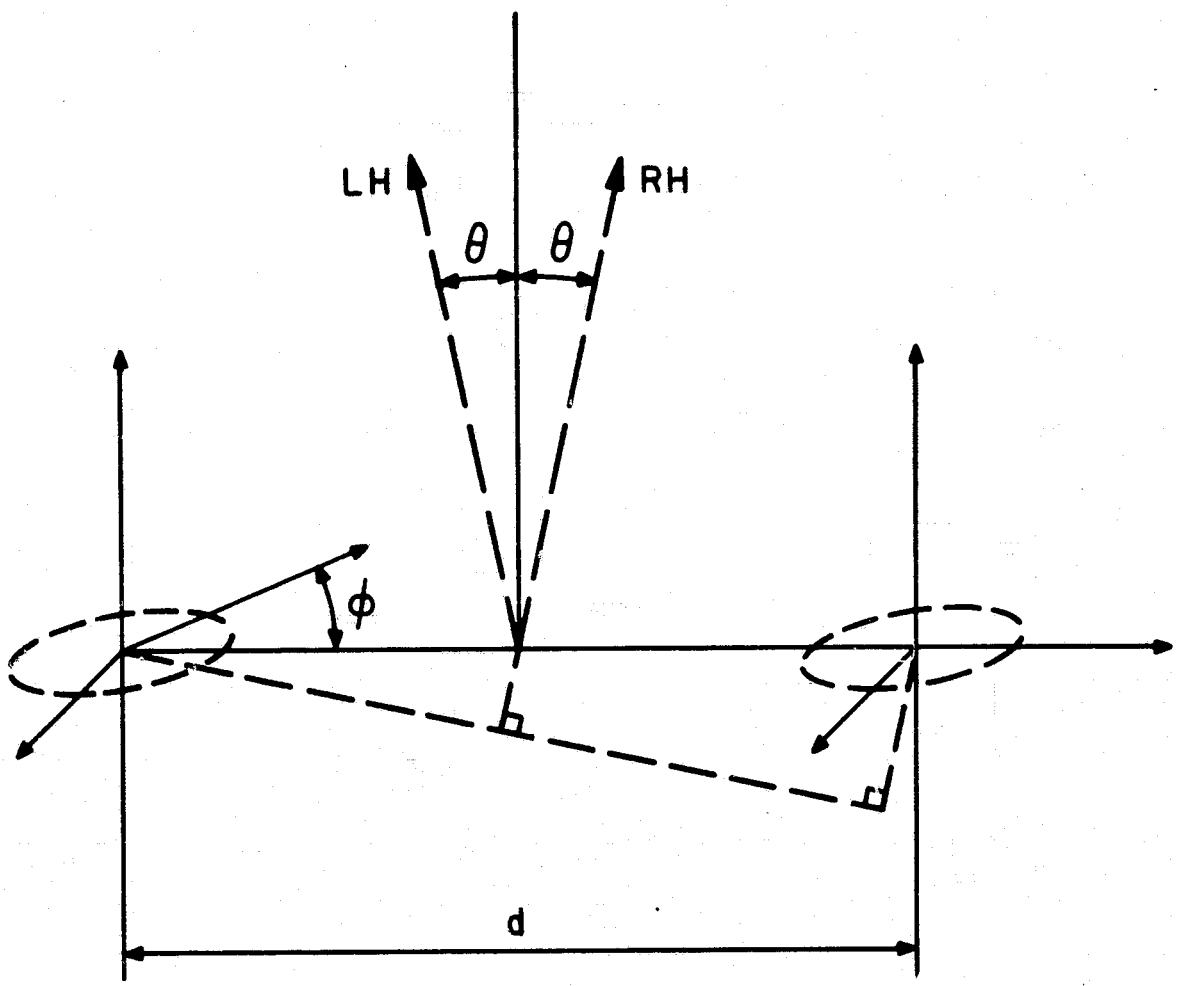

Fig. 3. Beam tilting in an array of circularly-polarized antennas.

It is obvious from Fig. 3 that the tilting angle θ can be controlled directly by the mechanical rotation ϕ of one of the sources.

In case that sources are not ideal and radiate some amount of the spurious left-hand polarized wave, the main lobe of the left-hand radiated field will be tilted the same angle in the opposite direction. This lobe represents the unwanted radiation and should be kept at a much lower level than the main lobe of the right-hand radiated field. Assuming that the level of the unwanted lobe should be suppressed by 25 db, the allowed AR of the circularly polarized source is

$$AR = \frac{1 + \frac{E_L}{E_R}}{1 - \frac{E_L}{E_R}} \leqq 1.12 .$$

It follows from the previous discussion that the source of a circularly polarized wave with an axial ratio better than 1.1 can represent a useful building block for frequency-independent phase shifters or for mechanically scanned arrays.

Experiments are being performed with two types of antennas -- helical and planar, equiangular-spiral antennas -- which appear to be suitable as sources of the circularly polarized wave. The results of this investigation will be reported soon.

THEORY AND DESIGN OF SINGLE BEAM FREQUENCY SCANNING DIPOLE ARRAYS

NSF Grant GP-2203
S. Cho (Prof. K. K. Mei)

The objective of this project is to design a frequency scanning dipole array which gives a single beam.

The theory of frequency scanning antennas is well-known. The conventional frequency scanning dipole arrays give two main beams. This project studies a new method of designing frequency scanning dipole arrays which will scan with a single beam.

The geometry of the array is shown in Fig. 1. The two-dimensional array consists of two sets of arrays -- one vertical (array A), the other (array B) is inclined at angle α. Their k-β diagrams are shown in Fig. 2. The angle α is so chosen that one beam of each array coincides. When each vertical array is considered as a single antenna, the method of pattern multiplication applies. The scanning beams are illustrated in Fig. 3.

An experimental model is being constructed.

OPTICAL ANTENNA ARRAYS

JSEP Grants AF-AFOSR-139-64 and 65
J. C. Gibson (Prof. M. J. Gans)

An investigation of the application of microwave array techniques to laser arrays has been made, and the results published.* An abstract of the report follows.

> Although there has been some investigation of the application of array techniques to laser arrays, it has been limited to very elementary models for the elements pattern, simple types of arrays, investigations of statistical variations between individual radiators, and problems involved with the partial coherence of laser radiation. This

*J.C. Gibson, "Laser Arrays," ERL Technical Report 65-21, July 23, 1965.

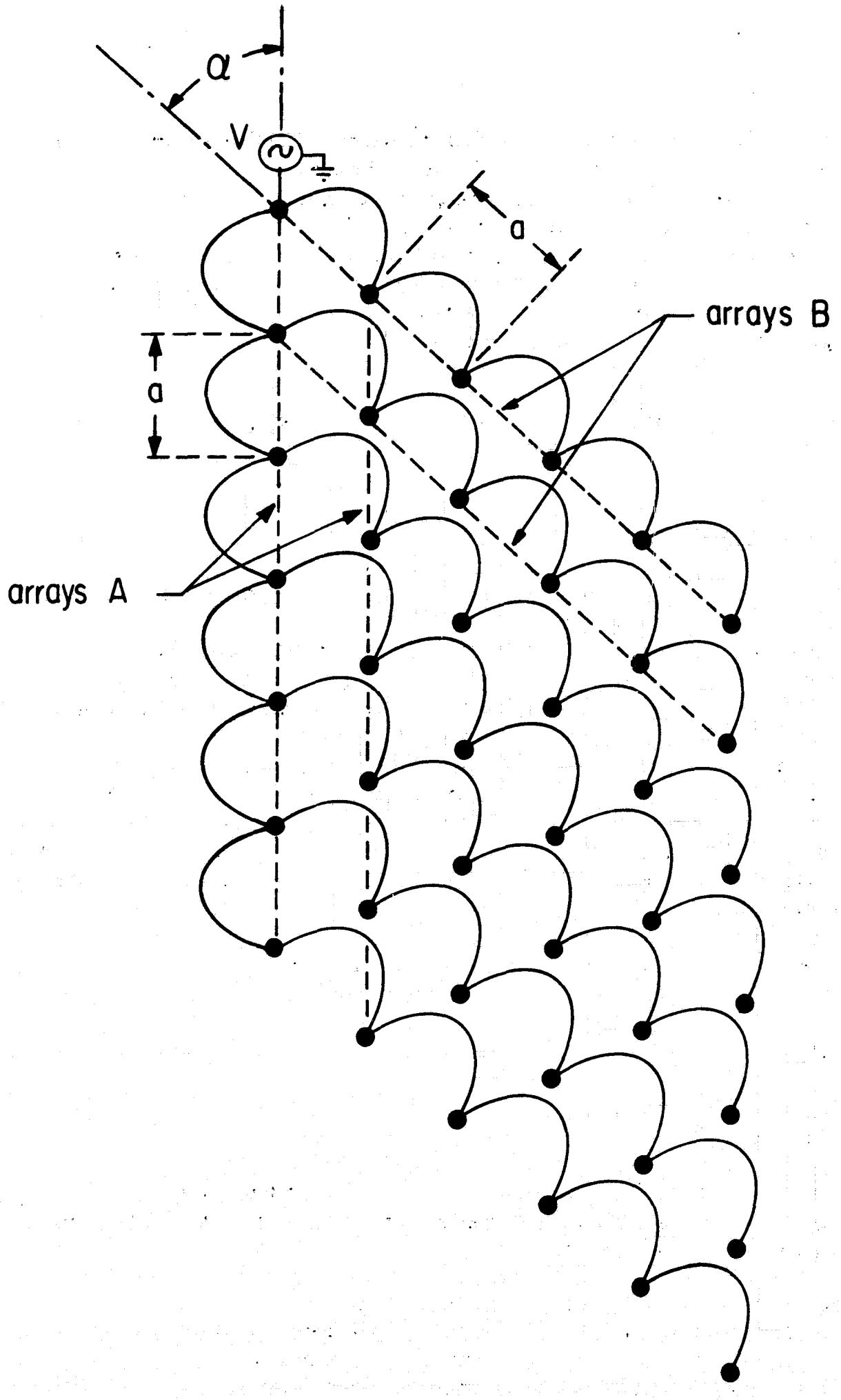

Fig. 1. Geometry of the frequency scanning arrays.

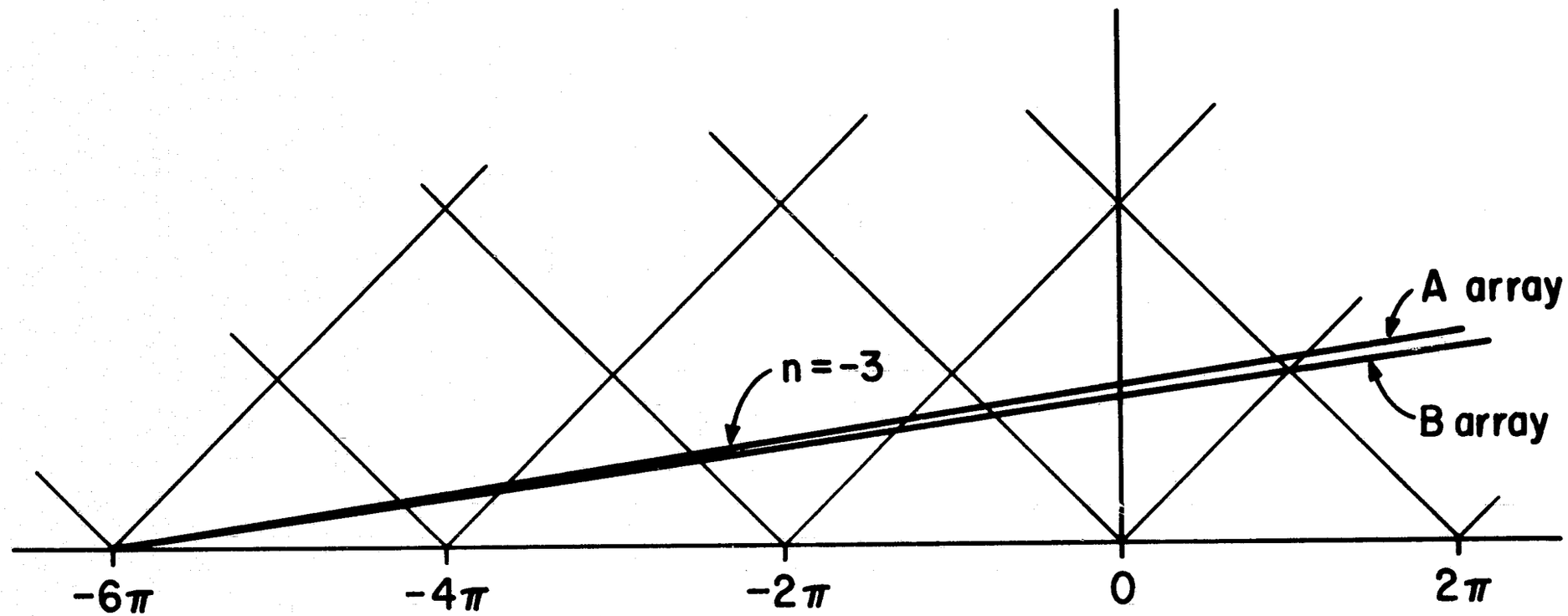

Fig. 2. k-β diagram of the frequency scanning arrays.

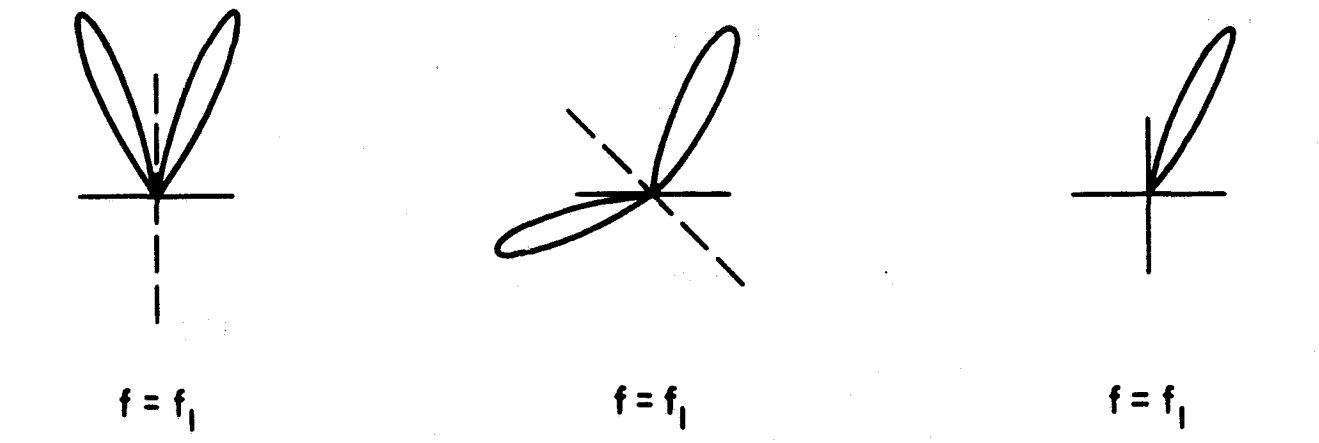

Fig. 3. (a) the radiation patterns of A-array at different frequencies,
(b) the radiation patterns of B-array at the corresponding frequencies,
(c) the resultant patterns of the scanning antenna at the corresponding frequencies.

paper deals in much more detail with the application of various types of array techniques. The laser is assumed to have a Gaussian field pattern distribution at its aperture pattern. The linear broadside array factor is applied to both the Gaussian element pattern and to an element consisting of a circular aperture uniformly illuminated with a plane wave. The Dolph-Tchebyscheff and binomial amplitude distribution array factors are applied to the Gaussian element pattern to reduce sidelobe levels with equal element spacing. Ishimaru's technique of unequal element spacing is applied to the Gaussian element pattern to reduce sidelobes, and then to suppress the secondary beam. The half-power beamwidths are calculated and compared, and the circular array and ring apertures are investigated for application to the Gaussian element pattern. Results concerning relative sidelobe levels and grating lobe levels are tabulated and compared. Conclusions are made concerning the feasibility of applying array theory to lasers with element spacings of hundreds of wavelengths.

RADIATION IN DISSIPATIVE MEDIA

ONR Contract Nonr-3653(11)

H. S. Lu (Prof. M. J. Gans)

1. Submerged Antenna

To improve the impedance of a submerged dipole antenna, a lumped circuit antenna has been considered. The antenna consists of periodic, parallel-conducting disks with LC elements between them. The L and C are calculated such that the impedance of the antenna will match this impedance of the medium. The theoretical analysis shows that this method cannot improve the gain of the dipole antenna; however, it was shown to be an effective way of controlling voltage distributions at the low frequencies involved in submerged antenna applications and could find use in the construction of aperture-type submerged antennas.

2. Distribution of Charges on a Sinusoidal Conducting Surface

To evaluate the possibility of sensing sound waves on the surface of the water by their effect on the charge distribution of the ambient dc electric field, a theoretical study of the charge distribution on a sinusoidal conducting surface was initiated. It was not possible to obtain the equation of the conformal mapping which would solve the problem; however, the eigenvalues and the eigenfunctions of this problem were found. The distribution of the charges was spanned by these eigenfunctions, but as far as numerical computation was concerned, it was felt that this was not a good approach.

3. Radiation from an Aperture in a Lossy Medium

By using Hodara's method, the radiation from an aperture in a lossy medium has been analyzed and computed. The solution does not include the surface wave. The further investigation on the surface wave is necessary for the complete description of the performance of this type of antenna.

SCATTERING OF E.M. WAVES BY A SEMI-INFINITE ARRAY OF CONDUCTING STRIPS

ONR Contract Nonr-3653(11)
H. S. Lu (Prof. K. K. Mei)

The objective of this project is to study the radiation characteristic of a semi-infinite Yagi array. The first step is to investigate the feasibility of using the Wiener-Hopf technique to solve the problem of scattering by such an array. The geometry of the conducting strips is shown in Fig. 1.

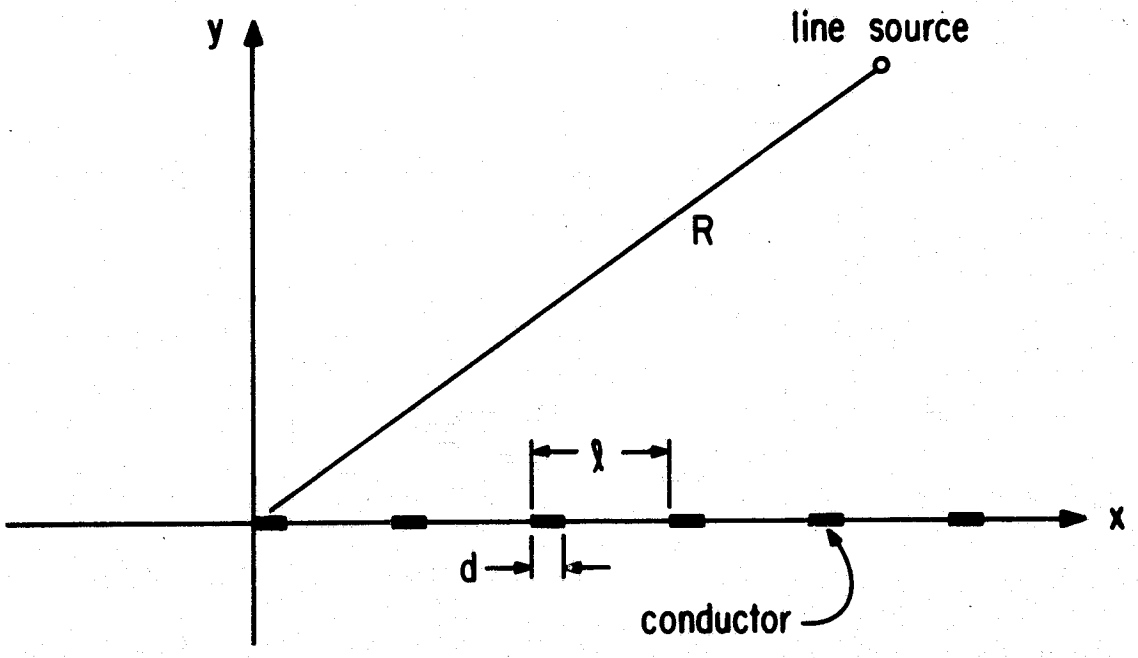

Fig. 1.

When $d << \lambda$, $d << \ell$, the sample technique can be applied. Let

$$j(x) = \sum_{m=0}^{\infty} J_m \, \delta(x - m\ell) ,$$

$$h(x) = \sum_{m=-\infty}^{\infty} H_0^{(1)} \left[k|m|\ell\right] \delta(x - m\ell) ,$$

and

$$e(x) = \sum_{m=0}^{\infty} E(m\ell\ ,\ 0)\,\delta\,(x - m\ell)\,,$$

where J_n is the total current on the nth conductor, $E(x, y)$ is the field of the line source.

From the boundary conditions, the following Wiener-Hopf integral equation is obtained.

$$e(x) = \int_{-\infty}^{\infty} j(y)\,h\,(x - y)\,dy \quad \text{for} \quad x \geq 0\,. \tag{1}$$

When the source is a large distance from the origin, the solution of Eq. 1 is given by the following expression for $j(x)$

$$j(x) = \frac{1}{\sqrt{2\pi}} \int_{-\infty+ib}^{\infty+ib} \frac{\left(\frac{Ae^{-i\left[R - \frac{\pi}{4}\right]}}{R}\right)\left(\prod_{m=-\infty}^{\infty}\sqrt{1 + \frac{k\cos\theta}{\frac{2m\pi}{\ell} - k}}\right)\left(\sum_{m=-\infty}^{\infty}\frac{1}{\alpha\ell - \ell k\cos\theta + 2m\pi}\right)}{\left(\prod_{m-\infty}^{\infty}\sqrt{1 + \frac{\alpha}{\frac{2m\pi}{\ell}}}\right)\left(\sum_{m=-\infty}^{\infty}\frac{1}{k^2 + (\alpha + \frac{2m\pi}{\ell})^2}\right)} e^{-i\alpha x}\,d\alpha$$

where A is a constant.

And the scattering field is

$$E_s(x,y) = \frac{1}{\sqrt{2\pi}} \int_{-\infty+ib}^{\infty+ib} \frac{\gamma^{-1} e^{-i\alpha x + \gamma y}\left(\frac{Ae^{i(R - \frac{\pi}{4})}}{\sqrt{R}}\right)\left(\prod_{m=-\infty}^{\infty}\sqrt{1 + \frac{k\cos\theta}{\frac{2m\pi}{\ell} - k}}\right)\left(\sum_{m=-\infty}^{\infty}\frac{1}{(\alpha\ell - \ell k\cos\theta + 2m\pi)}\right)}{\left(\prod_{m=-\infty}^{\infty}\sqrt{1 + \frac{\alpha}{\frac{2m\pi}{\ell}} - k}\right)\left(\sum_{m=-\infty}^{\infty}\frac{1}{\sqrt{k^2 - (\alpha + \frac{2m\pi}{\ell})^2}}\right)} d\alpha$$

where $\gamma = (\alpha^2 - k^2)^{1/2} = -i(k^2 - \alpha^2)^{1/2}$,

$$k = k_1 + ik_2,$$

$$k_2 \cos\theta < b < k_2,$$

the upper sign applies for $y \geq 0$, the lower for $y \leq 0$. This integration can be evaluated by the method of steepest decent, which will be investigated in the next report period.

F. SOLID-STATE ELECTRONICS

Research in solid-state electronics ranges from fundamental material studies, through device design and analysis to the study of component interactions and integrated component performance. Basic material studies are related to thin-film properties, semiconductor laser operation, epitaxial layer formation and properties, and the effects of high fields on materials. Device studies include considerations appropriate to field-effect operation, acoustoelectric interactions, and piezoelectric effects. In the integrated circuits area, considerations of design criteria for functional electronic blocks and basic system constraints are under study.

SURFACE MOBILITY IN SILICON MOS DEVICES

JSEP Grants AF-AFOSR 139-64 & 65
T. I. Kamins (Prof. R. Muller)

During this report period, an investigation was undertaken on the relation between gate voltage and surface mobility in silicon MOS devices. Initial measurements of I_d vs V_g led to a value of μ through the standard MOS formula

$$g_m = \frac{\mu_n C_0}{L} V_d. \qquad (1)$$

This method has two serious disadvantages. First, it is necessary to differentiate the curve in order to obtain g_m and hence μ. This operation is subject to serious errors since the deviation of the slope from a constant value is small. The second difficulty arises from the first-order nature of Eq. 1. The deviation of the formula from the actual physical situation may be due to effects other than the deviation of μ from a constant value. The results obtained with this method were of the form shown in Fig. 1.

When the inadequacy of the above method became apparent, we began investigating a method proposed by Grove [1] of Fairchild and used at IBM by Fang and Triebwasser [2]. In this method, the mobility

---

[1] A. S. Grove, O. Leistiko, Jr., & C. T. Sah, "Electron and Hole Mobilities in Inversion Layers on Thermally Oxidized Silicon Surfaces," IEEE Trans. On Electron Devices, 5, 248,1965

[2] F. Fang & S. Triebwasser, IBM J. Research & Development, 8, 410, 1964.

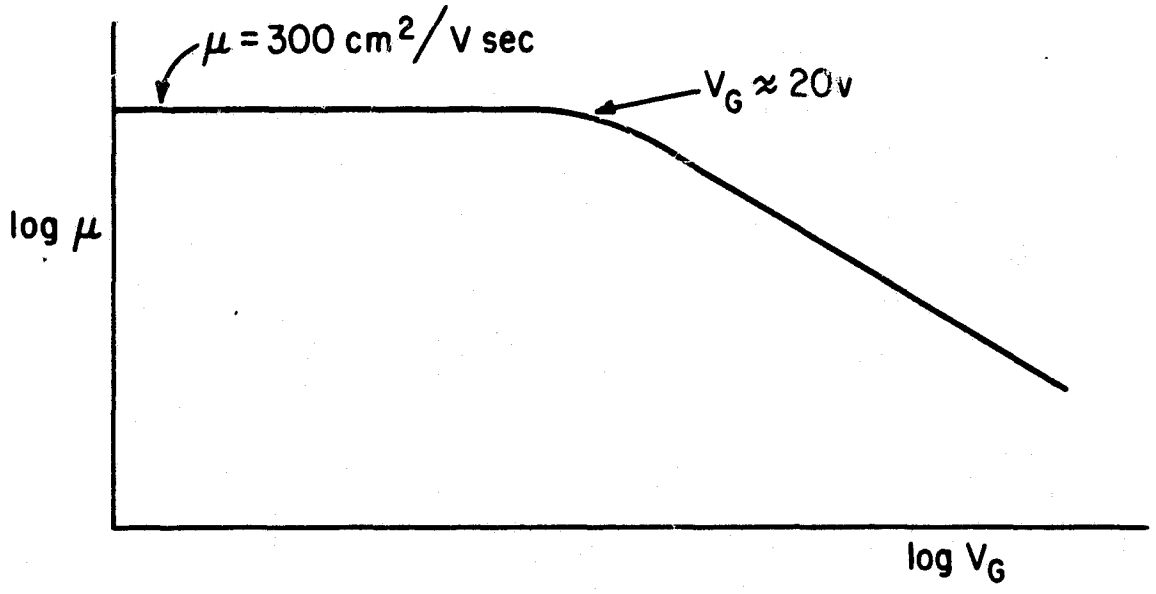

Fig. 1. Mobility as a function of gate voltage, determined from the formula $g_{sd} = -Z\mu_n Q_n / L$.

is related to the source-drain conductance through the expression

$$g_{sd} = -\frac{Z}{L}\,\mu_n Q_n , \qquad (2)$$

where μ_n is the mobility of the electrons within the inversion layer, ZLis the ratio of the channel width to the channel length, and Q_n/q is the number of electrons in the channel at zero source-drain voltage. The value of Q_n can be calculated as a function of U_s, the normalized band bending at the semiconductor surface, by the Kingston-Neustadter formulas [3] extended by Young [4]. Since g_{sd} is measured as a function of V_g, the applied gate voltage, and the relationship between V_g and U_s is known [5], the value of μ_n can be found as a function of V_g or V_s.

Figure 1 shows a typical mobility-vs-gate-voltage curve obtained from g_{sd} measurements. It can be seen that the mobility remains constant at a fraction of its bulk mobility up to about $V_g = 20$ volts then gradually decreases. The behavior is qualitatively similar to that found by Grove et al.[1], but differs somewhat quantitatively.

---

[3] R. H. Kingston and S. F. Neustadter, J. Appl. Phys., 26, 718, 1955.

[4] C. E. Young, J. Appl. Phys., 32, 329, 1961.

[5] T. I. Kamins, "Surface Mobility of Silicon MOS Devices," ERL Tech. Memo. M-120, University of California, Berkeley, May, 1965.

Grove found a low voltage mobility of 660 cm^2/V sec which begins to decrease at a critical field of 5×10^5 V/cm. Experiments in this laboratory indicate a low voltage mobility of about 300 cm^2/V sec with a critical field of 10^6 V/cm.

Our experimental results are not necessarily in conflict with those of Grove. Suppose that one mechanism limits the mobility at low gate voltages, while another mechanism dominates at high gate voltages. Since the low voltage mobility is constant, we may assume that the mechanism which dominates at low voltages is voltage independent. Now, suppose that the mechanism which dominates at high voltages is voltage dependent and that the total mobility is related to that due to the individual mechanisms by the expression [6]

$$\frac{1}{\mu_t} = \frac{1}{\mu_1} + \frac{1}{\mu_n} \quad . \tag{3}$$

This equation shows that a lower value of μ_1 would cause the critical voltage, at which the second term begins to dominate, to be higher. The mechanism which dominates at high voltages may be surface scattering from a partially diffuse surface as proposed by Schrieffer [7]. Figure 2 shows qualitatively how such mechanisms may combine.

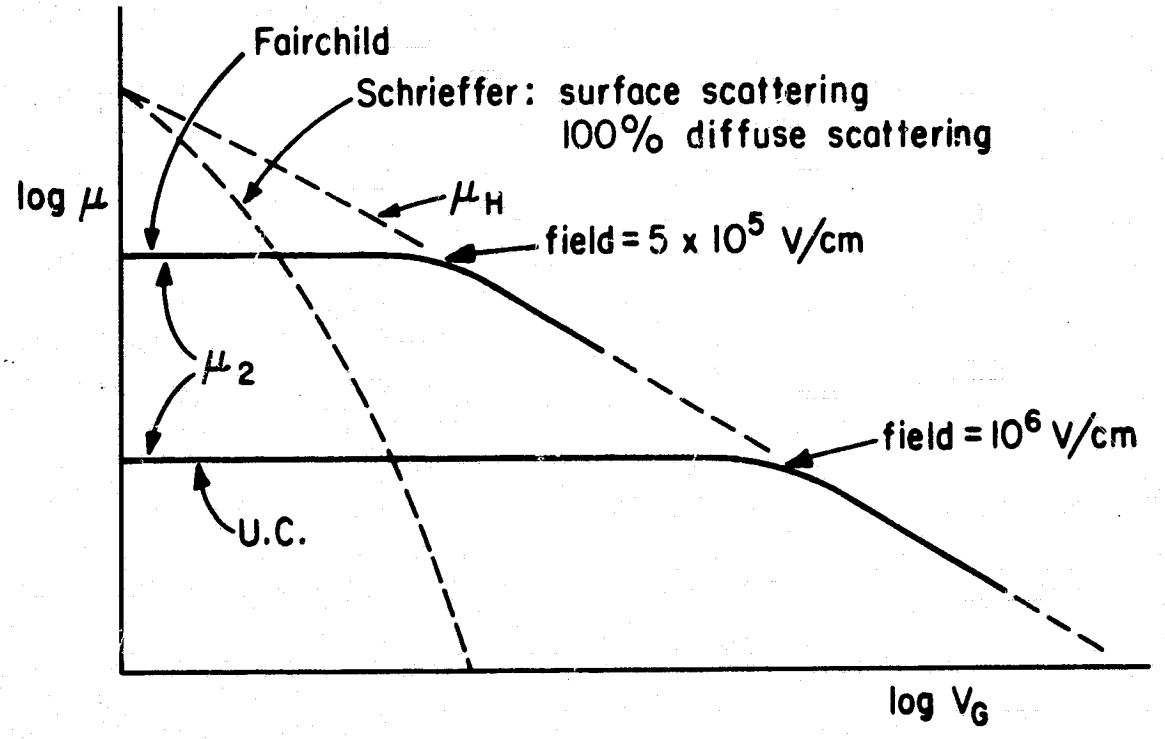

Fig. 2. Qualitative comparison of U.C. data with Fairchild data and Schrieffer theory.

[6] A. Waxman et al., J. Appl. Phys., 36, 168, 1965.

[7] J. R. Schrieffer, Phys. Rev., 97, 641, 1955.

A tentative outline of further work on this project follows. Devices with somewhat wider channel regions will be constructed, then an attempt will be made to obtain more consistent results for the μ vs V_g relation. In order to examine the region past the critical voltage, we will try to improve the low-voltage mobility obtained in this laboratory and hence, lower the value of the critical voltage. After the preliminary work is completed, an attempt will be made to investigate the temperature dependence of the region of decreasing mobility in an effort to determine the limiting mechanism effective in this region.

METAL-INSULATOR-SEMICONDUCTOR-PIEZOELECTRIC PRESSURE TRANSDUCER

University of California Support
J. Conragan (Prof. R. S. Muller)

A new electromechanical transducer that combines power gain with the transducing mechanism in one device has been designed, built, and tested. The device has been described in two publications [1], [2]. An abstract from the more complete discussion of the device as a transducer follows [2]:

> A deposited metal-insulator-piezoelectric-semiconductor (MIPS) transistor can be used as an electromechanical transducer, because of the sensitivity of the power-gain mechanism in a surface field-effect device to fixed charge in the channel. Close correspondence has been obtained between the theory of this effect and experimental observations on deposited CdS MIPS devices. The transducer action described here is quite different from that employed in other piezoelectric pressure transducers, and has some characteristics which are highly beneficial. Comparisons with conventional transducers are made, and design consideration of the MIPS transducer is discussed.

---

[1] R. S. Muller and J. Conragan, "Transducer Action in a Metal-Insulator-Piezoelectric-Semiconductor Triode," Appl. Phys. Letters, 6, p. 83, 1965.

[2] R. S. Muller and J. Conragan, "A Metal-Insulator-Piezoelectric-Semiconductor Electromechanical Transducer," presented at the Specialists' Conference on Thin-Film Active Devices, John Hopkins University, Baltimore, Maryland, April 14, 1965. To be published in IEEE Trans. on Electron Devices.

CdS THIN-FILM TRANSISTOR STUDIES

JSEP Grants AF-AFOSR 139-64 & 65
J. Fiebiger (Prof. R. S. Muller)

The substrate employed in making cadmium-sulfide coplanar TFT's is a significant factor in obtaining device reproducibility and uniformity. In order to obtain substrate conditions reproducible enough to give consistent device characteristics, a layer of silicon monoxide, approximately 1500 A thick, was deposited on the Corning 7059 substrate glass before the CdS was evaporated. It was observed that when the silicon-monoxide-coated slides were used, the deposited CdS film showed a very uniform coloration across the slide. Although several sets of TFT's were made in the same manner, only one slide yielded operable devices. On this slide, the characteristics of the three devices were very uniform. Further evaluation of SiO undercoating was dropped in favor of using evaporated high-purity quartz.

Evaporated quartz films can be used [1] to replace the SiO undercoating and insulation of the TFT. An evaporated quartz film over the undercoated TFT gives an essentially continuous glass envelope surrounding the device with only the leads passing through. Hence, one may achieve reproducible devices by the quartz undercoating and increase life as well as stability by encapsulating the TFT between two quartz films. R.C.A. has found that this procedure provides devices as stable as those kept in a vacuum encapsulation.

Techniques for quartz deposition have been evolved. Preliminary evaluation of the quartz films has been made by constructing parallel plate capacitors. (The quartz was evaporated from a tantalum boat at a temperature of 1810°C in a vacuum of 5×10^{-6} Torr.) The capacitors were found to be uniform in value to within 0.5% across the slide. The individual capacitances varied by less than 0.2% for a dc bias across them from zero to breakdown.

The transducer action of the CdS TFT's is currently under further investigation. An ultrasonic drill vibrating at a frequency of 20 KC has been used to strain the glass substrates of dc-biased TFT's. The ac output across the load resistor was a 20 KC near sinusoid with an amplitude of 0.5 volts. The transient response studies of the TFT's to a transient mechanical strain have been limited by the mechanical response of the substrates. In order to get a true measure of the transient response, deposition on new substrate materials is being investigated.

---

[1] P. K. Weimer et al., "Thin-Film Polycrystalline Field-Effect Triode," R.C.A. Second Quarterly Report, March 1965; ECOM - Contract DA 28-043-AMC-00231(E).

MICROWAVE MEASUREMENT OF EPITAXIAL LAYER CHARACTERISTICS

University of California Support
W. M. Gosney (Prof. R. S. Muller)

Bichara and Poitevin [1] related the complex reflection coefficient of incident microwaves to the resistivity and thickness of semiconductor epitaxial layers as well as to the resistivity of homogeneous semiconductor samples. In order to study this technique for measuring semiconductor resistivity, a microwave bridge circuit has been constructed (Fig. 1). It can measure the complex reflection coefficient of the semiconductor samples placed across the end of a waveguide. This bridge is to be calibrated by performing repeated measurements on known samples.

Until now, only homogeneous samples have been measured with this circuit. The preliminary results indicate that homogeneous resistivities of less than 1Ωcm cannot be accurately resolved by this circuit because the reflection coefficients approach that of a short circuit.

THIN-FILM RESISTORS

University of California Support
B. Lindgren (Prof. R. S. Muller)

The preparation of evaporated thin films of nichrome with a high resistivity and a low temperature coefficient of resistance has been studied. The problems of evaporation of an alloy, the composition of the resulting film, and the variation of the temperature coefficient of resistance were explored, and the preparation and properties of stable films of nichrome have been described in an internal report. The results include graphs of thickness vs resistance, temperature coefficient of resistance vs deposition rate, and percentage change in resistance vs annealing time. For accuracy and reproducibility, it was found that the film thickness should be greater than 100 angstroms.

---

[1] M. R. E. Bichara and J. P. R. Poitevin, "Resistivity Measurement of Semiconducting Epitaxial Layers by Reflection of Microwaves;" presented at the Congress of Precision Electromagnetic Measurements, National Bureau of Standards, Boulder, Colo., June 1964.

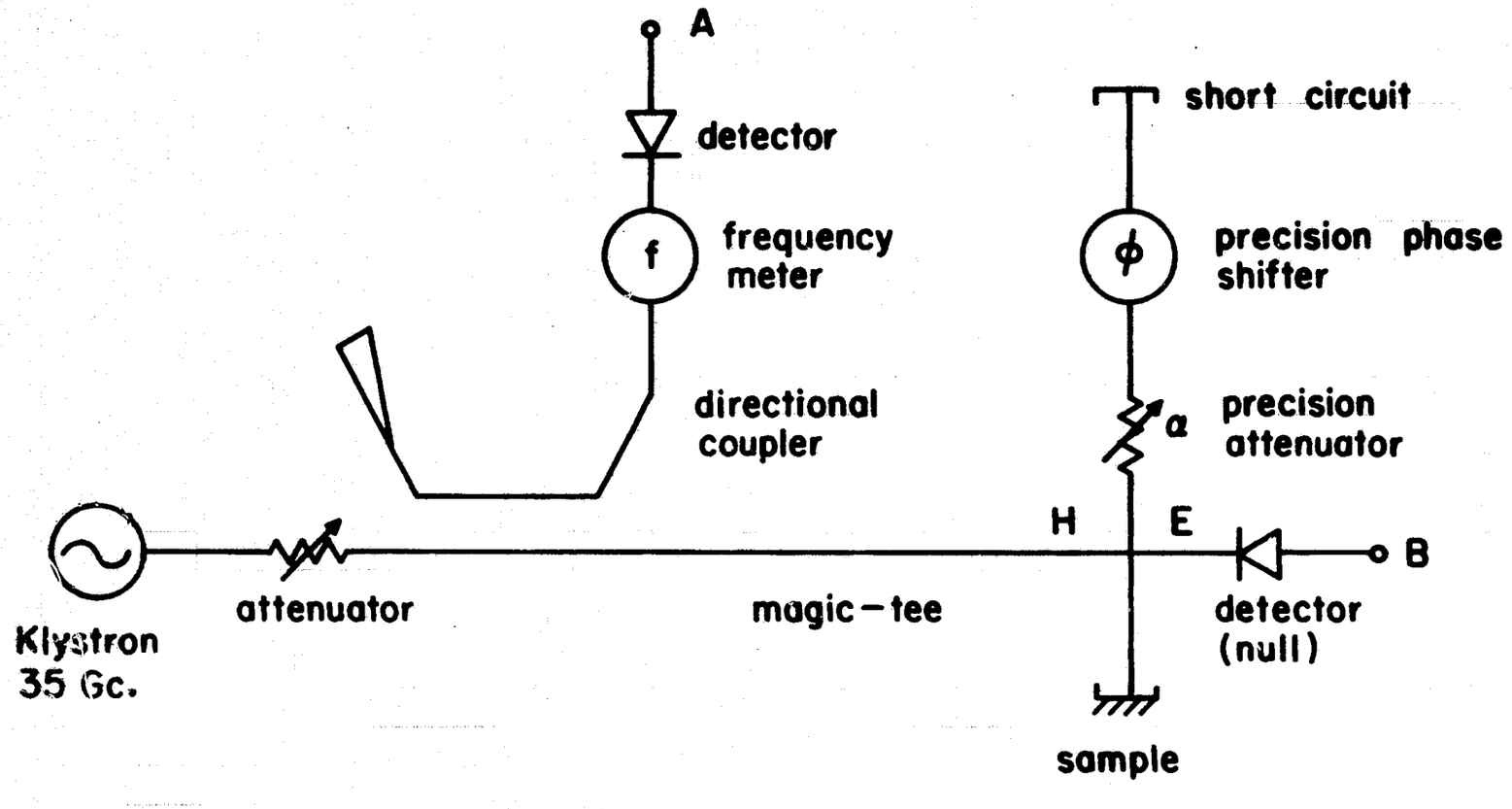

condition of balance:
adjust for null at point B

$$\text{Ref. Coeff.} = e^{-\frac{\alpha}{4.343}} \angle 2\phi$$

Fig. 1. Bridge circuit used to measure semiconductor characteristics with microwaves.

THERMALLY STIMULATED TRAP EMPTYING IN THIN CdS FILMS

University of California Support
D. Ciarlo (Prof. R. S. Muller)

The method of thermally-stimulated trap emptying was used to determine the energy levels and density of trapping states in thin CdS films. An analysis of the utility of this method as well as a discussion of trapping states in deposited films was completed. A report on this work is being written.

EPITAXIAL SILICON

JSEP Grant AF-AFOSR 139-65
R. Holmstrom (Prof. W. G. Oldham)

Since the epitaxial growth system was shut down for an extended period during the spring semester, attempts to produce any usable material have been unsuccessful. Silicon heated in the system has a haze on the surface which, when examined with a microscope, appears to have a uniform distribution of small pits. It is thought that the pitting is caused by contamination, either air leaking into the system or some residue in the system. Since pitting occurs when the wafer is heated in hydrogen, it is assumed that the source of contamination is not HCl or $SiCl_4$. In an attempt to eliminate the pitting, part of the system was rebuilt and all Teflon parts were replaced with stainless steel. The entire system was then leak tested under vacuum with a helium leak detector and now seems sufficiently leaktight. To eliminate the possibility that the wafer is the source of contamination, a more thorough cleaning process has been used. The hydrogen purifier (silver-palladium type) is the only remaining part of the system to be checked, and tests are under way to determine whether it is functioning properly.

SEMICONDUCTOR EVAPORATION IN ULTRA-HIGH VACUUM

JSEP Grant AF-AFOSR 139-65
Prof. W. G. Oldham

An ultra-high vacuum apparatus is under construction for the study of semiconductor epitaxy by evaporation, and associated problems. The complete system will consist of a vacuum apparatus (sorption-fore pumps, ion and sublimation high-vacuum pumps, and power supplies) and evaporation apparatus (electron beam heaters for source and substrate, source and substrate holders, jigging and arrangements for moving the substrates and shutters, and associated power supplies and control circuits).

The main parts of the high-vacuum system have been completed. The ion pump, sorption pumps, and vacuum chamber have been put into operation. On the initial pumpdown, following a 300°C backout for 12 hours, a pressure of less than 1×10^{-9} Torr was achieved.

Other parts of the system, namely, high-voltage supplies, filament supplies, and the evaporation station, are nearing completion. In connection with the project, three electron beam evaporation designs are presently being evaluated experimentally. They are sketched in Fig. 1. Design 1 is after Unvala and is a focusing arrangement for achieving a very local molten region in the water-cooled source. Design 2 is a defocusing scheme to obtain a uniform substrate temperature. Design 3 is a parallel beam arrangement, also for obtaining a uniform substrate temperature.

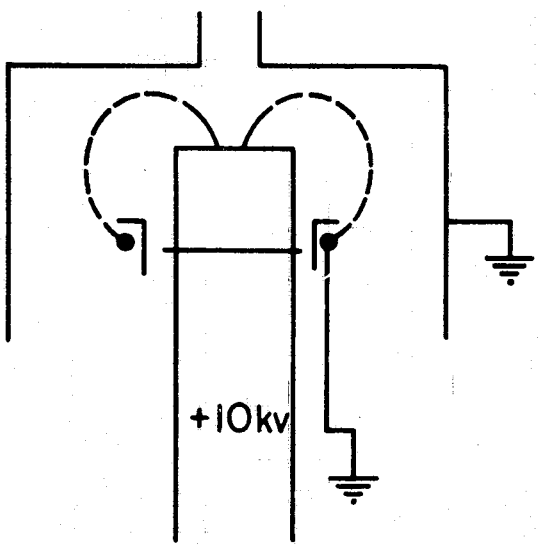

Design 1

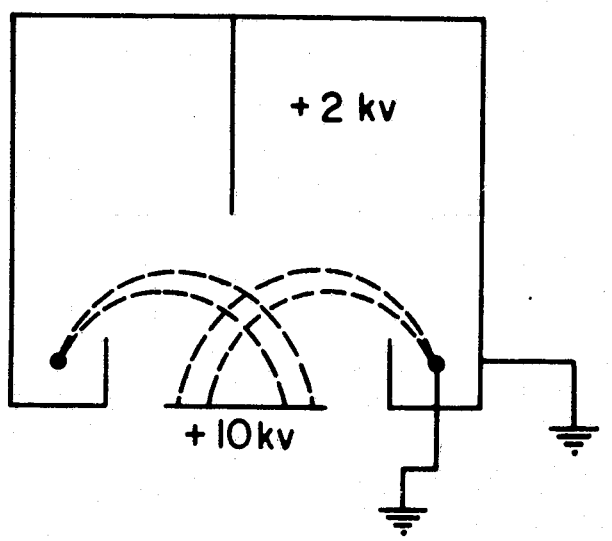

Design 2

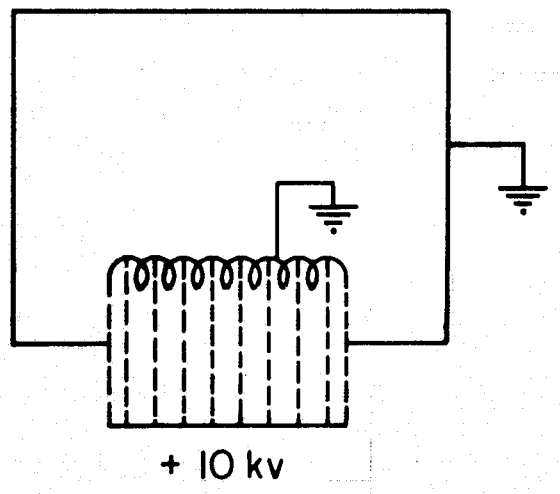

Design 3

STUDY OF MAGNETOACOUSTIC OSCILLATION IN YTTRIUM-IRON GARNET

AROD Grant DA-ARO-D-31-124-G557
G. Thomas (Prof. S. Wang)

The major purpose of this project is to investigate the coupling between the uniform magnetization, the spin-wave, and the elastic strain in yttrium-iron garnet (YIG).

When a spherical sample of YIG is placed in a strong dc magnetic field and pumped with a high-level, transverse-microwave field, it was observed by Comstock and others [1] that under certain conditions the magnetostatic mode and elastic mode will become unstable and will grow in amplitude exponentially until the growth is limited by other nonlinear effects. This acoustic mode can only occur if the threshold for elastic oscillation is lower than that for spin-wave instabilities.

So far, only the component of the acoustic mode parallel to the dc magnetic field has been observed. If the transverse component of the acoustic mode can be observed, then a complete description of the acoustic mode will be possible. The transverse component should be observable through a small pick-up coil placed near the sample. Work along these lines is in progress.

FIELD EFFECT IN GALLIUM ARSENIDE

University of California Support
M. Selser (Prof. W. G. Oldham)

The feasibility of constructing a gallium arsenide MOS transistor with a thermally grown oxide is being studied. Wafers of gallium arsenide cut on the different crystal planes have been oxidized. The (111) arsenic and gallium planes oxidize very slowly while the oxide on the (110) plane is irregular. The (100) plane gives an oxide with a very good appearance. Attempts to measure the surface state density were unsuccessful because of the low breakdown voltage of the oxide.

When the equipment assembled for the pyrolytic deposition of silicon dioxide is in working order, the properties of the gallium-arsenide-deposited oxide and the gallium-arsenide, thermal oxide-deposited silicon-dioxide systems will be studied.

A vacuum system for sealing ampoules for closed-tube diffusions is under construction. When this is completed, studies of diffusion into high resistivity (10^7 ohm-cm) gallium arsenide will be undertaken.

---

[1] R. L. Comstock, J. Appl. Phys., 34, 2427, 1964.

SECOND BREAKDOWN IN SILICON DIODES

ONR Contract Nonr-222(57)
M. Barnford (Prof. A. C. English)

In recent work, several techniques were devised to produce more certain evidence of a localized mesoplasma. By direct observation with the microscope, a glowing spot was observed on diode samples in second breakdown, and a diffraction grating spectrum had qualitatively a black-body distribution. Still more specifically, and going further than the original observations of Tauc and Abraham [1], we have observed and photographed tiny globules of molten silicon on the surface of a diode during high-current second breakdown. Figure 1 shows a typical edge view of the rim of a diode where the central portion has been roughened by the melting and several solidified globules are present. This shows that the estimates of maximum temperatures by Tauc and others are considerably short of reality.

To refine even further the identification of breakdown regions totally enclosed in the bulk silicon, considerable work was done with lapping and staining techniques. An attempt to induce second breakdown at a predetermined site by making contact to the junction with a hot-wire loop was unsuccessful. However, if the diffused, highly doped layer on the junction is etched to reduce the surface conductance, a wire point contact quite readily induces a second breakdown spot under the point. Figure 2 shows a typical distinctive stain pattern obtained by lapping through the junction region. The size of the stained region is larger by a factor of two than present theoretical estimates of the size of the melt. This is considered to be a good correlation for this stage of the investigation. Part of the stained region may be silicon that has been near the melting point but not melted. As predicted, the size of the stained region is proportional to current (in the one-to-four ampere range).

The search for microscopic breakdown regions over the whole of a diode junction is far too tedious and ambiguous and we found it necessary to fabricate, by etching, a number of "pedestal" diodes on the diode surface about 100 microns diameter to reduce the search volume. Each small diode on the silicon wafer base exhibited the same type of breakdown behavior as the original diode. The array of small diodes was polished off a few microns at a time and stained to bring out the evidence of breakdown. Previous work at much higher currents passed through a metal point contact had produced obvious surface cratering. In the present instance, no surface damage was visible after subjecting the pedestal diode to second breakdown. However, the stain, concentrated hydrofluoric acid with 0.1 per cent nitric acid, apparently attacks a heat-damaged region at a greatly increased rate and often produces craters a few microns in size (Fig. 3). The damaged region could be traced down in depth into the silicon until it disappeared (Fig.4).

---

[1] J. Tauc and A. Abraham, Phys. Rev., 108, 936, 1957.

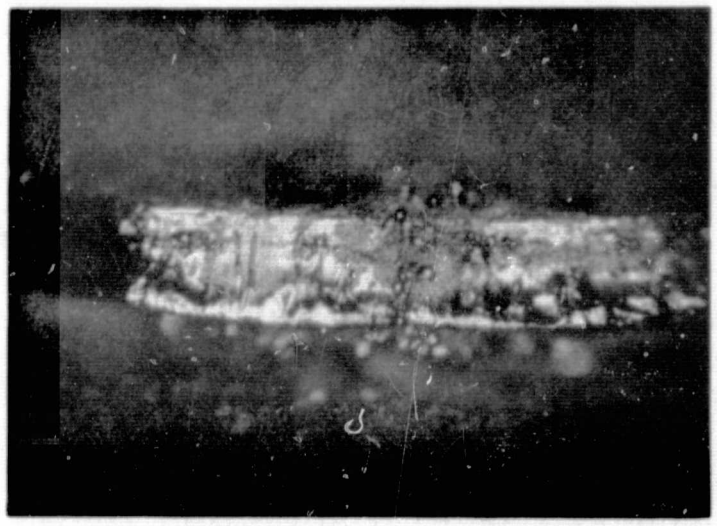

Fig. 1. Beveled edge of silicon junction diode after mesoplasma meets had been observed on the surface. (Mag. x 110).

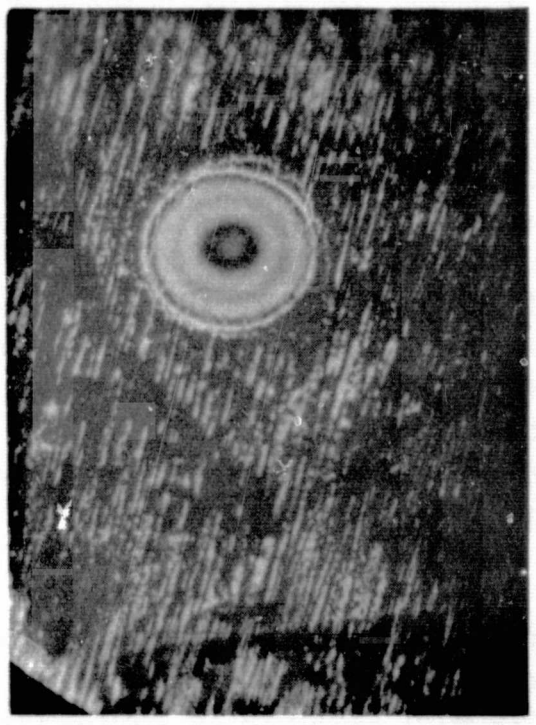

Fig. 2. Concentric circles on a grey background produced by lapping and staining after second breakdown. (Mag. x 280).

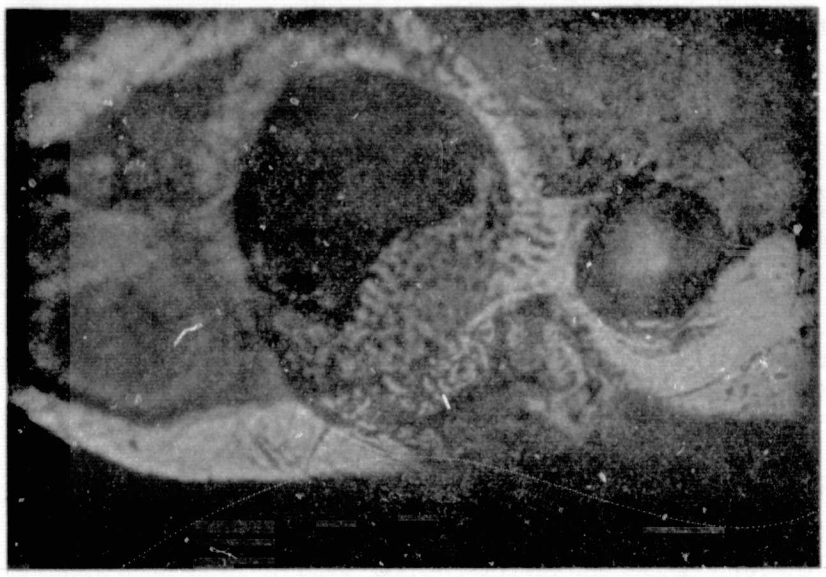

Fig. 3. Crater 6 μ deep with adjacent 4 μ crater. The 4 μ crater began as a shallow etch (a roughened area). (Magnification x 800)

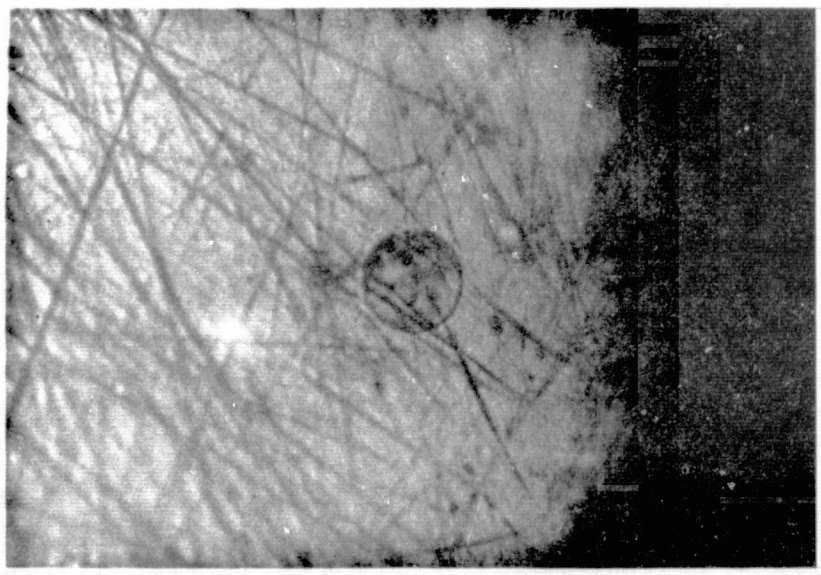

Fig. 4. Slightly indented region after a 6 μ deep crater had been followed down in 2 μ steps. There the stain evidence disappeared abruptly. (Magnification x 1000)

HIGH CURRENT BREAKDOWN IN AVALANCHE TRANSISTORS

ONR Contract Nonr-222(57)
H. Kawamoto (Prof. A. C. English)

The objective of this project is to study the detailed dynamic characteristics of a silicon transistor in so-called avalanche operation. Second breakdown was observed during transient operation in the order of nanoseconds under several circuit and temperature conditions.

The transient collector-to-emitter voltage and the collector current in the circuit (Fig. 1) were carefully measured with a sampling oscilloscope.

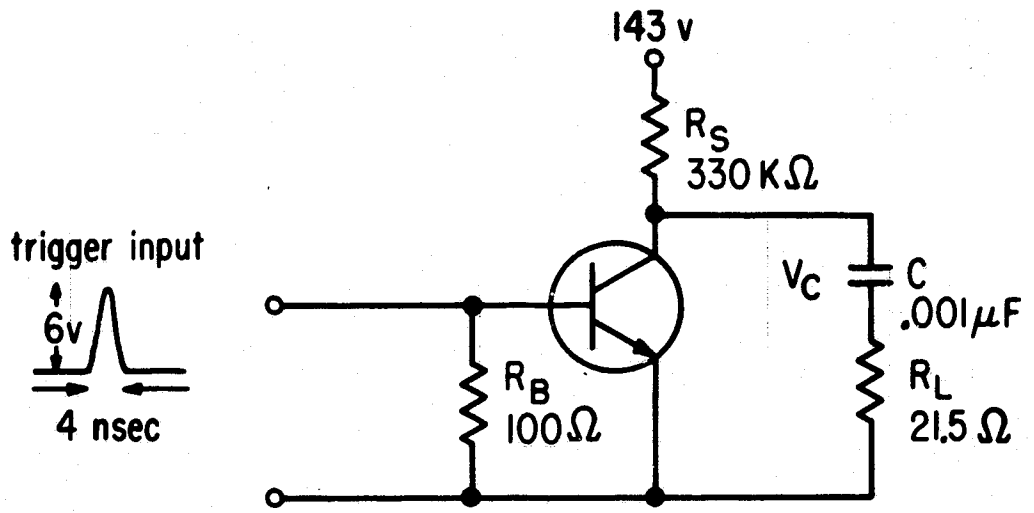

Fig. 1. Measuring circuit.

As a typical example, the voltage and current as a function of time are shown in Fig. 2, and the current-voltage characteristics are shown in Fig. 3. The phenomena encountered may be discussed with the aid of Fig. 4.

In the static condition the operation point stays at the point A which is the intersection of the 21.5-ohm load-line and the breakdown curve, I, with base and emitter shunted by 100 ohms. Upon the application of a positive base trigger, the operating point moves to the point B along the load-line. The transistor now dissipates high power, approximately 40 watts, the collector junction heats up, and it is believed that "pinch-in" concentrates the heat in a local region. While this occurs, the voltage across the capacitance decreases and the operating point moves to point C in about 90 nsec. At this point, second breakdown sets in and the collector voltage drops suddenly to the SB sustaining voltage at the point D, with the current at 2.2 amps. The operating point then moves down to the point E along a second breakdown characteristic curve in about 50 nsec as the capacitor discharges. Point E appears to mark the condition where heat dissipation permits the breakdown region to cool sufficiently to escape from second breakdown and return the characteristic to the origin in a

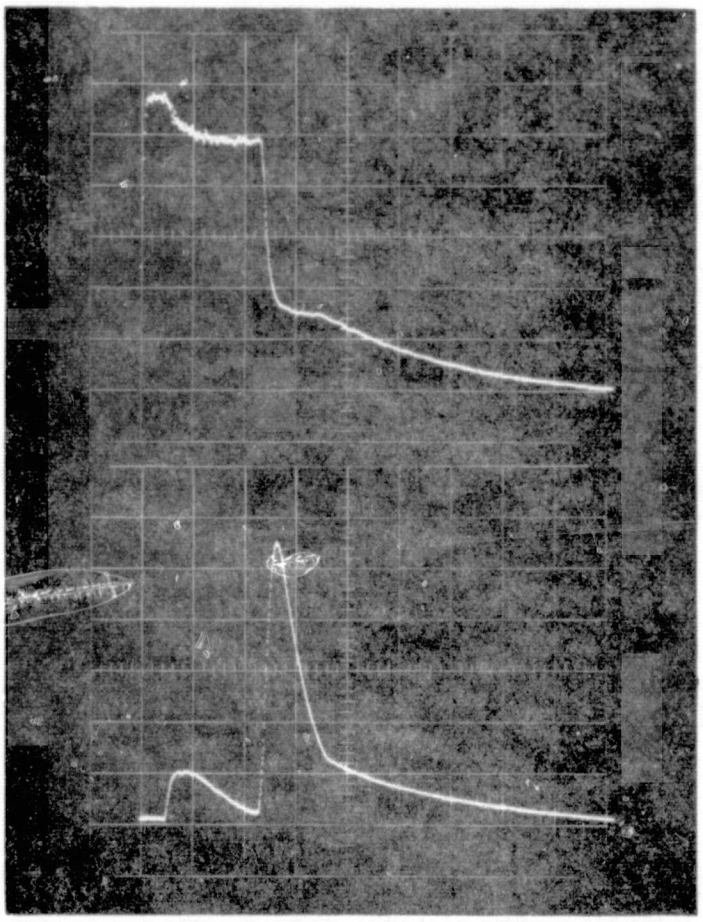

Fig. 2. Voltage (upper) and current (lower) wave-form as a function of time.
Upper: 20 volts/div, Ver
50 n sec/div, Hor

Lower: 0.4 amp/div, Ver
50 n sec/div, Hor

The origin is at (1.5, 1).

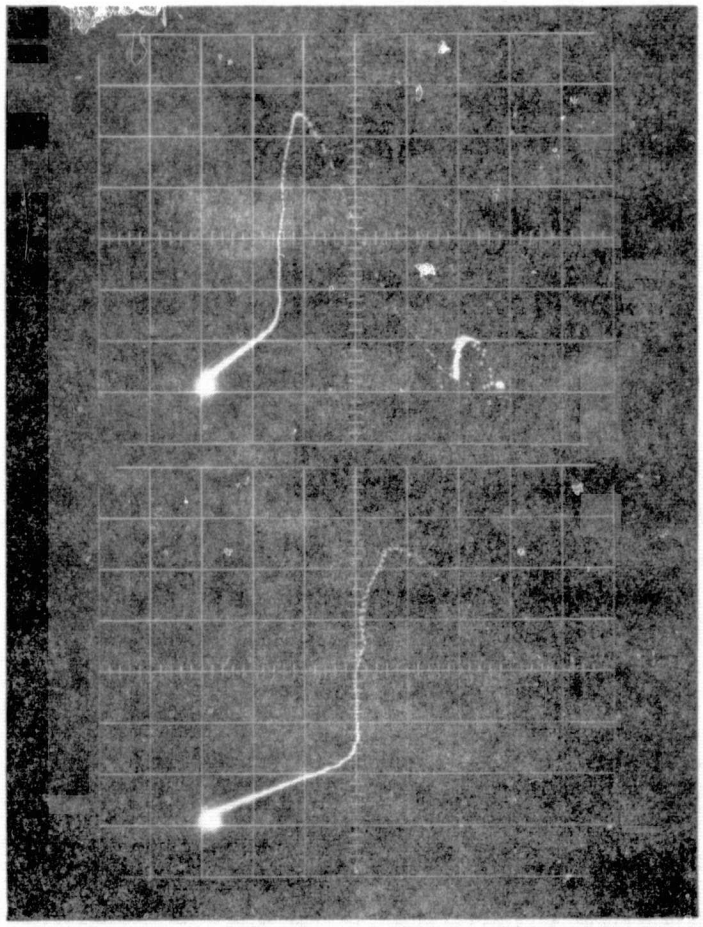

Fig. 3. Collector current (Ver) - collector voltage (Hor) characteristic in the transient operation.
Upper: 0.4 amp/div, Ver
20 volts/div, Hor

Lower: 0.4 amp/div, Ver
10 volts/div, Hor

The origin is at (2, 1).

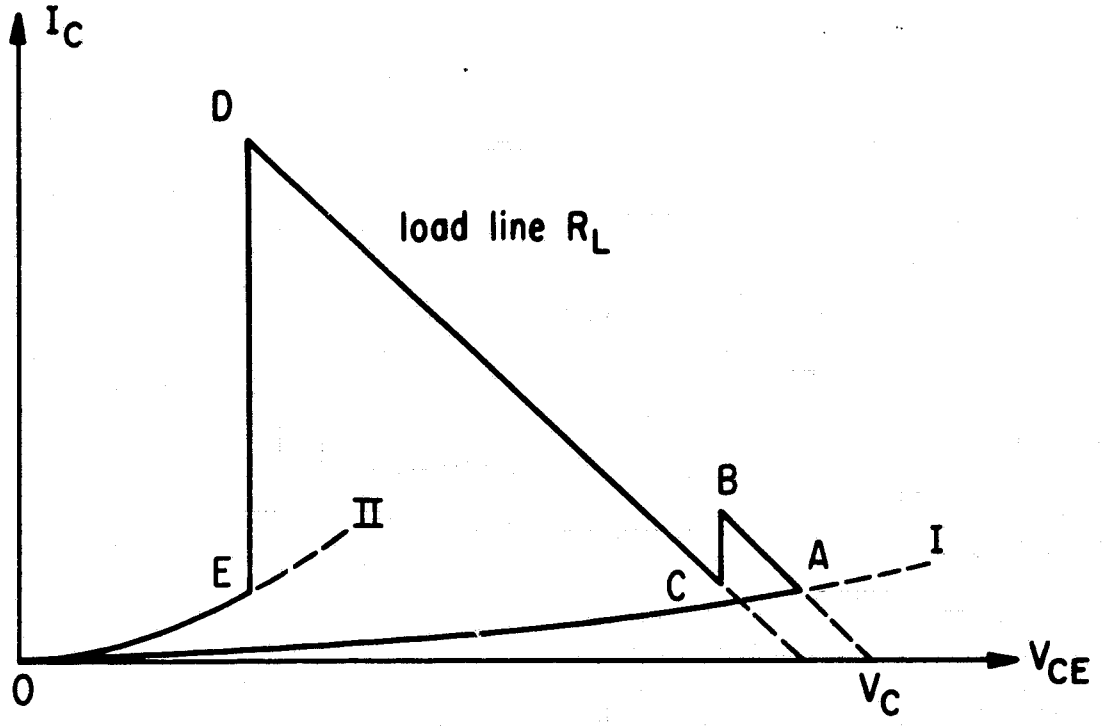

Fig. 4. The trace of the operating point in the I_C-V_{CE} domain.

normal breakdown condition under variable high-temperature conditions. It is believed that further study of these effects will provide vital information on operating conditions which are indefinitely stable, unstable in the sense of inducing modifications in the device characteristics and junction geometry, or destructively unstable.

BISTABLE AND MONOSTABLE INTEGRATED CIRCUITS

JSEP Grants AF-AFOSR 139-64 & 65
D. A. Hodges (Prof. D. O. Pederson)

In prior work by this group, it was shown that the dc configurations of all possible bistable circuits may be systematically developed with a controlled-conductance (controlled G) model for the active devices [1]. In subsequent work, systematic techniques are developed for generating monostable circuits and binary counters from dc bistable configurations [2]. In this work, simplified representation of the dc I, V

---

[1] L. O. Hill, D. O. Pederson, and R. S. Pepper, "Synthesis of Electronic Bistable Circuits," IEEE Trans. on Circuit Theory, Vol. CT-10, No. 1, pp. 25-35; March 1963.
[2] D. A. Hodges, D. O. Pederson, and R. S. Pepper, "Systematic Generation of Monostable and Counting Bistable Circuits," IEEE Trans. on Circuit Theory -- to appear in Dec. 1965.

characteristics of bistable and monostable circuits as viewed at all node pairs is used. Monostable circuits and binary counters are obtained by adding energy storage elements and triggering circuitry to dc bistable configurations.

During this report period, closer ties have been established between the controlled-G model and the electronic or other physical processes underlying device operation. It was found that for charge-control active devices, e.g., the bipolar junction transistor (BJT), the field-effect transistor (FET), and the vacuum tube (VT), the controlled-G model may be derived directly from the principles of charge-control operation. In these devices, a control charge, Q_c, applied at the control electrode (base, gate, or grid) determines the magnitude of the active charge, Q_a, in a one-to-one manner. The active charge flows from emitter to collector (source-drain, cathode-anode) in all active devices.

The collector current, I_2, is determined by the relation $I_2 = \frac{Q_a}{\tau_t}$, where τ_t is the average effective time for an active carrier to cross from emitter to collector. On the basis of these relations, the controlled G may be written as

$$G(V_1) = \frac{I_2}{V_2} = \frac{Q_a}{\tau_t} \frac{1}{V_2},$$

where V_1 is the control voltage which establishes Q_c.

The biasing, conduction, and control relations for charge-control devices are summarized in Fig. 1. Figure 1a shows electron-conducting devices and the appropriate controlled-G models. Note that the metal-oxide-semiconductor (MOS) FET may be represented by a slightly modified controlled-G model. Figure 1b shows hole conducting devices and the appropriate models. Figure 1c shows the qualitative nature of the controlled-G characteristics for all these devices when polarities are defined as shown in Figs. 1a and b. The BJT operates usefully only in the enhancement mode. The junction-type FET and the vacuum tube operate most commonly in the depletion mode. The MOS FET may be designed as either an enhancement or depletion-mode device. Such an intermediate characteristic is indicated by the dotted line in Fig. 1c.

Note that the controlled-G characteristic for a charge-control device always has a positive slope; that is,

$$\frac{dG(V_1)}{dV_1} \geq 0.$$

This inequality is one way of representing the phase-inverting behavior of all charge-control devices in the common-emitter connection.

It was found that other devices, not adequately described solely on the basis of charge-control concepts, also may be represented

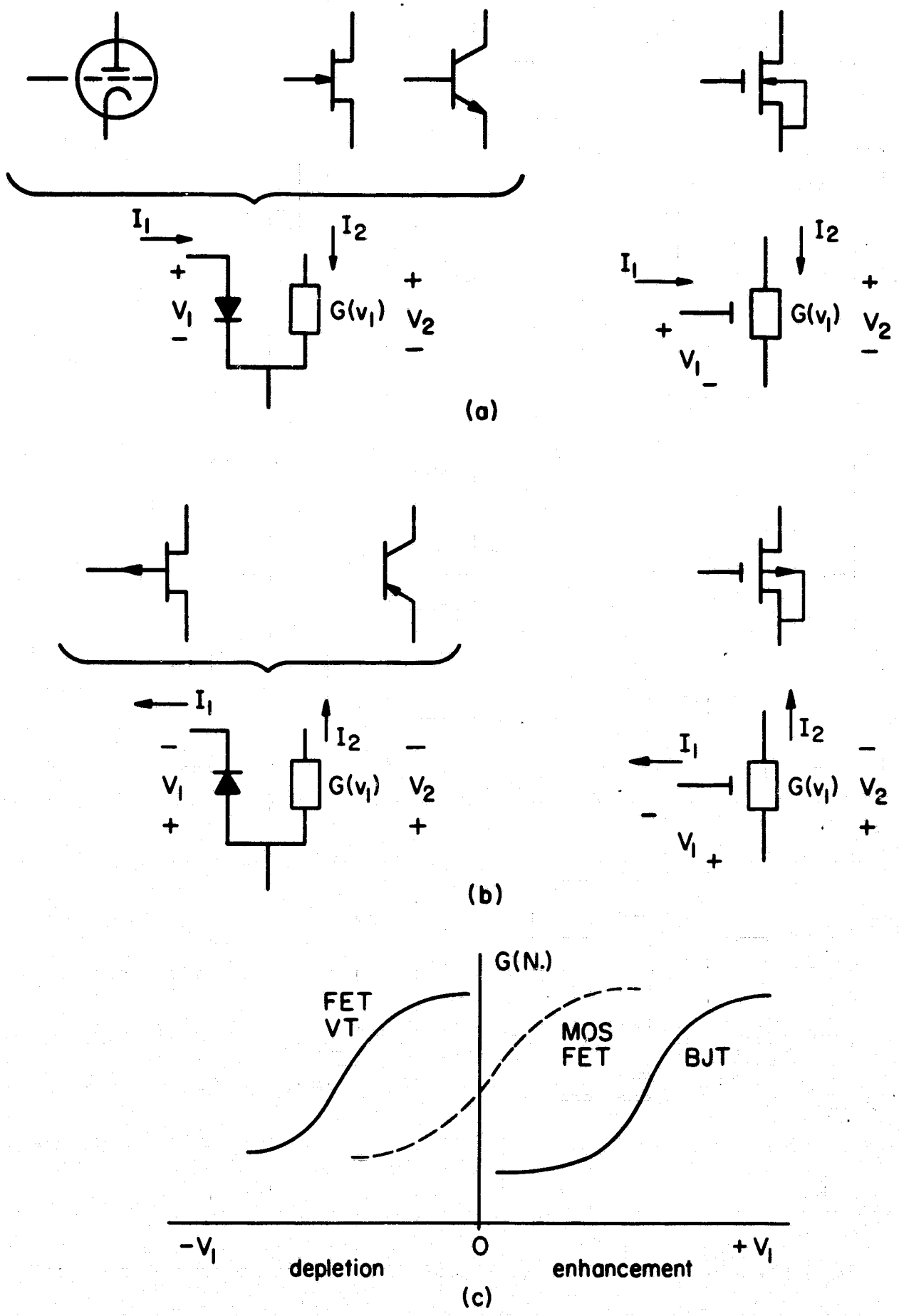
I1
I2
+
V1
−
G(v1)
+
V2
−
(a)
I1
I2
+
V1
−
G(v1)
+
V2
−
I1
I2
−
V1
+
G(v1)
−
V2
+
I1
I2
−
V1
+
G(v1)
−
V2
+
(b)
G(N.)
FET
VT
MOS
FET
BJT
−V1
0
+V1
depletion
enhancement
(c)

Fig. 1.

by the controlled-G model. Devices in this group include the tunnel diode, the unijunction transistor, the avalanche transistor, the magnetic relay, and the photon-coupled pairs. These devices may have phase-inverting or nonphase-inverting circuit behavior. A single nonphase-inverting device may be made bistable by adding a load and a dc source. We have shown that the terminal I, V characteristics of these non-charge-control devices in every case may be simulated with a properly chosen connection of two, charge-control, active devices.

A complete report on this project is being prepared.

INTEGRATED NEAR-HARMONIC OSCILLATORS

University of California Support
JSEP Grants AF-AFOSR-139-64 & 65
G. D. Hachtel (Prof. D. O. Pederson)

Potentially bistable oscillators are oscillators that can be made into bistable circuits by adding linear resistors and batteries. A study of the class of integrable, potentially bistable, near-harmonic oscillators was culminated during this period with the fabrication of a new type of integrated oscillator circuit. In addition, a procedure has been worked out for synthesizing integrable near-harmonic oscillators from integrable bistable circuits.

This brief statement of research conducted during this report period combines a description of the new integrated circuit with an example of the application of the synthesis procedure. The details on the research reported here will be published as a technical report titled, "Semiconductor Integrated Oscillators."

It has been shown that near-harmonic oscillation can always be realized by RC imbedding of an "OGS-derived activity block." By definition, an OCS-derived activity block is a 1-port or 2-port active-device configuration which exhibits an OCS (open-circuit-stable) negative-resistance characteristic. Further, it has been found that access ports which exhibit OCS negative resistance characteristics can be obtained by pliers entry into any active device lead in a large class of bistable circuits. The class referred to comprises those bistable circuits which incorporate two 3-terminal active devices, each of which are essential to the bistability. The active devices in this class of circuits can be bipolar transistors or field-effect transistors. These results have been used to establish a procedure for the synthesis of integrable, potentially bistable oscillators from integrable, bistable circuits.

The synthesis procedure is useful because it allows selection of a bistable circuit which is particularly suited for realization in integrated form. There will be six possible pliers entries into each bistable circuit; one of these entries must be selected on the basis of a particular oscillator application or for ease of integrated realization. The procedure then specifies how the near-harmonic oscillator is to be constructed around the chosen entry by adding (integrable) resistors and capacitors.

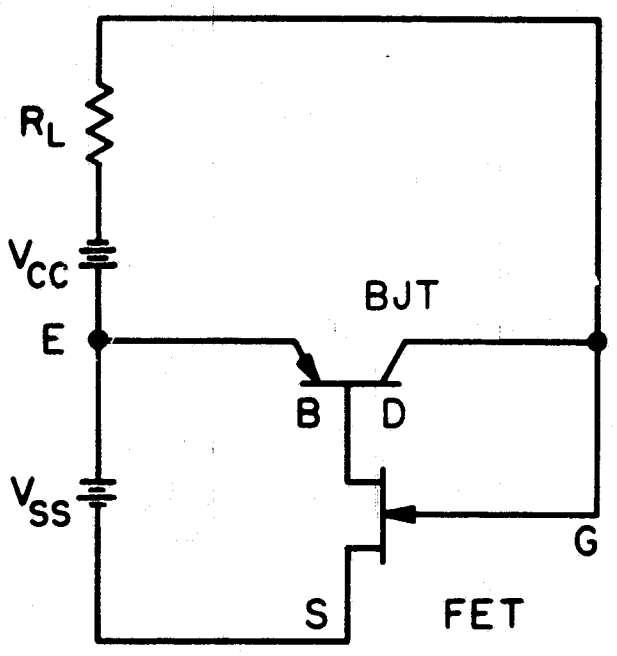

Fig. 1. BJT-FET (BIFET) bistable circuit.

A new integrated oscillator was synthesized in this way from the BJT-FET (bipolar junction transistor-field effect transistor) bistable circuit of Fig. 1. The source lead of the FET was selected for pliers entry for two reasons: First, it was found that this entry could be biased into the negative resistance portion of its dc characteristics by simply leaving the entry to be a dc open circuit. Second, this entry choice allowed the utilization of internal active device connections (beneath the surface of the integrated realization) and of parastic capacitances in the oscillator design. A discrete element prototype of the integrated oscillator is shown in Fig. 2. The OCS-derived 2-port activity block shown on the right of Fig. 2 exhibits an OCS negative-resistance characteristic at the source-emitter port. The simple RC 2-port imbedding network shown at the left of Fig. 2 realizes near-harmonic oscillation at a frequency roughly approximated by $\omega_0 = {}^{1}/\sqrt{R_1 R_2 C_1 C_2}$. The parameter values shown in Fig. 2 are those achieved in the actual integrated realization.

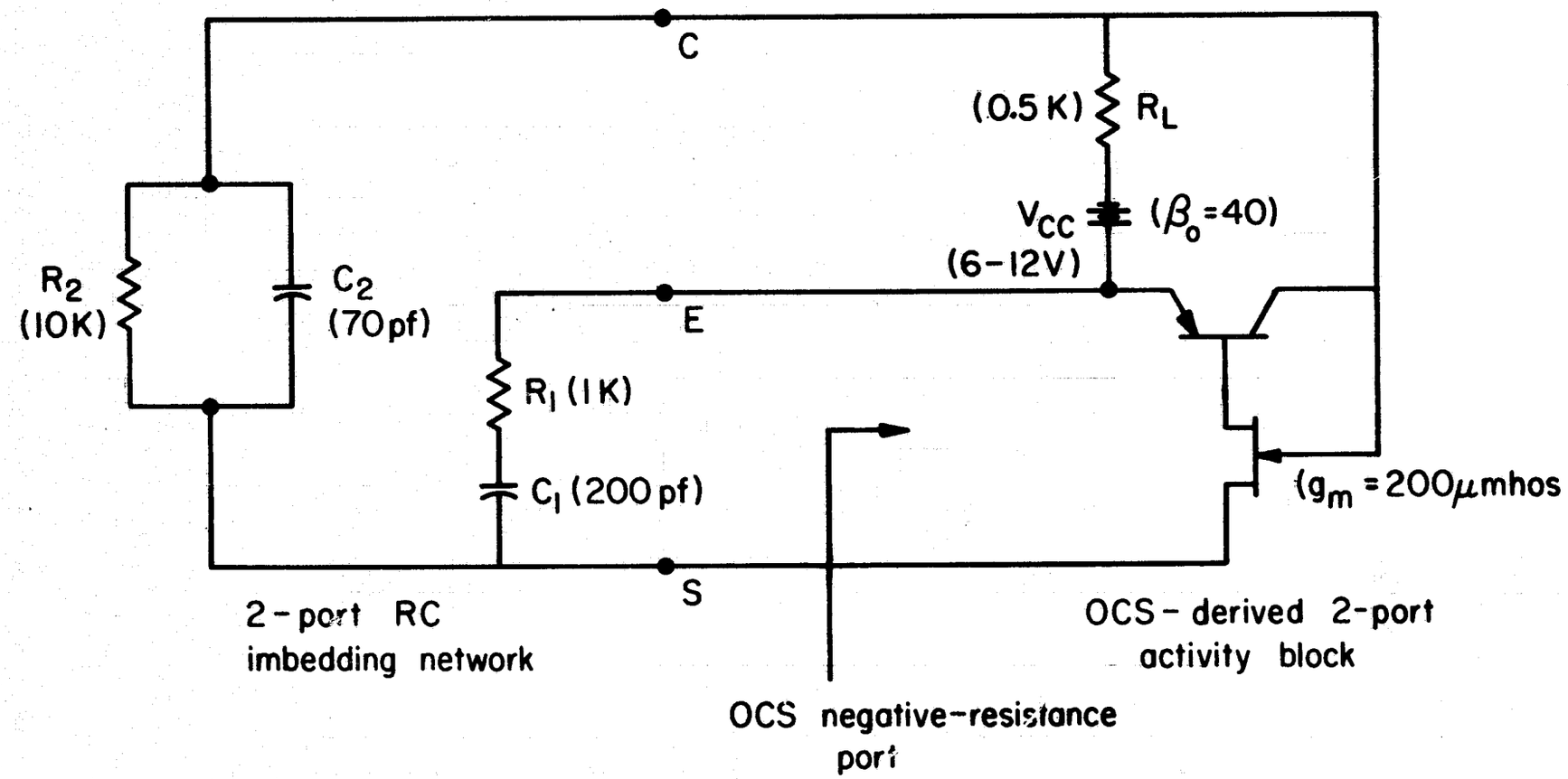

Fig. 2. Discrete element prototype of integrated potentially bistable oscillator.

An integrated realization of the prototype circuit of Fig. 2 is shown in Fig. 3. The BJT and FET active devices are grouped around the horseshoe (which constitutes the base of the BJT and the drain of the FET) at bottom-center in Fig. 2. On the left is an isolated diffused resistor box in which the resistors R_2 and R_L of Fig. 2 are realized. On the lower right another isolated-diffused resistor box contains the imbedding resistor R_1. The large white (aluminized) area at the top of the realization covers both of the two imbedding capacitors C_1 and C_2 of Fig. 2. (C_2 is located directly underneath C_1 and is therefore obscured by C_1.)

The circuit is designed so that no bias current is required at the source pliers entry. Thus, the circuit is able to operate from a single voltage supply (V_{CC} of Fig. 2). The integrated circuit was found to oscillate for V_{CC} in the range 6-12 volts. Measurements indicate that the integrated oscillator was capable of near-harmonic oscillation at frequencies in the expected range of 200-300 Kc for various values of bias voltage. For a limited range of bias conditions a nearly sinusoidal oscillation could be observed, with distortion less than 7% (mostly second harmonic). However, both the amplitude and the frequency of the oscillation were strongly dependent on the dc bias voltage. For example, voltage and temperature coefficients of frequency on the order of 20,000 PPM/Volt and -5000 PPM/°C, respectively, were typical measured values. The measured temperature coefficient was much larger than could be expected from the known temperature dependence of the integrated resistors and capacitors. It is believed that the large temperature coefficient is due to the temperature dependence of the distortion spectrum.

It is concluded that for integrated RC oscillators to achieve "state-of-the-art" performance, the following steps should be taken in a future design:

1. Employ negative-feedback desensitization techniques to stabilize the amplitude and reduce the distortion spectrum of the oscillation so that the limiting performance dictated by the RC imbedding elements can be achieved.
2. Vapor deposit thin-film RC imbedding elements onto silicon active device structure. (Thin-film components can have very low temperature coefficients.)

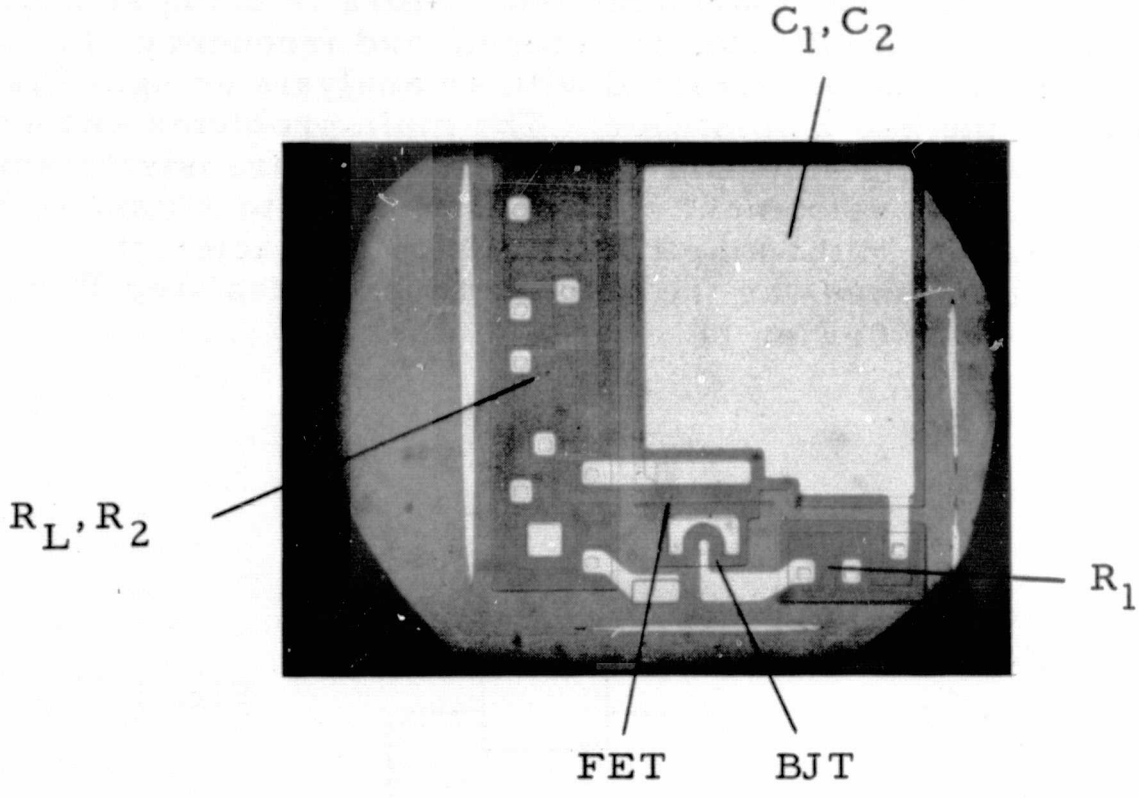

Fig. 3. Integrated potentially bistable near harmonic oscillator.

INTEGRATED OSCILLATOR REALIZATION

National Science Foundation and University of California Support
R.F. Adams (Prof. D.O. Pederson)

As a complimentary project to the previous topic, the realization of other integrated near-harmonic oscillators is being studied. As a first topic the output amplitude, waveform, and frequency of a Wien Bridge oscillator have been predicted with an analysis using measured characteristics of the basic amplifier. The main problems encountered have been those involving selection of a satisfactory transistor amplifier configuration and the development of a measurement technique of sufficient accuracy to obtain the amplifier transfer characteristic.

The starting point was the selection of the idealized Wien Bridge oscillator circuit (Fig. 1).

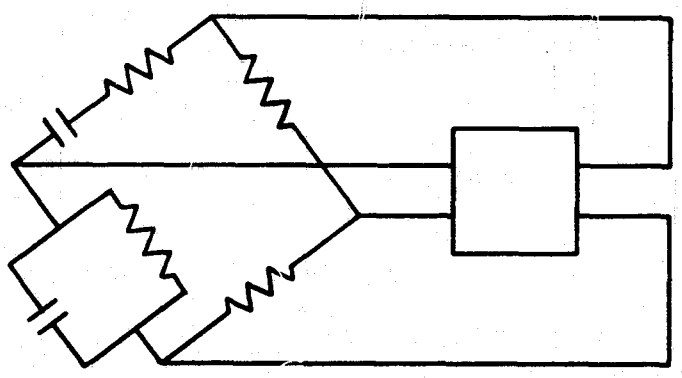

Fig. 1.

If we include the feedback elements in the amplifier block, we obtain Fig. 2.

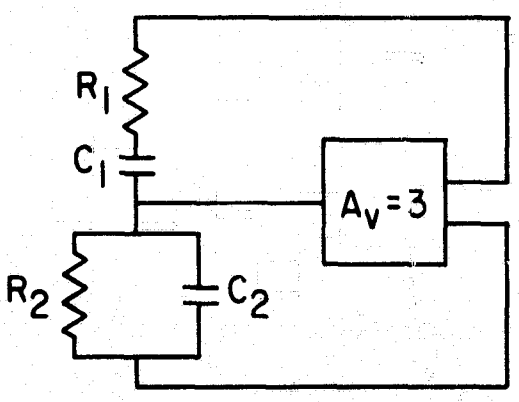

Fig. 2.

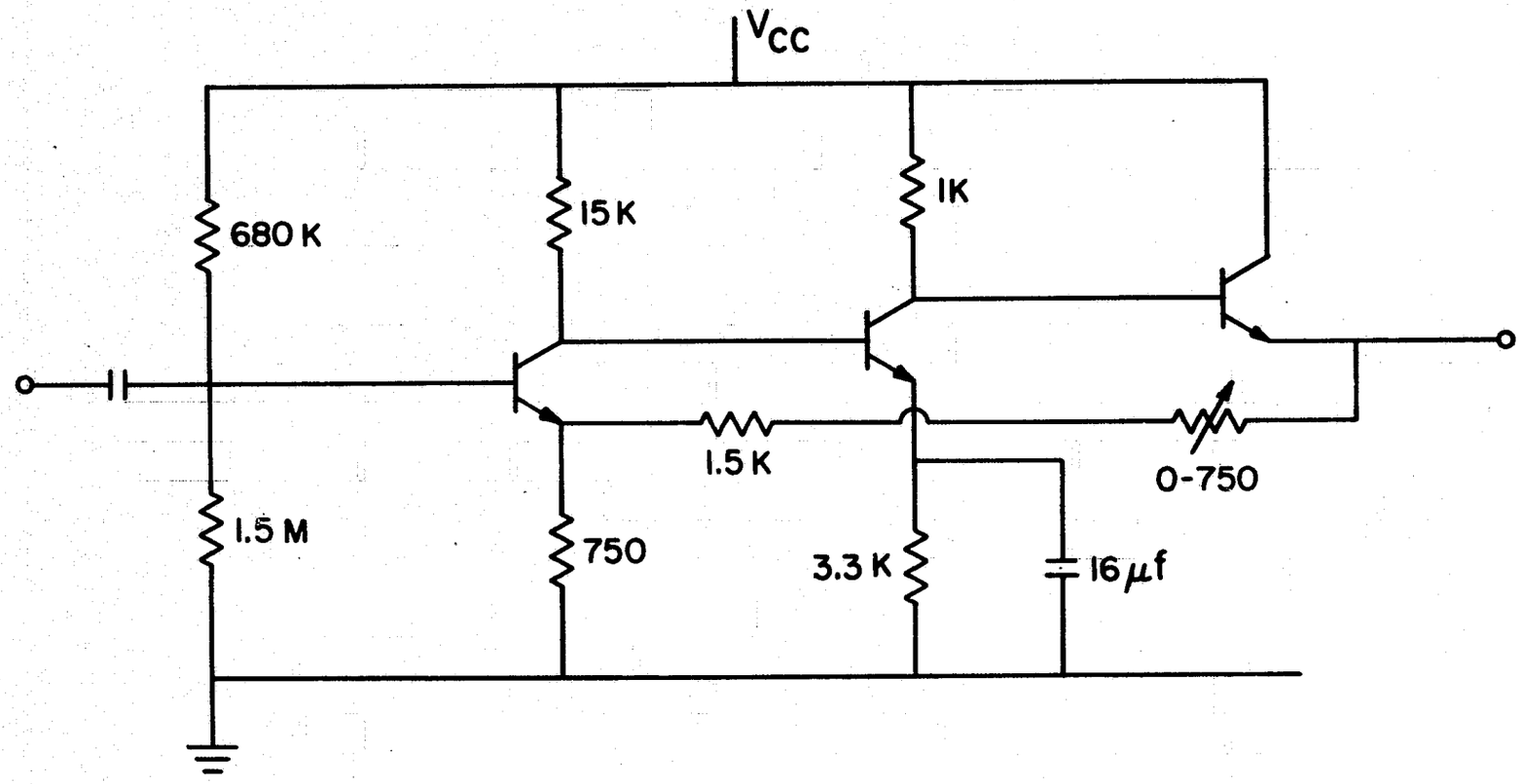

Fig. 3. Voltage amplifier.

The basic oscillator equation, in variational form, for this idealized circuit is :

$$v_1 + \frac{-\frac{1}{RC}p}{p^2 + 3\frac{1}{RC}p + \frac{1}{R^2C^2}} A_v(v_1) = 0$$

where $R_1 = R_2 = R$ and $C_1 = C_2 = C$ and where $A_r(v_1)$ is the nonlinear gain characteristic of the amplifier. If p is normalized with respect to $\frac{1}{RC}$, this can be written :

$$p^2 v_1 + p(3v_1 - A_r(v_1)) + v_1 = 0.$$

In order to apply this idealized equation to the experimental circuit, the actual amplifier must approximate an ideal voltage amplifier : Z in = ∞, Z out = 0, and $v_2 = A_v v_1$ with no phase shift. Several amplifiers, using both FET and BJT units, were tried. Many had to be rejected immediately because of phase shifting problems. Also some difficulty with amplitude stability was encountered with several amplifier configurations. For the final amplifier shown in Fig. 3, the input impedance requirement was solved by noting that the input impedance to the transistor amplifier can be modelled to a first-order approximation by a parallel R, C. Values for R_{in} and C_{in} were measured for the amplifier and the values of R_2 and C_2 were adjusted to incorporate the values. An input impedance of 10 Ω was achieved using an emitter follower, although some instability problems were encountered. High frequency transistors and direct coupling minimized excess phase shift and the instability problem could be neglected.

For the final amplifier, the nonlinear transfer characteristics as shown in Fig. 4 was measured. The difference equation, $3v_1 - A_v(v_1)$ had to be accurate to within a few percent to achieve reasonable predictions of output for near-harmonic oscillator operation. Using this characteristic together with the basic second-order oscillator equation, we can use conventional Leinard plane construction to obtain the limit cycle of the oscillator. This is shown in Fig. 5. From the limit cycle, the predicted output waveform of Fig. 6 is obtained using conventilanl methods. The experimental waveform is also shown in this figure. A Prediction of the output to within 2% of the frequency and 3% of the amplitude were achieved. Our efforts now are centered on the integrated realization of this circuit.

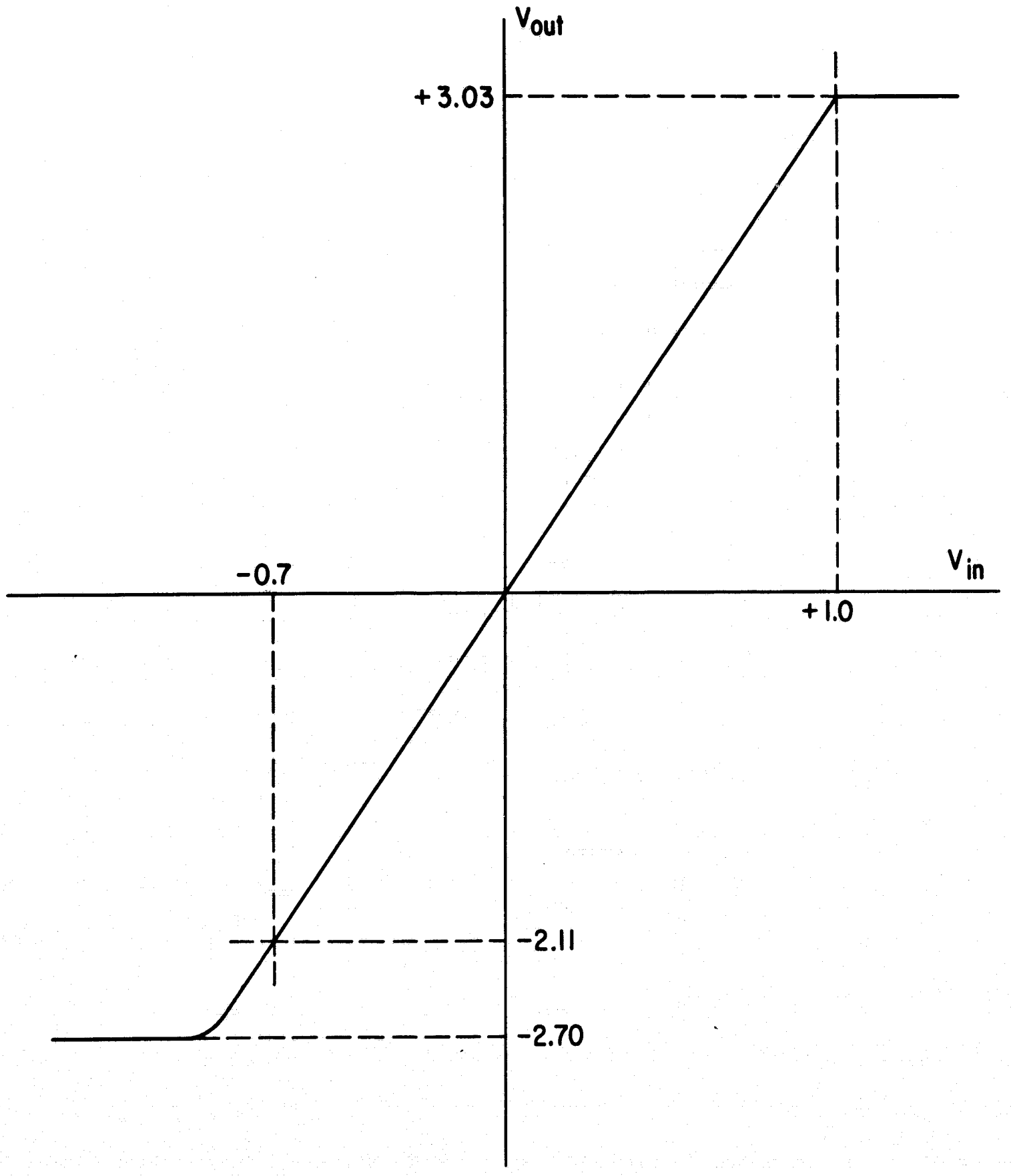

Fig. 4. Gain characteristic.

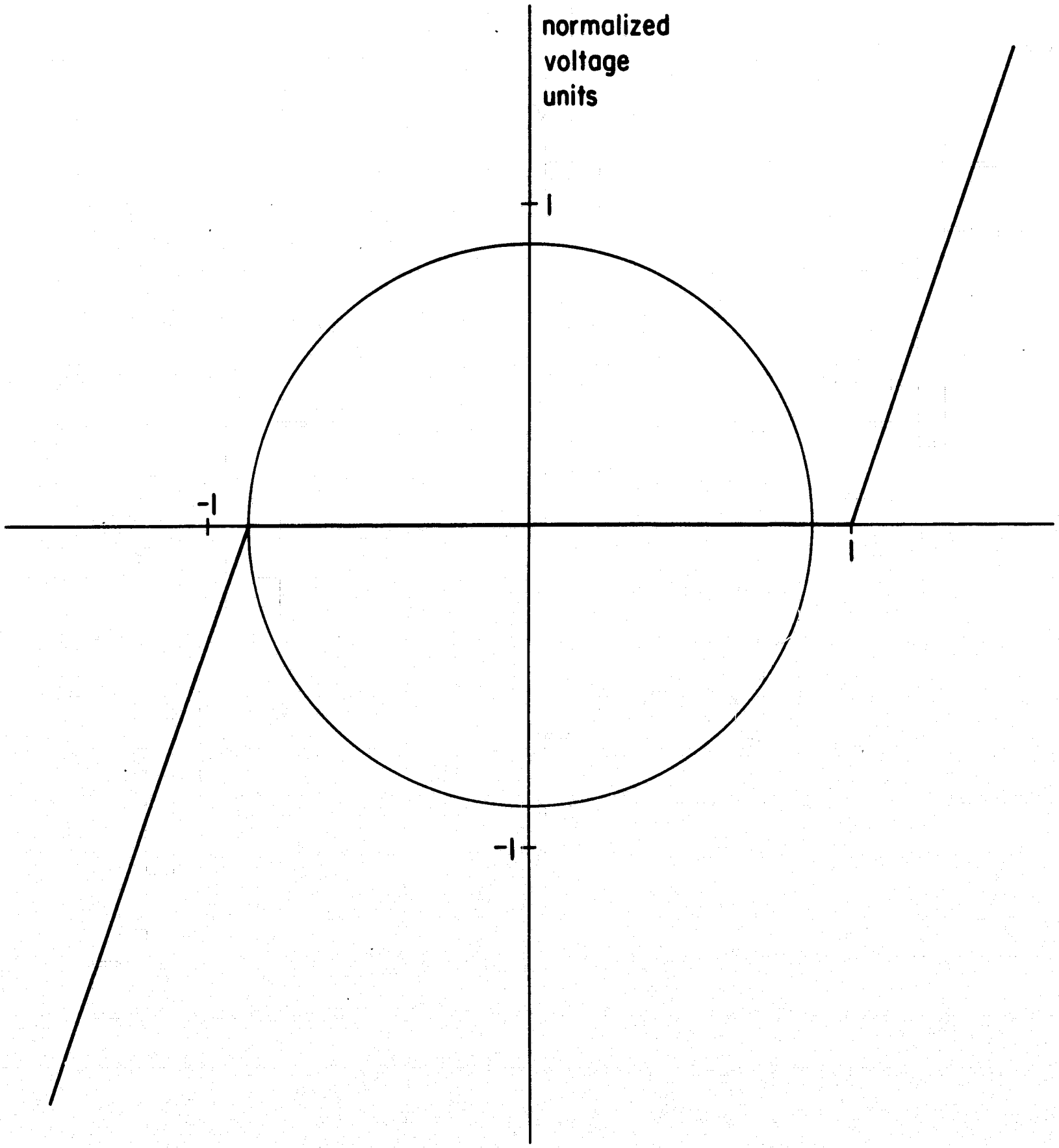

Fig. 5. Lienard plane.

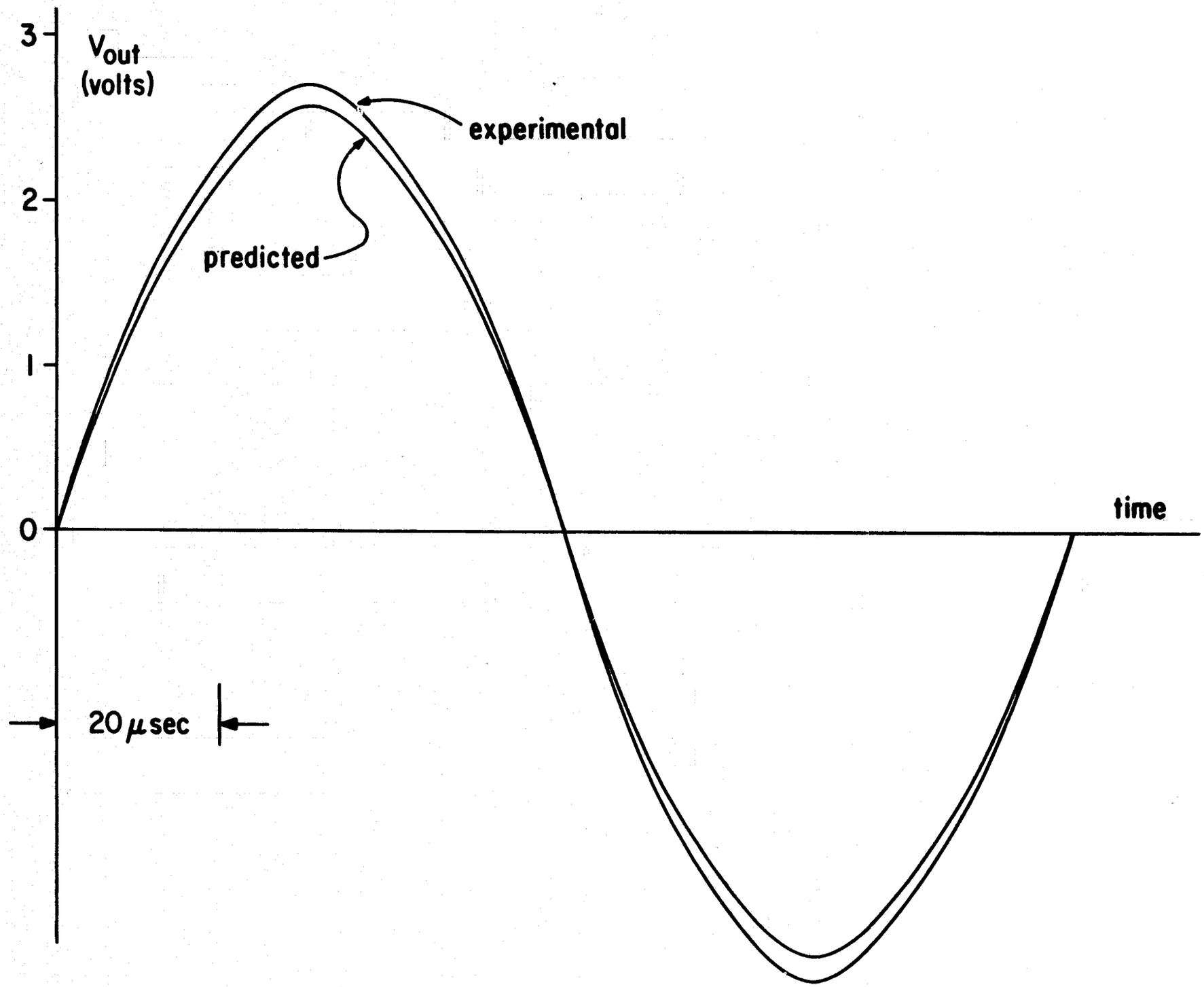

Fig. 6. Output waveform.

GUNN-EFFECT GALLIUM ARSENIDE OSCILLATORS

University of California Support
J-W Hwan (Prof. R. M. White)

Oscillations of current in GaAs diodes were first observed by Gunn in 1963[1,2] and later explained by Kroemer [3,4] in terms of negative differential mobility, features of the model having been worked out by Ridley and Watkins [5] and Hilsum [6]. These oscillations have been observed at fundamental frequencies up to 7.5 Gc in CW operation [7]. Relatively high efficiencies (e.g., 12% on pulsed operation) have been reported.

In this laboratory, Gunn effect diodes have been fabricated and tested. The primary objective is to explore the properties of the diode oscillators so as to permit characterizing them as microwave circuit elements. Thus tunability, effects of external load upon output power and frequency, effects of the sample resistance and capacitance on the optimum external circuit and so on are being examined. The Gunn diodes appear to be fundamentally different from negative resistance devices such as the tunnel diode in that oscillations will occur regardless of the external circuit conditions. However these conditions do have some effect on oscillation frequency, output power, etc.

Gallium arsenide diodes have been fabricated from undoped single-crystal material having resistivities between one and about two thousand ohm-centimeters. Making ohmic contacts to higher resistivity material has been difficult; pure tin contacts alloyed to GaAs in a forming gas atmosphere during induction heating have been moderately successful. An attempt (by Mr. Clapp, of this laboratory) to make

---

[1] J. B. Gunn, "Microwave Oscillations of Current in III-V Semiconductors," Solid State Communications, vol. 1, pp. 88-91, September 1963.

[2] J. B. Gunn, "Instabilities of Current in III-V Semiconductors," IBM Journal, vol. 8, pp. 141-159, April 1964.

[3] H. Kroemer and G. F. Day, "A Study of Solid State Microwave Devices and Phenomena," Interim Engineering Report No. 5, Varian Associates, Palo Alto, California, January 1965.

[4] idem, Interim Engineering Report No. 6, April 1965.

[5] B. K. Ridley and T. B. Watkins, "The Possibility of Negative Resistance Effects in Semiconductors," Proc. Phys. Soc., vol. 78, pp. 293-304, August 1961.

[6] C. Hilsum, "Transferred Electron Amplifiers and Oscillators," Proc. IRE, vol. 50, pp. 185-189, February 1962.

[7] B. W. Hakki and S. Knight, "Phenomenological Aspects of CW Microwave Oscillations in GaAs," to be published.

tin contacts by evaporation with the "ion plating" technique described by Mattox [8, 9] was successful with low resistivity GaAs but no success was had in using this technique to make good contacts to higher resistivity material (greater than 200 ohm-cm).

Short diodes were made(thickness of the samples smaller than 8 mils) and coherent oscillations having fundamental frequencies in the range from 0.5 to 1 Gc were observed. Threshold voltages were about 75 volts for 2 ohm-cm and 150 volts for 2000 ohm-cm resistivity samples, corresponding to electric fields of approximately 4200 volts/cm and 8500 volts/cm respectively. These diodes were tested in a tuneable half wavelength cavity. An improved cavity (permitting location of diode to be varied) and a special non-resonant mounting structure are now being used in tests of the effect of load impedance upon the oscillations.

CURRENT OSCILLATIONS IN PIEZOELECTRIC SEMICONDUCTORS

JSEP Grants AF-AFOSR-139-64 and 65
S. Joshi (Prof. R.M. White)

A number of workers [1-5] * have observed current saturation and current oscillations in single crystals of piezoelectric semiconductors such as CdS and ZnO when a pulsed voltage (to avoid overheating) of sufficient magnitude is applied across the crystals. At drift electric fields greater than $E = v_s/\mu$, where v_s is the velocity of sound, and μ is the electron mobility, the current begins to saturate, and, as the field is increased, oscillations of current appear (see Fig. 1 for typical characteristics). No completely satisfactory explanation for all features of the various oscillations has been proposed. However, in many ways the oscillations observed here resemble Gunn effect oscillations in GaAs. In the present case, the required negative differential mobility could result from the ultrasonic flux which is amplified to a high level in the piezoelectric semiconductor.

In support of the preceding statement, some characteristics of the oscillations will be described. In uniformly illuminated samples (the conductivity of the cadmium sulfide crystals studied here is conveniently controlled by incident illumination), the period of the oscillations is equal to or slightly less than the one-way transit time of sound between the electrodes on the crystal. In a nonuniformly illuminated sample, the period depends on the length of the illuminated region. Oscillations (in crystals about a centimeter long) are observed at frequencies at or below

---

[8] D.M. Mattox, "Metallizing ceramics using a gas discharge," Electronics Division Meeting of the American Ceramic Society, Philadelphia, Pennsylvania, Sept. 16-18, 1964.

[9] D.M. Mattox, "Film deposition using accelerated ions," Electrochemical Technology 2, No. 9-10, 295-298 (Sept. - Oct. 1964).

* These references appear on the next page.

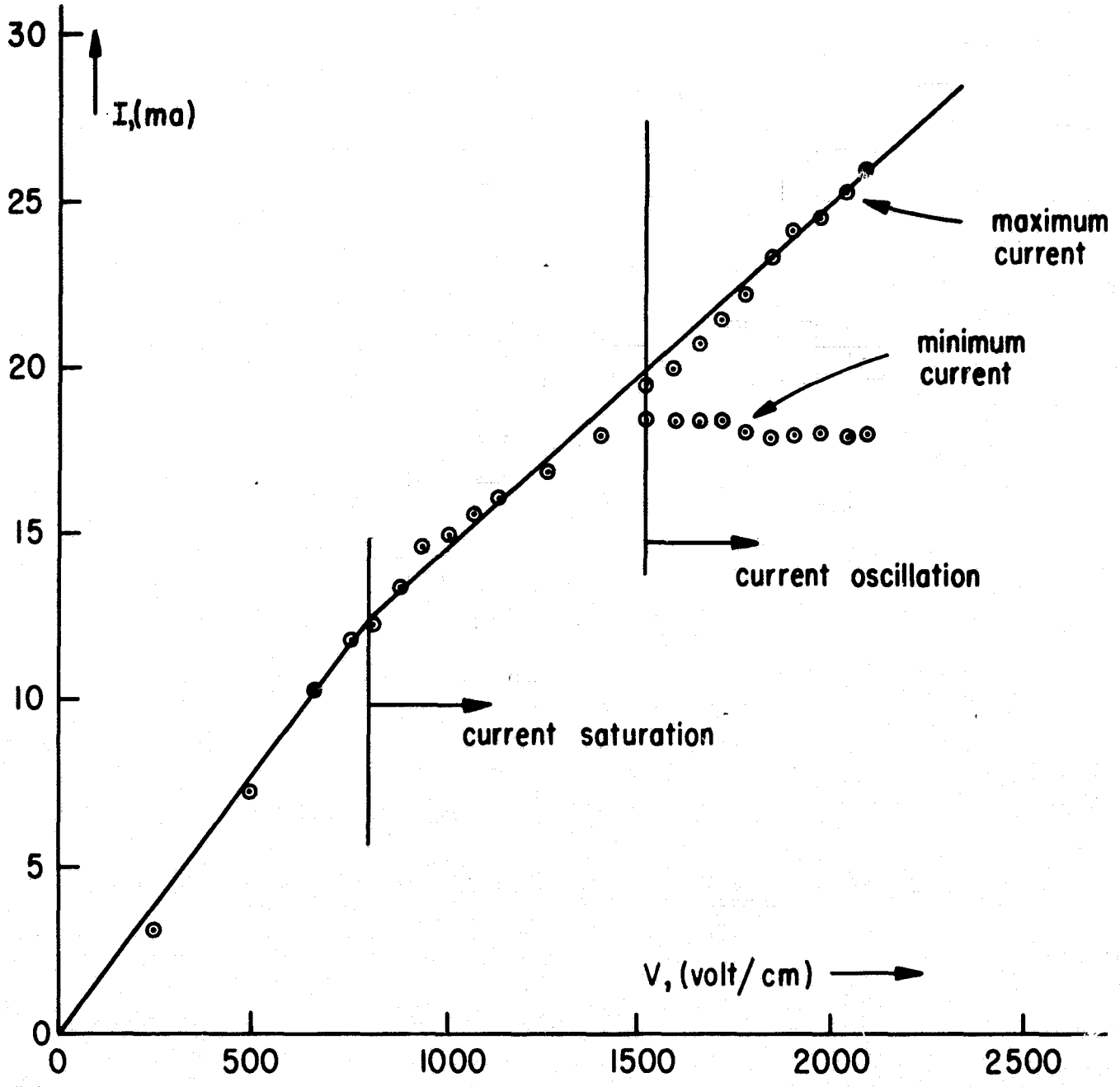

Fig. 1 a. Typical I-V characteristic of CdS diode oscillator.

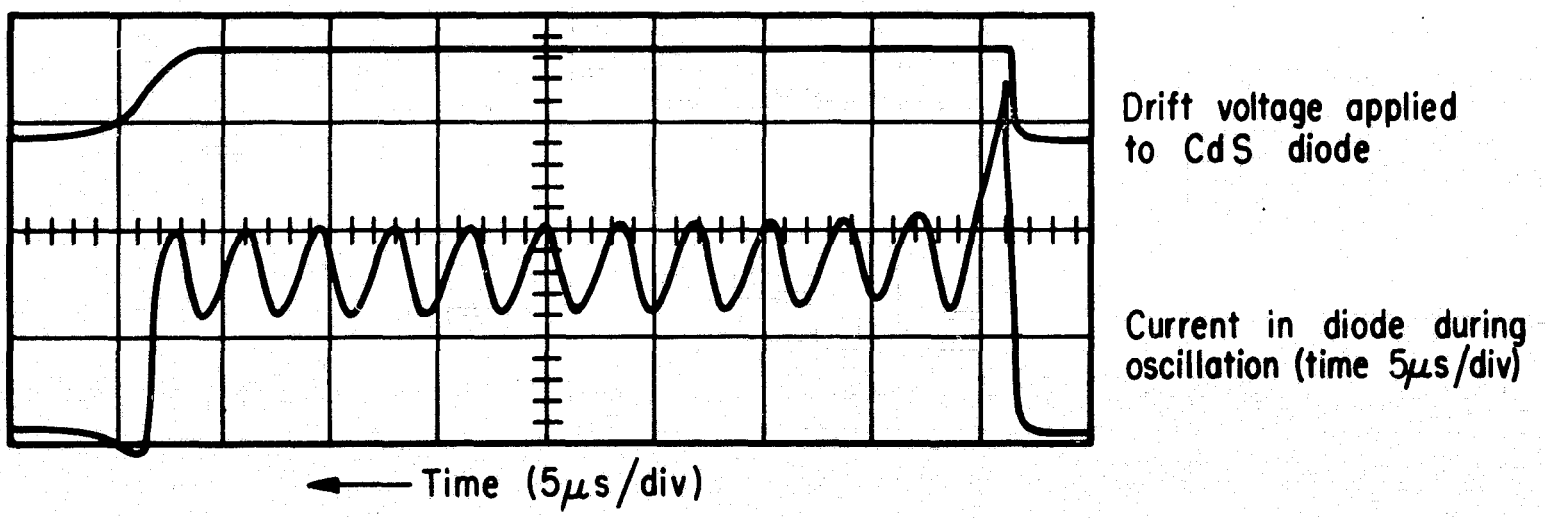

Fig. 1 b. Waveforms of typical CdS diode oscillator.

one megacycle, yet the calculated acoustic gain (which depends primarily on the conductivity) is very low at such frequencies, being a maximum instead at hundreds of megacycles. Oscillations are observed both with rapidly-rising drift voltages and with slowly-rising pulses; thus oscillation is not necessarily dependent on there being ultrasonic waves produced by the sudden application of the drift field to the piezoelectric crystal. In an oscillator having a slowly-rising drift pulse, ultrasonic flux from the thermal background may be amplified to produce the reduction of electron mobility which results in a reduced current through the sample.

If the slowing of electrons by high level ultrasonic flux is responsible for the current oscillations, then (as in the case of Gunn effect oscillations) one should be able to detect electric potential extrema moving through the crystal during oscillation. The potential extrema correspond to the movement of electron bunches. Gunn has reported observation of such extrema in GaAs moving with velocities of the order of 10^7 cm/sec. We have found similar motion in CdS. A small probe (the end of a miniature coaxial cable positioned about 0.005 inches from the CdS) was moved in the direction of current flow over the lateral surfaces of the CdS oscillators. Potential minima recurring at the oscillation frequency were found; the minima were particularly well defined near the positive (output) electrode (see Fig. 2), and in this region they appeared to move at a uniform velocity slightly in excess of the appropriate velocity of sound (i.e., the measured velocities of the potential minima ranged from 2.0 to 2.5×10^5 cm/sec in crystals oriented for shear wave interaction, the shear wave velocity being 1.75×10^5 cm/sec.) These measurements are in accord with the mechanism proposed above for the ultrasonic oscillations; it should be noted that evidence for this mechanism has also been observed recently by Sliva and Bray [6] in GaSb.

---

[1] R.W. Smith, "Current saturation in piezoelectric semiconductors," Phys. Rev. Letters, 9, 87 (1962).

[2] J.H. McFee, "Ultrasonic amplification and non-ohmic behavior in CdS and ZnO," J. Appl. Phys., 34, 1548 (1963).

[3] J. Kikuchi, "Continuous oscillation in CdSe observed by local illumination," Japan J. Appl. Phys., 2, 812 (1963).

[4] J. Okada and M. Machino, "Oscillations in Cds," Japan J. Appl. Phys., 2, 736 (1963).

[5] E.L. Adler and G.W. Garnell, "Current oscillations and negative resistance in CdS," Proc. IEEE, 53, 483 (May 1965).

[6] P.O. Sliva and R. Bray, "Oscillatory current vehavior in GaSb and its relation to spontaneous generation and amplification of ultrasonic flux," Phys. Rev. Letters, 14, No. 10, 372-376 (8 March. 1965).

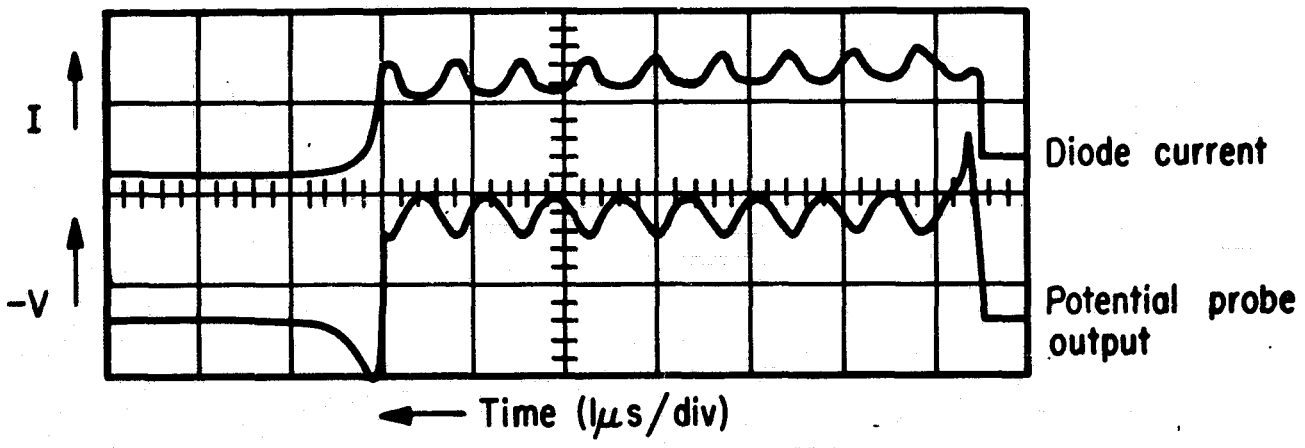

Fig. 2. Diode current and output of potential probe near positive electrode.

HEATING AND DISPERSION IN AN ULTRASONIC AMPLIFIER

University of California Support
Y.Z. Liu (Prof. R.M. White)

In an elastically active medium, such as that used in a piezoelectric semiconductor amplifier, gain is accompanied by dispersion. The gain, and hence, also the elastic wave velocity, in such a medium depend upon many factors including the electron mobility and the local drift electric field. Thus, local variations of any of these factors result in variations of gain and velocity. Typically, the temperature distribution (due to resistive heating and conductive cooling) is non-uniform and so will be the mobility. Electric field variations may exist as a result of electrode shape of a non-uniform distribution of the illumination often used to control the electrical conductivity.

It has been found that in a continuously-operating ultrasonic amplifier, the temperature distribution can result in substantial distortion of initially-plane elastic wavefronts and, thus, cause a large reduction in the response of the output transducer. In pulsed amplifiers, heating may be no problem, but a non-uniform drift electric field could produce wavefront distortion. The dependence of wave velocity on temperature and electric field has been calculated for CdS. One result of interest is that the change in wave velocity, v_s, due to a change of electron velocity with temperature in CdS may be of the same order or larger than the change in v_s characteristic of a passive medium in which only the elastic constant and density are temperature dependent.

SURFACE ELASTIC WAVES IN SEMICONDUCTORS

AROD Grant DA-ARO-D-31-124-G678 and University of Calif. Support
F. Voltmer (Prof. R.M. White)

Interactions between bulk elastic waves and electrons in piezoelectric semiconductors have been shown to result in wave attenuation or gain, and in oscillation. The details of the interaction depend upon such properties of the semiconductor as mobility, conductivity, and trapping. It is also possible to generate and detect surface elastic waves, that is, elastic waves which propagate along the free surface of a solid. Such waves, known also as Rayleigh waves, are analogous to gravity waves on the surface of a fluid; particle motion is confined to a region about one wavelength thick. It is the purpose of this project to study the interactions with electrons of such surface elastic waves in piezoelectric semiconductors.

Surface waves are being generated and detected with piezoelectric transducers attached to metal "combs" which contact the free surface of the solid as shown in Fig. 1; this transducer was first described by Viktorov [1] and has been employed more recently by Dransfeld and Arzt in the U.C. Department of Physics. Operation at frequencies up to 60 mc has been demonstrated, but much higher frequency operation appears possible.

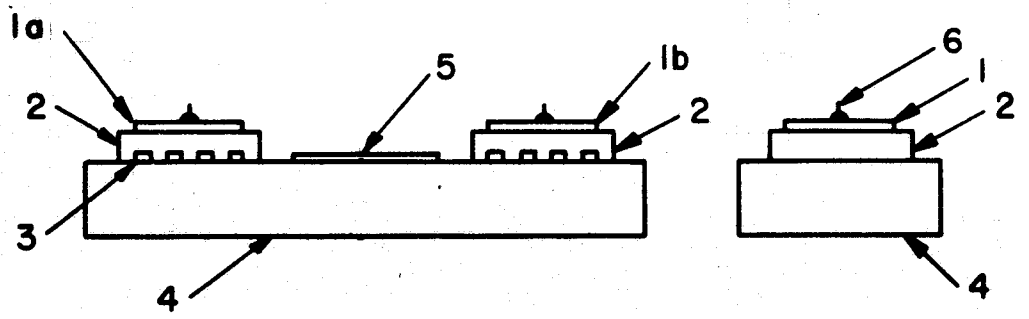

la, lb) Input and output compressional wave piezoelectric transducers; 2) metal comb; 3) comb teeth spaced one surface wave length; 4) fused silica plate; 5) film deposited on fused silica plate; 6) connecting lead for transducer.

Fig. 1. Surface plastic wave transducers.

---

[1] I.A. Viktorov, "Investigation of methods for exciting Rayleigh waves," Sov. Phys.-Acoustics I, 236-244 (1962).

Attention has been directed thus far to the generation and detection equipment and to qualitative observations of propagation and attenuation of surface waves in cadmium sulfide, a piezoelectric semiconductor. Because the comb transducer can produce compressional as well as surface waves, it is important to distinguish the surface waves from other wave types which produce a signal at the output transducer. Identification has been made in terms of the trapezoidal output signal characteristic of the surface waves and by the wave velocity, which is less than the bulk shear wave velocity by a fraction which depends for an isotropic substance only upon Poisson's ratio [2] .

One method of measuring the surface wave velocity is to determine the half-wavelength by moving an output comb transducer over the surface near the end of a plate (item 4 in Fig. 1); reflections at the right-hand end of the plate produce a standing surface wave whose periodic amplitude variations are easily detected. Such a measurement in fused silica gave a velocity 3.3×10^5 cm/sec in good agreement with the value 3.4×10^5 cm/sec calculated from the known elastic constants of fused silica. In an anisotropic medium, the possibility of surface wave propagation is open to question. Stonely has shown that in a hexagonal crystal, such as cadmium sulfide, surface waves can propagate along a free plane surface perpendicular to the c-axis.

Observations have been made here of photosensitive attenuation of 30 mc surface waves propagating on the surface of a fused silica plate on which a film of cadmium sulfide, a few microns thick, was vapor-deposited. This attenuation is now being studied in an attempt to correlate it with the properties of the film. In addition, photosensitive attenuation has been observed when single-crystal cadmium sulfide bars are interposed between two, fused silica plates in contact with surface-wave comb transducers. Electrically non-conducting transducers for direct contact to bulk, single crystals have been tested with success, preparatory to the study of surface-wave propagation, attenuation, and amplification in piezoelectric semiconductors.

SYNTHESIS OF INTEGRATED SELECTIVE AMPLIFIERS FOR SPECIFIED RESPONSE AND DESENSITIVITY

JSEP Grants AF-AFOSR-139-64 and 65
A.A. Gaash (Prof. D.O. Pederson)

This research project was completed during the period. The research results are reported in a Ph.D. dissertation of the same title and will also be issued as a technical report, an abstract of which follows.

The fundamental objective of this report is the realization of highly selective, bandpass network functions in the medium of semiconductor integrated circuitry. Realization of such

---

[2] H. Kolsky, Stress Waves in Solids, Oxford University Press, London, (1953).

circuit performance has to take into consideration the special properties of integrated, monolithic microcircuitry. In view of the unavoidable dependence of integrated passive and active components on environmental conditions and on manufacturing tolerances, synthesis procedures via sensitivity functions are explored. Attention is focused on closed sensitivity formulations in order to reveal extra degrees of freedom available for desensitization. To that end, various sensitivity functions in single-loop and multi-loop feedback structures are investigated. The effect on the variation of integrated passive components is then assessed. The corresponding sensitivity contributions are shown to be independent of the circuit configuration and are expressed in the form of sensitivity invariants.

Based on the sensitivity formulation, sensitivity criteria are incorporated into the synthesis procedures, permitting simultaneous realization of specified response and sensitivity. The procedures make use of multi-loop feedback structures, wherein redundant transmission loops are introduced together with the correlated nature of the time-dependent changes of integrated components.

To illustrate the synthesis procedures, the realization of totally desensitized, integrated, frequency-selective amplifiers is presented. This problem can not be solved by existing methods. Several representative design approaches are given and experimental realization is offered for each. Full agreement is found between experimental and theoretical results, confirming the feasibility of simultaneous realization of prescribed response and sensitivity.

INTEGRATED SELECTIVE AMPLIFIERS USING FREQUENCY TRANSLATION

JSEP Grant AF-AFOSR-139-65 and University of California Support
G.A. Rigby (Prof. D.O. Pederson)

The difficulties of realizing fully-integrated band-pass filters stem largely from the fact that no appreciable inductive energy storage is possible in the dimensions associated with integrated circuits. This limitation has led us to the use of a variety of active circuits using feedback or feedforward loops to achieve the required selectivity. These systems are severly limited by the temperature sensitivity of integrated circuit components and only the more sophisticated realizations have an acceptable degree of temperature stability. The use of acoustoelectric effects to make mechanical filter elements compatible with integrated circuits has received some attention and has a number of attractive features, although at present it appears to be limited to high-frequency applications.

The approach in this project is based on the formation of an actual band-pass to low-pass transformation in a system, thereby

changing the selective amplifier problem into the less formidable problem of realizing a stable lowpass transfer function in an integrated circuit. The class of system which uses this principle has been treated in considerable theoretical detail by a number of workers, but its applications have received relatively little attention in the area of integrated circuits.

The principle of this system can be seen from the example shown in Fig. 1. Each of the four identical channels consists of a low-pass amplifier with a cutoff frequency, ω_b. At the input and output of each channel is an analog multiplier driven from a clock signal at a frequency, ω_o, which becomes the center frequency of the pass band. The phasing of the multipliers is arranged in the cyclic form shown. If an input signal at a frequency ω_i is applied, the multipliers (assumed ideal) produce sum and difference frequencies at the input of each of the low-pass amplifiers. The sum frequency is heavily attenuated, since $\omega_b << \omega_o$, while the difference frequency is amplified if and only if it falls within the pass band of the amplifier. The output signals from the amplifiers are multiplied again with the correctly phased clock signal and the outputs, when summed, reform the input signal modified by an effective passband centered at ω_o with a bandwidth of ω_b. The reported realizations of this system have used sampling gates to achieve multiplier action with the consequent disadvantage that the output signal is rich in harmonics of the input frequency which are introduced by the gates and necessitate considerable filtering in addition to the basic system to restore a sinusoidal output. Furthermore, the nature of the sampling process places severe limitations on the magnitude of the center frequency. Such difficulties as these probably account for the limited results in integrated circuit form which has been shown in this technique.

In an attempt to overcome these problems an analog multiplier has been developed which approaches more closely the ideal operation described above. Its basic form is shown in Fig. 2. The emitter supply current, I_E, is modulated by a sinusoidal clock signal, i_E, while the input signal is applied to a differential current between the two bases. Using the simplest model of the transistors, one can show that the output from the multiplier when an input current i_i is applied is:

$$v_o = (I_E + i_E) R_L \cdot i_i R_i (q/kT).$$

Where q is the electronic charge, k is Boltzmann's constant and T is the absolute temperature of the devices. When full account is taken of the real nature of the transistors, this expression becomes far more complex and the achievement of optimum design and performance is far from a simple matter.

The project is being carried out in four stages:

(i) A general study of the realization of integrated selective amplifiers.

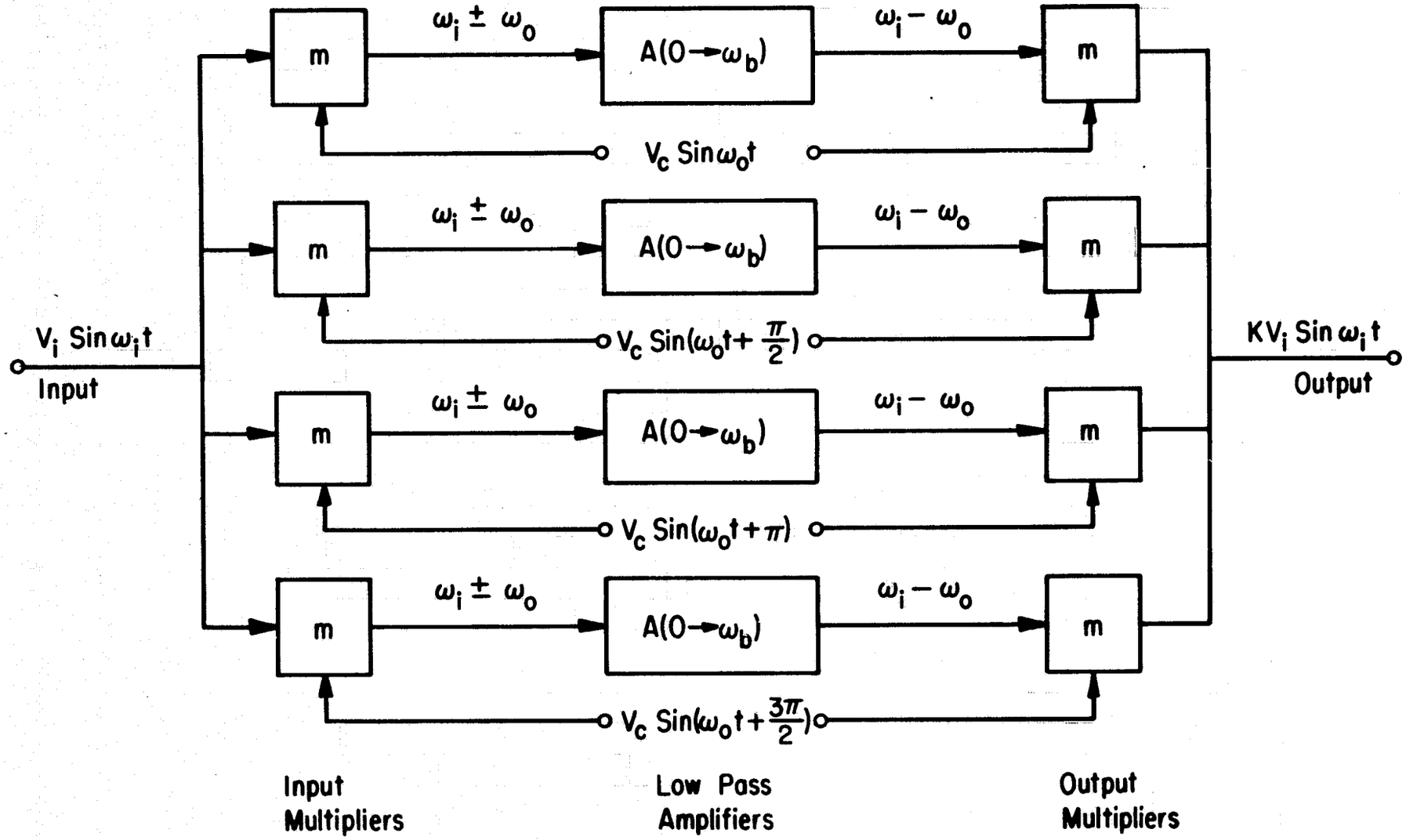

Fig. 1. Schematic diagram of 4-path band-pass amplifier using frequency translation.

(ii) An investigation of the theoretical aspects of the frequency translation scheme with particular emphasis on the use and design of analog multipliers. This stage is nearing completion, although further study of integrated multipliers is intended.

(iii) The design and construction of a complete system using lumped components. This stage has been irtually completed with the construction of an amplifier with a stable bandwidth of 43 Kc at a center frequency of 1.4 Mc. 12 transistors are used, not including the clock generator and power supplies. The dynamic range of the amplifier is approximately 500:1 with less than 5% distortion.

(iv) The development of a fully integrated form of this system. At this time, this phase has just been begun and no performance data is available.

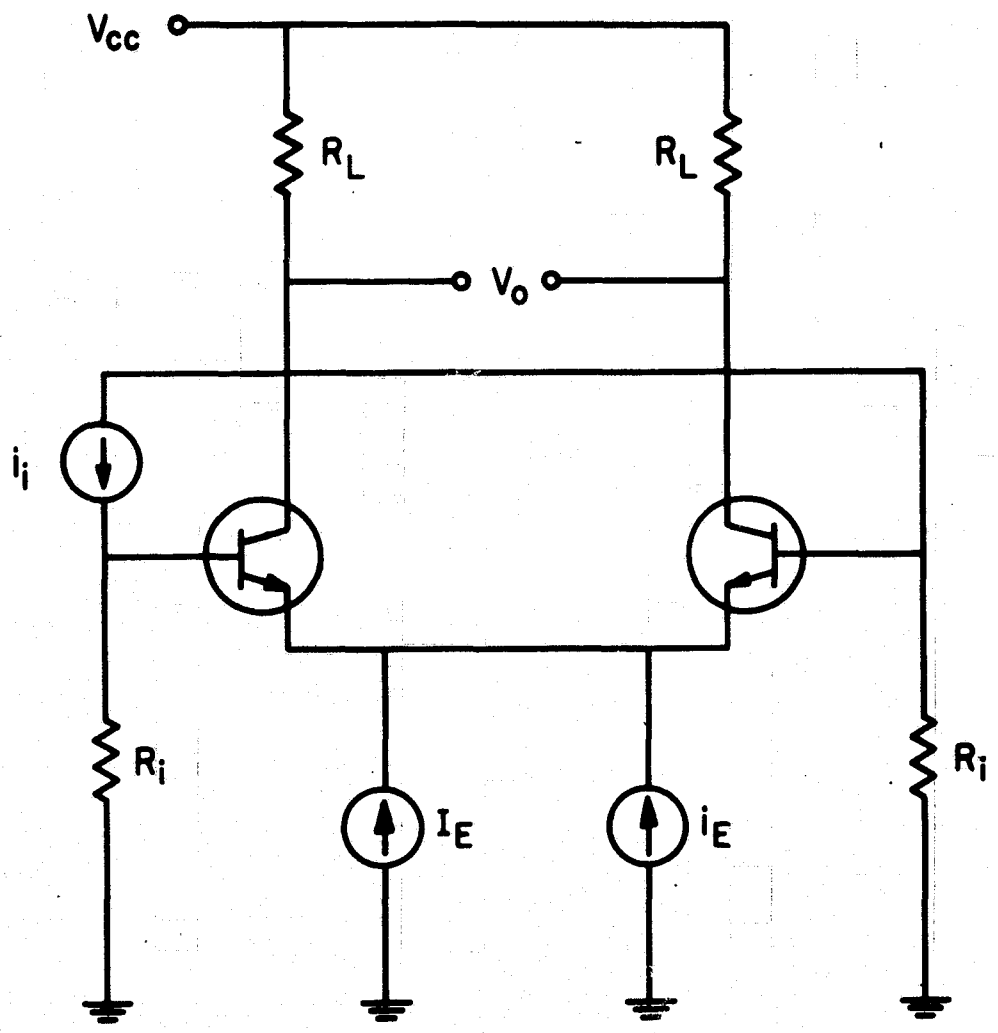

Fig. 2. Basic multiplier configuration.

INTEGRATED LOWPASS AMPLIFIERS

JSEP Grants AF-AFOSR-139-64 and 65
A. Brodersen (Prof. D.O. Pederson)

The realization of an integrated lowpass amplifier poses a number of conflicting constraints. The major problem is the determination

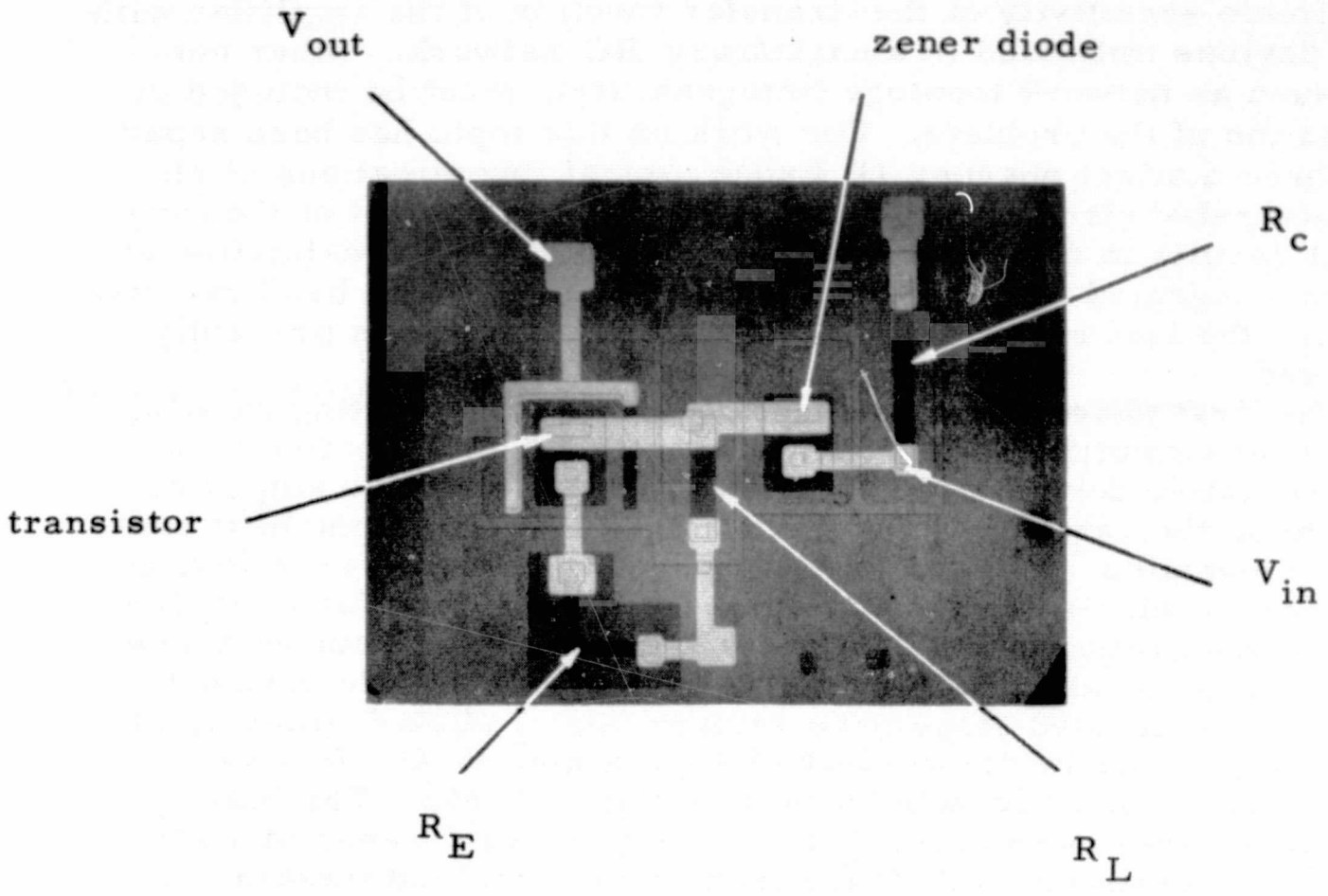

(a) Integrated amplifier.

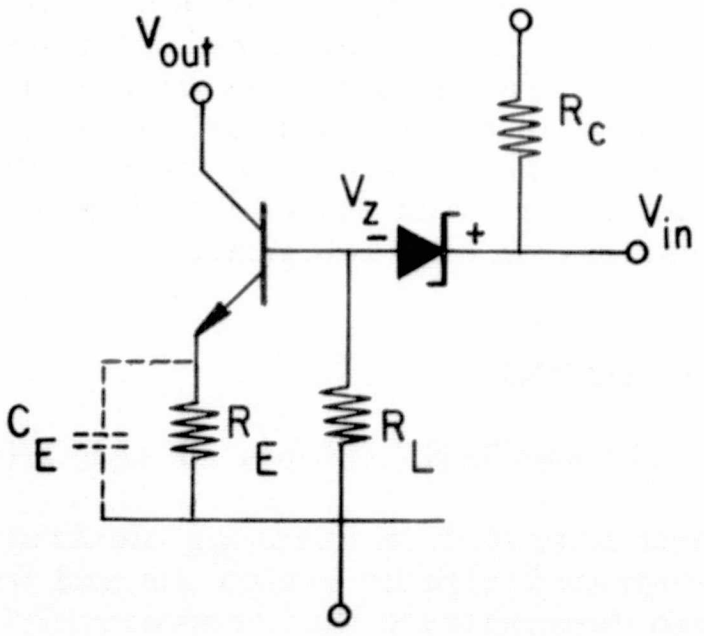

(b) Circuit schematic.

Fig. 1.

of the minimum sensitivity of the transfer function of the amplifier with the active devices imbedded in an arbitrary RC network. Other constraints, such as network topology (integrability), must be included in the formulation of the problem. Our work on this topic has been separated into three distinct phases: (1) Experimental investigations of elementary integrated circuits to gain insight; (2) Employment of theoretical circuit results to obtain fundamental limitations; (3) Realization of an optimum integrated lowpass amplifier. The first phase has been completed during the last report period and the second phase is presently being pursued.

The first phase of this project consisted of evaluating existing types of lowpass amplifier stages which employ bipolar junction transistors as the active devices. From among the five possible amplifier stages studied, the series RC feedback stage emerged as the best candidate for integration. The series RC feedback stage has excellent dc stability, ease of biasing and easily achieved ac coupling for cascaded stages. The integrated amplifier and its discrete-component prototype are shown in Fig. 1a and 1b, respectively. Both ac and dc measurements with the integrated stage have verified the predicted behavior of the stage. A gain-bandwidth product of approximately 40 Mc was observed, and the gain magnitude curve was flat to 15 Mc. The bias constancy of the stage was checked over a temperature range of 25 °C to 100 °C. The operating point of the transistor remained invariant as designed because of the cancelling temperature coefficients of the network.

The second phase of the project is the application of existing theoretical circuit results to the design of specified classes of lowpass amplifiers. Our approach uses first traditional circuit analysis to obtain the first-order restrictions and behavior of the desired RC imbedding network. Design criteria for this aspect includes a Butterworth characteristic. These results are then used to reformulate the problem in terms of the state variables. The state characterization exhibits the element values of the network in an explicit manner which makes the study of the sensitivity of the amplifier more tractable. The final results will be used to design a minimum sensitivity lowpass amplifier of desired or specified transmission characteristics.

SCANNING ELECTRON MICROSCOPY

AFAL Contract AF33(615)-2306 and JSEP Grants AF-AFOSR-139-64 & 65

The first area of our research in scanning electron microscopy is that of semiconductor integrated-circuit evaluation and testing. Our objectives in this area are to demonstrate that scanning electron beams can produce useful quantitative information about semiconductor integrated circuits, and to ascertain the limits of accuracy of this information. We are interested both in accuracy associated with spatial variations, which shall be termed "resolution," and with the measurement

accuracy of certain material parameters, such as doping level, diffusion length, lifetime, etc. The resolution obtainable in measuring semiconductor parameters will always be a function of the electron scattering in the target, which determines the electron-beam energy loss with distance from the point of bombardment, and the exit position of both back-scattered and secondary electrons from the sample. For this reason considerable effort was devoted to measurements relating to electron penetration and scattering, both along and perpendicular to the primary beam axis.

A second area of our research is the exploration of new areas for application of the scanning electron microscope, of basic improvement to the instrument's performance, and in improved methods of displaying information generated by the microscope. The scanning microscope used in the work reported below was built at the University of California and is described briefly in ERL Technical Memorandum M-100.

INSTRUMENT IMPROVEMENT

Profs. T. E. Everhart, R. F. W. Pease, and Mr. S. R. Pedersen

During this period the final magnetic lens, which was designed last summer was installed. After the aperture traverse mechanism was modified, this lens brought about a decrease in minimum spot diameter to less than 500 A. Unfortunately the gain so derived was partly offset by 60-cps magnetic fields causing undesirable spot movement of about 1000 A peak-to-peak. In spite of adding more magnetic shielding this effect still sets a limit to the useful resolution of the microscope. A field cancellation system is now being considered.

A new amplifier has been constructed which allows three different video signals to be mixed before the display CRT. This amplifier was necessary for the deflection modulation display discussed below.

SEMICONDUCTOR DEVICE MEASUREMENTS

P. Hoff (Prof. T. E. Everhart)

The purpose of this research is to develop electron-beam techniques for measuring semiconductor device parameters, such as oxide thickness, junction depth, metal lead thickness, lifetime, etc. By correlating these electron-beam measurements with more conventional measurements, we hope to evaluate the usefulness of the electron-beam measurements.

During this report period a mathematical model was developed to predict the electron beam-induced (EBI) current through a reverse-biased p-n junction which is parallel to the device surface. The model is based on the following assumptions: (1) that the hole-electron pairs created in the semiconductor device are proportional to the energy dissipation in the device, and (2) that the depth-dose function of Grün is a

valid representation of the energy lost with penetration depth into the device [1]. This function is approximated by a cubic power series, and the appropriate differential equation for minority carrier motion in the semiconductor is solved under the assumptions of small signals by applying the appropriate boundary conditions. The spatial distribution of carriers is determined vs the electron range R, using the surface recombination velocity, the minority carrier diffusion constant D, and the junction depth beneath the surface d, as parameters. In general, a rather complicated expression for the current through the reverse-biased p-n junction results; if we assume that $(R/L_n)^2 << 1$, where L_n is the minority carrier diffusion length, this complicated expression reduces to:

$$I_p = \frac{r V_0 I_0}{V_a} \left[\frac{1 + 0.41 \frac{v_s R}{D_n}}{1 + \frac{v_s d}{D_n}} \right] . \qquad (1)$$

In this equation, V_0 and I_0 are the primary beam voltage and current, respectively, V_a is the average excitation energy required to produce a hole-electron pair, r is the fraction of the incident beam power dissipated in the material, and the other parameters are defined above.

Brown develops a simpler model, assuming that energy loss per unit length is constant for depths less than electron-range R, and zero for depths greater than R [2]. Under the same assumptions made for the above equation, his corresponding equation is

$$I_p = \frac{r V_0 I_0}{V_a} \left[\frac{1 + 0.5 \frac{v_s R}{D_n}}{1 + \frac{v_s d}{D_n}} \right] . \qquad (2)$$

These expressions are quite similar, which suggests that under the above assumptions the electron-beam induced current through a p-n junction parallel to the surface is relatively insensitive to the exact distribution of energy loss with distance into the target. Comparisons of the more general expression derived by Brown and the more general expression derived in our work have not yet been completed.

Our analysis has also been carried out for a device covered by an oxide layer. The expression for the electron-beam induced current through a minor junction at distance d beneath the surface, in this case takes the form of

---

[1] See for example B.W. Schumacher, Electron and Ion Beam Science and Technology, pp. 5-70, ed. by R. Bakish, John Wiley & Sons, Inc., New York, (1965).

[2] A.V. Brown, IEEE Trans. on Electron Devices, Vol. ED-10, pp. 8-13, (1963).

$$I_p = \frac{r V_0 I_0}{V_a} \left[\frac{(1 - B_1) + \frac{v_s R}{D_n} (0.41 - B_2)}{1 + \frac{v_s d}{D_n}} \right] \qquad (3)$$

In the above equation, B_1 and B_2 are power series in t/R, where t is the oxide thickness.

Concurrently, experiments have been conducted with a 2N706 transistor to verify the model being developed. Thus far, the model and the measurements agree qualitatively; however, not all device parameters have been measured in alternative ways and therefore a complete quantitative check on the electron-beam measurements is not yet available.

TRANSVERSE SCATTERING OF ELECTRONS

W. W. L. Ho (Prof. T. E. Everhart)

The purpose of this work is to study the transverse scattering of kilovolt energy electrons in semiconductors (or other solids) using the scanning electron microscope (SEM). One attractive method of performing such measurements requires a thin planar region, which is perpendicular to the sample surface and which will measure all hole-electron pairs created within it. The depletion layer of a planar p-n junction perpendicular to the sample surface is such a region. However, electron-beam-excited carriers created outside the junction region by a primary beam normally incident to the sample surface may diffuse to the junction region and also be measured as an electron-beam-induced (EBI) current. It is desirable to avoid transverse scattering caused by a surface oxide; however, devices without a passivating surface oxide have unstable characteristics. Preliminary measurements have indicated many problems; additional measurements are planned on custom-made semiconductor samples, and on metal-oxide-metal samples, with a field across the oxide barrier. All experiments being planned involve the basic planar geometry discussed above.

ELECTRON SCATTERING MEASUREMENTS

Prof. R. F. W. Pease

The purpose of the current research on electron scattering measurements is to investigate the spatial scattering of electrons in a solid target with primary electrons in the range of from 5 to 30 kV.

The method is illustrated in principle in Fig. 1. The scattered electrons emerge over a relatively large area. When the electron beam impinges at a point well to the left of the electrode edge A, virtually no scattered electrons traverse the insulating film underneath the top electrode and no appreciable current is recorded on the micromicroammeter. As the beam is scanned to the right the induced current I_D will rise while

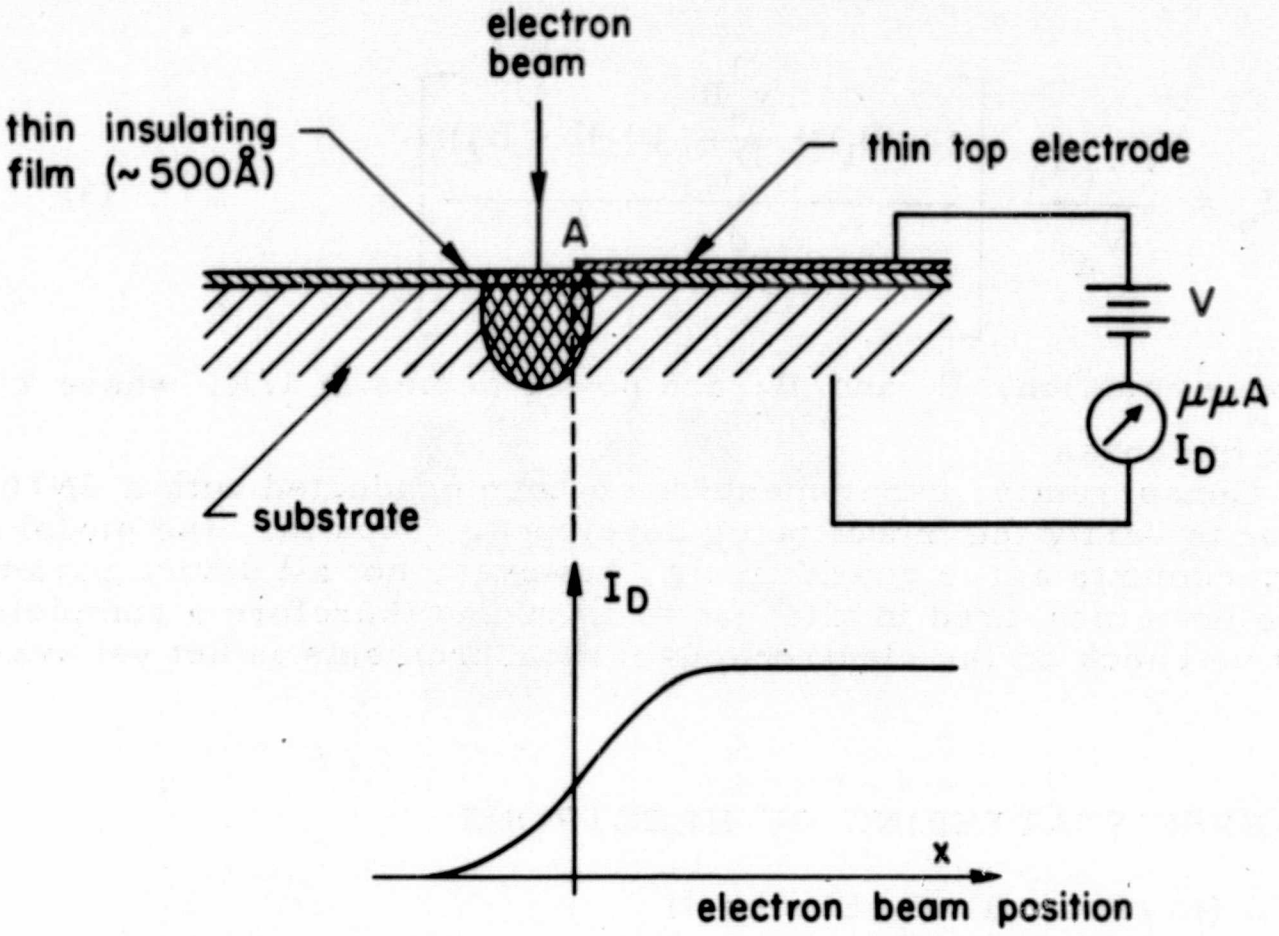

Fig. 1. Schematic view of experimental arrangement.

the area of scattered electrons is passing point A; thus by plotting electron beam position against induced current, a measure of the area of scatter at the surface can be obtained. By coating the target assembly with another insulating film and evaporating on a known depth of substrate material (Fig. 2) a measure of the area of scatter at a known depth can be obtained.

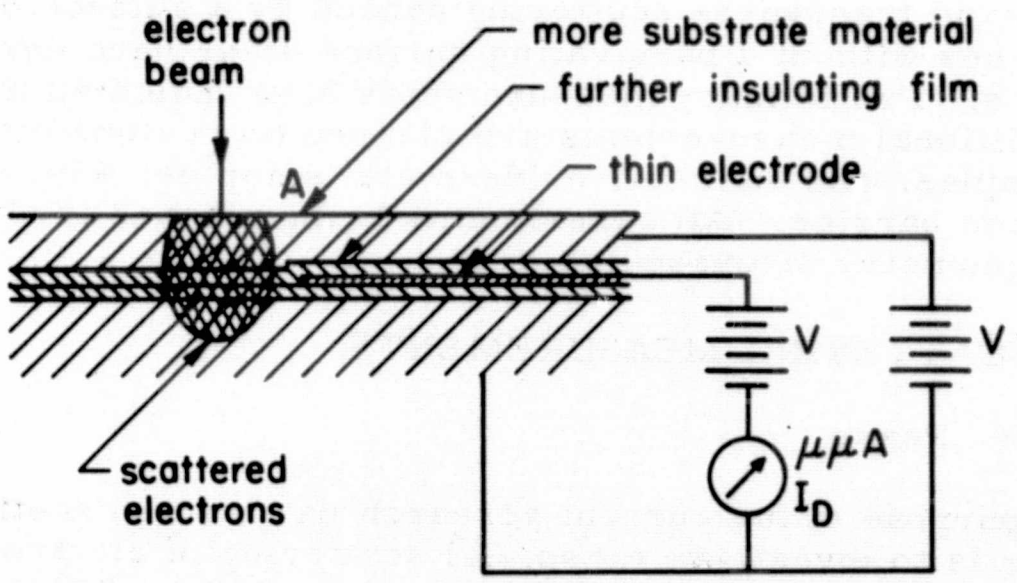

Fig. 2. Schematic view of proposed experimental arrangement.

Experimental Work

Experiments conducted thus far have used the setup shown in Fig. 1. The first practical problem was preparing a specimen with a very low (10^{-10} A) leakage current. So far specimens of Si with thermally grown SiO_2 and an Al top electrode have been successfully made; however, the SiO_2 had to be at least 1000 A thick if the bonding of a lead to the top electrode was not to short circuit the insulating film. However, specimens were also made with 700 A film of SiO_2 which had only pressure contacts to the top electrode which did not cause a short circuit.

The second problem was the unstable value of I_D due, presumably, to space charge arising from the carriers trapped in the SiO_2 film. McKay overcame this problem using a pulse technique [3], but in our experiment it was found that by adjusting the bias voltage V a stable I_D resulted. For lower values of V the value of I_D gradually decreased (over a period of minutes) and for higher values of V, I_D gradually increased. A value of V $\_$ 30 volts was found to give stable I_D across 1500 A SiO_2; this represents a field of 2×10^6 volts cm^{-1}. This effect will be investigated further.

The third problem was to ensure that the induced current was a direct measure of the electron current transversing the film. This was checked by simultaneously measuring I_D for different values of primary beam current I_B with the impact point being to the right of A in Fig. 1. It was found that proportionality between I_B and I_D existed for $I_B \leq 2 \times 10^{-11}$ A; above this value the induced current appeared to depend upon how well the beam was focused a well-focused beam giving less I_D than a defocused one.

A micrograph (X 6,500) of a specimen is shown in Fig. 3. The Al electrode is on the right. The regular (small scale) serrations are due to 60 cps beam wobble (see Instrument Section). The irregularity of the edge of the electrode gives a measure of merit for the present technique of depositing the top electrode using photo-resist techniques.

Figure 4 shows some typical results obtained with this specimen. Several observations can be made.

(i) the area of scattered electrons at the surface appear to be not more than about 1 micron diameter for 25 kV primary electron energy. This should be compared with the estimated effective range [4] of electrons in Si which comes to 5μ.

(ii) the line marking the position of the edge passes through a point of less tha $1/2\, I_D$ in two out of three cases, while it was expected

---

[3] K. G. McKay, Phys. Rev. 77, pp. 816-825, (1950).

[4] J. E. Holliday and E. J. Sternglass, J. Appl. Phys. 30, 1428, (1959).

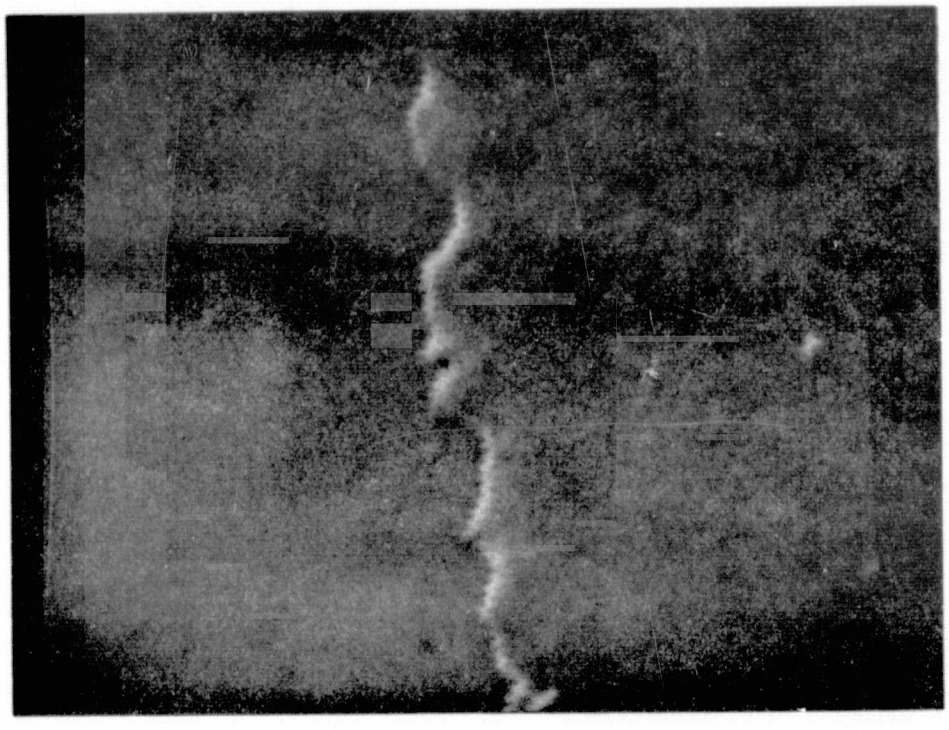

Fig. 3. Scanning electron micrograph x 6,500 of electrode edge. Electrode area is on the right.

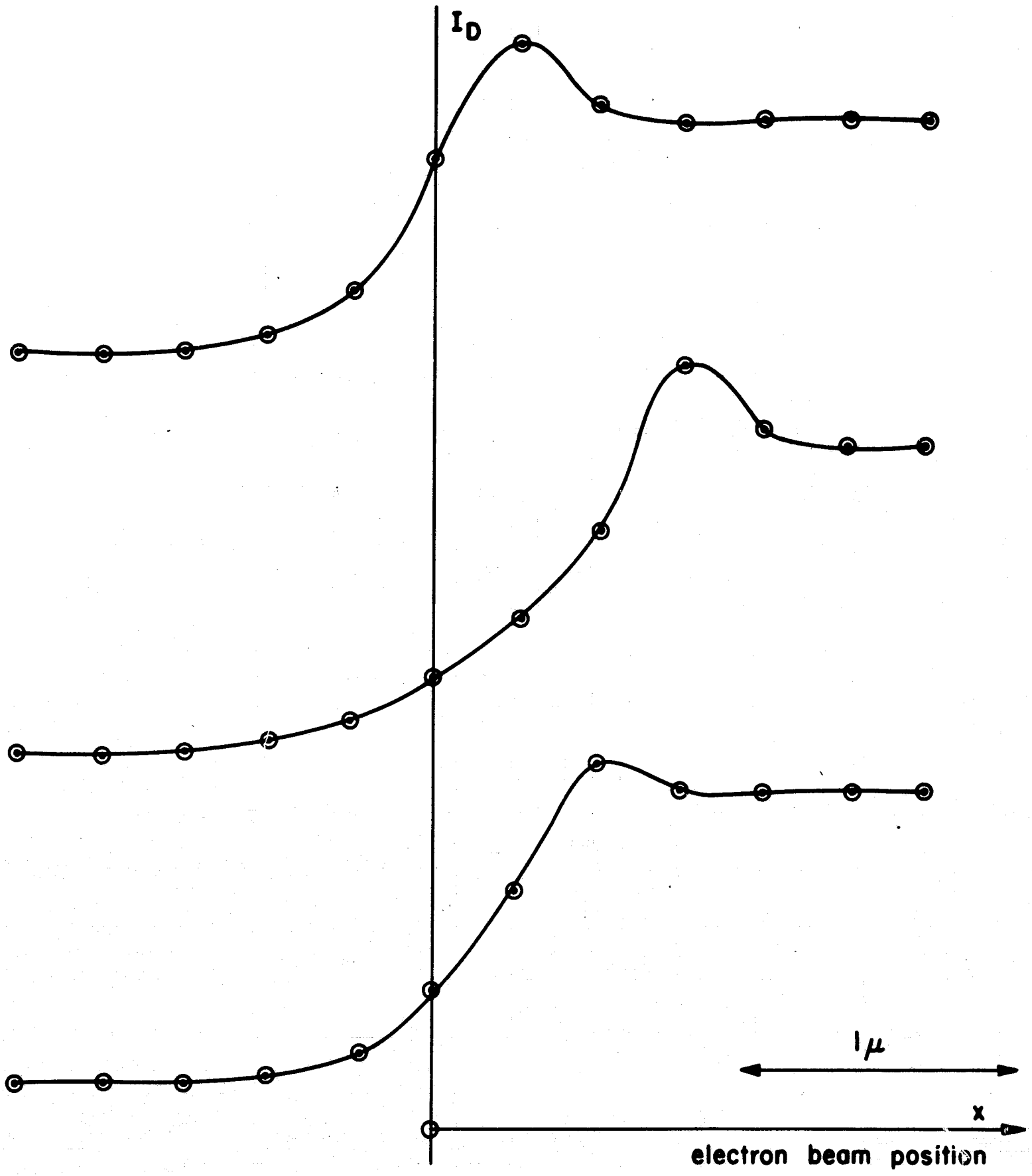

Fig. 4. Variations in I_d as electron beam is scanned across electrode edge at $x = 0$. The three curves represent reading for three different positions of the edge.

that the hole electron pairs created to the left of the electrode would diffuse towards the electrode and contribute to I_D.

(iii) most of the readings showed a peak in I_D when the point of impact was some way (between 0.3μ and 0.5μ) to the right of the electrode edge. A satisfactory explanation for this effect is still being sought.

Conclusions and Future Work

Using the method outlined, reproducible results have been achieved. It should be pointed out that the method does not give a direct measure of the number of electrons traversing the film but rather the energy dissipated in the film and this may be expected to increase with decreasing electron energy. When the method can be extended to aluminum targets and 30 kV beam, the results will be compared with those of an alternative method [5] using a reflection point projection technique in which the error is in the other direction.

At present the method is limited in accuracy by the 60 cps trouble with the SEM and is restricted by the difficulty of preparing pinhole-free thin insulating film substrates other than Si. It is hoped that both these problems can be overcome and that measurements can also be made in depth as shown in Fig. 2.

ELECTRON EXPOSURE OF SILICON-OXIDE SURFACES

Prof. T. E. Everhart

O'Keefe [6] recently reported that silicon oxide exposed to electron bombardment chemically etched three times more rapidly than unbombarded oxide. However, this technique requires exposures of approximately 1 coulomb/cm^2, compared with 10^{-5} coulomb/cm^2 required for KPR exposure [7]. The technique may be attractive for certain devices requiring high precision of registration of small areas, however, and for this reason, preliminary experiments were undertaken to evaluate the spatial resolution of the technique. Line patterns were exposed on one-micron thick oxide, and on a half-micron thick oxide, using various charge density exposures. Lines spaced by eight microns were very clearly resolved on one-micron thick oxide, and lines spaced by four microns were clearly resolved on the half-micron oxide. More careful and extensive experiments seem justified to evaluate this technique, and will be carried out as time and effort permit. Figure 5 shows a micrograph of lines spaced by 8 microns taken in the scanning electron microscope. Note that these lines are very uniformly spaced and are clearly resolved.

[5] R. F. W. Pease, J. Sci. Inst., 42, pp. 158-159, (1965).

[6] T. O'Keefe, Late Newspaper Spring Meeting, Electro-Chemical Society, San Francisco, May 1965.

[7] 4th Interim Engineering Report, Contract No. AF 33(657)-9897, 6 June - 6 September 1963.

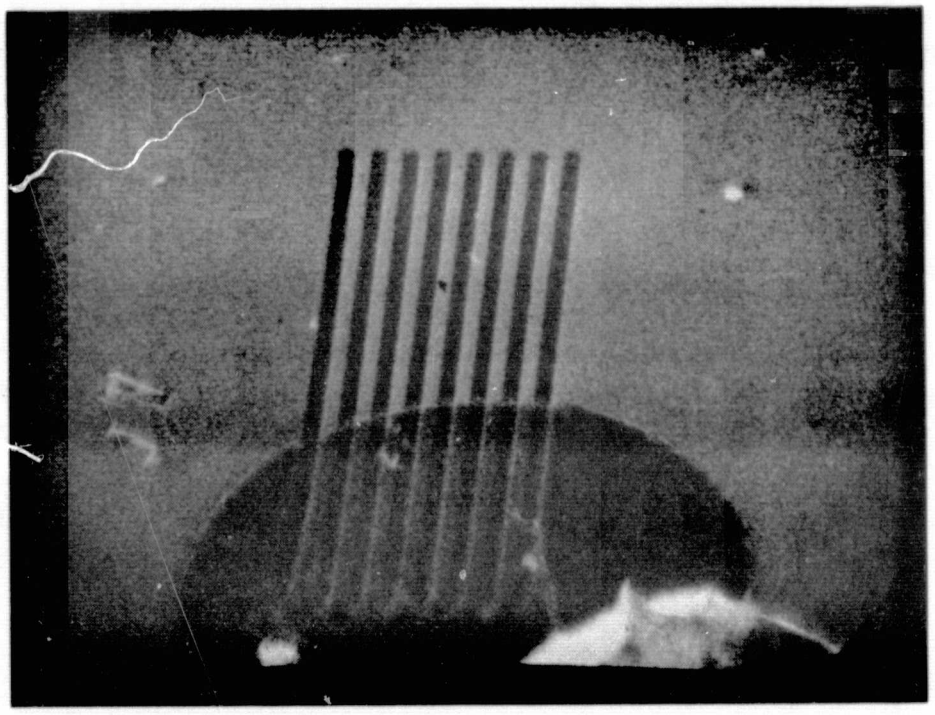

Fig. 5. Scanning electron micrograph of differentially etched lines in Silicon oxide, as explained in text.

DEFLECTION MODULATION DISPLAY

Prof. T. E. Everhart

A novel method of displaying information generated in a scanning electron microscope has been developed during the past period; it has been termed a deflection modulation display (DMD). In this display a constant current cathode-ray tube (CRT) beam is swept in a raster pattern, and the video signal is used to deflect the beam in one dimension producing a three-dimensional appearing display with a noticeably higher information content than is normally present in an intensity-modulated display (IMD), such as is used in television. There is some overlap of information in the deflection modulation display which can be distracting. An example of this display is shown in Fig. 6. Figure 6a shows a 64 line display where each line is clearly resolved and the deflection amplitude can be measured. Figure 6b shows the same area with a 256 line display where the lines are clearly resolved only in certain areas. Figure 6c shows that by rotating the deflection yokes in the column the areas of information overlap can be changed and the maximum information areas can be altered. A display similar to this using fewer lines has been described by Johnston [8] for electron beam current density measurements, and bv Grigson, for a scanning electron diffraction display using a chart recorder [9].

DEPLETION-WIDTH AND DOPING MEASUREMENTS

N. C. MacDonald (Prof. T. E. Everhart)

The depletion-region-width at the surface of an n-plus-p junction which had been angle-lapped at approximately 30° was measured as a function of applied bias, V, using the SEM. The depletion width was proportional to $V^{1/2}$; the doping of the high-resistivity p-type region was determined to be 6×10^{13} atoms/cc using this method, while the expected value based on surface resistivity measurements was 4×10^{13} atoms/cc. Thus the correlation is quite good. Additional measurements are planned to correlate with the theory of Davies and Gentry [10].

---

[8] T. W. Johnston, Proc. IEE, 105, Pt. B, Supplement No. 12, (1958).

[9] C. W. Grigson, private communication (1964).

[10] R. L. Davies and F. E. Gentry, IEEE Trans. on Electron Devices, vol. ED-11, pp. 313-323, (1964).

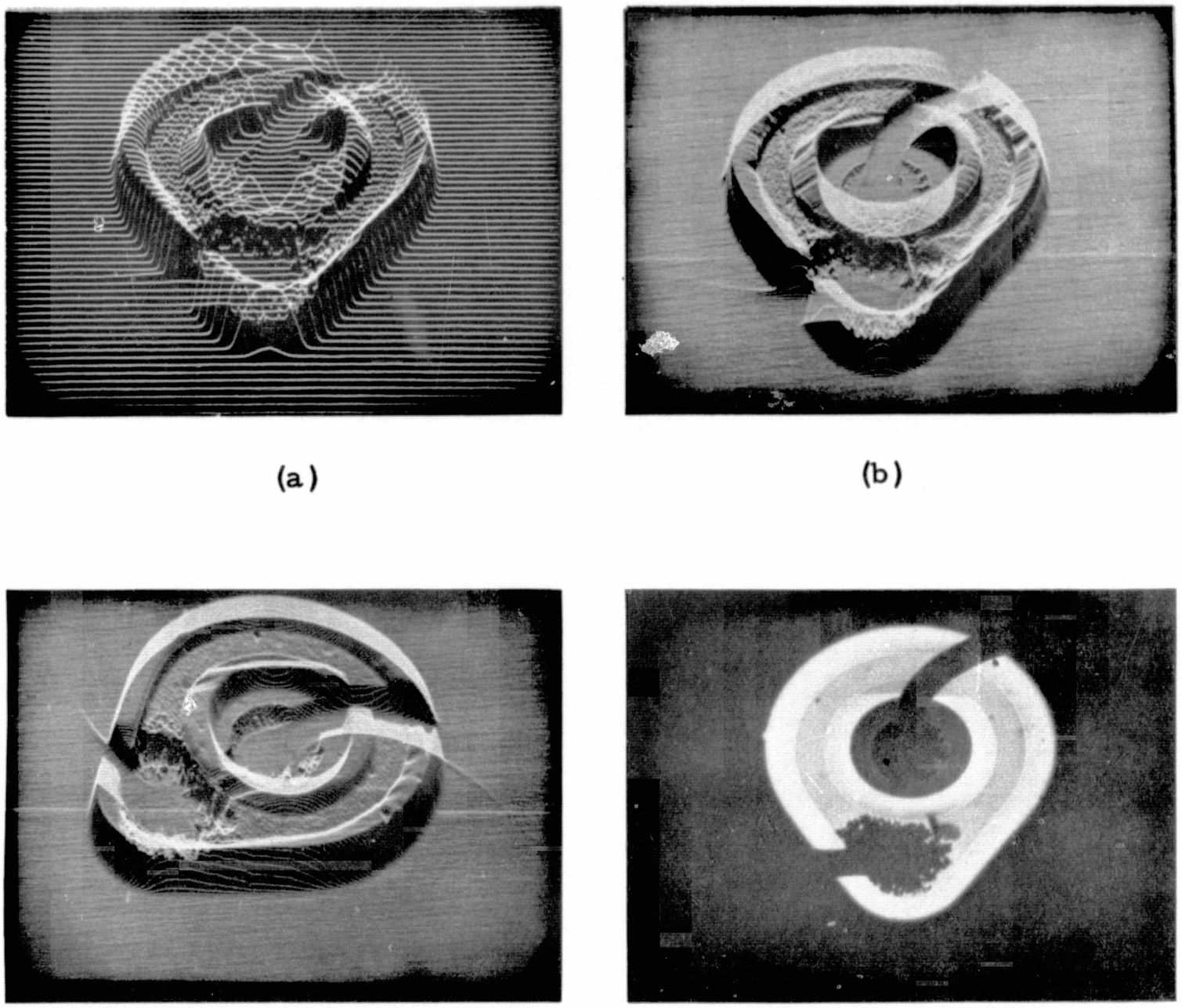

(a) (b)

(c) (d)

Fig. 6. Micrograph illustrating the deflection modulation display.

BLANK PAGE

H. SYSTEMS

General system theory includes many overlapping areas such as control theory, circuit theory, communication theory, information theory and coding, finite state automata, pattern recognition, and techniques of mathematical programming. These areas, though different in their motivation and application, have a great deal in common conceptually, as well as in the approaches and techniques encountered in them. Among the general system concepts we might list "linearity," "equivalence," "stability," and "fuzzy sets," while techniques such as mathematical programming, successive approximation procedures, and tools of probability theory are used almost universally.

The specific problems reported here have a much greater degree of cohesion than is suggested by their titles alone. The cementing matter is system theory which provides for continuous interactions among all these topics.

THE PROBLEM OF NEURON MODELING

AFOSR Grant AF-AFOSR 292- 64
J. G. Blanchard (Prof. E. I. Jury)

A simplified model of a neural element which can be of interest in the study of sensory receptors and the transmission of information to axons is the subject of a paper submitted for publication.* A mathematical definition of the elements of this model is given. It is also shown that this model satisfactorily describes the main electrical properties encountered in the electrical behavior of a neural membrane and that a digital simulation can be easily achieved.

OPTIMAL COMPENSATOR FOR RANDOM DISTURBANCES

NSF Grant GP-2413
B. Gillet (Prof. O. J. M. Smith)

It is assumed that a feedback system with random commands, random load disturbances, and a fixed dynamic output member preceded by a saturating amplifier, can be controlled by a nonlinear optimal controller. The design can be automatically adjustable such that each parameter in the nonlinear decision controller is significantly adjusted to minimize the system error power.

---

*IEEE Trans. on Biomedical Engineering.

The design of this controller is a function of both the spectra of the signals and the dynamics of the output member.

A simulation, in the case of a second-order dynamic output member, has been made on the analog computer according to the following block-diagram

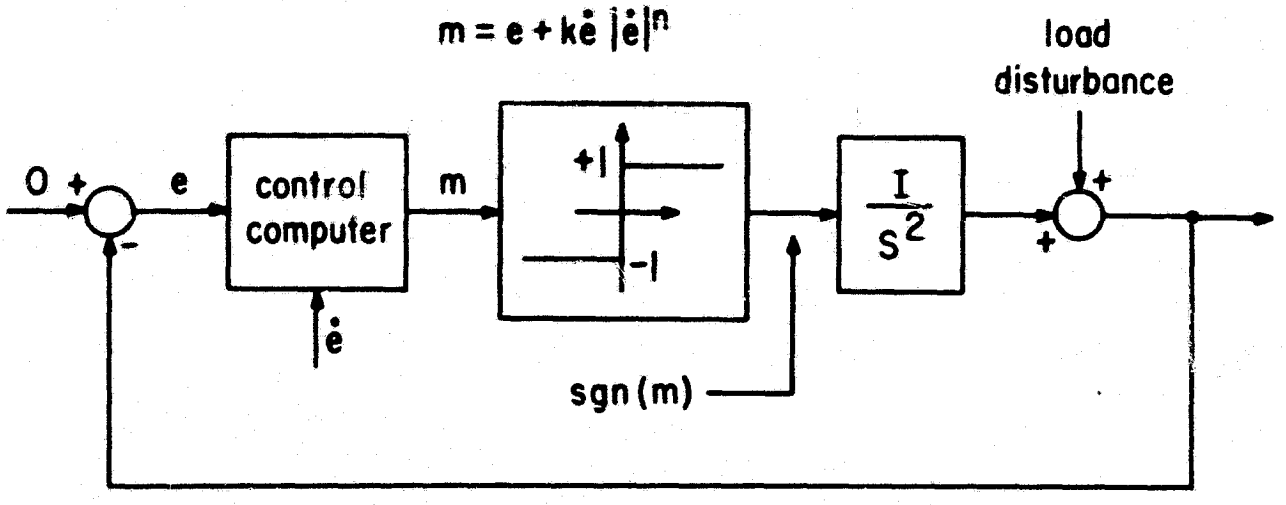

In the particular case of a square wave disturbance, a phase-plane analysis yielded the values of the parameters k and n. The same method should be applied to other classes of disturbances.

OPTIMAL CONTROL OF CONTINUOUS-TIME STOCHASTIC SYSTEMS BASED ON NOISY OBSERVATIONS

JSEP Grants AF-AFOSR-139-64 & 65
R.E. Mortensen (Prof. L.A. Zadeh)

More than a year ago, Kushner [1] * published a somewhat heuristic derivation of a nonlinear, stochastic, partial differential equation which, he asserted, is obeyed by the conditional probability density for

---

*References for this section are listed on page

the current state of a continuous-time dynamical system, given the entire past history of the noisy observations of its output. In the same paper, he sketched how this equation could be applied to the stochastic optimal control problem. Using the probability density itself to represent the current state of the system so far as the controller's knowledge of it is concerned, Kushner used dynamic programming to obtain a function space version of the stochastic Hamilton-Jacobi equation.

Kushner's approach represents a very creative idea. Unfortunately, in addition to having a rather high heuristic content, his work contains certain errors. But if his approach can be carried through in a completely rigorous way, it will in fact represent the complete, although abstract and theoretical, solution to the stochastic optimal control problem.

Recently, Bucy [2] presented his version of a derivation of the partial differential equation for the conditional probability density. His published treatment is however quite sketchy and some of the steps are somewhat obscure.

References 1 and 2 represent only a portion of the effort that has been directed towards obtaining the equation for the conditional density [3 - 5]. The basic difficulty, which these workers attempt to surmount by various techniques, is that a rigorous treatment of the problem must proceed from the theory of probability measures in function space.

Almost twenty years ago, Doob [6] discussed the problem of establishing a probability measure on function space. He noted that the approach one would like to take was blocked by what then appeared to be certain fundamental obstacles. In 1959, Nelson [7] presented a treatment of the problem which overcame many of the obstacles Doob noted.

Nelson published another paper in 1964 [8] and used his approach specifically to construct the Wiener integral. This paper should be carefully compared with another treatment of the subject by Kac [9]. One will note that the difficulties observed by Kac disappear under Nelson's treatment.

Nelson's approach is as follows: Rather than use the standard Kolmogorov [10] method to construct a measure, which consists of first defining a sigma-field of measurable sets, then assigning a measure to each of the sets in the sigma-field by means of a countably additive set function, Nelson uses an analytic approach. He first imbeds the desired function space in a much larger space, which is, however, a compact Hausdorff space under the appropriate topology. Rather than define the measure first then the integral, Nelson defines the integral first. He starts by defining the integral only for the tame functions on the compact Hausdorff space. This integral is a continuous, linear functional, bounded in norm. By the Stone-Weierstrass theorem [11], the class of tame functions can be extended to the class of all continuous functions on the space. By the Hahn-Barach theorem [12], the domain of the integral can be extended to this class of continuous functions. Finally, by the Riesz representation theorem [12], this integral implies a measure which is a countably additive set function over the sigma-field generated by the closed sets.

In the particular case of Wiener measure, Wiener space is a subset of the big compact Hausdorff space. However, Nelson has no difficulty in showing that this subset has measure one. This concludes Nelson's treatment.

So far, we are still working with the relative topology in Wiener space, which is the topology of pointwise convergence [13]. However, it is easy to show that Wiener space is a separable Banach space [12] under the uniform norm (sup norm), and hence satisfies the second axiom of countability [13]. Now, the topology associated with the uniform norm is, of course, the strong topology. We would like to have every set in the sigma-field generated by the strong topology on Wiener space to be Wiener measurable. It is not difficult however to show that this is so. We may take as a base [13] for the strong topology a class of sets, all of which are Borel sets in the pointwise topology. Every set in the base is thus Wiener measurable under Nelson's definition. But since the second axiom of countability is satisfied, every set in the strong topology can be represented as a countable union of sets in the base and we have the desired result.

We now restrict our attention to the class of stochastic dynamical systems which generate automorphisms in Wiener space. This class includes most of the systems of practical interest.

The measure induced on function space by the sample functions of the dynamic system is thus defined in terms of Wiener measure through this automorphism. By using the Radon-Nikodym theorem [14], there is no difficulty in defining a function-space version of the desired conditional-probability measure. When this measure is restricted to the state space of the system, it is easy to show that it is a regular conditional measure, at least when the dynamic system satisfies certain Lipshitz conditions. By then showing that this measure on the state space is absolutely continuous with respect to Lebesgue measure, we obtain a rigorous definition of the desired probability density.

As Bucy [2] points out, in order to obtain the dynamic equation obeyed by the conditional density it is necessary to employ the Ito [15] stochastic differential. Furthermore, to interpret what constitutes a solution to the equation, it is necessary to employ the Ito stochastic integral [16].

Having obtained the dynamic equation for the conditional density in a rigorous manner, one may then approach the stochastic optimal control problem much as Kushner [1] suggests, via dynamic programming. Kushner's sketch of a derivation of the stochastic Hamilton-Jacobi equation in function space can be refined and completed by employing the Frechet derivative [17]. Furthermore, it is possible to develop an algorithm for actually solving this equation by use of quasi-linearization.

In the above, we have employed two very important and entirely distinct generalizations of the ordinary notions of derivative and integral. On the one hand, we have the Nelson integral and the Frechet derivative in function space; on the other, we have the Ito stochastic integral and differential. The function-space integral and the stochastic integral

both go back to Norbert Wiener's pioneering work which was far ahead of its time in the early 1920's. The function space derivative was originally introduced by Volterra. A similar concept was given by Gateaux. The rigorous definition is due to Frechet and, more recently, Dieudonne. Finally, the stochastic differential is original with Ito.

We may expect that function space integrals and derivatives, and stochastic integrals and differentials, will be a standard part of the tool kit of the control system scientist of tomorrow, and will be employed routinely to solve the challenging problems of the future.

The preceding discussion will be developed in detail in a forthcoming thesis.

REFERENCES

[1] H.J. Kushner, "On the differential equations satisfied by conditional probability densities, with applications," J. Math. Anal. and Appl., Vol. 8, (1964).

[2] R.S. Bucy, "Nonlinear filtering theory," (correspondence) IEEE Trans. Automatic Control, April 1965.

[3] R.L. Stratonovich, "Conditional Markov processes," Theory of Probability and its Applications, Vol. 5, (1962).

[4] R.L. Kashyap, "On the partial differential equation for the conditional probability distribution for nonlinear dynamic systems with noisy measurements," Division of Engineering and Applied Physics, Harvard University, Cambridge, Mass.

[5] E. Wong and M. Zakai, "On conditional Markov processes," unpublished manuscript.

[6] J.L. Doob, "Probability in function space," Bull. Amer. Math. Soc., Vol. 53, pp. 15-30, (1947).

[7] E. Nelson, "Regular measures on function space," Annals of Math., Vol. 69, pp. 630-643, (1959).

[8] E. Nelson, "Feynman integrals and the Schroedinger equation," J. Math. Phy., March 1964. Vol. 5, No. 3, pp. 332-343. See appendices A and B.

[9] M. Kac, Probability and related topics in Physical Sciences, Interscience, New York, (1959). See Chap. 4, "Integration in Function Spaces and Some Applications."

[10] A.N. Kolmogorov, Foundations of the theory of probability, Chelsea, New york, pp. 27-33 (1956).

[11] R.C. Buck, (editor), Studies in Modern Analysis, Prentice-Hall, Englewood Cliffs, N. J., pp. 30-87, (1962).

[12] N. Dunford, and J.T. Schwartz, Linear Operators, Part I: General Theory, Interscience, New York, (1964).

[13] J.L. Kelley, General Topology, D. Van Nostrand Company, Inc., Princeton, (1955).

[14] P.R. Halmos, Measure Theory, D. Van Nostrand Company, Inc., Princeton, (1950), pp. 128-130.

[15] K. Ito, Lectures on Stochastic Processes, Tata Institute for Fundamental Research, Bombay, India, (1961).

[16] J.L. Doob, Stochastic Processes, John Wiley and Sons, Inc., New York, (1953), pp. 436-451.

[17] L.A. Liusternik and V.J. Sobolev, Elements of Functional Analysis, Ungar, New York, (1961), Chap. VI.

TIME OPTIMAL CONTROL OF NONLINEAR SYSTEMS

NSF Grant GP-2413
C.D. Cullum (Prof. E. Polak)

During this report period, a number of nonlinear, time-optimal, regulator problems have been investigated using the principle of equivalence discussed by this author in other reports.* These problems take the following forms:

Problem I:

State Equations of the System

$$\dot{x}_1 = f_1(x_2),$$

$$\dot{x}_2 = f_2(x_3),$$

$$\dot{x}_3 = u, \qquad u \text{ is a scalar}$$

where $f_i(x)$, $i = 1, 2$ are differentiable functions satisfying,

a) $f_i(0) = 0$

b) $f_i'(x) > 0 \quad \forall\ x$

Problem

Given an arbitrary initial state, find the measurable control function $u(t)$ with $|u(t)| \leq 1$ which brings the state of the system to the origin in minimum time.

* Electronics Research Laboratory Quarterly Progress Reports No. 10, p. 61; and No. 15, p. VII-11.

Problem II:

System

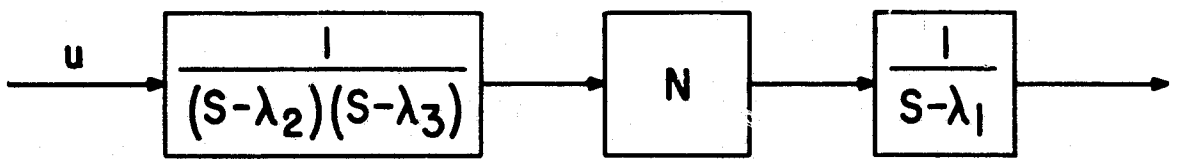

State Equations

$$\dot{x}_1 = \lambda_1 x_1 + N(x_2 + x_3),$$

$$\dot{x}_2 = \lambda_2 x_2 + (\lambda_2 - \lambda_3)\, u,$$

$$\dot{x}_3 = \lambda_3 x_3 - (\lambda_2 - \lambda_3)\, u,$$

where i) $\lambda_1, \lambda_2, \lambda_3 < 0$, $\lambda_2 \neq \lambda_3$

ii) $N(x)$ is a differentiable nonlinear function satisfying,

a) $N(0) = 0$

b) $N'(x) > 0 \quad \forall\ x.$

Problem

Same as in Problem I.

Using Pontryagin's maximum principle it has been shown for these problems that every optimal control is bang-bang with at most two switchings. It still remains to be shown that every control function which is bang-bang with at most two switching is optimal for some point, hereafter referred to as property (A). It is reasonable to believe that this is true for the systems considered, and a proof is the goal of current investigation. It can be stated that every system of the form given in Problem I or Problem II possessing property (A) will be equivalent to a linear system with real eigenvalues. This means that a computational procedure for the solution of such nonlinear, time-optimal, control problems can be formulated in terms of the known solution of the time optimal control problem for a linear system with real eigenvalues.

The computational procedure for the solution of such nonlinear problems utilizes the 1-1, onto map f from the state space X of the nonlinear system to the state space Y of a linear system with real eigenvalues (referred to as the prototype system) whose inverse function f^{-1} is defined by the following rule:

(a) To each state $y \in Y$ is associated the optimal-control function $u_{(0,t_1]}$, which brings the linear system from the initial state y to the origin in minimum time.

(b) Since the set of optimal-control functions for the linear and nonlinear systems are identical, there exists an initial state of the nonlinear system, $x \in X$, which is brought to the origin in minimum time by the control $u_{(0,t_1]}$ defined in (a). This state x is found by solving the state equations of the nonlinear system backward in time from the origin using the control $u_{(0,t_1]}$.

(c) Then f^{-1} is defined by $f^{-1}(y) = x$, where x is determined according to a and b.

In order to compute f^{-1} it is necessary and sufficient to know (1) the nonlinear system equations, and (2) a computational algorithm for solving the linear time optimal control problem. In all cases examined to date f has turned out to be a homeomorphism with f and f^{-1} piecewise differentiable. Thus it is possible to obtain $y = f(x)$ (and therefore the corresponding optimal control function) for any $x \in X$ by straighforward iterative techniques for inverting f^{-1}.

It should be noted that a critical part of the procedure is the possession of a computational algorithm for solving the linear time optimal control problem. Such algorithms have been developed [1], [2], but none can yet be called completely satisfactory from the standpoint of speed of convergence and ease of application. Future research will consider the problem of obtaining a prototype problem equivalent to the linear and nonlinear problems discussed above, but whose computational algorithm will involve direct calculation rather than iterative techniques.

ESTIMATIONS AND CONTROL OF NONLINEAR PHYSICAL SYSTEM

NASA Grant NSG-354 (Supplement 2)
T.C. Gaw (Prof. M. Aoki)

The problem under investigation is a class of adaptive control systems. It is assumed that the system dynamics is governed by

$$\frac{dx}{dt} = f(x,u,t),$$

where x = state variables, and

u = control.

The output or observation $y = h(x)$ + noise is assumed to be contaminated with noise of unknown probability distribution and the control u satisfies the equation

$$\frac{du}{dt} = g(u,t,y).$$

The purpose of this project is to find the best estimate of the state variables $x(t)$ under the circumstances given above. Using the criterion

$$F[\,u(t),\ \hat{x}(t),\ t\,] = \int_0^t dt \left\{ [\,k_1 \hat{x}^2(t) + k_2 u^2(t)\,] + 2[\,y(t) - h\hat{x}(t)\,]^2 \right\},$$

and invoking the invariant imbedding technique, the following results are obtained

---

[1] L.W. Neustadt, "Synthesis of Time Optimal Control Systems," J. Math. Anal. and Appl. 1, pp. 484-492 (1960).

[2] J.H. Eaton, "An Iterative Solution to Time Optimal Control," J. Math. Anal. and Appl., Vol. 5, No. 2, pp. 329-344 (1962).

$$\frac{d\partial}{dt} \simeq \partial\left[\, 2f_s + \frac{2k_2 c}{k_1 s - \lambda\,(y - h(s)\,dh/ds}\,\right]$$

$$-\partial^2\left[\, k_1 - 2\lambda\left[\, y(t) - h(s)\right]\frac{d^2h(s)}{ds^2} + \lambda\,\frac{dh(s)}{ds}\,\right], \qquad (1)$$

$$\frac{ds}{dt} = f - \partial\left[\, k_1 s = \lambda(y - h(s))\,\frac{dh}{ds}\,\right], \qquad (2)$$

where $x = s$ (present estimate),

$u = c$,

$f_s = \frac{\partial f}{\partial s}$.

To test the applicability of the above technique, a few computer runs will be made. The solution of Eq. 2 will be compared with the solution of the state variables obtained from known noise characteristics.

GAIN FUNCTION CHARACTERIZATION OF SYSTEMS

NASA Grant NSG-354 (Supplement 2)
D. Chazan (Prof. C.A. Desoer)

In the study of control systems it is almost universally assumed that the behavior of a (continuous time) control system is described by a differential equation partial or otherwise. In this work a different and more general description of control problems has been investigated which does not involve any differential euqations and attempts to reduce the problem to essentials. An inquiry was made into the possibility of translating some of the results of control theory into this setting. The answer obtained was in the positive at least in the special case that was studied.

At the base of this approach lies the concept of a gain function which assigns to every pair of states in the state-fine space the gain incurred in going from one state to the other. Such gain functions satisfy the following semi group condition:

$$C_{t_1 t_2}(x,y) = \sup\left[\, C_{t_1 t_3}(x,z) + C_{t_3 t_2}(z,y)\right] \qquad (1)$$

whenever $t_1 \leq t_3 \leq t_2$ (see quarterly report No. 14), and may be used to define a generalized system which is not necessarily describable by a differential equation. Thus a valid and mathematically interesting problem is the characterization of functions satisfying Eq. 1. A complete solution to this problem would certainly produce a generalized maximum principle as a by-product. The following is a first step in this direction:

Theorem: Let X be a locally convex linear topological space. Let T_t be a one parameter time group of continuous linear transformation on X which is continuous in t is some well defined sense. If $C_{t_1 t_2}(x, y)$ is a gain junction (i.e. it satisfies Eq. 1), $C_{t_1 t_2}(x, y) = C_{0, t_2 - t_1}(0, y - T_{t_2 - t_1} x)$, $C_{0,t}(0, x)$ is upper semi continuous in x and whenever $t_n \longrightarrow 0$ $C_{0, t_n}(0, x_n) \longrightarrow -\infty$ unless $x_n \longrightarrow 0$ then the function $C_{0, t}(\cdot, \cdot)$ is convex. Furthermore it is possible to obtain a complete characterization of $C_{0, t}(0, \cdot)$ which in the special case when X is a Banach space and T_t is continuous in t uniformly on X reduces to:

$$C_{0,t}(0, x) = \sup\left\{\int_0^t c(u(t)\, dt : \dot{x} = Ax + u, x(0) = 0, x(t) = 0\right\}$$

for some convex function $c(\cdot)$ on X and a continuous linear operator A.

STABILITY OF NONLINEAR SINGLE-LOOP FEEDBACK SYSTEMS

NASA Grant NSG-354 (Supplement 2)
C.T. Lee (Prof. C.A. Desoer)

We consider the system S shown in Fig. 1

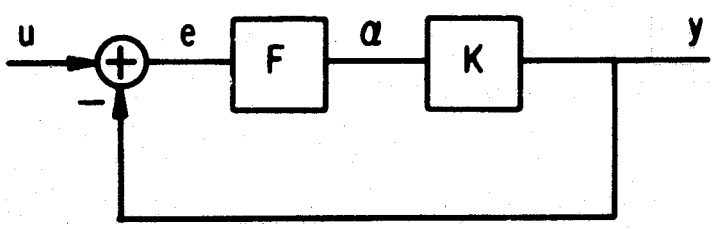

Fig. 1. The system S .

It is a single-input single-output feedback system. The system is characterized by following operator equations.

$$\begin{aligned} e &= u - y \ , \\ \alpha &= Fe \quad , \\ y &= K\alpha \quad , \end{aligned} \tag{1}$$

where F and K are operators.

(1) may be written as

$$(I + KF)\, e = u \qquad (2)$$

$$y = KFe\,. \qquad (3)$$

We shall introduce some notations before proceeding to the problems

1. H : a real Hilbert space, $\langle \cdot\,, \cdot \rangle$ will denote the scalar product in H, and $\|\cdot\|$ corresponding norm.

2. Let x be a real valued function defined on $[0, \infty)$. Let us call P_T the projection operator such that

$$(P_T x)(t) = x(t) \qquad \text{for } 0 \leq t \leq T$$

$$= 0 \qquad \text{elsewhere}\,.$$

3. H_e : an extension of H such that

   a) the elements of H_e are functions defined on $[0, \infty)$

   b) if $x \in H_e$

   $P_T x \in H$ for all finite T.

4. An operator $F: H_e \longrightarrow H_e$ is said to be of a finite gain if there are two real numbers $g(F)$ and r_F such that

   $\|P_T Fx\| \leq g(F)\, \|P_T x\| + r_F$ for all $T \geq 0$ and for all $x \in H_e$.

5. L^2 : a set of square integrable real valued functions on $[0, \infty)$.

6. L_e^2 : a set of locally square integrable real valued functions on $[0, \infty)$. L_e^2 is an extension of L^2.

7. An operator F is said to be nonanticipative if and only if

$$P_T F = P_T F P_T \qquad \text{for all } T \geq 0$$

8. We shall often write x_T for $P_T x$, and we adopt the following conventions

$$\|x\|_T \triangleq \|x_T\| \qquad \forall\, x \in H_e\,,$$

$$\langle x, y \rangle_T \triangleq \langle x_T, y_T \rangle \qquad \forall\, x, y \in H_e$$

The main results obtained shall be stated as following theorems

Theorem 1

Consider the operator Eq. 2

Suppose that

i) all solutions of (2) for $u \in H$ belong to H_e

ii) $F: H_e \longrightarrow H_e$ and $K: H_e \longrightarrow H_e$

iii) there are sequences of real numbers

$$\{k_i^{(1)}\}_{i=0}^{i=n}, \{k_i^{(2)}\}_{i=0}^{i=n}, \{k_i^{(3)}\}_{i=0}^{i=n}, \{k_i^{(4)}\}_{i=0}^{i=n}, \{P_i\}_{i=0}^{i=n}$$

such that for all $x \in H_e$ and for all $T \geq 0$

$$< x, Fx >_T \geq \sum_{i=0}^{n} \{k_i^{(1)} \|x\|_T^{P_i} + k_i^{(2)} \|Fx\|_T^{P_i}\},$$

and

$$< Fx, KFx >_T \geq \sum_{i=0}^{n} \{k_i^{(3)} \|Fx\|_T^{P_i} + k_i^{(4)} \|KFx\|_T^{P_i}$$

where

$$0 \leq P_0 < P_1 < \cdots < P_n$$

$$1 < P_n .$$

Under the above assumptions all solutions of (2) for $u \in H$ belong to H provided that one of the following two conditions is satisfied.

a. $k_n^{(1)} + k_n^{(4)} > 0$ and $k_n^{(2)} + k_n^{(3)} \geq 0$, F is of finite gain.

b. $k_n^{(1)} + k_n^{(4)} \geq 0$ and $k_n^{(2)} + k_n^{(3)} > 0$, $K: H \longrightarrow H$.

Many researchers [1], [2] have investigated the stability of the nonlinear system S. Theorem 1 is more general than those obtained by Sandberg [1] and Zames [2] under somewhat less restrictive assumptions.

The next result is a special class of nonlinear system shown in Fig. 1.

We shall make the following assumptions:

Assumptions

F1. The operator F is characterized by

$$(Fe)(t) = \alpha(t) = \varphi[\, e(t)\,],$$

where the nonlinear characteristic φ is a piecewise continuous function defined on $(-\infty, \infty)$.
Furthermore,

F2. $\quad 0 \leq e\varphi(e) \leq ke^2 \quad$ for all $-\infty < e < \infty$,

and $\quad \varphi(0) = 0.$

Fe. $\quad \int_0^{\sigma} q(\xi)\, d\xi \longrightarrow \infty \quad$ as $|\sigma| \longrightarrow \infty$.

K1. The subsystem K is characterized by its input-output relation

$$y = z + k\alpha,$$

where $z(\cdot)$ is the zero input response which depends on the state of K at time 0, and K is a nonanticipative operator mapping from L^2 into itself.

K2. The operator DK is also assumed to be a nonanticipative operator mapping from L^2 into itself where $(DKx)(t) \triangleq \frac{d}{dt}(Kx)(t)$.

K3. For all initial states, $z(\cdot)$ and $\dot{z}(\cdot)$ are in L^2, and $z(0)$ is finite.

K4. The zero input response of the feedback system S for all initial states is assumed to be locally square integrable, i.e., $y(\cdot) \in L_e^2$ for all $z(\cdot)$ satisfying K3.

---

[1] I.W. Sandberg, "Some Results on the Theory of Physical Systems Governed by Nonlinear Functional Equations," Bell System Technical Journal, Vol. XLIV, May 1965 p. 871-898.

[2] G. Zames, "On the Stability of Nonlinear Time-Varying Feedback Systems," NEC Proceeding Sept.,1964 p. 725-730.

Remark

In fact K1, K2, and K3 imply K4 because $z(\cdot)$ and $k\alpha$ are differentiable and hence $y(\cdot)$ is continuous.

Theorem 2

Consider the system S shown in Fig. 1. Let $u = 0$. Suppose that the assumptions F1 - F3 and K1 - K4 are satisfied. Under these assumptions if there are positive numbers q and δ such that

$$< x, (K + q\,DK + \frac{1}{k})\, x > \geq \delta \|x\|^2 \quad \forall\, x \in L^2 ,$$

then the zero input response of the feedback system S is bounded square integrable functions for all initial states, i.e.,

$$y(\cdot) \in L^\infty \cap L^2 .$$

Theorem 2 is an extension of Popov's Theorem for stability. In refs. [3] and [4] the subsystem K is assumed to be a linear time invariant system. However,in Theorem 2 no assumption is made concerning linearity or time invariance.

Part of Theorem 2 has been reported and proved [5]. The significance of this result is the fact that it is derived without using Liapunov's functions. Asympotic stability, i.e., $y(t) \to 0$ as $t \to \infty$, can be also obtained by making additional assumptions on the subsystem K . A slightly more general result has been obtained.

Theorem 3

Let $u = 0$. Suppose that the assumptions F1 - F3 and K1 - K4 are satisfied. Under these assumptions if there is a positive number δ and if there is a monotonically decreasing function $q(\cdot)$ such that

$$0 < \epsilon \leq q(t) \leq q(0) < \infty$$

and

$$< x, (K + q\,DK + \frac{1}{k})\, x > \geq \delta \|x\|^2 \qquad \forall\, x \in L^2$$

---

[3] M. Aizerman and F.R. Gantmacher, "Absolute Stability of Regulator Systems," (Translated from Russian by E. Polak) San Francisco, Holden Day, 1964.

[4] C.A. Desoer, "A Generalization of the Popov Criterion," IEEE Trans., AC-10, 2, p.182-184, April 1965.

[5] C.A. Desoer and C.T. Lee, "Stability of Single-Loop Feedback Systems," Notes on System Theory, VII Feb. 1965.

then, for each initial state, the zero input response of the feedback system S is bounded and square integrable function over $(0, \infty)$ i.e.,

$$y(\cdot) \in L^{\infty} \bigcap L^{2} .$$

Remark

Theorem 2 is in fact a special case of Theorem 3, i.e., $q(t) = q = \text{const.}$

Since frequency domain analysis is not applicable to the general nonlinear system, all the results mentioned above are derived in time domain. Further extension of Theorem 2 to higher order systems is under investigation.

All the results obtained are being prepared for publication.

THE ABSOLUTE STABILITY OF CERTAIN NONLINEAR FEEDBACK SYSTEMS

AFOSR Grant AF-AFOSR-292-64
A. Dewey (Prof. E.I. Jury)

Systems are being investigated for which the Popov stability criterion [1] fails to guarantee absolute stability for nonlinearities in the entire Hurwitz sector. That is for systems where we cannot prove, using the Popov theorem that linearization will give correct results for the stability of the system.

In a recent memorandum [2], a third-order system is given for which Aizerman's conjecture does not hold. That is, a linearized version of this system is asymptotically stable in the large, but the nonlinear system exhibits a stable limit cycle. The transfer function of the linear part of this feedback system is

$$G(s) = \frac{2s^2 - 1}{2(s+1)(s^2+1)}$$

The results were obtained by analog computer simulation, but have recently been checked by obtaining a digital computer solution.

To obtain information about the stability of such systems when the Popov theorem does not hold, certain new inequalities have been obtained by making stronger restrictions on the nonlinear element. In an earlier technical memorandum [3], the following results are described.

---

[1] M.A. Aizerman and F.R. Yantmacher, "Absolute Stability of Regulator Systems," Holden Day, San Francisco, 1964.

[2] A.G. Dewey and E.I. Jury, "A Note on Aizerman's Conjecture," ERL Internal Tech. Memo M-115, May 20, 1965.

[3] A.G. Dewey and E.I. Jury, "A Stability Inequality for a Class of Nonlinear Feedback Systems," ERL Internal Tech. Memo M-114, April 21, 1965.

The system is described by the equation

$$-\sigma(t) = z(t) + \int_0^t g(t-\tau)\,\xi(\tau)\,d\tau\,, \quad t \geq 0\,, \tag{1}$$

where $\xi(t)$ is the output of a time-invariant memoryless nonlinear gain element with input $\sigma(t)$ such that $\xi(t) = \phi[\sigma(t)]$ for all $t \geq 0$. It is assumed that $\phi(\sigma)$ is a continuous function such that $\phi(0) = 0$ and $0 \leq \phi(\sigma)/\sigma \leq k < \infty$ for all $\sigma \neq 0$. This inequality restricts the nonlinear function to a sector in the σ, ϕ plane and we will refer to this as a nonlinearity in the sector $[0,k]$. The following further restriction is made:

$$0 \leq \frac{d\phi}{d\sigma} \leq k_2 \text{ where } k_2 \geq k. \tag{2}$$

This will be referred to as a slope restriction $[0, k_2]$. It is assumed that for all initial states, $z(t)$, $\dot{z}(t)$, and $\ddot{z}(t)$ are bounded elements of $L_2(0,\infty)$ and that $g(t)$ and $\dot{g}(t)$ are elements of $L_1(0,\infty)$.

Let $G(j\omega)$ be the Fourier transform of $g(t)$, then the following theorem can be shown.

Theorem 1 If there exists a finite number q and a finite number $\mu \geq 0$ such that for all $\omega \geq 0$

$$\mathrm{Re}\left\{(1 + j\omega q)\,G(j\omega)\right\} + \frac{1}{k} + \mu\,\omega^2\left\{\mathrm{Re}\,G(j\omega) + \frac{1}{k_2}\right\} > 0 \tag{3}$$

then the system is asymptotically stable in the large.
For the case when $k_2 = k$, inequality (3) reduces to

$$\mathrm{Re}\left\{\left[1 + \frac{j\omega q}{1+\mu\omega^2}\right]\quad G(j\omega)\right\} + \frac{1}{k} > 0. \tag{4}$$

Inequality (4) has also been shown to be valid when $G(s)$ has simple poles on the imaginary axis of the S-plane.

Recently some simple extensions to Theorem 1 have been obtained. If in place of inequality (2) we have

$$-k_1 \leq \frac{d\phi}{d\sigma} \leq k_2 \quad \text{where} \quad k_1 > 0 \tag{5}$$

then inequality (3) becomes

$$\mathrm{Re}\,(1+j\omega q)\,G(j\omega) + \frac{1}{k} + \mu\,\omega^2\left\{\frac{1}{k_1 k_2} + \left(\frac{1}{k_1} - \frac{1}{k_2}\right)\mathrm{Re}\,G(j\omega) - |\,G(j\omega)\,|^2\right\} > 0\,.$$

In the Memorandum, examples are given of systems which can be proved to be stable using inequality (4) but cannot be treated by the Popov theorem.

CAUSALITY AND STABILITY OF FEEDBACK CONTROL SYSTEMS

JSEP Grants AF-AFOSR-139-64 & 65
C.T. Chen (Prof. C.A. Desoer)

During this report period, the following work was completed:

1. On the Causality of Sampled-Data Feedback Systems.

Consider the sampled-data feedback system shown in Fig. 1; k is a constant gain, G is a linear, time-invariant system. Let

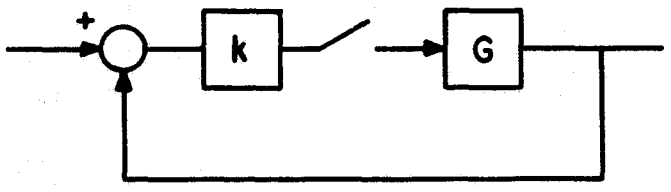

Fig. 1.

$G(z)$ and $\{g(n)\}_{n=-\infty}^{\infty}$ be the transfer function and the sampled impulse response of G. Let $\{h(n)\}_{n=-\infty}^{\infty}$ be the impulse response of the closed loop system, then

$$h(n) = k\, g(n) - k \sum_{n=-\infty}^{\infty} g(n-m)\, h(m), \text{ for all } n.$$

A system is defined to be causal if its sampled impulse response is identical to zero for $n < 0$ (n the set of integers).

Theorem: Consider the sampled-data system shown in Fig. 1. Assume G is causal, i.e., $g(n) = o$ for $n < o$, then the feedback system is causal.

If and only if

$$1 + k\, g(o) \neq 0,$$

or

$$\lim_{\delta \to \infty} [1 + k\, G(z)] \neq o.$$

2. On the Stability of Feedback Control Systems with Perturbation Gain

It is proved that in the linear time-varying feedback system, if the total gain deviation from a constant gain is finite and the constant gain feedback system (no gain deviation) is stable, then the response of the time-varying system to any bounded input is bounded; furthermore, the response of the time-varying system tends to that of the constant gain system as $t \to \infty$. Similar results are obtained for the sampled-data feedback system.

A report on this topic was recently published [1] and more general results have since been obtained.

3. On the Stability of Nonlinear Sampled-Data Feedback Systems

This work is a generalization of Tsypkin's stability criterion for a class of time-varying nonlinear sampled-data feedback systems. An article on this work has been accepted for publication in the Journal of the Franklin Institute.

ON SOME PROPERTIES OF CONTROL SYSTEMS WITH DIGITAL FEEDBACK

JSEP Grants AF-AFOSR-139-64 & 65
E.T. Schoen (Prof. C.A. Desoer)

A class of accurate measuring instruments operate on a digital force balance principle. The analog input of the instruments is balanced by a sequence of standard shape pulses of both polarities at a fixed sampling rate; the polarity of the pulses is determined by some decision function on the state of the system at the sampling instants. The fixed shape of the pulses eliminates troubles due to the nonlinearity of the feedback torquer, while the fixed sampling rate allows counting to replace integration with respect to time.

A block diagram of this class of systems is shown in the following:

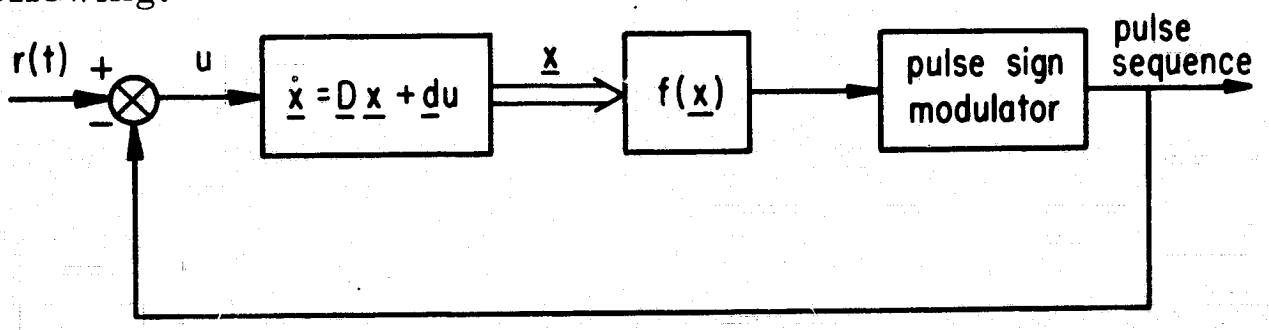

[1] "On the Stability of Feedback Control Systems with Perturbation Gain," Notes on System Theory, Vol. VII, ERL, Univ. of Calif., Berkeley, May 1965.

where $f(\underline{x})$ represents the decision function for the polarity of the pulses.

The pulse sign modulator samples $f(\underline{x})$ at a constant sampling rate and emits a pulse of corresponding polarity. $\underline{D}$ and $\underline{d}$ represent the dynamics of the measuring instrument and any compensation introduced.

In the research undertaken, the behavior of these systems under constant or no input was studied. These systems can be described by a nonlinear vector difference equation of the form

$$\underline{x}\,(k+1) = \underline{A}\,\underline{x}\,(k) - \underline{b}\ \mathrm{sgn}\ f(\underline{x}(k)) = F(\underline{x}(k))$$

Systems of this class exhibit sometimes many possible limit cycles and nonperiodic oscillations, which can be detrimental to their application.

In the study tools for the analysis of this class of systems were found. These consist of conditions for the possibility and methods for converting the above systems into equivalent finite state machines. Several theorems and methods that provide these tools are presented in the following.

1. Sufficient Conditions for Periodicity

Theorem I: Given an autonomous discrete time system described by the vector difference equation

$$\underline{x}_{n+1} = \underline{F}\,(\underline{x}_n)$$

Suppose there exists a bounded invariant limit set D for this system.

Let the output y(k) be given by

$$y(k) = g(\underline{x}(k))$$

It is assumed that $g(\cdot)$ can attain only a finite number of distinct values for all $\underline{x} \in D$. If there exists a partition of D into a finite number of sets $\overline{D_j}$ obeying the following four conditions:

(1) $D_i \cap D_j = \phi$ for $i \neq j$

(2) $\bigcup D_i = D$

(3) For all j, the function $g(\cdot)$ is constant on D_j

(4) $\underline{F}(D_j) C D_i$ (for some i that may be identical with j), for all j.

Then, the output sequence $\{y(k)\}$ is eventually periodic for all initial states of the system.

Remarks:

I: If the set D is only an invariant set (F(D)CD) but not a limit set, the same conclusion holds provided the initial state is in D.

II: If the system described by the mapping $\underline{x}_{n+1} = \underline{F}(\underline{x}_n)$ is a pulse sign modulation system with a linear time invariant finite dimensional plant, the output and state relations become $F(\underline{x}) = \underline{A}\underline{x} - \underline{b}\ \mathrm{sgn}\, f(\underline{x})$; $y(k) = \mathrm{sgn}\, f(\underline{x}(k))$. In this case the existence of a partition of the invariant limit set D, obeying conditions (1) - (4) implies that the sequence $\{y(k)\}$ is eventually periodic and the motion of the state point $\underline{x}(k)$ is asymptotically periodic for all initial states.

2. Stability of a Pulse-Sign Modulated Sequence

Definition: A PSM (Pulse Sign Modulated) sequence is said to be stable if the mapping from the state space to the sequence space is continuous; i.e., that a sufficiently small perturbation of the state point does not cause any change in the pulse sequence (since the smallest change in the pulse sequence is of finite magnitude).

Definition: A periodic motion of a PSM system is said to be stable if a sufficiently small perturbation of the state point does not cause the PSM sequence to change and the perturbation of the state space trajectory dies out as $t \to \infty$.

3. Existence Theorem:

Theorem II: Given an autonomous, linear, finite dimensional plant with PSM feedback. Suppose there exists a bounded invariant set D. If the system possesses only a finite number of stable periodic modes,(PSM patterns) and no nonperiodic or unstable periodic ones, then there exists a partition of the invariant set D into sets D_j obeying all the conditions of Theorem I.

4. Construction of the Partition.

The following procedure leads in a finite number of steps to the partition of the invariant set D.

Assume an invariant limit set D for the system is known. Assume that the switching surface $f(\underline{x}) = 0$ divides the state space into two simply connected parts: $f(\underline{x}) \geq 0$ and $f(\underline{x}) < 0$. The equation describing the state point motion is $\underline{x}(k+1) = \underline{A}\underline{x}(k) - \underline{b}\ \mathrm{sgn}\ f(\underline{x}(k)) = \underline{F}(\underline{x}(k))$.

Let $P_1 : \{\underline{x} \mid f(\underline{x}) \geq 0,\ \underline{x} \in D,\ f(\underline{A}\,\underline{x} - \underline{b}) < 0\}$

$P_{j+1} : \{\underline{x} \mid f(\underline{x}) \geq 0,\ \underline{x} \in D,\ \underline{A}\,\underline{x} - \underline{b} \in P_j\}$ $\quad j = 1, 2, \ldots$

$P_\infty : \{\underline{x} \mid f(\underline{x}) \geq 0,\ \underline{x} \in D,\ \underline{A}\,\underline{x} - \underline{b} \in P_\infty\}$

$N_1 : \{\underline{x} \mid f(\underline{x}) < 0,\ \underline{x} \in D,\ f(\underline{A}\underline{x} + \underline{b}) \geq 0\}$

$N_{j+1} : \{\underline{x} \mid f(\underline{x}) < 0,\ \underline{x} \in D,\ \underline{A}\,\underline{x} + \underline{b} \in N_j\}$ $\quad j = 1, 2, \ldots$

$N_\infty : \{\underline{x} \mid f(\underline{x}) < 0,\ \underline{x} \in D,\ \underline{A}\,\underline{x} + \underline{b} \in N_\infty\}$

By their definition the sets P_j and N_j obey conditions (1) ÷ (3) of Theorem I. Check if $\underline{F}(P_1) \subset N_j$ (some j) and $\underline{F}(N_1) \subset P_i$ (some i); if yes the partition is finished. If no, generate the inverse images of $F(P_1)' \cap N_j$, $\forall_j$ in $D \cap \{\underline{x} \mid f(x) \geq 0\}$ and the inverse images of $F(N_1) \cap P_i$, $\forall_i$ in $D \cap \{\underline{x} \mid f(x) < 0\}$; for the new sets generated check again property (4) of theorem I; repeat this process until property (4) is obeyed. (It was shown that this procedure leads to the desired partition in a finite number of steps and without generating any redundant sets.)

5. Implications

Having found the invariant limit set D and its partition we have found the following facts about the system:

a. Identification of all possible modes of oscillation.

b. Reduction of the invariant set to its minimal size (only those sets in D that are reachable from other sets in D are retained).

c. Neighborhood properties of modes are determined.

d. The stability of oscillation of each mode can be determined by measurement of the smallest perturbation of the periodic state point that will cause the PSM sequence to change.

e. Pull-in regions to different modes can be found.

f. Properties of the switching function $f(\underline{x})$ in enhancing or disturbing certain modes can be evaluated.

6. Method of Finding an invariant limit set by Lyapunov's 2nd Method.

Given the state transition relation,

$$\underline{x}(k+1) = \underline{F}(\underline{x}(k)).$$

Let $V(\underline{x})$ be a Lyapunov function, i.e., obeying the conditions:

a. $V(\underline{0}) = 0$, $V(\underline{x}) > 0$ for $\underline{x} \neq \underline{0}$

b. $V(\underline{x})$ is continuous in $\underline{x}$

c. $V(\underline{x}) \to \infty$ when $\|\underline{x}\| \to \infty$.

Let $\Delta V(\underline{x}(k)) \triangleq V(\underline{x}(k+1)) - V(\underline{x}(k)) < 0$ for all $\underline{x}(k) \in \Omega^c$, where Ω is a compact set including the origin.

Let $Q \triangleq \Omega \cup \underline{F}(\Omega)$.

Then, the smallest set of the form $\{\underline{x} : V(\underline{x}) \leq C\}$ for some C that includes the set Q is an invariant limit set for the system. In fact any set $V \leq C_1$ with $C_1 > C$ is also an invariant limit set for the same system.

NONLINEAR DISCRETE SYSTEMS

AFOSR Grant AF-AFOSR-292-64
A.J. Rault (Prof. E.I. Jury)

It has been shown that discrete Voltera series approximate arbitrarily closely the solution of nonlinear difference equations of the form

$$L[\,y(m)\,] + F[\,y(m),\ y(m+1), \ldots y(m+n)\,] = X(m), \qquad (1)$$

where L is a linear time-invariant difference operator and F is a multinomial in y(m) and its n following samples. The input output relation of a system described by Eq. 1 has the following representation

$$y(m) = Y_1 + Y_2 + \cdots + Y_p \ldots,$$

where

$$Y_i = \sum_{k_1=0}^{m} \cdots \sum_{k_i=0}^{m} g_i (m-k_1, \ldots, m-k_i) \prod_{j=1}^{i} X(k_j).$$

A multidimensional Z transform has been defined and its properties have been developed. It enables us to extend the properties of convolution to this representation of nonlinear discrete systems. Then, block diagram and operator manipulations similar to those in the linear case can be made use of.

The technique of "associating variables" has been developed, which permits the inversion from the multidimensional Z domain to the time domain without any restriction. Practical examples showing the advantages of the method over previous numerical methods such as the Z convolution, have been worked out. This research has been summarized in Electronics Research Laboratory Technical Memorandum M-112, "Nonlinear Sampled-Data Systems and Multidimensional Z Transform". The abstract follows:

> Discrete Volterra series is shown to approximate arbitrarily closely the response of nonlinear sampled-data systems. A multidimensional Z-transform calculus is developed which makes it possible to generalize the property of convolution to nonlinear discrete systems; operator notation can then be used to analyze the problem. A typical example is taken and a representation of the system is obtained from which the transient response is easily computed.

The next area of research to be investigated is the stability of linear and nonlinear time varying sampled-data systems.

TIME OPTIMAL CONTROL OF A CLASS OF PULSE WIDTH MODULATED SAMPLED DATA SYSTEMS

NASA Grant NsG-354 (Supplement 2) and NSF Grant GP-2413
M. Canon and C.D. Cullum (Prof. E. Polak)

By combining work by M.D. Canon on the time optimal control of pulse amplitude modulated linear discrete systems* and the work of C.D. Cullum and E. Polak on the equivalence of optimal control problems†

---

*Described

† ERL Consolidated Quarterly Progress Report No. 15, Aug. 16-Nov. 15, 1964, p. VII-11

a computational algorithm has been developed for the optimal control of a class of pulse width modulated linear sampled data systems. The class of problems considered and the algorithm developed are described in the following.

1. PWM Linear Sampled Data System

It is assumed that the plant is described by a set of linear differential equations of the form

$$\dot{\underline{x}} = \underline{A}\underline{x} + \underline{b}u$$

$$A = \begin{pmatrix} \lambda_1 & & 0 \\ & \ddots & \\ 0 & & \lambda_n \end{pmatrix} \qquad \lambda_n < \lambda_{n-1} < \cdots < \lambda_1 < 0$$

$$\underline{b} = \text{col}\,(b_1, \ldots, b_n)$$

$$\underline{x} = \text{col}\,(x_1, \ldots, x_n)$$

$$u = \text{scalar}$$

The state of the system is assumed to be sampled once every second (on a normalized time scale), and the control function u(t) is given by

$$u(t) = \begin{cases} \text{sgn}\, u_n & n-1 \leq t < n-1+|u| \\ 0 & n-1+|u_n| \leq t < n \end{cases}$$

where the u_n $n = 1, 2, \ldots$ are constants satisfying $|u_n| \leq |$ for all n. The optimal control problem is stated in the following form:

Given that the system is in an initial state $\underline{x}_0$ at $t = 0$, find a control sequence $u_1, u_2, \ldots, u_N$ which brings the system to the origin in a number of sampling periods, N, which is less than or equal to the nunber of sampling periods required with any other control sequence.

The following definitions are used in the discussion of the algorithm:

$$\underline{w}_i(u_i) \triangleq e^{-(i-1)\underline{A}}\left[e^{-\underline{A}|u_i|} - \underline{I}\right]\underline{b}$$

$$\underline{r}_i \triangleq \underline{w}_i(1) = e^{-(i-1)\underline{A}}\left[e^{-\underline{A}} - \underline{I}\right]\underline{b}$$

$$\text{sat}(x) \triangleq \begin{cases} x & \text{if } |x| \leq 1 \\ \text{sgn}\, x & \text{if } |x| > 1 \end{cases}$$

$$R_N \triangleq \left\{\underline{x}_0 / \underline{x}_0 = -\sum_{i=1}^{N} \underline{w}_i(u_i)\,\text{sgn}\, u_i,\ |u_i| \leq 1,\ i=1, \ldots, N\right\}$$

= the set of states from which the origin is reachable in N samplings periods or less.

2. Optimal Control Algorithm

The algorithm is based on the following conjectured theorem.

Theorem: Under the conditions of the problem stated above, the sets $C_N \subset E^n$, $N = n, n+1, \ldots$ defined by

$$C_N = \{ \underline{c} / \text{the set of indices } \{ i / i \leq N, | < \underline{r}_i, \underline{c} > | \leq 1 \} \text{ has cardinality } \geq n \}$$

have the properties that

(a) C_N is homeomorphic to R_N for every $N \geq n$ with the homeomorphism $f: C_N \rightarrow R_N$ given by

$$\underline{f}(\underline{c}) = - \sum_{i=1}^{N} \underline{w}_i \, (\text{sat} < \underline{n}, \underline{c} >) \, \text{sgn} < \underline{r}_i, \underline{c} >$$

(b) for any $\underline{x}_0 \in R_N$ there exists a control sequence $u_1, u_2, \ldots, u_N$ which brings the system from the initial state $\underline{x}_0$ to the origin in N sampling periods, which is given by $u_i = \text{sat} < \underline{r}_i, \underline{f}^{-1}(\underline{x}_0) >$ $i = 1, \ldots, N$

(c) $\underline{f}$ and $\underline{f}^{-1}$ are piecewise differentiable. Some remaining details of the proof of this theorem are being worked out and it is expected that the material will be submitted for publication in the near future.

Given the initial state, $\underline{x}_0$, of the system, the basic procedure used in this algorithm is to examine successively R_n, $R_{n+1}, \ldots$ to determine whether $\underline{x}_0$ belongs to these sets, stopping at the first N for which $\underline{x}_0 \in R_N$. This N represents the minimum number of sampling periods to bring the system to the origin. To determine whether $\underline{x}_0$ is in R_N for a fixed N, the algorithm seeks a solution of the equation

$$\underline{f}(\underline{c}) = \underline{x}_0$$

with $\underline{c} \in C_N$. This is accomplished using standard techniques for the solution of a set of nonlinear equations. If a solution is not found, N is increased by one and the procedure is repeated. If a solution, $\underline{c}_0 \in C_N$, is found, then an optimal control is given by

$$u_i = \text{sat} < \underline{r}_i, \underline{c}_0 > \qquad i = 1, \ldots, N.$$

The procedure described here has not been tested in practice. However, an equivalent procedure involving a more complicated function f was examined using a second-order system with initial states less than or equal to 20 sampling periods from the origin. Typical computation times for initial states picked at random were of the order of

4 to 5 seconds or less on an IBM 7094 computer. The authors expect to obtain considerable computational experience with this algorithm during the next few months. The relative simplicity of the present procedure, as compared with the one for which computation times were quoted, would lead one to suspect that these times could be reduced by a factor of two or more. The actual times obtained will be reported in the next progress report.

REAL-TIME IDENTIFICATION OF TRANSFER

NASA Grant NsG-354 (Supplement 2)
K.Y. Wong (Prof. E. Polak)

A new method of real-time identification of a transfer function under normal operation with noise disturbance is discussed. The problem is stated and a summary is given of the writer's previous result in using testing function to convert the problem of estimating the coefficients of a differential equation into one of estimating the coefficients of an algebraic equation. An outline is also given of the use of instrumental variables to obtain a consistent estimate of the desired parameters. It is shown that the solution can be re-written into a recursive form, enabling the estimates of the parameters to be up-dated. The optimal shape of the testing function with respect to a suitable criterion is also discussed.

1. Problem Statement

Assume that the input $u(t)$ and the output $V(t)$ of time invariant system obey the differential equation:

$$a_2 \frac{d^2V}{dt^2} + a_1 \frac{dV}{dt} + a_0 V = b_1 \frac{du}{dt} + u. \qquad (1)$$

However, $V(t)$ cannot be observed, but $v(t)$ can be measured, where

$$v(t) = V(t) + e(t),$$

$e(t)$ is a stationary noise process with zero mean (not necessary white noise). We assume that the variables $v(t)$ and $u(t)$ have been observed over some interval of time which we then divided into subintervals of length T. The problem is to estimate the coefficients a_2, a_1, a_0, b_1.

A second-order system is chosen for convenience of illustration; the theory that follows can be trivially extended to higher order systems.

Let $g(t)$ be a continuous function such that

$$g(0) = g^{(1)}(0) = g^{(2)}(0) = g(T) = g^{(1)}(t) = g^{(2)}(T) = 0.^{*} \qquad (2)$$

The function $g(t)$ will be called a testing function. Multiplying both sides of Eq. 1 by $g(t)$ and integrating from zero to T, we get,

---

* $g^{(j)}(t)$ denotes the jth derivative of $g(t)$.

$$a_2\int_0^T g(t)\ V^{(2)}(t)\ dt + a_1\int_0^T g(t)\,V^{(1)}\,dt + \int_0^T g(t)\,V(t)\,dt$$

$$= b_1\int_0^T g(t)\,u^{(1)}(t)\,dt + \int_0^T g(t)\,u(t)\,dt\ . \qquad (3)$$

Equation 3, after integration by parts, gives

$$a_2\int_0^T g^{(2)}(t)\,v(t)\,dt + a_1\int_0^T -g^{(1)}(t)\,dt + a_0\int_0^T g(t)v(t)\,dt + b_1\int_0^T g^{(1)}(t)a(t)\,dt$$

$$= \int_0^T g(t)\,u(t)\,dt + \sum_{j=0}^{2}(-1)^j a_j\int_0^T g^{(j)}(t)\ e(t)\ dt.$$

Note that the integrals

$$\int_0^T g^{(j)}(t)\ v(t)\ dt, \qquad j = 0, 1, 2,$$

and

$$\int_0^T g^{(j)}(t)\ u(t)\ dt, \qquad j = 0, 1,$$

can easily be computed and that

$$\sum_{j=0}^{2}(-1)^j\ a_j\ \int_0^T g^{(j)}(t)\ e(t)\ dt$$

is the disturbance quantity. The process of multiplying by a testing function and integrating from 0 to T can now be repeated on the observed data v(t), u(t), for t in the time intervals [T, 2T], [2T, 3T] ..... and so on. These will be referred to as the first, 2nd, etc. intervals of integration. Let us define

$$x_{kj} \triangleq (-1)^j\int_0^T g^{(j)}(t)\ v(t)\ dt \quad j = 0, 1, 2 \qquad (4a)$$

$$x_{k3} \triangleq \int_0^T g^{(1)}(t)\ u(t)\ dt \qquad (4b)$$

$$y_k \triangleq \int_0^T g(t)\, u(t)\, dt \tag{4c}$$

$$\epsilon_j \triangleq \sum_{j=0}^{2} (-1)^j a_j \int_0^T g^{(j)}(t)\, e(t)\, dt \tag{4d}$$

$$a_3 \triangleq b_1 \tag{4e}$$

The index k in Eq. 4 refers to the interval of the integration. The following set of algebraic equations is then obtained.

$$\begin{bmatrix} x_{10} & x_{11} & x_{12} & x_{13} \\ x_{20} & x_{21} & x_{22} & x_{23} \\ \vdots & \vdots & \vdots & \vdots \\ x_{N0} & x_{N1} & x_{N2} & x_{N3} \end{bmatrix} \begin{bmatrix} a_0 \\ a_1 \\ a_2 \\ a_3 \end{bmatrix} = \begin{bmatrix} y_1 \\ y_2 \\ \vdots \\ Y_N \end{bmatrix} + \begin{bmatrix} \epsilon_1 \\ \epsilon_2 \\ \vdots \\ \epsilon_N \end{bmatrix}$$

In symbolic matrix notation, Eq. 5 can be written as

$$X_N \underline{a} = \underline{y}_N + \underline{\epsilon}_N \,. \tag{5}$$

Define

$$\underline{X}_k \triangleq \begin{bmatrix} X_{k0} \\ X_{k1} \\ X_{k2} \\ X_{k3} \end{bmatrix} \tag{6}$$

Note that $E(x_{kj}\, e_j) \neq 0$; $k = 1, 2, \ldots N$; $j = 0, 1, 2$ *

The problem of estimating the coefficients of the differential Eq. 1 is transformed into finding a statistical estimate of $\underline{a}$ in Eq. 5.

---

* "E" denotes expectation.

2. Use of Instrumental Variables to Obtain Consistent Estimates

Suppose we generate a vector instrumental stationary stochastic process $\{\underline{z}_k\}$ where

$$\underline{z}_k \triangleq \begin{bmatrix} z_{k0} \\ z_{k1} \\ z_{k2} \\ z_{k3} \end{bmatrix} \tag{7}$$

and k is the timing index, such that

$$\text{(i)} \quad E\left(\underline{z}_{Nj}\ \underline{\epsilon}_N^T\right) = 0, \qquad j = 0, 1, 2, 3,$$

where $\underline{z}_{Nj}$ is a vector with elements $(z_{1j}, z_{2j}, \ldots z_{Nj})$, and $\underline{\epsilon}_N^T$ is the transpose of $\underline{\epsilon}_N$;

$$\text{and} \quad \text{(ii)} \quad E\left(\underline{z}_{Nj}\ \underline{x}_{nj}\right) \neq 0, \quad j = 0, 1, 2, 3, \tag{8}$$

where $\underline{x}_{Nj}$ is the jth column vector defined by the matrix X_N in Eq. 5.

Now use the estimator $\hat{a}_N = \left(Z_N^T\ X_N\right)^{-1} Z_N^T\ y_N$ (9)

where

$$Z_N = \begin{bmatrix} z_{10} & z_{11} & z_{12} & z_{13} \\ z_{20} & z_{21} & z_{22} & z_{23} \\ \vdots & \vdots & \vdots & \vdots \\ z_{N0} & z_{N1} & z_{N2} & z_{N3} \end{bmatrix}$$

Therefore $\hat{a}_N = \underline{a} + \left(\frac{1}{N}\ Z_N^T\ X_N\right)^{-1} \left(\frac{1}{N} Z_N^T\ \underline{\epsilon}_N\right)$.

By Slutsky's Theorem [1]

$$\operatorname*{plim}_{N\to\infty} \hat{a}_N = \underline{a} + \left[\operatorname{plim}\left(\frac{1}{N} Z_N^T\ X_N\right]^{-1} \left[\operatorname{plim}\left(\frac{1}{N}\ Z_N^T\ \underline{\epsilon}_N\right)\right]\right. *$$

---

[1] S. Wilks, Mathematical Statistics, John Wiley and Sons, Inc. New York, (1962), p. 102.

* "plim" denotes a limit in probability.

It can be shown that (a) $\underset{N\to\infty}{\text{plim}} \frac{1}{N} Z_N^T X_N = E\, \underline{z}_k \underline{x}_k^T \triangleq \Sigma_{zx}$ (10)

where $\underline{x}_k$ was defined in Eq. 6, and it is assumed that the 4 x 4 square matrix has finite components; and

$$\text{(b)}\quad \text{plim}\left(\frac{1}{N} Z_N \underline{\epsilon}_N\right) = 0;$$

therefore plim $\hat{a}_N = \underline{a}$. If the noise process e(t) is white, the asymptotic variance of a_N has been proved to be $\frac{\sigma^2}{N} \Sigma_{zx}^{-1} \Sigma_{zz} \Sigma_{xz}^{-1}$ (11)

where Σ_{zz}, Σ_{zx}, Σ_{xz} are 4 x 4 square matrices defined similarly as in Eq. 10 and $\sigma^2 = E\,\epsilon_k^2$.

If e(t) is not white, an asymptotic expression for the variance of a_N can still be obtained but it is more complicated than Eq. 11. The measurable output v(t) of Eq. 1 is correlated with u(t), but u(t) is independent of e(t); hence an obvious way to generate the instrumental variable process is to derive it from u(t).

3. Recursive Estimate

Let X_{N+1}, Z_{N+1}, Y_{N+1} be partitioned as follows:

$$X_{N+1} = \begin{bmatrix} x_{10} & x_{11} & x_{12} & x_{13} \\ x_{20} & x_{21} & x_{22} & x_{23} \\ \cdot & \cdot & \cdot & \cdot \\ \cdot & \cdot & \cdot & \cdot \\ \cdot & \cdot & \cdot & \cdot \\ x_{N0} & x_{N+1} & x_{N+1} & x_{N3} \\ \hline x_{N+1,0} & x_{N+1,1} & x_{N+1,2} & x_{N+1,3} \end{bmatrix} = \begin{bmatrix} X_N \\ \\ \\ \\ \hline m_{N+1} \end{bmatrix}$$

$$Z_{N+1} = \begin{bmatrix} Z_N \\ \hline \\ q_{N+1} \end{bmatrix}, \qquad y_{N+1} = \begin{bmatrix} y_N \\ \hline \\ y_{N+1} \end{bmatrix}$$

It has been shown that the estimator a_N in Eq. 9 obeys the following recursive relation:

$$\hat{a}_{N+1} = \hat{a}_N - \left[P_N q_{N+1}^T (1 + m_{N+1} P_N q_{N+1}^T)^{-1}\right] \left[m_{N+1} \hat{a}_N - Y_{N+1}\right] \quad (12)$$

and

$$P_{N+1} = P_N - P_N a_{N+1}^T (1 + m_{N+1} P_N a_{N+1}^T)^{-1} m_{N+1} P_N$$

with $P_N \triangleq (Z_N^T X_N)^{-1}$. Note that $(1 + m_{N+1} P_N q_{N+1}^T)$ is a scalar.

4. Optimal Shape of the Testing Function

For a functional of optimality of the testing functions, with T given, we chose

$$\rho(T) = \frac{\int_0^T \int_0^T R_s(s-t)\, g(t)\, g(s)\, dt\, ds}{\int_0^T \int_0^T R_n(s-t)\, g(t)\, g(s)\, dt\, ds}, \quad (13)$$

where $R_s(t)$ = autocorrelation function of $V(t)$, and

$R_n(t)$ = autocorrelation function of $e(t)$.

Both $R_s(t)$ and $R_n(t)$ are assumed to be known. We shall now show how to choose a continuous function $g(t)$ that maximizes $\rho(T)$ subject to the boundary conditions of Eq. 2.

Case A: $R_n(t) = \delta(t)$, i.e., $e(t)$ is a white-noise process.

It is well known that $g(t)$ maximizes the ratio (without boundary conditions)

$$\frac{\int_0^T \int_0^T R_s(s-t)\, g(t)\, g(s)\, dt\, ds}{\int_0^T g^2(s)\, ds} \quad (14)$$

if and only if it satisfies the following integral equation:

$$\int_0^T R_s(s-t)\, g(s)\, ds = \lambda_{max}\, g(t)\,, \tag{15}$$

where λ_{max} is the maximum eigenvalue of Eq. 15. If the maximization of the ratio in Eq. 14 is subject to h boundary conditions, then the maximum of the ratio in Eq. 14 $\rho(T)$, by the Courant mini-max lemma [2], satisfies the relation

$$\lambda_{h+1} \leq \lambda(T) \leq \max,$$

where λ_{h+1} is the (h+1)st largest eigenvalue of Eq. 15.

Solution of the integral equation (Eq. 15) by analytical methods is difficult in practice; hence, approximations in $L^2_{[0,\,T]}$ are used. Let

$$R_s(s-t) \approx \sum_{i=1}^{M} \sum_{j=1}^{M} \gamma_{ij}\, \psi_i(t)\, \psi_j(s)\,, \tag{16}$$

where

$$\gamma_{ij} \triangleq \int_0^T \int_0^T R_s(s-t)\, \psi_i(t)\, \psi_j(s)\, dt\, ds\,, \tag{17}$$

where $\{\psi_i(t)\}$ is a complete orthonormal basis for $L^2_{[0,T]}$. With this series expansion of $R_S(s-t)$, the finding of an approximation solution of Eq. 15 with or without constraints of Eq. 2 on g(t), leads to a matrix eigenvalue problem. If the Fourier transform of $R_s(t)$ is a ratio of polynomials in ω^2, and if $\{\psi_i(t)\}$ are chosen to be sine and cosine functions, then γ_{ij} can be computed readily by the residue method of complex variable theory.

It would be desirable to know $\rho(T)$ explicitly as a function of T, since then it would be possible to make a better choice of T; unfortunately $\rho(T)$ can only be computed for a range of T by repeatedly solving Eq. 15. On the other hand, upper and lower bounds for $\lambda_{max}(T)$ can be easily obtained as functions of T without solving the integral equation. It has been proved by Bellman and Letter [3] that

---

[2] R. Courant and D. Hilbert, Methods of Mathematical Physics, Interscience (1953), p. 31.

[3] R. Bellman and R. Latter, "On the integral equation $\lambda f(x) = \int_0^a K(x-y)\, dy$," Proc. Amer. Math. Soc., 3, pp. 884-891 (1952).

$$\frac{2}{T}\int_0^T (T-t)\, R_s(t)\, dt \leq \lambda_{\max}(T) \underset{0\leq x\leq T}{\text{Max}} \int_0^T R_s(x-y)\, dt, \qquad (18)$$

In particularly, if $R_s(t)$ is a function which decreases monotonically for $|t| \uparrow \infty$ the right hand side of the inequality (Eq. 18) reduces to

$$2\int_0^{\frac{T}{2}} R_s(t)\, dt .$$

When the Fourier transform of $R_s(t)$ is a rational polynomial in ω^2, certain necessary conditions, as well as some sufficient conditions for the location of the zeros and poles of the Fourier transform of $R_s(t)$, have been developed to ensure the monotonicity of $R_s(t)$.

Case B: When $R_N(t) \neq \delta(t)$, the optimization problem in Eq. 13 can be solved by expanding $R_s(s-t)$ and $R_N(s-t)$ into series of sine and cosine terms, and the problem again reduces to a matrix eigenvalue problem.

5. Conclusions

The method of identification outlined in this report can be used in systems under normal operation condition and it can update the estimate easily when new data are received. Further work will be carried out choosing an optimal interval of integration and an optimal set of instrumental variables.

DECOMPOSITION OF LARGE SYSTEMS

NASA Grant NsG-354 (Supplement 2)
P. Varaiya (Prof. L.A. Zadeh)

A basic problem in nonlinear programming is the following:

Maximize $\{f(x) \mid g(x) \geq 0,\ x \geq 0\}$ NP

where $x \in E^n$, $g: E^n \longrightarrow E^m$ is a differentiable mapping, and f is a real-valued, differentiable function. Necessary conditions for the solution of the NP problem were first formulated by Kuhn and Tucker [1]. Their result essentially consists of a non-trivial extension of the classical theory of Lagrange multipliers.

---

[1] H.W. Kuhn and A.W. Tucker, "Nonlinear Programming," Proceedings of the Second Berkeley Symposium on Mathematical Statistics and Probability, Berkeley and Los Angeles, University of California Press,(1951), pp. 481-492 .

Some effort [2] has since been devoted to extend the K.T results to problems where the variables range over more general spaces or are subject to more general constraints. We have considered the following problem:

$$\text{Maximize } \{f(x) \mid g(x) \in \Omega_Y,\ x \in \Omega\} \qquad P$$

where X and Y are real Banach spaces, $x \in X$, $\Omega \subseteq Y$ is an arbitrary set and $\Omega_Y \subseteq Y$ is a closed convex set. $g: X \rightarrow Y$ and $f: Y \rightarrow$ Reals are arbitrary Frechet-differentiable functions. The necessary conditions which we obtain are very analogous to those of Kuhn and Tucker and are based on the well known geometric fact that two disjoint closed convex sets one of which is compact, can be strictly separated by a closed hyperplane. Such a general viewpoint also lends insight into some theoretical aspects of optimal control and shows the essential similarilty between the structure of problem P and those of optimal control. Thus the necessary conditions for the solution of problem P then gives us (local) maximum principles for both discrete -- and continuous -- time optimal control problem. Moreover, in the case of discrete time problems, we can assume that the state vector and the control belong to any real B-spaces. This allows us to obtain necessary conditions for the solution of stochastic discrete time optimal control problems.

Finally we show that the problem P is related to a saddle-value or game-theoretic problem. This viewpoint helps us to develop techniques for the solution by decomposition of some large nonlinear programming problems. Some of these decomposition results will appear in the Fall issue of the Control Section of SIAM Journal. Most of these results will be published soon as an ERL Report. In the near future we hope to obtain more algorithms for the practical solution of these problems and extend the theory to cases where we have a vector-valued or "minimax" type cost function.

A NEW ALGORITHM FOR A CLASS OF QUADRATIC PROGRAMMING PROBLEMS WITH APPLICATION TO CONTROL *

NASA Grant NsG-354 (Supplement 2)
M. Canon (Prof. E. Polak)

An algorithm is given which can be used to solve the following optimal control problems for linear discrete time systems: minimum energy, minimum time, and minimum energy plus time. Each of the optimal control problems is reduced to solving a simple quadratic programming problem (QPP) or a finite sequence of such problems. A new algorithm is given for solving the QPP, and computational results are included.

---

[2] K.J. Arrow, L. Hurwicz, and H. Uzawa, Studies in Linear and Nonlinear Programming, Stanford University Press, Stanford, California, (1958).

* This paper will appear in the SIAM Journal on Control, Sept. 1965.

Many algorithms are available in the literature for solving the minimum time problem [1 - 3] as well as quadratic programming problems [4, 5], but in most cases these algorithms cannot be used for computing optimal controls in a feedback mode because of the large computation times involved. The primary justification for further consideration of these problems is in decreasing the computation time.

PAM sample data system

Let X be a discrete, time invariant system described by the linear vector difference equation

$$\underline{x}_{k+1} = A\,\underline{x}_k + \underline{b}\,u_{k+1}, \qquad k = 0, 1, \ldots, \qquad (1)$$

where $\underline{x}_k \in E^n$ is the state of X at time k, A is an $n \times n$ constant nonsingular matrix, $\underline{b} \in E^n$ is a constant vector, and the scalar input u_k is constrained in magnitude by $-1 \leq u_k \leq 1$. Note that no difficulties are encountered for the multiple input case, i.e., where $u_k \in E^r$, $r \leq n$. We assume a single input in order to symplify notation. For a given input sequence $u_1, u_2, \ldots, u_k = \underline{u}_k$, it is assumed that the energy supplied to the system X is given by

$$J(\underline{u}_k) = \sum_{i=1}^{k} u_i^2$$

Given $\underline{x}_0$, the initial state of X, we can iterate Eq. 1 and express $\underline{x}_k$ and the control sequence $\{u_j : j = 1, 2, \ldots, k\}$:

$$\underline{x}_k(\underline{x}_0, \underline{u}_k) = A^k\left(\underline{x}_0 + \sum_{i=1}^{k} A^{-i}\,\underline{b}\,u_i\right). \qquad (2)$$

---

[1] Wing, J. and Desoer, C.A., "The Multiple Input Minimal Time Regulator Problem", IEEE Trans. on Automatic Control, Vol. AC-8, No. 2, pp. 125-136, 1963.

[2] Whalen, B.H., "On Optimal Control and Linear Programming," IRE Trans. on Automatic Control (Correspondence), Vol. AC-7, pp. 45-46, 1962.

[3] Tou, J.T., "Optimum Control of Discrete Systems Subject to Saturation, "IEEETrans. on Automatic Control, pp. 88-89, Jan. 1964.

[4] Beale, E.M.L.," On Quadratic Programming", Naval Res. Log. Quart., 6, pp. 227-244, Sept. 1959.

[5] Wolfe, P., "The Simplex Method for Quadratic Programming," Econometrica, 27, pp. 382-398, 1959.

Definition: A control sequence $\underline{u}_k$, of length k, is said to belong to the constraint set Ω if $|u_i| \leq 1$, $i = 1, 2, \ldots, k$.

Problem I. Minimum Energy Problem

Given the initial state $\underline{x}_0$ of X, an integer $N \in \{1, 2, \ldots\}$, and a desired terminal state $\underline{z}_N \in E^n$, find a control sequence $\underline{u}_N^0$ which minimizes

$$J(\underline{u}_N) = \sum_{i=1}^{N} u_i^2 \tag{3}$$

subject to the n + N constraints

$$\underline{x}_N(\underline{x}_0, \underline{u}_N) = \underline{z}_N, \tag{4}$$

$$\underline{u}_N \in \Omega. \tag{5}$$

Let $\underline{r}_i = A^{-i} \underline{b}$, i=1, 2, . . . , N, then Eq. 4 can be written as

$$\sum_{i=1}^{N} \underline{r}_i u_i = (A^{-N} \underline{x}_N - \underline{x}_0) \triangleq \underline{v}_N .$$

Since $\underline{x}_0$, N, and $\underline{z}_N$ are given, $\underline{v}_N$ is known and hence the minimum energy problem can be restated in the following equivalent form :

minimize $$J(\underline{u}_N) \tag{6}$$

subject to $$\sum_{i=1}^{N} \underline{r}_i u_i = \underline{v}_N , \tag{7}$$

$$\underline{u}_N \in \Omega . \tag{8}$$

It is easily shown that if the constraints, Eqs. 7 and 8 admit at least one solution, then the minimum energy problem has a solution. More precisely, if we let $R_N = \{ \sum_{i=1}^{N} \underline{r}_i u_i : \underline{u}_N \in \Omega \}$, then a solution to Problem I exists iff $\underline{v}_N \in R_N$.

Problem II. Intercepting a Moving Target in Minimum Time

Let $\underline{z}_N \in E^n$, N=1, 2, . . ., represent a moving target at time N. Given the initial state $\underline{x}_0$ of X, and the target $\{\underline{z}_N : N=1, 2, \ldots\}$, find a control sequence $\underline{u}_N \in \Omega$, of minimum length N, such that $\underline{x}_N(\underline{x}_0, \underline{u}_N) = \underline{z}_N$. As in Problem I, define $\underline{r}_i = A^{-i}\,\underline{b}$ and $\underline{v}_i = (A^{-i}\underline{x}_i - \underline{x}_0)$, i=1, 2, ... An equivalent formulation is: find the smallest integer N such that

$$\sum_{i=1}^{N} \underline{r}_i\, u_i = \underline{v}_N ,$$

$$\underline{u}_N \in \Omega .$$

Note that a solution to this problem exists iff $\underline{v}_N \in R_N$ for some finite integer N. Clearly, a solution to Problem II can be obtained by finding the smallest N for which Problem I has a solution.

Problem III. Minimum Energy Plus Time

Given $\underline{x}_0$ and the target state $\underline{z}_N \in E^n$ at time N, n=1, 2, . . ., find a control sequence $\underline{u}^0_N$ which minimizes

$$Q(\underline{u}_N, N) = \alpha N + \sum_{i=1}^{N} u_i^2, \qquad \alpha > 0$$

subject to the constraints $\underline{x}_N(\underline{x}_0, \underline{u}_N) = \underline{z}_N$ and $\underline{u}_N \in \Omega$. As before, this problem is reducible to the following: find a control $\underline{u}^0_N$ which minimizes $Q(\underline{u}_N, N)$, subject to the constraints $\underline{v}_N = \sum_{i=1}^{N} \underline{r}_i\, \underline{u}_N \in \Omega$. It is easily shown that this problem has a solution iff $\underline{v}_N \in R_N$ for some N, and, furthermore, that a solution can be obtained by solving, sequentially, Problem I starting with N=1, N=2, etc.

Problem IV. Intercepting a Moving Target on a Subspace

In some cases it is not required that the system state agree with the target state in all coordinates; e.g., it may be required that the system state and the target agree in position and velocity. In general it may be required that a linear function of the system state agree with a linear function of the target state. We can formulate this problem as follows. Let H be an s x n matrix and let $\{\underline{z}_N : N=1, 2, \ldots\}$ be the

target. The problem is to find a control sequence $\underline{u}_N \in \Omega$, of minimum length N, such that

$$H\,\underline{x}_N(\underline{x}_0, \underline{u}_N) = H\,A^N\underline{x}_0 + \sum_{i=1}^{N} H\,A^{N-i}\,\underline{b}\,u_i = H\,\underline{z}_N .$$

Defining,

$$\hat{\underline{r}}_i = H\,A^{i-1}\underline{b} \qquad i=1, 2, \ldots$$

$$\hat{\underline{v}}_i = H\,(\underline{z}_i - A^i\underline{x}_0).$$

An equivalent formulation is to find the smallest integer N for which

$$\sum_{i=1}^{N} \hat{\underline{r}}_i\, u_{N+1-i} = \hat{\underline{v}}_N$$

$$|\,u_{N+1-i}\,| \leq 1, \quad i=1, 2, \ldots, N.$$

It is clear that Problem IV is of the same form as Problem II, and, therefore, a solution can be obtained as described in Problem II. Note, however, that if the target state and the system state need only agree in position, then the problem reduces to the time optimal control of a first order system.

Analysis We have shown that solutions to the four problems stated above can be obtained by solving sequentially Problem I. Therefore, we shall limit our discussion to this problem, and state briefly how a solution is obtained. For a proof of the theorems and lemmas which follow, the reader is referred to reference [6].

Lemma 1: If $\underline{u}_N^0$ is the solution to the minimum energy problem (Problem I), then there exists a constant vector $\underline{c} \in E^n$ such that $u_i^0 = \text{sat} < \underline{r}_i, \underline{c} >$, i=1, 2, . . . , N.*

We have previously remarked that a solution to the minimum energy problem exists iff $\underline{v}_N \in R_N$, consequently, using Lemma 1 we have:

---

[6] Canon, M.D. and Eaton, J.H., "A New Algorithm for a Class of Quadratic Programming Problems with Application to Control," presented at First International Conference on Programming and Control, to appear SIAM Journal on Control, Sept. 1965 .

* sat $y \triangleq y$ if $|y| \leq 1$, $\triangleq y/|y|$ if $|y| > 1$

Theorem 1: Each point $\underline{v}_N \in R_N$ can be represented in the form

$$\underline{v}_N = \sum_{i=1}^{N} \underline{r}_i \text{ sat} < \underline{r}_i, \underline{c} > \triangleq \underline{f}_N(\underline{c})$$

for some vector $\underline{c} \in E^n$.

The minimum energy problem has been reduced to finding a vector $\underline{c} \in E^n$ such that $\underline{v}_N = \underline{f}_N(\underline{c})$, i.e., inverting $\underline{f}_N$. Note that $\underline{f}_N$ maps E^n onto R_N, however, the mapping is not one to one. We next show that it is possible to restrict the domain of $\underline{f}_N$, to a subset of E^n, in such a manner as to make $\underline{f}_N$ a bijective bicontinuous function. Since we wish to find an algorithm for determining $\underline{c}$ given $\underline{v}_N$ (or determining if a solution exists, i.e., if $\underline{v}_N \in R_N$) the continuity of $\underline{f}_N^{-1}$ is of major importance.

Definition: For each $\underline{c} \in E^n$, let $I_N(\underline{c}) \subset \{1, 2, \ldots, N\}$ be an index set such that if $i \in I_N(\underline{c})$ then $| < \underline{r}_i, \underline{c} > | \leq 1$; $\bar{I}_N(\underline{c})$ denotes the complement of this set relative to $\{1, 2, \ldots, N\}$. Using this notation $\underline{f}_N(\underline{c})$ can be written as

$$\underline{f}_N(\underline{c}) = \sum_{i \in I_N(\underline{c})} \underline{r}_i \text{ sat} < \underline{r}_i, \underline{c} > + \sum_{i \in \bar{I}_N(\underline{c})} \underline{r}_i < \underline{r}_i, \underline{c} >$$

Definition: Let $C_N \subset E^n$ be the set of all points $\underline{c} \in E^n$ for which the vectors $\{\underline{r}_i : i \in \bar{I}_N(\underline{c})\}$ span E^n.

It is now possible to prove:

Theorem 2: The mapping $\underline{f}_N : C_N \longrightarrow R_N$ is a homeomorphism.

Using the continuity of $\underline{f}_N^{-1}$, a finite step algorithm has been developed for inverting $\underline{f}_N$ [6]. If there is no solution to $\underline{v}_N = \underline{f}_N(\underline{c})$, then the algorithm terminates in a finite number of steps. Thus, it can be determined in a finite number of steps whether $\underline{v}_N \in R_N$, and, as a result, solutions to Problems II through IV can be obtained in a finite number of steps.

To test the computational efficiency of this algorithm time optimal controls of length 20 sampling periods or less were computed for a fourth order system (i.e., $\underline{r}_i \in E^4$). Using an IBM 7090 computer

the maximum computation time was 0.4 seconds. In solving the minimum time problem for an optimal control of length 20 sampling periods the minimum energy problem is solved 20 times. Thus for N = 20, Problem I can be solved in approximately 0.07 seconds.

A NEW APPROACH TO THE SOLUTION OF QUADRATIC PROGRAMMING PROBLEMS

NASA Grant NsG-354 (Supplement 2)
M. Canon (Prof. E. Polak)

All the algorithms presently available for solving quadratic programming problems (QPP) share one common feature, viz., at each step of the algorithm the boundary conditions are satisfied and the value of the cost function is reduced. In this note we show how the QPP can be reduced for solving a set of simultaneous nonlinear equations. A finite-step algorithm has been developed for solving these equations.

The Quadratic Programming Problem

Find n real variables $x_1^0, x_2^0, \ldots, x_n^0$ (representing an n-vector $\underline{x}^0$) which minimize

$$J(\underline{x}) = \langle \underline{x}, Q\underline{x} \rangle + \langle \underline{x}, \underline{d} \rangle \qquad (1)$$

subject to the constraints

$$A\underline{x} = \underline{b} \qquad (2)$$

$$x_i \geq 0, \quad i=1, 2, \ldots, n \qquad (3)$$

Here Q is a symmetric, positive semi-definite n x n matrix, A is an m x n matrix of full rank, $\underline{d} \in E^n$ and $\underline{b} \in E^m$ are constant vectors. Let N(Q) and N(A) denote, respectively, the null space of the operators Q and A. It is assumed that $N(Q) \cap N(A) = \{\underline{0}\}$, the zero vector.

Definition: An n-vector $\underline{x}$ is said to belong to the constraint set Ω, if $x_i \geq 0$, i=1, 2, . . . , n.

Definition: Let $\mathcal{A}$ be the image of the constraint set Ω under the linear transformation A, i.e., $\mathcal{A} = \{A\underline{x} : \underline{x} \in \Omega\}$.

In a straightforward manner one can prove the following:

Lemma 1: If $\underline{b} \in \mathcal{A}$, then the QPP has a solution; furthermore, if $N(Q) \cap N(A) = \{\underline{0}\}$, then the solution is unique.

Necessary and Sufficient Conditions for Optimality

Following Kuhn and Tucker [1] we introduce a scalar valued function $H(\underline{c}, \underline{x})$ defined by

$$H(\underline{c}, \underline{x}) = < c, A x > - J(\underline{x}),$$

where $\underline{c} \in E^m$, $J(\underline{x})$ and A are defined above. Let $(H_{\underline{x}0})_i$, i=1, 2, . . . , n denote the ith component of the partial derivative of H with respect to $\underline{x}$, evaluated at $\underline{x} = \underline{x}^0$ and $\underline{c} = \underline{c}^0$. After a slight modification of the Kuhn and Tucker theorem [1], it is possible to prove Theorem 1.

Theorem 1: A necessary and sufficient condition for $\underline{x}^0$ to be a solution of the QPP is the existence of a vector $\underline{c}^0 \in E^m$ such that

$$\text{(i)} \quad \text{If } x_i^0 = 0, \text{ then } (H_{\underline{x}0})_i \leq 0 \tag{4a}$$

$$\text{(ii)} \quad \text{If } x_i^0 > 0, \text{ then } (H_{\underline{x}0})_i = 0 \tag{4b}$$

It turns out that Eq. 2 implies $H(\underline{c}^0, \underline{x}^0) = \max_{\underline{x} \in \Omega} H(\underline{c}^0, \underline{x})$.

The Vector-Valued Function f

For ease in explanation, let us assume that Q is positive definite. A slight modification of the following argument is necessary under the more general assumption $N(Q) \cap N(A) = \{\underline{0}\}$.

Let $\underline{g}$ be the vector function mapping E^m into Ω defined as follows: to each $\underline{c}^0 \in E^m$, $\underline{g}(\underline{c}^0)$ is that point in Ω which satisfies Eq. 4,i.e.,

$$H(\underline{c}^0, \underline{g}(\underline{c}^0)) = \max_{\underline{x} \in \Omega} H(\underline{c}^0, \underline{x}). \tag{5}$$

It is easily shown that $\underline{g}$ is a function, i.e., to each $\underline{c}^0 \in E^m$ there is one, and only one, $\underline{x}^0 \in \Omega$ satisfying Eq. 3. One can now associate to each $\underline{c} \in E^m$ a point $\underline{a} \in \mathcal{A}$ by the composite function $A \circ \underline{g} = \underline{f}$, where A is the matrix in Eq. 2. By Lemma 1, a solution to the QPP exists if the linear equality constraint, Eq. 2, is replaced by $A \underline{x} = \underline{a}$, for all $\underline{a} \in \mathcal{A}$. Consequently, it follows from Theorem 1, that for every $\underline{a} \in \mathcal{A}$ there exists a $\underline{c} \in E^m$ such that $\underline{f}(\underline{c}) = \underline{a}$; clearly, $\underline{f}$ is continuous. We have proved Theorem 2.

---

[1] H.W. Kuhn and A.W. Tucker, "Nonlinear Programming," Proc Second Berkeley Symposium on Mathematical Statistics and Probability, University of California Press, Berkeley, 1951, pp. 481-492.

Theorem 2: The mapping $\underline{f}: E^m \to \mathcal{R}$ is continuous and onto, furthermore, if $\underline{a} = \underline{f}(\underline{c}) = (A \circ \underline{g})\,\underline{c}$, then $\underline{g}(\underline{c})$ is the solution to the QPP:

$$\text{minimize} \qquad J(\underline{x})$$

$$\text{subject to} \qquad A\underline{x} = \underline{a}$$

$$\underline{x} \in \Omega ,$$

The QPP has now been reduced to inverting the equation $\underline{f}(\underline{c}) = \underline{b}$. A finite step algorithm has been developed for performing this inversion and a computer program has been written and tested on several problems. Preliminary computational results are favorable.

SELF-ORGANIZING CONTROL SYSTEMS

AFOSR Grant AF-AFOSR-292-64
R.P. Iwens (Prof. E.I. Jury)

In general two kinds of learning can be distinguished, i.e., learning from a teacher, and learning by experience. In the first kind of learning the knowledge exists and must only be efficiently transferred from the teacher to the pupil. In a sense, all conventionally designed control systems may be regarded as belonging to learning systems of the first kind. Here learning systems of the second kind are considered where learning is accomplished by utilizing the system experience. A self-organizing or learning control system is able to learn which control to apply to the plant so that the plant is controlled in a near optimum manner. The criterion of optimality considered here is minimum time control.

The problem of learning is viewed as a problem in pattern recognition and a pattern space is defined as an augmented state space. The members of this pattern space are the plant control patterns which must be classified into different categories, each category corresponding to a certain control choice $u_i \in \Omega_u$, where Ω_u is the set of admissible controls. A heuristic training program has been developed with the aid of which the system learns how to establish the different categories in pattern space so that a near optimum control results.

1. Heuristic Training Program

From observations of the behavior of the plant under the influence of the admissible controls $u_i \in \Omega_u$, sample control patterns are collected. The control associated with a sample control pattern is termed a desirable control if during the time when this control is applied the second and/or third time derivative of the weighted norm of the state vector remains negative. (Driving the state vector to the origin is considered equivalent to reducing the system error to zero.) Each

trial control is applied for a predetermined sampling period T. If it is uncertain if the applied control was desirable, the sample control pattern is discarded. The trial control choice is altered each time after an undesirable control choice has been made. The sample control patterns thus collected serve as training patterns for the control-pattern-classifier. The pattern space is bounded and partitioned into pattern categories corresponding to different control choices by using a training algorithm proposed by F. Rosenblatt and B. Widrow. A partition of the pattern space into only two categories is considered here. The assumed form of the discriminant functions were either polynomials or truncated orthogonal expansions. The training algorithm adjusts the coefficients (called weights), $W_1, \ldots, W_M$ which appear in the assumed form of the discriminant function. After the program has determined the proper weights for the discriminant function, the controller has learned how to control the plant, i.e., it is able to drive the system error to zero. The controller measures the plant patterns every T seconds, classifies the pattern into the appropriate category and then applies the corresponding control. The control law thus obtained is, however, not time optimal since the discriminant function will only be a very crude approximation to the time optimal switching boundary. The cost functional of the system may now be considered a function of the weights, $W_1, \ldots, W_M$, of the discriminant function. Gradient techniques are used to adjust these weights further by seeking the minimum of the cost functional $J = f(W_1, \ldots, W_M)$. The main problem encountered here is that $f(W_1, \ldots, W_M)$ is most likely not convex.

a. Example

The regulator system with time varying gain $K(t)$, as shown in Fig. 1, is to learn to reduce the system error to zero in minimum time.

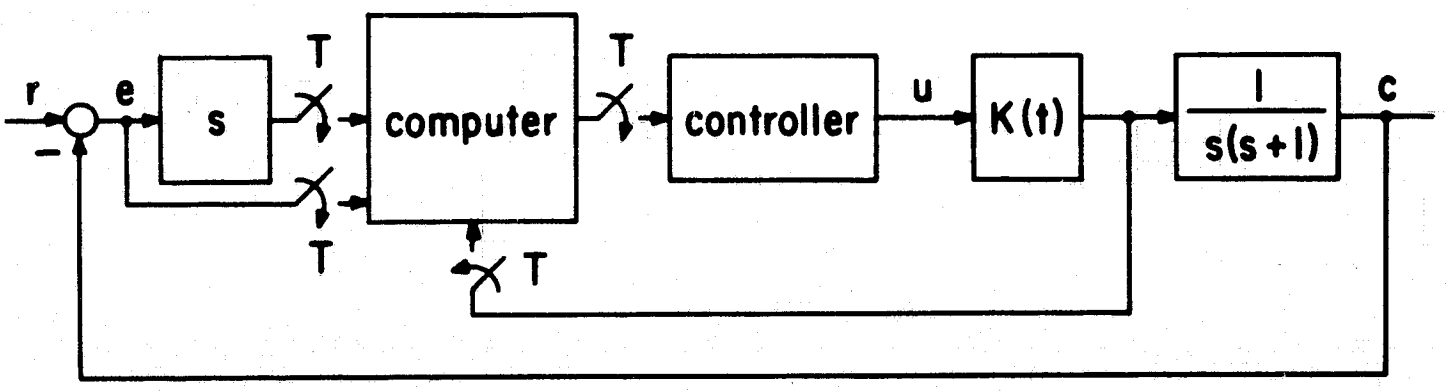

Fig. 1.

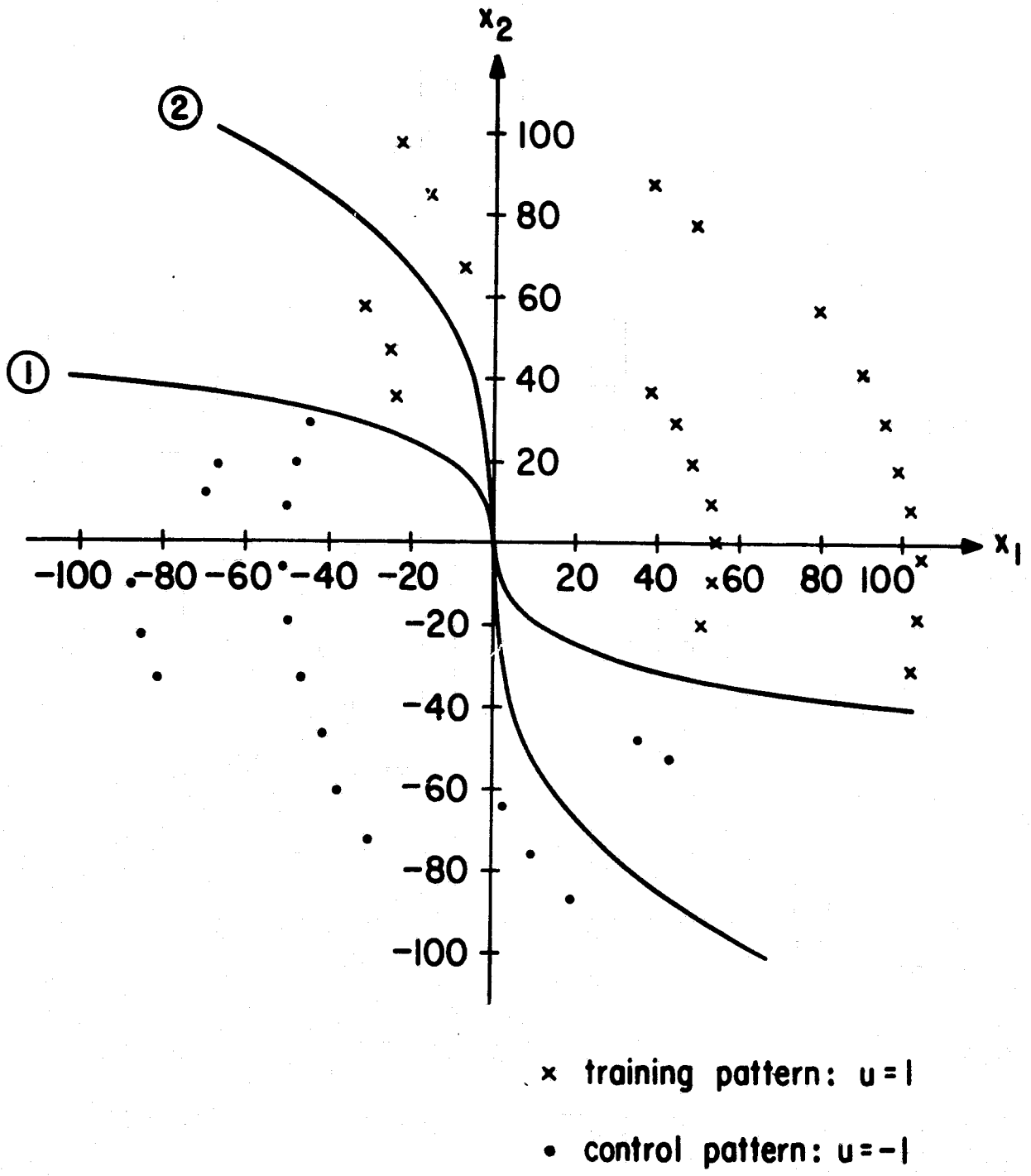

① decision surface obtained from classifier training procedure

② after gradient techniques were applied

Fig. 2. Establishing decision surface from training patterns.

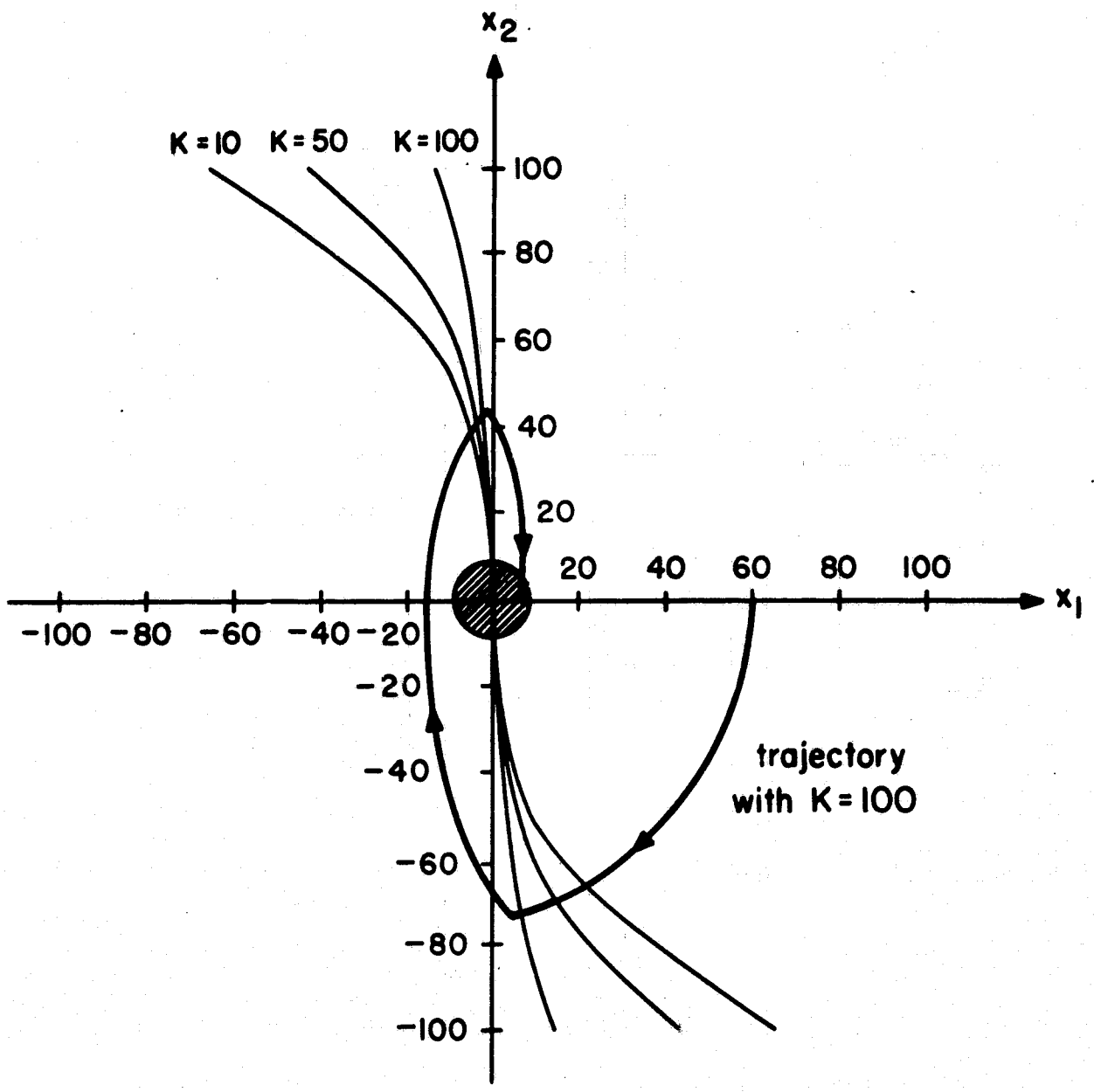

Fig. 3. Learned decision surfaces for three different K's.

The pattern space is the three-dimensional space

$$\mathcal{P} = \{\underline{P} \mid \underline{P} = (x_1, x_2, K) ; e = x_1, \dot{e} = x_2 \}$$

Figure 2 shows some of the collected training patterns for K = 10. It also shows the discriminant function decision surface separating the two pattern categories, and the adjusted decision surface after gradient techniques were applied. Figure 3 shows the "learned" decision surfaces for three different gains. A typical trajectory using T = 0.05 sec is also shown. To avoid small limit cycles around the origin, the system may be operated in a linear negative feedback mode once the trajectory has entered the cross-hatched circle around the origin.

b. Evaluation

The main advantages of this approach to learning systems is that the learning period is short and the memory requirements during the learning process, as well as afterwards when the system is in actual operation, are quite small. This is because all of the information necessary to control the plant is contained in the weights of the discriminant functions. Large memory requirements are some of the main difficulties of other methods which have been proposed for implementing self-organizing systems.

For the example given above the following computer data applies: Computing time on the IBM 7094 : 4.15 minutes of total learning time. Memory requirements: (a) During learning process: 2, 500 words, (b) After learning is completed: 60 words.

Further research in this area should be directed towards seeking better methods of obtaining a good set of training patterns and in extending the method to other optimality criteria.

A report on this research will be published in the near future as an ERL technical memorandum from the Electronics Research Laboratory, University of California, Berkeley.

STUDIES IN PATTERN CLASSIFICATION

AROD Grant DA-ARO-D-31-124-G576 and NSF Grant GP-2413
N. Sugino (Prof. E. Wong)

During the reporting period, classification methods based on distance concepts have been studied. Specifically, a new and simple proof of the Sebestyen's "best" metric problem [1] in the signal space was obtained. Mathematically, one of the "best" distance problems is reduced to: Given sample vectors $\xi_i (i = 1, \ldots, M)$ in En, find an n x n matrix A such that

$$\overline{D}^2 \triangleq \frac{1}{M^2} \sum_{i=1}^{M} \sum_{j=1}^{M} (\xi_i - \xi_j)' A (\xi_i - \xi_j) \text{ is minimized subject to}$$

[1] G.S. Sebestyen, Decision Making Processes in Pattern Recognition, The Macmillan Company, New York, N. Y., (1962).

$|A| = 1$ and A being positive definite and symmetric.

Let $R \triangleq \frac{1}{M} \sum_{i=1}^{M} (\xi_i - \mu)(\xi_i - \mu)'$, where $\mu \triangleq \frac{1}{M} \sum_{i=1}^{M} \xi_i$. Then, by letting

$x_\ell \triangleq \left((\xi_1 - \mu)^{(\ell)}, \ldots, (\xi_M - \mu)^{(\ell)} \right)'$, $(\ell = 1, \ldots, n)$, where $(\xi_i - \mu)^{(\ell)}$ $(i = 1, \ldots, M)$ denotes the ℓth component of $(\xi_i - \mu) \in En$, we find that $|R|$ becomes a Gram determinant. Hence, by virtue of characteristics of a Gram determinant and the projection theory in En, we can easily get the solution.

At present, an attempt is being made to explore the possibility of applying the concept of vector criteria [2] to the problems in pattern classification. Let us consider the problem of classifying $x \in En$ into one of two non-empty categories, $C_1 \subset En$ or $C_2 \subset En$, where $C_1 \cap C_2 = \{\phi\}$. Our attempt is to accomplish the classification by the decision criteria;

$$\text{decide} \quad x \in C_1 \quad \text{if} \quad \mathbb{D}_{C_1}(x) > \mathbb{D}_{C_2}(x)$$

$$\text{decide} \quad x \in C_2 \quad \text{if} \quad \mathbb{D}_{C_1}(x) < \mathbb{D}_{C_2}(x),$$

where $\mathbb{D}_{C_1}(x)$ and $\mathbb{D}_{C_2}(x)$ are functions on En to Em $(n, m > 1)$.

ITERATIVE APPROACHES TO CLASSIFICATION, GAME STRATEGIES AND MATHEMATICAL PROGRAMMING

AROD Grant DA-ARO-D-31-124-G576
L. Barbosa (Prof. E. Wong)

After a set of N measurements is chosen, a pattern can be associated with an N-dimensional vector. Given two sets A and B of vectors representing patterns of two categories, the problem of classification is how to design a machine capable of distinguishing vectors belonging to set A from those belonging to B.

The sets A and B are said to be linearly separable whenever there exists a hyperplane π in E_N such that the sets A and B lie in different π-half-spaces. Equivalently, the sets A and B are said to be linearly separable if there exists a vector w in E_N and a scalar t satisfying:

---

[2] L.A. Zadeh, "Optimality and Non-Scalar-Valued Performance Criteria," IEEE Trans. on Automatic Control, Vol. AC-8, pp. 59-60; January, 1963.

$$w \cdot x > t \text{ for all } x \in A$$

$$w \cdot x < t \text{ for all } x \in B$$

For simplicity, one can define a set $\mathcal{A}$ augmenting the vectors x ($x \in A \cup (-B)$) to $a = (x, -1)$:

$$\mathcal{A} \triangleq \{a = (x, -1); x \in A \cup (-B)\}$$

and after augmenting w to $g = (w, t)$, results: classes A and B are linearly separable if there exists a vector $g \in E_{N+1}$ such that

$$g \cdot a > 0 \quad \text{for all } a \in \mathcal{A} .$$

In the following, some results on procedures to find the vector g will be presented. Since, in general, one cannot be sure of the linear separability of the classes, it is advantageous that the procedures converge even in the case of nonseparable (linearly) classes.

1. Continuous Procedures

If classes A and B are linearly separable, one can, without loss, admit the existence of a vector y and a scalar θ such that

$$y \cdot a > \theta > 0 \quad \text{for all } a \in \mathcal{A} . \tag{1}$$

Consider the following procedure:

$$\dot{g} = \sum_j |a_j \cdot g|^{\epsilon} a_j H_j(g) ,$$

$$a_j \in \mathcal{A} ,$$

$$H_j(g) = \begin{cases} 1 \text{ if } a_j \cdot g \leq 0 \\ 0 \text{ otherwise.} \end{cases}$$

We succeeded on the proof of the following results:

1.1 Procedure (1) converges for $\epsilon > 0$. The rate of convergence is at least $1/t$.

1.2 Under existence of w such that $w \cdot a_j \geq 0$ for every $a_j \in \mathcal{A}$, with $w \cdot a^* > \theta > 0$ for some $a^* \in \mathcal{A}$, procedure (1), with $\epsilon > 0$, would converge to g^* satisfying

$$g^* \cdot a_j \geq 0 \quad \text{for all } a_j \in \mathcal{A}$$

$$\|g^*\| \neq 0 ,$$

provided $g_0 \cdot w > \theta$ (put $g_0 = \sum_j a_j$ for instance).

The rate of convergence is at least 1/t.

1.3 Under existence of y such that $y \cdot a_j > \theta > 0$ for every $a_j \in \mathcal{A}$ procedure (1) terminates (that is, will reach equilibrium in finite time) for $0 < \epsilon < 1$. Furthermore, choosing g_0 such that $g_0 \cdot y > \theta$ (put g_0 = some $a_j \in \mathcal{A}$, for instance), procedure (1) terminates at g^* such that

$$g^* \cdot a_j \geq \text{for all } a_j \in \mathcal{A}$$

$$\|g^*\| \neq 0.$$

2. Modification of Brown-von-Neumann Procedure

The continuous approach of Brown-von-Newmann to solve a symmetric matrix game can be modified according to the preceding ideas, in order to increase its rate of convergence. Here, one seeks a strategy y for player II satisfying

$$u_i(y) \triangleq a_i \cdot y \leq 0 \quad \text{for all } a_i \in \mathcal{A}$$

(here a_i is the ith line of an antisymmetric matrix).

Define

$$\phi(u_i) \triangleq |a_i \cdot y| \cdot H_i(y) \text{ with } H_i(y) = \begin{cases} 1 \text{ if } a_i \cdot y \geq 0 \\ 0 \text{ otherwise} \end{cases}$$

$$\phi_\epsilon(y) = \sum_i \phi^\epsilon(u_i) = \sum_i |a_i \cdot y|^\epsilon \; H_i(y) .$$

Consider the procedure:

$$\begin{cases} \dot{y}_j = \phi^\epsilon(u_j) - y_j \phi_\epsilon(y) \\ y(0) \text{ - an arbitrary strategy} \end{cases} \tag{2}$$

(For $\epsilon = 1$ this is the Brown-von-Newmann procedure)

Then, one can prove:

2.1 Procedure (2) converges to an optimal strategy for $\epsilon > 0$

2.2 At each instant, y(t) is a strategy (that is, $\sum y_i = 1$, $y_i \geq 0$)

2.3 The rate of convergence approaches an exponential as $\epsilon \longrightarrow 0$

Remark: According to 1.2, procedure (1) could also be used to solve symmetric games by adjoining a N x N unit matrix of the game (to ensure that $y_i \geq 0$).

3. Discrete Procedures

The following iteration proceudre is a discrete version of procedure (1):

$$g_{n+1} = g_n + \alpha_n \sum_{j \in J_n} |a_j \cdot g_n|^{\epsilon} a_j, \quad J_n = [j_i \cdot a_i \cdot g_n < 0, \ a \in \mathcal{A}] \qquad (3)$$

g_0 = arbitrary, in the span of a_j's

One can prove:

3.1 The sequence $\|g_m\|$ resulting from (3) is bounded

($\|g_m\| < k$) for $0 \leq \epsilon < 1, \alpha_n < A$.

3.2 Procedure (3) will converge for $0 \leq \epsilon < 1$ provided

$$\sum_{\alpha_n \longrightarrow \infty}, \ \sum \alpha_n^2 < \infty$$

3.3 If there exists a g^* such that

$$g^* \cdot a_j \geq 0 \text{ for all } a_j \in \mathcal{A}, \text{ and}$$

$$g^* \cdot a^* > \theta > 0 \text{ for some } a^* \in \mathcal{A}$$

then procedure (3) under conditions 3.2 will converge to some g^{**} satisfying

$$\|g^{**}\| \neq 0$$

$$g^{**} \cdot a_j \geq 0 \text{ for all } a_j \in \mathcal{A}$$

provided

$$g_0 \cdot g^* > \theta$$

3.4 If there exists a y such that

$$y \cdot a_j \geq \theta > 0 \text{ for all } a_j \in \mathcal{A}$$

procedure (3) terminates under conditions 3.2.

By termination we mean that after a finite number of iterations n_0, $g_{n_0+k} = g_{n_0}$ for any $k \geq 0$.

Remark: As in the continuous case, according to 3.3, procedure (3) could be used to solve a symmetric matrix game if an N x N unit matrix is adjoined to the game matrix in order to ensure the positiveness of all components of g. The rate of convergence of procedure (3) is better than $1/\ln n$. In order to improve this rate, a modification of (3) yields:

3.5 Define $\phi_n \triangleq \sum_{j \in J_n} | a_j \cdot g_n |^{1+\epsilon}$. Then procedure (3) will converge

for $0 \leq \epsilon <$ with $\alpha_n = k\phi_n \frac{1-\epsilon}{1+\epsilon}$, $k < \frac{2}{L^2 M^{2/1+\epsilon}}$,

where $L = \max_{a_i \in \mathcal{A}} \|a_i\|$

M = number of vectors a_i in $\mathcal{A}$.

The rate of convergence is at least exponential.

FACTORIZATION OF LINEAR CYCLE SETS

ONR Contract NOMN-333(53)
C.J. Tan (Prof. A. Gill)

An autonomous linear sequential circuit $\mathcal{A}$ is described by: (a) A finite field $GF(p) = \{0, 1, \ldots, p-1\}$, where p is prime and all operations are modulo p; (b) an n-dimensional vector space S_n over GF(p); a vector $\underset{\sim}{s}$ of S_n is called a state of $\mathcal{A}$; (c) an n x n characteristic matrix $\underset{\sim}{A}$ over GF(p). If the state of $\mathcal{A}$ at any time t (where t assumes integral values only) is $\underset{\sim}{s}$, then the state at time t + 1 is $\underset{\sim}{A}\underset{\sim}{s}$.

The state graph of $\mathcal{A}$ consists of p^n vertices, one for each vector of S_n. A directed bran ch leads from vertex $\underset{\sim}{s}_i$ to vertex $\underset{\sim}{s}_j$ if and only if $\underset{\sim}{s}_j = \underset{\sim}{A}\underset{\sim}{s}_i$. Here we shall restrict ourselves to nonsingular matrices $\underset{\sim}{A}$, in which case the state graph of $\mathcal{A}$ consists of cycles only. If a state graph contains μ_i cycles of length k_i, the graph can be characterized by an expression of the form

$$\Sigma = \mu_1 \{k_1\} + \mu_2 \{k_2\} + \cdots + \mu_r \{k_r\}, \qquad (1)$$

which is called a cycle set. A cycle set Σ characterizing the state graph of an autonomous linear-sequential circuit with a nonsingular characteristic matrix is called a linear-cycle set. If the matrix is $\underset{\sim}{A}$, Σ is said to be the cycle set of $\underset{\sim}{A}$.

Let $\underset{\sim}{A}$ be the companion matrix of $[\,p(x)\,]^e$, where $p(x)$ is an irreducible polynomial over GF(p) of degree h. Elspas [1] showed that, in this case, the cycle set of $\underset{\sim}{A}$ is given by

$$\Sigma = 1\,\{1\} + \frac{p^h-1}{k_1}\,\{k_1\} + \frac{p^{2h}-p^h}{k_2}\,\{k_2\} + \frac{p^{3h}-p^{2h}}{k_3}\,\{k_3\} + \cdots$$

$$+ \frac{p^{eh}-p^{(e-1)h}}{k_e}\,\{k_e\}, \qquad (2)$$

where k_1 is the least integer such that $p(x)$ divides $1-x^{k_1}$; $k_j = p^{r_j} k_1$, where r_j is the least integer such that $p^{r_j} \geq j$. Such a cycle set is called a canonical-cycle set. It can be shown that h is the least integer such that k_1 divides p^h-1. The expression k_1, therefore, cannot be a multiple of p.

A term $\mu_i\,\{k_i\}$ in a cycle set is called a cycle term of period k_i. Addition of cycle terms is defined only when they are of the same period:

$$\mu_i\,\{k_i\} + \mu_j\,\{k_i\} = (\mu_i + \mu_j)\,\{k_i\}. \qquad (3)$$

Multiplication of cycle terms is defined by:

$$\mu_i\,\{k_i\} \cdot \mu_j\,\{k_j\} = \mu_i\mu_j\,\gcd(k_i, k_j)\{\mathrm{lcm}(k_i, k_j)\}. \qquad (4)$$

Multiplication of cycle sets is defined as follows: If Σ is as given in Eq. 1, and

$$\Sigma' = \mu'_1\,\{k'_1\} + \mu'_2\,\{k'_2\} + \cdots + \mu'_s\,\{k'_s\}, \qquad (5)$$

then $\Sigma\Sigma'$ is a cycle set given by the sum of all products $\mu_i\,\{k_i\} \cdot \mu'_j\,\{k'_j\}$, evaluated by Eq. 4. Thus, cycle set multiplication is both associative and commutative.

Elspas [1] showed that a cycle set Σ is linear (i.e., realizable by an autonomous linear sequential circuit) if and only if it is expressible as a product of canonical cycle sets. This expression is referred to as a canonical factorization of Σ. The circuit realization (by means of feedback shift registers) of a linear cycle set whose canonical factorization is known can be readily derived from the corresponding factors. A cycle set is said to be irreducible, if it is not expressible as the product of two or more linear cycle sets.

---

[1] B. Elspas, "The Theory of Autonomour Linear Sequential Networks," Trans. IRE, Vol. CT-6, pp. 45-60 (1959).

Elspas asserted (without proof) that the canonical factorization of a cycle set (and as a special case, of a canonical-cycle set) is unique. The first undertaking in this project was to prove that this assertion is not correct, although a canonical cycle set is indeed irreducible. An algorithm was constructed for the division of one linear cycle set by another, to result in a quotient which is a linear-cycle set; this algorithm serves as a proof for the uniqueness of such a division wherever it can be carried out. Finally, an improved procedure was devised for the canonical factorization of an arbitrary linear cycle set.

STABILITY ANALYSIS OF MONOTONE FEEDBACK SHIFT REGISTERS

ONR Contract Nonr-222(53)
C.J. Tan (Professor A. Gill)

A special class of feedback shift register, called monotone feedback shift registers (MFSR's) were found to be useful in a number of error-correction applications. In this project, a general stability test was formulated for MFSR's, using Boolean matrices.

STUDIES IN NONLINEAR MODULAR SEQUENTIAL CIRCUITS

JSEP Grants AF-AFOSR-139-64 & 65
J.P. Jacob (Prof. A. Gill)

Problems in sequential circuits or synthesis of Boolean functions can be viewed as mappings from binary Galois fields into themselves. We will try to illustrate the first part of this statement below (Fig. 1 and sequel); the second part has been treated previously [1].

Once this has been recognized, we can start using properties of Galois fields mappings [2]. Unfortunately, these are of theoretical nature and do not give us a lead as to how to find the hardward which corresponds to them. The objective of the first part of our work was to fill this gap. Reference [1] exhibits all our results in this topic; the main result is the presentation of the logical circuit which multiplies two elements of a binary Galois field (in accordance with the rules of this field, of course). This multiplication is performed in one clock pulse, as opposed to other methods [3] using shift registers. An

[1] J.P. Jacob, "The design of circuits for performing operations and computing functions over finite fields," ERL Tech. Memo. M-106, University of California, Berkeley.

[2] L.E. Dickson, Linear Groups, Dover Publications Inc., New York, N.Y., 1958.

[3] W.W. Peterson, Error-Correcting Codes, J. Wiley and Sons, N.Y., 1961.

immediate corollary of the above result is the design of a logical circuit which realizes a polynomial function on a binary Galois field.

As a second part of our studies, we considered applications of these results: shift-register generators, decoders, synthesis of Boolean functions using only NOR gates (Sheffer stroke operations), etc. These assorted topics share the fact that they can all be viewed as mappings of finite fields into themselves.

Consider the generalized sequential circuit in Fig. 1 where the boxes labelled D_i represent delays (or memory elements) and, as usual, α_i and β_i are either 0 or 1.

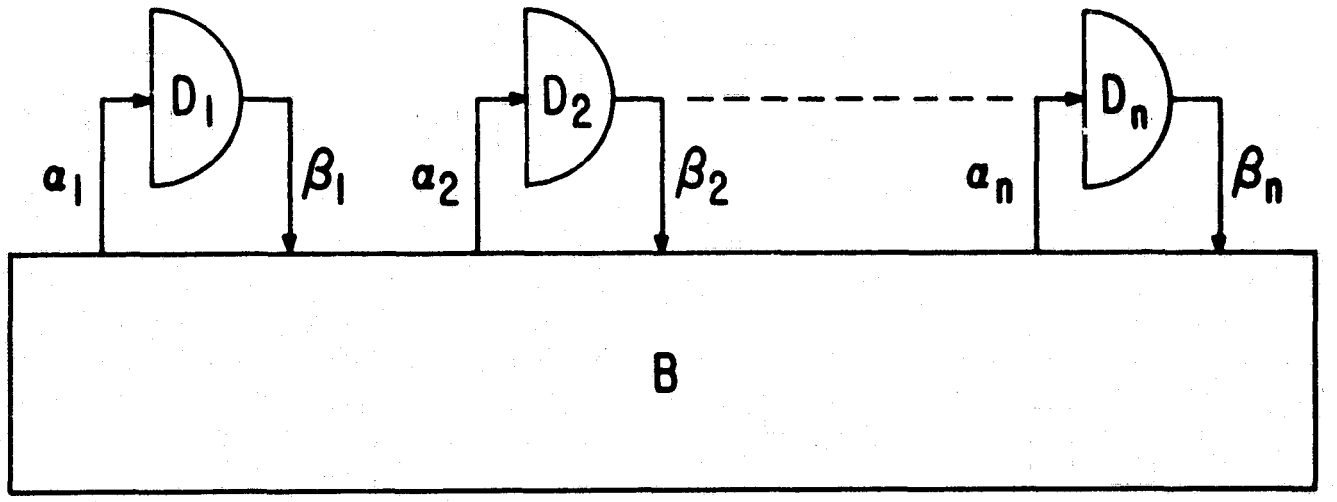

Fig. 1. Generalized sequential circuit.

We assume that our circuit has exactly n delays, i.e., box B contains no delay. It consists only of logic and a clock pulse generator. Figure 1 may represent a shift register generator [3] as shown in Fig. 2. In our approach we do not need to discriminate between linear and non-linear shift registers, or, more generally, between linear or nonlinear generalized sequential circuits.

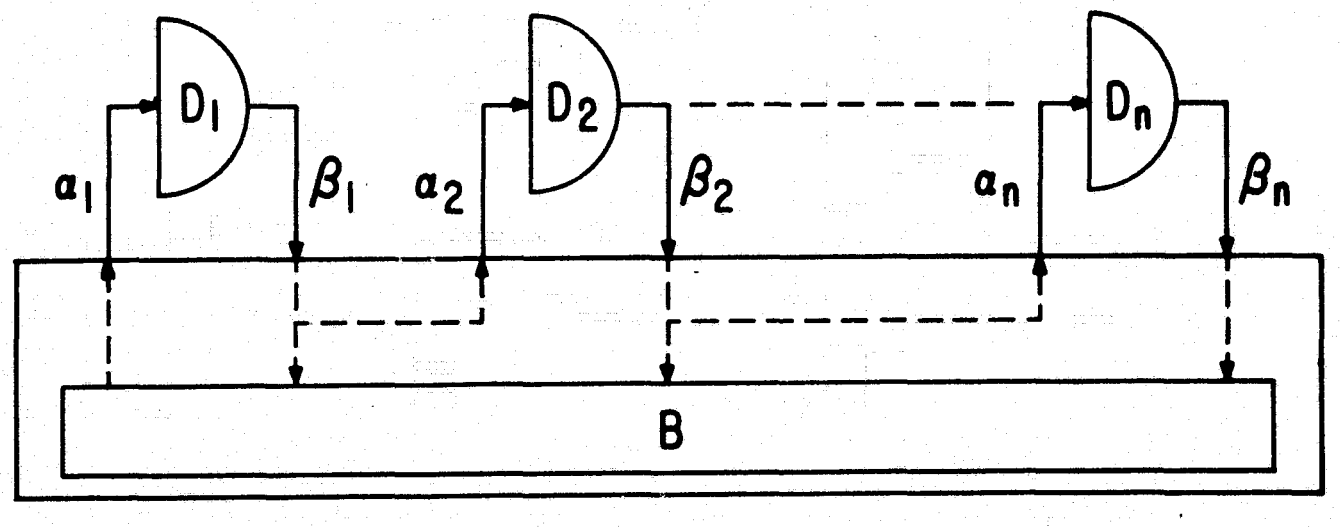

Fig. 2. The shift-register.

At each clock pulse one may look at the set of outputs $(\beta_1, \beta_2, \ldots, \beta_n)$ and identify this collection with an element of the finite field containing 2^n elements, called G.F. (2^n). There are as many different ordered collections $(\beta_1, \beta_2, \ldots, \beta_n)$, with $\beta_i \in \{0, 1\}$ as elements in G.F. (2^n), namely, 2^n. One of the ways of making the identification is to think of the elements of G.F. (2^n) as if they were polynomials of degree n in an indeterminate x and coefficients 0 or 1. In the sequel the reader is assumed to be familiar with this kind of representation. We associate each β_i with one and only one coefficient of this polynomial. The choice is arbitrary but for simplicity we will associate β_i with the coefficient of x^{i-1}.

We now look at Fig. 1 again and see that, at a given clock pulse n, box B has an input an element of G.F. (2^n) and maps this element into another element in G.F. (2^n), associated with the collection $(\alpha_1, \alpha_2, \ldots, \alpha_n)$. Since $(\alpha_1, \alpha_2, \ldots, \alpha_n)$ will be the output at clock pulse n + 1, we call this transformation the "successor transformation" or, better, the "successor mapping."

Box B is hence characterized by the mapping it performs. Since the mappings of G.F. (2^n) into itself can be represented by a polynomial function [2] and since a polynomial function has a given standard way of realizing it (see claim in second paragraph) we have a "convenient way" -- synonym for "canonical way" -- of representing any generalized sequential circuit.

From the above, it can be immediately concluded that we can obtain, via shift-registers, properties of finite fields. This result is trivial but nevertheless curious. In Fig. 3, for instance, the output of box B exhibits, at each clock pulse, an automorphic image of the element initially placed in the memory. In other words, the circuit of Fig. 3 finds all the automorphisms of any element of G.F. (2^4). Similar results can be obtained for isomorphisms [1]. A possible application of this "isomorphism" would be a transformer of codes, i.e., a device mapping a fixed length code into an isomorphic one.

We previously showed [1] how to obtain box B when the mapping polynomial is given. If, however, only the successor mapping is given, one has to find its mapping polynomial. A computational aid has been devised for doing so [4]. In general, the mapping polynomial would require as many nonzero coefficients (as much "memory") as the number of given points but in certain particular cases of importance, less memory is required.

---

[4] A. Gill and J.P. Jacob, "The Application of Galois Field Theory to a Class of Recognition Problems," to be published.

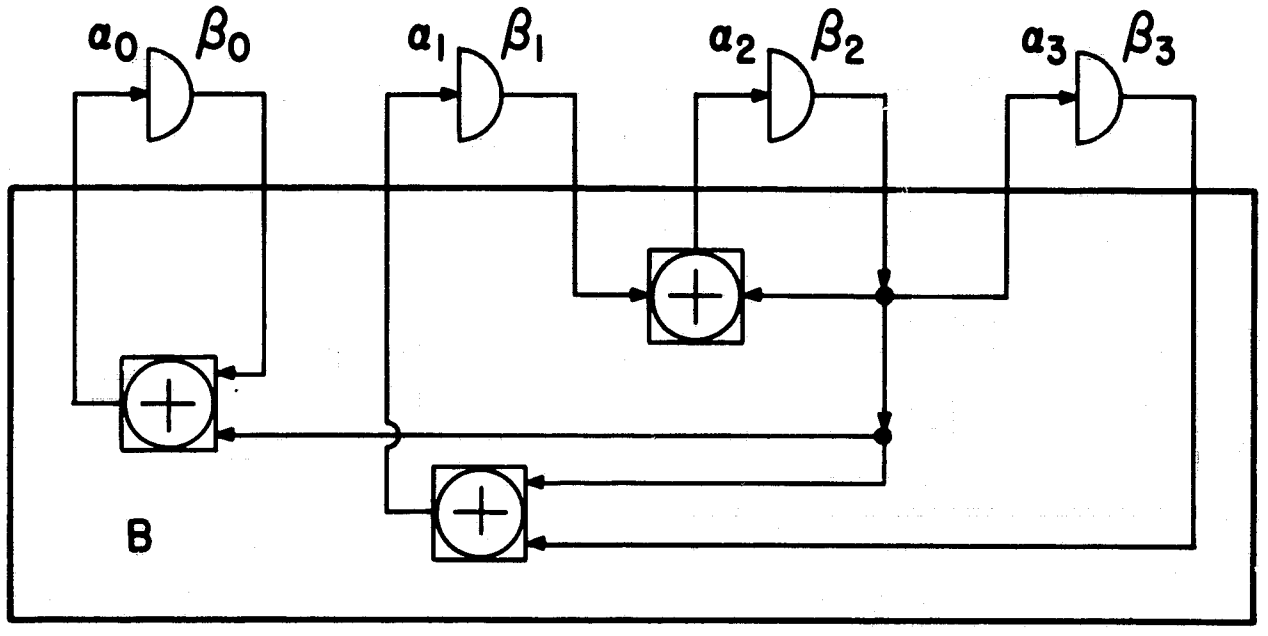

Fig. 3. A generator of automorphisms for G. F. (2^4). Box B contains only NOR gates. At each clock pluse the input to box B is an automorphic image of the element initially placed in the memory. Box B is just a squarer in G. F. (2^4).

THE THEORY OF SEQUENTIAL RELATIONS

AFOSR Grant No. AFOSR-639-64
J.N. Gray, (Prof. M.A. Harrison)

The theory of sequential machines with an initial state is well-developed. This report concerns a generalization of sequential machines by discarding the requirement of an initial state. This paper presents our results concerning the closure and decidability properties of the classes of sets defined by these more general machines.

A sequential machine S is a system $< \Sigma, \Delta, S, f, g >$, where Σ is a finite non-empty input alphabet, Δ is a finite non-empty output alphabet, S is a finite non-empty set of internal states, f is the transition function $f: \Sigma \times S \to S$, and g is the output function $g: \Sigma \times S \to \Delta$.

Let $R \subseteq (\Sigma \times \Delta)^*$, then R is a sequential relation over $\Sigma \times \Delta$, $SR/(\Sigma \times \Delta)$, if and only if (iff) there exists a sequential machine $\mathcal{S} = < \Sigma, \Delta, S, f, g >$ such that $R = \{(x, y) \in (\Sigma \times \Delta)^* \mid s \in S, g(x, s) = y\}$. In this case R is the relation computed by $\mathcal{S}$ denoted $R(\mathcal{S})$. On the other hand, if there is a state s in $\mathcal{S}$ such that $R = \{(x, y) \in (\Sigma \times \Delta)^* \mid g(x, s) = y\}$ then R is said to be a sequential function over $\Sigma \times \Delta$.

The following are our results:

1. Necessary and Sufficient Conditions for Sequential Relations

Proposition 1.1. The set $R \subseteq (\Sigma \times \Delta)^*$ is $SR/(\Sigma \times \Delta)$ iff there exists a finite number of sequential functions $g_i, \ldots, g_n$ such that

(a) $R = \bigcup_{i=1}^{n} g_i$

(b) $\forall\, i \leq n, \forall\, \sigma \in \Sigma, \exists\, j \leq n, \forall\, x \in \Sigma, {}^* g_i(\sigma x) = g_i(\sigma)\, g_i(x)$.

Alternatively.

Proposition 1.2. The set $R \subseteq (\Sigma \times \Delta)^*$ is $SR/(\Sigma \times \Delta)^*$ iff there exists a finite number of sequential functions, $g_i, \ldots, g_n$ such that

(a) $R = \bigcup_{i=1}^{n} g_i$

(b) R is suffix closed.

Following are some of the important properties of any sequential relation R over $\Sigma \times \Delta$; for the pertinent definitions see [1].

(a) R is regular over $(\Sigma \times \Delta)^*$,

(b) R is length preserving,

(c) R is prefix and suffix closed,

(d) R is strongly extendable,

(e) If $\Delta \leq \Gamma$, then R is $SR/(\Sigma \times \Gamma)$,

(f) R is infinite.

2. Closure Properties

The following table summarizes the closure properties for the set of all sequential relations over $\Sigma \times \Delta$.

---

[1] C.C. Elgot, (1961) "Decision problems of finite automata design and related arithmetics," Trans. Amer. Math. Soc., 98, 21-51.

TABLE 1

The set of all sequential relations over $\Sigma \times \Delta$ closed under

	$\lvert\Delta\rvert$	$\lvert\Delta\rvert > 1$
Complementation	no	no
Union	yes	yes
Intersection	yes	no
Symmetric difference	no	no
Composition	yes	yes
Converse	yes	no
Concatenation	yes	no
Iteration	yes	no
Transpose	yes	no

Further, the Kleenean closure [2] of all $SR(\Sigma \times \Delta)$ relations is the class of all $(\Sigma \times \Delta)^*$ regular sets.

3. Decidability Questions

The answers to these questions were by far the most difficult to obtain. We have considered three cases. We are given [1 - 3] a set $R \subseteq \Sigma^* \times \Delta^*$ which is given as:

(1) The behavior of a finite automaton,

(2) A sequential transduction,

(3) The language generated by a context free grammar.

In each case we asked: Is there an algorithm for deciding whether R is $SR/(\Sigma \times \Delta)$; further, if R above is $SR/(\Sigma \times \Delta)$ then is

---

[2] M. O. Rabin, D. L. Scott, "Finite automata and their decision problems," IBM J. Res. and Develop., 3, pp. 114-125, (1959).

[3] N. Chomsky, "Formal properties of grammars," Handbook of Mathematical Psychology, II, J. Wiley and Sons, Inc., N. Y., (1963).

there a synthesis method for a sequential machine such that $R = R(\mathcal{S})$.

A rather long but elegant argument disclosed the following:

Proposition 3.1. If $R \subseteq (\Sigma \times \Delta)^*$ is the behavior of finite automaton $\mathcal{A}$ then there is an effective procedure for deciding whether R is $SR/(\Sigma \times \Delta)$. If R is $SR/(\Sigma \times \Delta)$, then there is a synthesis method for sequential machine $\mathcal{S}$ such that $R = R(\mathcal{S})$.

The following proposition hinges on the fact that it is decidable whether a sequential transduction is a regular set. If it is not a regular set it is not $SR/(\Sigma \times \Delta)$, and if it is regular then we can decide if it is $SR/(\Sigma \times \Delta)$.

In any case:

Proposition 3.2. If $R \subseteq \Sigma^* \times \Delta^*$ is a sequential transduction then it is decidable whether R is $SR/(\Sigma \times \Delta)$. If R is $SR/(\Sigma \times \Delta)$ then there is a synthesis method for sequential machine $\mathcal{S}$ such that $R = R(\mathcal{S})$.

In light of proposition 3.2 the following result is quite surprising.

Proposition 3.3. If R is $SR/(\Sigma \times \Delta)$ and S is a sequential transduction over $\Sigma \times \Delta$ then it is recursively unsolvable to decide whether $R \cap S$ is empty, finite or infinite.

However proposition 3.3 does make the following credible.

Proposition 3.4. It is recursively unsolvable if a context-free language over $(\Sigma \times \Delta)^*$ is $SR/(\Sigma \times \Delta)$.

TWO-WAY DETERMINISTIC PUSHDOWN STORAGE AUTOMATA

JSEP Grants AF-AFOSR-139-64 & 65
AF-AFOSR-639-65
O.H. Ibarra (Prof. M.A. Harrison)

The study of artificial languages was initiated by Chomsky in 1955 in an attempt to find a mathematical model for studying natural languages. Since then, several papers relating to this theory have been written. The following important results are known:

(1) A set of strings over a finite alphabet Σ is a one-sided linear language if and only if it is accepted by a finite automaton [1];

(2) A set of strings over a finite alphabet Σ is a context-free language if and only if it is accepted by a nondeterministic pushdown storage automaton [2 , 3]; and

---

[1] N. Chomsky, "On certain formal properties of grammars," Information and Control , 2, pp. 137-167 , (1959).

[2] N. Chomsky, "Context-free grammars and pushdown storage," Quarterly Progress Report No. 65 , Research Laboratory of Electronics, M.I.T., pp. 187-194 (1962).

[3] M.P. Schutzenberger, "Context-free languages and pushdown automata," Information and Control 6, pp. 246-264, (1963).

(3) A set of strings over a finite alphabet Σ is a context-sensitive language if and only if it is accepted by a nondeterministic linear bounded automaton [4, 5].

Here, we try to generalize the notion of a pushdown automaton by allowing it to move both ways on the input tape, and at the same time restricting the machine to operate deterministically. We shall call this type of a machine a two-way deterministic pushdown storage automaton (twdpda). Unlike the equivalence of one-way and two-way finite automata [6, 7], we showed that twdpda's are more powerful than one-way deterministic pushdown storage machines. We have exhibited a number of non-context-free languages which are twdpda definable. It is not yet known whether the class of context-free languages is a proper subset of the class of twdpda definable sets, although we suspect this is not so.

Relations to one-tape and two-tape automata were studied. We have shown that if the amount of pushdown tape necessary for a two-way computation is linearly bounded by the length of the input tape, a deterministic linear bounded automaton exists which accepts the same set of tapes as the given twdpda. We believe that a slight modification of the proof will give a stronger result of the form: the set of tapes accepted by a twdpda is a context-sensitive language.

On the closure properties we have shown the following: Twdpda definable sets are closed under transposition and intersection. Closure under the operations of complementation, union, complex product, and star operation is not yet known.

Decidability problems were studied in detail. Some of the decision problems which we have shown to be effectively unsolvable are: Let L_1, L_2 be arbitrary twdpda definable sets and R an arbitrary one-sided linear language.

(1) Is L_1 empty, finite, infinite, regular, context-free?

(2) Is $L_1 \cap L_2$ empty, finite, infinite, regular, context-free?

(3) Is $L_1 = \Sigma^*$?

(4) Is $L_1 \subseteq R$?

(5) Is $L_1 \leq L_2$?

(6) Is $L_1 = L_2$?

---

[4] P.S. Landweber, "Three theorems on phrase structure grammars of type 1," Information and Control 6 , pp. 131-137, (1963)

[5] S.Y. Kuroda, "Classes of languages and linear bounded automata," Information and Control 7 , pp. 207-223, (1964)

[6] M.O. Rabin and D. Scott, "Finite automata and their decision problems," IBM J. Res. and Dev., V. 3, pp. 114-125, (1959).

[7] J.C. Shepherdson, "The reduction of two-way automata to one-way automata," IBM J. Res. and Dev., V. 3, pp. 198-200, (1959).

REGULAR EXPRESSIONS FOR BINARY MACHINES

NSF Grant GP-2413
L. Lecoq (Prof. A. Gill)

In this project, an algorithm was developed for finding the regular expression for a sequential machine directly from the logical circuit of the machine. The following were obtained as by-products: (a) An algorithm for describing all cycles originating in a specified state, (b) description of all proper paths originating from a specified state, and (c) specialization of the results to input-independent machines.

THE CYCLE STRUCTURE OF NON-LINEAR AUTONOMOUS SEQUENTIAL CIRCUITS

NSF Grant SP-2413
Y. Zalcstein (Prof. A. Gill)

The action of a non-singular autonomous sequential circuit divides the state space into disjoint cycles. A given circuit realizes a cycle set $\{N_1[T_1], \ldots, N_K[T_k]\}$ if and only if it divides the state space into N_1 cycles of length T_1, N_2 cycles of length $T_2 \ldots N_k$ cycles of length T_k, where $\sum_{i=1}^{k} N_i T_i =$ cardinality of state space. The basic problems are:

(1) To characterize the cycle sets realizable by non-singular autonomous sequential circuits, and

(2) To find out whether a realizable cycle can be realized by a parallel or series-parallel connection of simpler circuits.

In this generality the problems have never been attacked. The linear case is completely solved, but the problem for non-linear circuits is considerably more difficult. Our study of the literature shows that the only attempts to attack the non-linear case were concerned with realizing a single cycle of a given length and not with the complete cycle structure of the circuit.

By analogy with the linear cases the conjecture is that the "building blocks" in Prob. (2) are the feedback shift registers (FSR's). Consequently we have been investigating the cycle structure of FSR's. The rough picture emerging from the analysis is that the cycle structure depends heavily on how "close" the feedback function is to the identity function. The cycles get shorter as we get closer to the identity. We are not yet able to formulate the rough description above in precise mathematical terms, but pursuing this idea we have developed a graph theoretic method for enumerating realizable cycle sets.

Since the number of non-singular feedback functions of n variables increases exponentially with n, it is important to be able to treat instead of functions, their equivalence classes under the relation "realizing the same cycle set." A careful analysis shows that the existing methods for enumerating Boolean functions do not apply [1]. All these methods are based on invariance of functions under permutations of the domain. However, the set of non-singular functions is not a subalgebra of the algebra of all Boolean functions; moreover, it behaves poorly under the action of permutations. Therefore, new techniques are needed. We have tried to extend the range of the functions and consider permutations on these extended ranges.

WEIGHT DISTRIBUTIONS IN PARITY CHECK CODES

ONR Contract Nonr-222(53)
J. Kurzweil (Prof. A.J. Thomasian)

According to Shannon's coding theorem, codes chosen at random are, on the average, good codes. Nevertheless, the immensity of the computation involved places, in general, a practical roadblock in the way of determining whether a particular code, selected at random, is a good code.

The purpose of this inquiry is to discover, through a combination of analytic and computational techniques, a method for significantly reducing the computation required to determine whether a code is good. The class of codes under consideration are parity check codes over the binary field.

A parity check code is defined by a (kxn) matrix G of 0's and 1's having linearly independent rows. The code words are all 2^k linear combinations of the rows of the matrix so that the code words form a k-dimensional subspace of an n-dimensional vector space. It follows that the code words form an additive group under vector addition modulo 2 with the all zero n-tuple as the identity and, in fact, parity check codes are isomorphic to all block length group codes.

The rows of the matrix G form the basis for the subspace of code words and through the use of elementary row operations the basis can be changed so that the matrix is in rational canonical form:

$$G = [\, I_k \mid P_{kx(n-k)} \,]$$

where I_k is the kth order identity matrix, and P is some kx(n-k) matrix of 0's and 1's. Note that this form of representation clearly points out the independence of the rows of G. The first k digits are information digits; the last (n-k) are parity check digits.

The set of n-tuples orthogonal to all elements of the subspace generated by G is called the dual code of G. This dual code is generated by the matrix H where

---

[1] M.A. Harrison, Ph.D Thesis, Univ. of Michigan, 1963.

$$H = \left[P^T_{(n-k)xk} \mid I_{n-k} \right], \quad H^T = \left[\frac{P_{kx(n-k)}}{I_{n-k}} \right],$$

so

$$GH^T = HG^T = I_k P + P I_{n-k} = 0_{kx(n-k)} .$$

Definition: The Hamming distance between two n-tuples is the number of places in which they differ, or equivalently, the number of 1's in their vector sum modulo 2, i.e., the weight of their sum.

Because of the group properties of the code words, the sum of any two code words is itself a code word so that the distance between any two code words is the weight of some code word. Let $N_d(c_m)$ $(d=1, 2, \ldots, n;\ m = 1, 2, \ldots, 2^k) \triangleq$ the number of code words at distance d from a particular code word, c_m. As a result of the group properties of the code words, $N_d(c_m)$ is independent of c_m. It follows that the distance properties of the code are completely determined by the listing of N_d with respect to the all-zero code word. This is simply a list of the weights of the code words and the minimum distance between codewords, which determines the error-correcting capability of the code, is the smallest weight of a non-zero code word.

If a code is to correct e errors, the smallest distance between code words, i.e., the smallest weight of a non-zero code word, must be at least $d = 2e + 1$. Thus, the weight of each row of G should be at least $d = 2e + 1$ and the weight of each row of P should be at least 2e. Similarly, the weight of any sum of x rows of P should have weight at least $(2e + 1-x)$.

The Gilbert and Elias bounds are, respectively, lower and upper bounds on the error-correcting capability of a code.

Define: $R \triangleq k/n$; $h(p_r) = 1-R$; $h(x) = -x\log_2 x - (1-x)\log_2(1-x)$.

Gilbert bound $\triangleq$ there exists a code with $d \gtrsim np_r$

Elias bound $\triangleq$ for every code, $d \lesssim 2np_r(1-p_r)$

The problem can now be stated more precisely. A code is considered to be good if the smallest weight of a code word exceeds the Gilbert bound. The question is whether it is necessary to calculate all 2^k code words to discover this. Certainly when k becomes large the amount of calculation that would be required increases exponentially.

The first result is that for rates $R > R'$, where R' will be defined, it is not necessary to calculate all 2^k code words to determine whether the code is good. Let $\ell \triangleq$ the number of rows of G that are added to obtain a codeword. There are $\binom{k}{\ell}$ such code words resulting from adding rows of G, ℓ at a time. The totality of code words is $\sum_{\ell=0}^{k} \binom{k}{\ell} = 2^k$. Asymptotically $\binom{k}{k/2} \doteq 2^k$

so that in order to reduce significantly the number of calculations required to show whether a code is good, it must be sufficient to calculate only the code words in one of the tails of the binomial distribution. Note that a code word obtained from ℓ rows of the generator has ℓ ones in its information symbols. Referring to the Elias bound as d_E, if $d_E = \ell_E$ then <u>all</u> code words whose weight is below d_E are contained in the set of code words obtained by adding ℓ_E or fewer rows to G. Thus if $\ell_E < \frac{k}{2}$ only $\sum_{\ell=0}^{\ell_E} \binom{k}{\ell} \doteq (\ell_E)^k < < \binom{k}{k/2} \doteq 2^k$ code words must be calculated.

In order to calculate ℓ_E/k we note that $\frac{k}{n} \ell_E/k = \frac{d_E}{n} = 2p_r(1-p_r)$ or equivalently $Ry_E = 2p_r(1-p_r)$, $y_E = \frac{2p_r(1-p_r)}{R}$. Thus:

R	y_E
.40	.795
.45	.622
.50	.492
.55	.399
.60	.315
.65	.243
.70	.189
.75	.144

with y_E decreasing as R increases so that for $R > 1/2$ there is a significant reduction in calculation while checking all code words below the Elias bound.

A further reduction in calculation can be made if it is considered sufficient to check whether any code words fall below the Gilbert bound. Here $y_G = \frac{p_r}{R}$ and

R	y_G
.30	.63
.35	.48
.40	.37
.45	.28
.50	.22
.55	.17
.60	.14
.65	.11

Thus, a significant reduction of calculation is achieved for $R > 1/2$. The problem now is to achieve a similar reduction for $R < 1/2$.

This problem is being attacked in two ways. The first is essentially algebraic and tries to make use of the MacWilliams weight formula which related the weight distribution of a code to that of its dual. The hope is to obtain information about codes with $R < 1/2$. Pertinent information about codes with $R > 1/2$ can be obtained with relatively few calculations, as demonstrated above.

The second approach is essentially probabilistic and seeks to discover where to look in order to find bad code words. Consider a parity check matrix G chosen at random. Let ℓ be the number of one's in the information sequence of some code word in the space of G; equivalently, ℓ is the number of rows of G that were added to obtain the code word. Let δ be the number of one's in the parity check sequence of the code word. Thus,

$$E\ \{\ \text{a random (n-k) - tuple has weight } \delta\ =\ \binom{n-k}{\delta} \cdot \frac{1}{2^{(n-k)}}\ .$$

The weight of a code word is $d = \ell + \delta$ so that

$$E(N_d^{(\ell)}) = \binom{k}{\ell} \binom{n-k}{\delta} \frac{1}{2^{(n-k)}}\ .$$

Since

$$\binom{n}{pn} \doteq 2^{nh(p)} \text{ as } n \to \infty\ , \text{ we have}$$

$$E\left(N_d^{(\ell)}\right) \doteq 2^{n[\frac{k}{n} h(\ell/k) + (\frac{n-k}{n})\, h\,(\frac{\delta}{n-k}) + (\frac{k}{n} - 1)]}$$

and letting

$$\frac{k}{n} = R,\ \ \ell/k = y,\ \frac{d}{n} = x,$$

we have

$$E(N_d^{(\ell)} \doteq 2^{n\alpha} \text{ where } \alpha = (1-R)\{h\,(\frac{x-Ry}{1-R}) = \frac{R}{1-R}\ h(y) - 1\}\ .$$

Where $\alpha > 0$, $E(N_d^{(\ell)})$ is large and where $\alpha < 0$, it is small. This serves as a quide to evolving a probabilistic search procedure for discovering bad code words.

It should be noted that $X_{min}\ \big]_{\alpha=0,\ R \text{ fixed}} = p_r$, the Gilbert bound.

In summary, the problem being dealt with is how to bring the calculation involved in discovering whether a parity check code selected at random is good, into the realm of possibility. One important, though somewhat intuitive, result has been obtained for $R > 1/2$, and two lines of inquiry are being pursued to obtain results for $R < 1/2$.

CONSTRUCTIVE DERIVATION OF THE CAPACITY OF A BAND-LIMITED CHANNEL*

JSEP Grant AF-AFOSR-139-64
L. Seidman (Prof. D.J. Sakrison)

We consider digital communications using a channel which adds white Gaussian noise of two-sided spectral density N_0 with the constraints that the signals have duration T sec, each signal must have energy less than PT, and the energy content of each signal outside the band $\pm$ W c.p.s. is less than ϵ PT, $0 < \epsilon < 1$. We have, with the use of prolate spheroidal functions, given a constructive proof of the fact that the capacity of this channel is

$$C = W \log_2 \left(1 + \frac{(1 - \epsilon P)}{2N_0 W}\right) + \frac{\epsilon P}{2N_0} \log_2 e \text{ bits/sec.}$$

SIGNAL DESIGN FOR BANDLIMITED GAUSSIAN CHANNELS

JSEP Grant AF-AFOSR-139-65
L. Seidman (Prof. D.J. Sakrison)

The problem considered is that of choosing signals to be used for digital communication over a coherent channel with additive white Gaussian noise. We assume that the signals are essentially limited to time T and bandwidth W, and represent each signal as a point in a real Euclidean space of [2WT] dimensions, in the usual way. We further assume that the signals are equi-probable and that either the energy of each signal or the (statistical) average power of all the signals is constrained, and that the objective is to minimize the probability of error.

The method of Lagrange multipliers has been interpreted to provide a simple method of locating certain signal sets at which probability of error is stationary with respect to the class of signals which satisfy the energy constraints with equality. In the case where the number of signals equals [2WT] + 1, we can show that the minimum probability of error occurs on the constraint. In particular, we have shown that the regular simplex signals yield a stationary point which is not a maximum. Balakrishnan [1] proved that the simplex is a local minimum of probability in the case where the energy of each signal is constrained by complicated procedures. Our approach is a simple one which applies more generally.

---

* Reported in Notes on System Theory, Vol. VII, Electronics Research Laboratory, Univ. of Calif., Berkeley, pp. 135-140 (May 1965).

[1] A. V. Balakrishnan, "A contribution to the sphere packing problem of communication theory," J. Math. Anal. and Appl., 3, (1961), pp. 485-506.

Unfortunately, we do not yet have a method for proving that a given signal configuration is a local minimum rather than a type of saddle point. A more detailed discussion of these results is expected to appear in the next issue of "Notes on System Theory", (to be published as an ERL report, Spring 1966).

LOWER BOUNDS ON MEAN-SQUARED ERROR

NASA Grant NSG-354 (Supplement 2)
B. Haskell (Prof. D.J. Sakrison)

Consider the single parameter transmission system shown above, where the channel has capacity C bits/sec. The mutual information between the input and output per unit time is less than or equal to C. We wish to maximize this transmitted information while at the same time minimizing the mean squared error,

$$\delta^2 = \iint (\lambda-\hat{\lambda})^2 \; p(\hat{\lambda}/\lambda) \; p(\lambda) \, d\lambda \; d\hat{\lambda} \qquad (1)$$

$p(\hat{\lambda}/\lambda)$ is the transition probability density function and $p(\lambda)$ is the a priori density function.

For a given $p(\lambda)$, define the rate distortion function as the minimum mutual information possible if the mean-squared error is less than or equal to D.

$$R(D) = \min_{p(\hat{\lambda}/\lambda)} \iint p(\hat{\lambda}/\lambda) \; p(\lambda) \; \log_2 \frac{p(\hat{\lambda}/\lambda)}{p(\lambda)} \, d\lambda \, d\hat{\lambda}, \qquad (2)$$

where $p(\hat{\lambda}/\lambda)$ is varied over the class defined by

$$\delta^2 = \iint p(\hat{\lambda}-\lambda)^2 \; p(\lambda/\lambda) \; p(\lambda) \; d\lambda \, d\hat{\lambda} \leq D. \qquad (3)$$

If T is the time devoted to the transmission of one parameter, then

$$R(D) \leq CT. \tag{4}$$

An equivalent statement is that if $CT = R(D)$, then $\delta^2 \geq D$. (5)

Similarly, if $p(\hat{\lambda}/\lambda)$ is varied over a subclass of that defined by inequality (3) and $R_1(D)$ is obtained, then when using a system in this class, $CT = R_1(D)$ implies that $\delta^2 \geq D$. (6)

Consider the a priori density function

$$p(\lambda) = \begin{cases} \frac{1}{2} & |\lambda| \leq 1 \\ 0 & \text{elsewhere} \end{cases} \tag{7}$$

Using statement (6) we can show that for a PCM system [1]

$$\delta^2 \geq \frac{1}{3} 2^{-2CT}, \tag{8}$$

and we can find a lower bound on the mean-squared error when using PAM, PPM, or FSK. By means of a lower bound on R(D), derived by Shannon, we can also show that for any system [2]

$$\delta^2 \geq \frac{2}{\pi e} 2^{-2CT} \tag{9}$$

These are plotted in Fig. 1.

The PCM lower bound and the absolute lower bound have been derived geometrically for the case of gaussian white noise. It is shown that the bounds can be generalized. (These results are presented in detail in the Master's II report by B.G. Haskell, "Pulse Modulation.")

COMPARISON OF SEQUENTIAL AND NONSEQUENTIAL DETECTION SYSTEMS WITH UNCERTAINTY FEEDBACK

AFOSR Grant AF-AFOSR-230-64
Professor G.L. Turin

We previously found optimal signals for, and evaluated the performance of, a binary, sequential detection system in which the detector constantly feeds back to the transmitter its "state of uncertainty" concerning what is being sent. We have now analyzed a similar nonsequential detection system. Comparison of the results of

---

[1] A similar result is shown by A. J. Viterbi, "Maximum SNR for Digital Communications," IEEE Trans. on Communications Systems Vol. CS-12, No. 1, March, 1964.

[2] This result is also derived in Wozencraft and Jacobs, Principles of Communication Engineering, to be published, John Wiley and Sons, Inc.

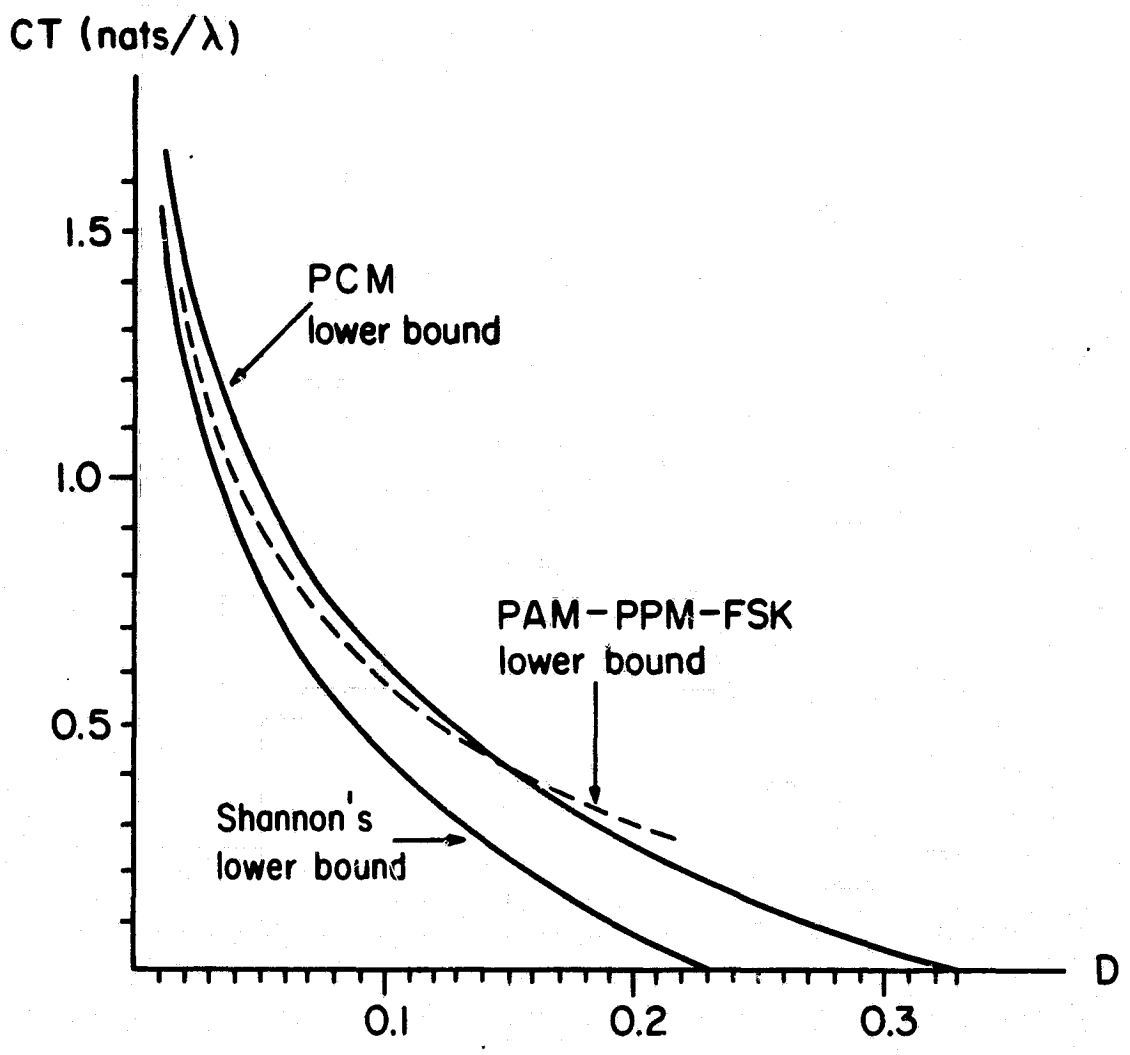

Fig. 1. Lower bounds on δ^2.

the two studies shows that: (1) when the prescribed peak-to-average power ratio is small, the sequential system operates with a 6-db average-power advantage over the nonsequential system; (2) when the prescribed peak-to-average power ratio is large, the sequential system operates with a 6-db peak-power advantage over the nonsequential system. In both systems, the performance improves rapidly as the peak-power constraint is relaxed, i.e., as the prescribed peak-to-average power ratio in increased.

An article based on this work has been accepted for publication by IEEE Transactions on Information Theory.

STUDIES OF SEQUENTIAL DETECTION SYSTEMS WITH UNCERTAINTY FEEDBACK

AFOSR Grant AF-AFOSR-230-64
J.F. Hayes (Prof. G.L. Turin)

Recently, Turin [1-2] considered the problem of signal design for sequential detection systems employing a feedback channel (Fig. 1). In this work he assumes negligible delays in the forward and feedback channels. He also assumes that there is negligible noise in the feedback channel. We have extended this work to systems where these assumptions may not be justified.

Consider the communication system shown in Fig. 1. We have a binary message source whose output, ± 1, is encoded by the modulator into the signals $s_{\pm}(w(t), t)$. At time $t = t_0$ the transmitter begins sending one of these signals, corresponding to the current output of the message source. (The argument in $s_{\pm}(\cdot, T)$, viz., $w(t) = y(t-T_R) + n_2(t)$, is a signal plus noise received at the transmitter via the feedback channel.) The transmitted signal $s_{\pm}(w(t), t)$ is received delayed and corrupted by noise, and is transformed by the probability computer into a statistic $y(t)$. Then, when $y(t)$ reaches the threshold Y_+ or Y_- the receiver takes the transmitted signal to be $s_+(w(t), t)$ or $s_-(w(t), t)$, respectively. More precisely, we let $y(t) = \ln \frac{P(H+/z(\tau), t_0 \leq \tau \leq t)}{P(H-/z(\tau), t_0 \leq \tau \leq t)}$ where $P(H+/z(\tau); t_0 \leq \tau \leq t)$ and $P(H-/z(\tau); t_0 \leq \tau \leq t)$ are the a posteriori probabilities that the output of the message source is + 1 or - 1, respectively. For this definition of $y(t)$ the probability of error can be expressed as a function of the thresholds.

As noted above, the receiver feeds $y(t)$ back to the transmitter until a threshold is reached. This fed-back signal, besides synchronizing the receiver and the transmitter, also is used to control the transmitted

[1] G.L. Turin, "Signal Design for Sequential Detection Systems with Feedback" IEEE Trans. Information Theory, July 1965.
[2] G.L. Turin "Signal Design for Sequential Detection Systems," Univ. of California, Berkeley, ERL Tech. Memo M-69, May 6, 1964.

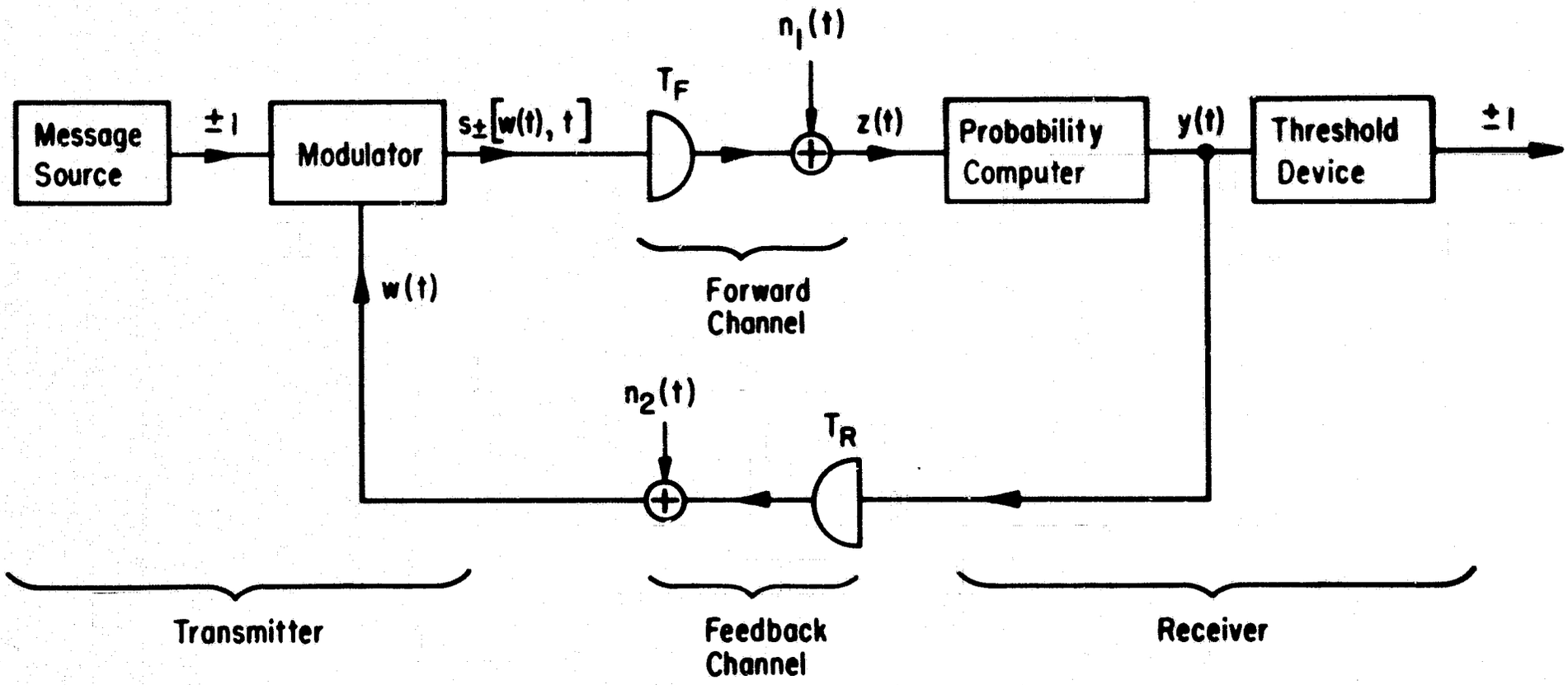
Message Source
±1
Modulator
s±[w(t), t]
T_F
$n_1(t)$
z(t)
Probability Computer
y(t)
Threshold Device
±1
w(t)
Forward Channel
$n_2(t)$
T_R
Transmitter
Feedback Channel
Receiver

Fig. 1.

signal. The purpose of this control is to minimize the average time of transmission of a particular signal, subject to average-power and peak-power constraints on the transmitted signal.

We assume that the forward and the feedback channels are coherent. The forward channel is disturbed by additive white Gaussian noise. We assume further that the noise in the feedback path is additive Gaussian and confined to the "band" of $y(t)$. We also assume that the noise in the feedback path is small relative to the signal in the feedback channel and the noise in the forward channel. We may then ignore its effect on the statistic $y(t)$; in fact, the feedback noise then manifests itself only by its deleterious effect on the average power available to the transmitted signal.

To make the problem tractable, we assume that $s_{\pm}(y(t),t) = \pm U_{\pm}(y)\,\sigma(t)$, where $U_{+}(y) + U_{-}(y) = 1$. Following a procedure similar to Turin's [1] we calculate the average transmission time of a signal, the average transmitted energy, and the average transmitted power. We then proceed to find the $s_{\pm}(y(t),t)$ which minimizes the average transmission time within the boundaries imposed by the peak- and average-power constraints. The forms of the expressions for the average power and the average transmission time show that the solution lies on one or both of these boundaries.

If the solution lies on the average power boundary, we are forced to assume that $s_{\pm}(y,t) = \pm KU_{\pm}(y)$ in order to make the problem tractable. In the case where $n_2(t) = 0$, the result is

$$s_{\pm}(y,t) = \frac{\pm K}{1+\epsilon^{\mp y}}$$

where

$$K^2 = 2\left(P_{ave}\frac{-N_{01}\ln 2}{T_R+T_F}\right) + \sqrt{2\left(P_{ave}\frac{-N_{01}\ln 2}{T_R+T_F}\right) + \frac{P_{ave}N_{01}}{T_R+T_F}}\,.$$

$T_R + T_F$ is the roundtrip delay, N_{01} is the single-ended noise power density in the forward channel. P_{ave} is the average power, and $Y = Y_+ = -Y_-$ is the threshold level.

In general, when $n_2 \neq 0$, the solution is

$$s_{\pm}(y,t) = \frac{\pm K\int_{-Y}^{Y} \epsilon^{\pm\xi/2 - \left|\frac{\xi}{2}\right| - \frac{(\xi-y)^2}{2N_2}}\,d\xi}{\int_{-Y}^{Y} \epsilon^{\xi/2 - \left|\frac{\xi}{2}\right| - \frac{(\xi-y)^2}{2N_2}}\,d\xi + \int_{-Y}^{Y} \epsilon^{-\xi/2 - \left|\frac{\xi}{2}\right| - \frac{(\xi-y)^2}{2N_2}}\,d\xi}$$

where N_2 is the mean-square noise in the feedback path. We can find K for a particular set of system parameters by setting the average transmitted power equal to P_{ave}. When a solution has been obtained, we must check to be sure that it lies within the peak-power boundary. This leads to a lower bound on $\gamma = \frac{P_{peak}}{P_{ave}}$ where P_{peak} is the maximum allowable peak power.

When $\gamma = 1$, the solution is on the peak-power boundary. The optimal signals are then $s_{\pm}(y,t) = \pm P_{peak}$.

For intermediate values of γ, the solution lies on both boundaries. It is difficult to find a solution in this case. We are reduced to assuming signals of the form $s_{\pm}(y,t) = \pm K\left[\frac{1-\lambda_0}{2} \pm \frac{\lambda_0}{1+\epsilon^{\pm y}}\right]$. This signal is a linear interpolation between extremes (i.e., for large γ and $n_2(t) = 0, \lambda_0 = 1$, or $\gamma = 1, \quad \lambda_0 = 0$). The constants K and λ_0 can be computed from the peak- and average-power constraints with equality holding.

Systems using the derived signals are evaluated with respect to a comparison system, which sends constant signals for a fixed length of time and uses nonsequential detection. The basis for comparison is the average transmitted power for a given probability of error and average time of transmission.

Many of the results are in rather complicated forms which are difficult to evaluate analytically. During the next report period we plan to make machine computations, which should yield more insight into these results. For example, various approximations have been made in obtaining our results, and machine calculations should indicate the range of parameter values for which these approximations hold.

OPTIMUM UNCERTAINTY FEEDBACK FUNCTIONS

NSF Grant GP-2413
S. Sugimoto (Prof. G.L. Turin)

Turin [1] has formulated a problem of the optimization of uncertainty feedback functions for detection systems with a noiseless and delayless feedback channel. For the symmetric case, he has given the optimum uncertainty feedback functions

$$U_+(y) = \frac{1}{2} \text{ and } U_+(y) = \frac{1}{1+e^{y}} \text{ for } \alpha = 1 \text{ and } \alpha > \alpha' = \frac{Y}{\ln 2},$$

$Y \gg 1$, respectively, where α is defined to be the ratio of the allowable peak power to the average power of the transmitter and Y is the prespecified threshold parameter.

We have found an exact expression for α' as a function of Y:

[1] G.L. Turin, "Signal Design for Sequential Detection Systems," IEEE Trans. on Information Theory, July 1965.

$$\alpha' = \frac{Y\dfrac{e^Y}{1+e^Y}\,2\,\dfrac{e^Y-1}{e^Y+1}}{\dfrac{Ye^Y}{1+e^Y}+\ell n\dfrac{2}{1+e^Y}}$$

In order to get the solutions for $1 < \alpha < \alpha'$, we have restricted ourselves to the class of functions

$$U_+(y,\lambda) = \frac{1}{1+e^{\lambda y}} ,$$

as proposed by Turin, and have given the curve of the optimum λ as a function of $\frac{\alpha}{Y}$.

We have defined a loss coefficient $\mathcal{L}(\lambda)$, which indicates the power disadvantage when we use $\lambda = 1$ instead of $\lambda = \lambda_{opt}$, and have calculated it with Y as the parameter.

We are now considering m re general methods of finding the optimum U_+ for the case $1 < \alpha < \alpha'$.

RANDOM SIGNAL DESIGN

AFOSR Grant AF-AFOSR-230-64
A. Al-Shalchi, (Prof. Turin)

Given a zero-mean Gaussian noise process, $x(t,\omega)$, with a jointly continuous covariance function $K_0(t,s)$, we are interested in designing a zero-mean Gaussian signal process whose presence can be detected with good reliability in a finite observation interval T.

Since the covariance is continuous, the pr ocess is continuous in the quadratic mean [1]. Then the process is continuous in probability, and thus there exists a measurable and separable process $\tilde{X}(t,\omega)$ such that $P[\tilde{x}(t,\omega) = x(t,\omega)] = 1$ for every $t \in T$ [2]. Then $\tilde{x}(t,\omega)$ and $x(t,\omega)$ have the same joint n-dimensional distributions $P[x_{t_1},\ldots,x_{t_n}]$ and $P[\tilde{x}_{t_1},\ldots,\tilde{x}_{t_n}]$ for all n.

One can index the random process by using the eigenfunctions $\{\phi_i\}_1^\infty$, of the covariance function of the noise; the associated eigenvalues are $\{\alpha_i\}_1^\infty$.

---

[1] N. Loeve, Probability Theory 2nd Ed., Van Nostrand Co., Inc. p, 470.

[2] J.J. Doob, Stochastic Processes, J. Wiley and Sons, Inc., p. 61 Thm. 2.6.

We obtain:

$$x_i = \int_0^T \phi_i(t)\, \tilde{x}(t, \omega)\, dt, \tag{1}$$

where $x(t)$ is the received signal,

x_i are Gaussian, have zero mean, and

$E x_i x_j = \alpha_i \delta_{ij}$.

These integrals can be shown to exist almost surely. Let us specify the process by writing the density $P_0^{(n)}(x_1, \ldots x_n)$ for all n. It can be shown that this specification is equivalent to that obtained by samples along the time axis, i.e., $P[x_{t_1}, \ldots, x_{t_n}]$ for all n [3].

For the signal process, let us use a zero-mean Gaussian process, independent of the noise. The covariance function of the received signal plus noise is $K_1(t, s) = K_0(t, s) + K_s(t, s)$ where $K_s(t, s)$ is the signal covariance function. We shall assume $K_s(t, s)$ to be of the following form:

$$K_s(t, s) = \sum_{i=1}^{N} \gamma_i \phi_i(s)\, \phi_i(t) . \tag{2}$$

Since $K_0(t, s)$ is continuous, the eigenfunctions are also continuous. Therefore, $K_s(t, s)$ is continuous. Again there exists a separable and measurable process which, when indexed by its eigenfunctions as in Eq. 1, provides a representation of the process equivalent to sampling along T. The received signal is $x = x_{noise} + x_s$, where

$$x_s(t) = \sum_{i=1}^{N} \xi_i(\omega)\, \phi_i(t) , \tag{3}$$

where $\{\xi_i\}$ are independent, zero-mean Gaussian random variables with var $\xi_i = \gamma_i$. The design problem is to choose $\{\gamma_i\}_1^N$ so as to satisfy the design constraints and minimize the probability of error.

Using Equation (3) for the design of signals, we note that one needs to design filters whose impulse responses are $\{\phi_i(t)\}_1^N$. As i

---

[3] T.T. Kadota, "Optimum Reception of Binary Gaussian Signals" B.S.T.J. No. 6, November 1964. Appendix D, p. 2801.

increases, the $\{\phi_i(t)\}_1^N$ may become quite oscillatory, and bandwidth limitations may come into play. Thus, our use of a finite number of eigenfunctions satisfies a bandwidth criterion. More specifically, the choice is made as follows: We would agree on some operator B which would limit a function to a "frequency band". Then, the energy in the band and in $[0, T]$ is:

$\int_0^T [B\psi(t)]^2 dt$. Thus from $\{\phi_i(t)\}_1^\infty$ we choose $\{\phi_i(t)\}_1^N$ such that

$$\int_0^T [B\phi_i(t)]^2 dt \Big/ \int_0^T \phi_i^2(t)\, dt \qquad (4)$$

is greater than some fixed number.

The second constraint is that on signal power which is a random variable:

$$\frac{1}{T}\int_0^T x_s^2(t)\,dt = \frac{1}{T}\int_0^T \left[\sum_{i=1}^N \xi_i \phi_i(t)\right]^2 dt = \frac{1}{T}\sum_{i=1}^N \xi_i^2 . \qquad (5)$$

We shall work with the expected signal power,

$$S = \frac{1}{T}\sum_{i=1}^N E\,\xi_i^2 = \frac{1}{T}\sum_{i=1}^N \gamma_i , \qquad (6)$$

and require $S \leq S_0$, some upper bound on signal power.

1. Optimum Detector Suppose we take n samples of the received signal as in Eq. 1. Then we obtain the density functions $P_0^{(n)}(x_1, \ldots, x_n)$ and $P_1^{(n)}(x_1, \ldots, x_n)$. Also let Π_1, Π_0 be the a priori probabilities of signal and no signal respectively.
The test:

$$\Pi_1 P_1^{(n)}(x_1, \ldots, x_n) > \Pi_0 P_0^{(n)}(x_1, \ldots, x_n) \Longrightarrow \text{Signal}$$

$$\Pi_1 P_1^{(n)}(x_1, \ldots, x_n) < \Pi_0 P_0^{(n)}(x_1, \ldots, x_n) \Longrightarrow \text{No signal}$$

minimizes the probability of error $P_e^{(n)}$, when n samples are used [4].

---

[4] C.W. Helstrom, Statistical Theory of Signal Detection, Pergamon Press, p. 73, 64, (1960).

This error probability is:

$$P_e^{(n)} = \Pi_1 \int P_1^{(n)}(x, \ldots, x_n)\, dx_1, \ldots, dx_n + \Pi_0 \int P_0^{(n)}(x_1, \ldots, x_n) dx_1, \ldots, dx_n$$

$$\{\Pi_1 P_1^{(n)}(x, \ldots, x_n) \qquad \{\Pi_1 P_1^{(n)}(x_1, \ldots, x_n)$$

$$< \Pi_0 P_0^{(n)}(x_1, \ldots, x_n)\} \qquad > \Pi_0 P_0^{(n)}(x_1, \ldots, x_n)\} \tag{7}$$

From the optimality of the test we have

$$P_e^{(n+1)} \leq P_e^{(n)} \text{ all } n. \tag{8}$$

Since we agreed to let $\gamma_i = 0$ for $i > N$, the test using N samples is optimum, which can be seen as follows:

$$P_0^{(n)}(x_1, \ldots, x_n) = \prod_{i=1}^{n} \frac{e^{-x_i^2/2\alpha_i}}{\sqrt{2\Pi\alpha_i}}, \tag{9}$$

$$P_1^{(n)}(x_1, \ldots, x_n) = \prod_{i=1}^{n} \frac{e^{-x_i^2/2(\alpha_i+\gamma_i)}}{\sqrt{2\Pi(\alpha_i+\gamma_i)}}.$$

Since $\gamma_i = 0$ for i 2 N, then

$$\frac{\Pi_1 P_1^{(n+N)}(x_1, \ldots, x_{n+N})}{\Pi_0 P_0^{(n+N)}(x_1, \ldots, x_{n+N})} = \frac{\Pi_1 P_1^{(N)}(x_1, \ldots, x_N)}{\Pi_0 P_0^{(N)}(x_1, \ldots, x_N)} \quad \text{all } n,$$

so the tests are identical and $P_e^{(n+N)} = P_e^{(N)}$ all n. Then the test on $\{x_1, \ldots, x_N\}$ is optimum.

The probability of error can be bounded by:

$$P_e^{(n)} \leq \sqrt{\Pi_1 \Pi_0} \int_{\substack{-\infty < x_i < \infty \\ \text{all } i}} \sqrt{P_1^{(n)}(x_1, \ldots, x_n)\, P_0^{(n)}(x_1, \ldots, x_n)}\, dx_1 dx_2, \ldots, dx_n \tag{10}$$

Using Eq. 10, the bound can be calculated:

$$P_e^{(N)} \leq \sqrt{\Pi_1 \Pi_0} \prod_{i=1}^{N} \sqrt{2}\, \frac{\sqrt[4]{c_{i+1}}}{\sqrt{c_{i+2}}} \quad \text{where } c_i = \gamma_i/\alpha_i. \tag{11}$$

Since

$$\frac{d}{dc_i} \ell n \sqrt{\Pi_1 \Pi_0} \prod_{i=1}^{N} \frac{\sqrt{2}\sqrt[4]{c_{i+1}}}{\sqrt{c_{i+2}}} = -\frac{c_i}{4(c_{i+1})(c_{i+2})}, \qquad (12)$$

the bound is monotonically decreasing with c_i increasing. Since the bandwidth constraint is already satisfied, the design problem is reduced to choosing $\{c_i\}_1^N$ so as to minimize the bound on the probability of error and satisfy the signal power constraint $\frac{1}{T} \sum_{i=1}^{N} c_i \alpha_i \leq S_0$.

This can be done using the method of Lagrange multipliers. The answers are as one would have reasoned physically: make c_i large where α_i is small, i.e., put large signal power where there is small noise power. One does best by letting the signal power take its largest allowable value.

An expression for $\frac{\partial \ell n Pe}{\partial c_i}$ has been derived. It is not as simple as that of Eq. 12, but is negative also. Thus we have the monotonic behavior with the $\{c_i\}$ in the exact probability of error also.

2. The Use of Different Eigenfunctions Up to this point, we were using the same eigenfunctions for the noise and signal covariances. One might wonder whether the use of different eigenfunctions can decrease the probability of error, subject to the constraints on signal power and bandwidth. We propose to answer this question as follows; we have two covariances:

$$K_0(t, s) \text{ and } K_1(t, s) = K_0(t, s) + K_s(t, s). \qquad (13)$$

where $K_s(t, s)$ is arbitrary for the time being and $K_0(t, s)$ is positive definite.*

---

* This is assumed so as to avoid giving $K_0(t, s)$ a non-trivial zero space, because then $\underline{K}_0^{-1/2}$ is not unique. (See pages 299-300 of Root: "Singular Gaussian Measures in Detection Theory" W.L. Root, which is Chap. 20 of "Proceedings of the Symposium on Time Series Analysis" held at Brown University, June 11-19, 1962.

Next, let $\{\theta_i(t)\}_1^N$ be orthonormal on $[0, T]$, and let us write $K_s(t, s)$ as:

$$K_s(t, s) = \sum_{i=1}^{N} c_i \underline{K}_0^{1/2} \theta_i(t) \; \underline{K}_0^{1/2} \theta_i(s) \tag{14}$$

(where $K_0^{1/2} \underline{K}_0^{1/2} \theta_i(t) = \int_0^T K_0(t, s) \theta_i(s) \, ds$ . .)

The signal power S is:

$$S = \frac{1}{T} \sum_{i=1}^{N} c_i \int_0^T \int_0^T \theta_i(t) K_0(t, s) \, dt \, ds. \tag{15}$$

If we set $\{\theta_i = \phi_i\}_1^N$ in Eq. 15, we obtain Eq. 6, which is expected.

It can be shown that the probability of error, as well as the bound, are functions of $\{c_i\}_1^N$, of the same form as betore (e.g., Eq. 11). The design problem now has two parts: First we let $\{c_i\}_1^N$ be fixed, then choose $\{\theta_i\}_1^N$ so as to minimize

$\int_0^T \int_0^T \theta_i(t) \; K_0(t, s) \, \theta_i(s) \, dt \, ds$, subject to bandwidth constraints.

This minimizes expression (15) for the signal power when the $\{c_i\}_1^N$ are fixed. In other words, it allows us to use as large $\{c_i\}_1^N$ as allowable within the signal power constraints. This is desirable since we have previously pointed out that the probability of error and the bound on it are monotonically decreasing in $\{c_i\}_1^N$. Once $\{\theta_i\}_1^N$ are chosen, the second step is to find the best $\{c_i\}_1^N$ so as to minimize the bound of Eq. 10, subject to the constraint on signal power in Eq. 15. The results depend on how the bandwidth is defined.

Let us consider the case when the covariance function of the noise $K_0(t, s)$ is a "satisfactory" choice for defining B in equation (4), i.e., $B \psi_i(t) = \int_0^T K_0(t, s) \psi_i(s) \, ds \quad 0 \leq t \leq T$. An example of when $K_0(t, s)$ may be satisfactory is if $K_0(t, s)$ is stationary, and its Fourier transform has a low pass form or any other satisfactory

approximation to a bandlimiting operation. In the case where $K_0(t, s)$ is satisfactory for defining B, one can show that the best choice of the eigenfunctions is $\{\phi_i\}_1^N$, where $\{\phi_i\}_1^N$ are the noise eigenfunctions chosen starting from the smallest allowable noise eigenvalue.

The best number of eigenfunctions to which to allot signal energy may not always be N. Using a large number of eigenfunctions lowers c_i, the signal-to-noise ratio for each of the components of the random signal, and that may reduce the probability of error, but it may increase it also.

Example: Let $K_0(t, s)$ have eigenvalues $\{\alpha_i\}_1^{\infty}$

where $\alpha_i = \alpha$, $i = 1, \ldots, N$, where N is fixed by bandwidth limitations on the designed signal for which we have now: $K_s(t, s) = \sum_{i=1}^{N} \gamma_i \phi_i(t) \phi_i(s)$

$$\gamma_i = \begin{cases} c\alpha_i = c\alpha & i = 1, \ldots, M \quad M \leq N \\ 0 & i > M \end{cases}$$

$$S = cM\alpha/T$$

Using the bound of Eq. 10, $P_{eM} \leq \sqrt{\Pi_1 \Pi_0} \left[\frac{\sqrt{2} \sqrt[4]{1 + \frac{TS}{\alpha M}}}{\sqrt{2 + \frac{TS}{\alpha M}}} \right]^M$

This bound has a minimum at $M = \frac{0.9TS}{\alpha}$. We have made an approximate calculation of the probability of error and it exhibited a minimum at approximately the same value. These minima are not sharp and we plan to make a more accurate calculation of the probability of error.

3. Stationary Processes The detection of the processes defined above requires knowing the exact time the signal is received, because one is transmitting the signal for an interval T seconds long, and also the detector depends on the eigenvalues of the covariances, which may depend on the time when the observation started. In the case where the noise and signal covariances are stationary, it would be convenient to transmit the signal process for a sufficiently long duration of time, so that when one detects within this time duration, he can choose any interval of length T. Due to the stationarity of the covariances, they would look the same on any interval of length T, i.e., $K(t, s) = K(t-t_1, s-t_1)$ where t_1 is the start of the observation interval T. Thus the detectors would have the same form also.

Because of this useful property of stationary covariances, one might try to approximate the covariances obtained from the design procedure in the previous section by stationary covariances, and estimate the change in the probability of error.

A FIRST-PASSAGE PROBLEM FOR A MULTIDIMENSIONAL GAUSSIAN MARKOV PROCESS

NSF Grant GP-2413
S. Weinstein (Prof. G.L. Turin)

Gaussian Markov processes are found in digital communication systems in which the channel disturbance is approximated by an additive, white, Gaussian noise. Any linear processing in the receiver amounts to one or more weighted integrations, producing Gaussian Markov processes. These processes, considered as a vector process $\underline{X}$, are completely described by the first-order transition density, $p(\underline{X}_2, t_2/\underline{X}_1, t_1)$.

For sequential-detection schemes, one wishes to find the expected length of a test for a given false-alarm probability and detection probability. It is possible, starting from the Fokker-Planck "backward equation", to derive a differential equation whose solution is the expected testing time under a given hypothesis about which signal was transmitted. Sometimes this is a one-dimensional equation (one Gaussian Markov process only), as for example in a binary communication system.

In the present work, a digital communication system was postulated in which one of M constant-amplitude signals occupying disjoint frequency bands may be transmitted. The sequential-decision scheme chosen for analysis was as follows: at every time during the course of the test, compute $z_i(t)$, the logarithm of the a posteriori probability of the ith signal. Determine the difference $\max z_i(t) - \max z_j t)$, $j \neq$ index of $\max z_i(t)$. When this difference first equals some threshold "a", which depends on the prescribed error probability, the test concludes with the selection of the kth signal if k is the index of $\max z_i(t)$. Note that if k is the index of the "winning" signal, the test concludes only when all M-1 differences $z_k(t) - z_j(t)$, $j \neq k$ have exceeded the threshold "a" at least once.

For large signal-to-noise ratio, the M-1 differences described above form (approximately) an (M-1)-dimensional Gaussian Markov process under each hypothesis. The differential equation for the expected test length is

$$-1 = \sum_{i=1}^{M-1} K_i \frac{\partial \overline{T}(\underline{x})}{\partial x_i} + \frac{1}{2} \sum_{i=1}^{M-1} \sum_{j=1}^{M-1} k_{ij} \frac{\partial^2 \overline{T}(\underline{x})}{\partial x_i \partial x_j}$$

where $\underline{x} = (x_1, \ldots, x_{M-1})$ is the initial value of the (M-1)-dimensional random process,

$\overline{T}(\underline{x})$ = is the expected testing time, given the initial position $\underline{x}$,

K_i = S is the squared amplitude of the signals,

$$k_{ij} = \begin{cases} 2N_0S, & i=j \\ N_0S, & i \neq j \end{cases},$$

N_0 is the spectral density of the noise in the channel, and the boundary conditions are

$$\overline{T}(\underline{x}) = 0, \ \underline{x} \in \{\underline{x} : x_i \geq a_1 \ i = 1, \ldots, M-1\} .$$

The threshold for M = 3 is shown below. It is seen that we have a problem of first passage into a quadrant (or higher dimensional analog) of the Gaussian-Markov plane. It has not been possible to find $\overline{T}(\underline{x}_0)$ analytically, but computer simulation is feasible.

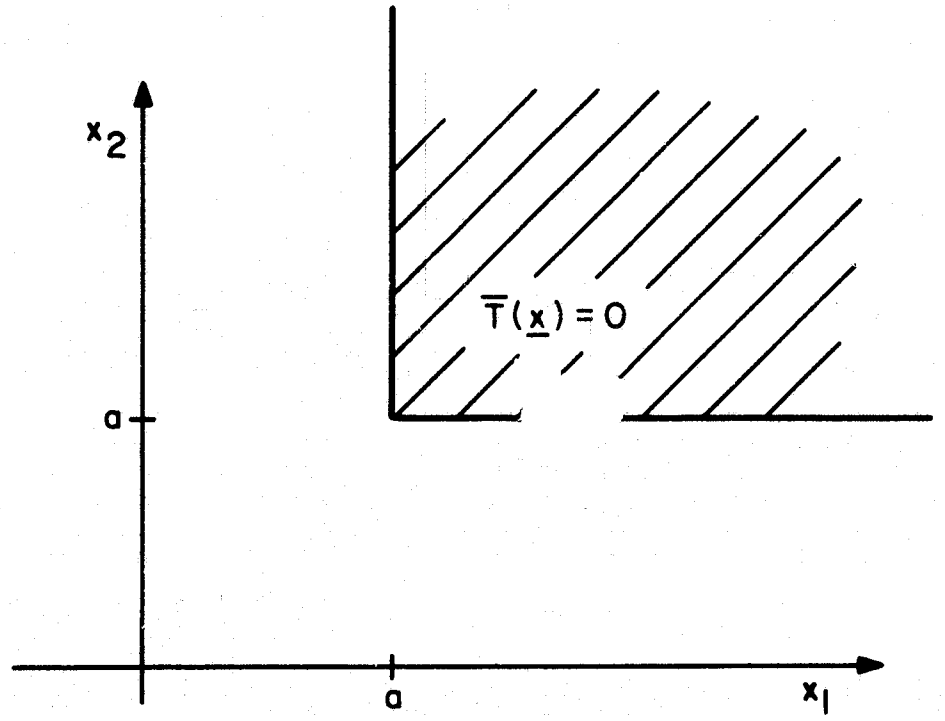

MEAN AND COVARIANCE OF NONSTATIONARY SHOT NOISE

NSF Grant GP-2413
L. Gurley (Prof. G.L. Turin)

We consider shot noise produced by a Poisson process whose mean rate ν is time-varying. Let $p(m;s,t)$ be the probability that m shots occur in the time interval $[s,t]$, $m = 0, 1, 2, \ldots$, $-\infty \leq s \leq t \leq \infty$; we assume

$$p(m;s,t) = \frac{[\psi(s,t)]^m \exp[-\psi(s,t)]}{m!},$$

where $\psi(x,t) = \int_s^t \nu(\tau)\,d\tau$ and $\nu(t)$ is then the "mean rate" of occurrence of shots, in the sense that

$$\nu(t) = \lim_{h \to +0} \frac{E[\text{number of shots in } (t, t+h)}{h}.$$

The expression for $p(m;s,t)$ may be derived from the assumptions

$$\text{(i)} \quad \lim_{h \to +0} \frac{p(1;s,s+h)}{h} = \nu(s) \text{ exists},$$

$$\text{(ii)} \quad \lim_{h \to +0} \sum_{k=2}^{\infty} \frac{p(k;s,s+h)}{h} = 0,$$

(iii) successive shots are independent

Conditions (i), (ii), and (iii) are assumed to apply, for instance, to emission of photoelectrons due to light of varying intensity.

We assume $\nu(t)$ measurable, $\psi(s,t) < \infty$ for finite s, t and, for the moment, $\nu(t) > 0$ a.e.

The shot noise process $x(t)$ is assumed to be a linear superposition of pulses, of finite pulse length δ, the starting time of each pulse corresponding to a shot. Thus, if $\{t_k, k = 1, 2, \ldots\}$ are the times of occurrence of the (countable) shots, and $f(t)$ is the form of a pulse starting at $t = 0$,

$$X(t) = \sum_{k=1}^{\infty} f(t - t_k)$$

We begin by defining the one-to-one transformation T of the real line onto itself by

$$\tau = T(t) = \int_0^t \nu(x)\,dx,$$

thus defining a new time scale. On the new time scale

$$\hat{p}(m;\sigma,\tau) = \text{Prob}[\,m \text{ shots occur in } (\sigma,\tau)\,]$$

$$= \frac{[\tau-\sigma]^m e^{-(\tau-\sigma)}}{m!} ,$$

which we recognize as the probability law of a stationary Poisson process with a mean rate of unity. We recall that, for a stationary Poisson process, if we consider any finite time interval, the times of occurrence of the shots are conditionally uniformly distributed in the interval and conditionally independent, given the total number of shots in the interval. Thus, considering the time interval $t = T_1$ to $t = T_2$, corresponding to $\tau = \gamma_1$ to $\tau = \gamma_2$ we have, for $T_1 + \delta \leq t \leq T_2$

$$EX(t) = \sum_{m=0}^{\infty} \hat{p}(m;\gamma_1,\gamma_2) \int_{\gamma_1}^{\gamma_2} \frac{d\tau_1}{\gamma_2-\gamma_1} \cdots \int_{\gamma_1}^{\gamma_2} \frac{d\tau_m}{\gamma_2-\gamma_1} \; X(t)$$

$$= \sum_{m=0}^{\infty} \hat{p}(m;\gamma_1\,\gamma_2) \sum_{k=1}^{m} \int_{\gamma_1}^{\gamma_2} \frac{d\tau_1}{\gamma_2-\gamma_1} \int_{\gamma_1}^{\gamma_2} \frac{d\tau_m}{\gamma_2-\gamma_1} f\left(t - T^{-1}(\tau_k)\right)$$

$$= \int_{\gamma_1}^{\gamma_2} f\left(t - T^{-1}(\tau)\, d\tau\right)$$

$$= \int_{T_1}^{T_2} f(t-x)\nu(x)\, dx$$

$$= \int_{-\infty}^{\infty} f(t-x)\,\nu(x)\, dx$$

since $\sum_{m=0}^{\infty} m \cdot \hat{p}(m;\gamma_1,\gamma_2) = \gamma_2 - \gamma_1$ and since $f(t)$ is of duration δ.

Similarly for $T_1 + \delta < t_1,\ t_2 \leq T_2$

$$EX(t_1)\,X(t_2) = \sum_{m=0}^{\infty} \hat{p}(m;\tau_1,\tau_2) \int_{\tau_1}^{\tau_2} \frac{d\tau_1}{\tau_2-\tau_1} \cdots \int_{\tau_1}^{\tau_2} \frac{d\tau_m}{\tau_2-\tau_1}\, X(t_1)\ X(t_2)$$

$$= \sum_{m=0}^{\infty} \hat{p}(m;\tau_1,\tau_2) \left[\sum_{k=1}^{m} \sum_{j=1}^{m} \int_{\tau_1}^{\tau_2} \frac{d\tau_1}{\tau_2-\tau_1} \cdots \right.$$

$$\left. \int_{\tau_1}^{\tau_2} \frac{d\tau_m}{\tau_2-\tau_1}\, f(t_1 - T^{-1}(\tau_k))\, f(t_2 - T^{-1}(\tau_j)) \right]$$

The m^2 term of the above double sum may be divided into two groups; the m terms for which $k = j$ and the $m^2 - m$ terms for which $k \neq j$ when $k = j$, the m - fold integral above becomes

$$\int_{\tau_1}^{\tau_2} \frac{d\tau_1}{\tau_2-\tau_1} \cdots \int_{\tau_1}^{\tau_2} \frac{d\tau_m}{\tau_2-\tau_1}\, f(t_1 - T^{-1}(\tau_k))\, f(t_2 - T^{-1}(\tau_k))$$

$$= \frac{1}{\tau_2-\tau_1} \int_{\tau_1}^{\tau_2} f(t_1 - T^{-1}(\tau))\, f(t_2 - T^{-1}(\tau))\, d\tau$$

$$= \frac{1}{\tau_2-\tau_1} \int_{-\infty}^{\infty} f(t_1 - x)\, f(t_2 - x)\ \nu(x)\, dx .$$

Similarly, when $k \neq j$, the integral becomes

$$\left(\frac{1}{\tau_2-\tau_1}\right)^2 \int_{-\infty}^{\infty} f(t_1 - x)\ \nu(x)\ dx \int_{-\infty}^{\infty} f(t_2 - y)\ \nu(y)\ dy .$$

Thus

$$EX(t_1)\,X(t_2) = \sum_{m=0}^{\infty} \hat{p}(m;\tau_1,\tau_2)\left[\frac{m}{\tau_2-\tau_1}\int_{-\infty}^{\infty} f(t_1-x)\,f(t_2-x)\,\nu(x)\,dx\right.$$

$$\left. + \frac{m^2-m}{(\tau_2-\tau_1)^2}\int_{-\infty}^{\infty} f(t_1-x)\,\nu(x)\,dx\int_{-\infty}^{\infty} f(t_2-y)\,\nu(y)\,dy\right]$$

$$= \int_{-\infty}^{\infty} f(t_1-x)\,f(t_2-x)\,\nu(x)\,dx + \int_{-\infty}^{\infty} f(t_1-x)\,\nu(x)\,dx\int_{-\infty}^{\infty} f(t_2-y)\,\nu(y)\,dy$$

$$= \int_{-\infty}^{\infty} f(t_1-x)\,f(t_2-x)\,\nu(x)\,dx + EX(t_1)\cdot EX(t_2).$$

Hence

$$\mathrm{Cov}[\,X(t_1)\,X(t_2)] = \int_{-\infty}^{\infty} f(t_1-x)\,f(t_2-x)\,\nu(x)\,dx.$$

1. Relaxation of the hypothesis $\nu > 0$

The assumption $\nu(t) \geq 0$ a.e. may be relaxed to $\nu(t) \geq 0$ a.e. by the following argument: if, on some non-degenerate interval (a, b) $\nu(t)$ is identically zero, we have

$$\tau_0 \triangleq T(t), \quad t \in (a, b).$$

We then set $T^{-1}(\tau_0) = a$; T^{-1} is thus defined for the interval (α, β), where $\alpha = T(-\infty)$, $\beta = T(+\infty)$. Clearly, any $\tau = T(t)$ is in (α, β) and preceding derivation remains valid.

2. Extension to the case of random mean rate

The physical example in mind here is photoelectronic emission produced by light of randomly-varying intensity. We assume the mean rate is a non-negative measurable random function of time, almost surely, almost everywhere (implying that almost every realization of

the random function is a measurable, almost-everywhere, non-negative function of time).

Thus, we consider the conditional probability

$$P[\text{m shots occur in } [s,t) \mid \nu(r),\ -\infty < r < \infty]$$

$$= p_{\nu}(m;s,t)$$

$$= \frac{[\psi(s,t)]^m \exp[-\psi(s,t)]}{m!},$$

where $\psi(s,t) = \int_s^t \nu(\tau)\, d\tau$, $\nu(t)$ is now the random mean rate and

$\psi(s,t)$ is now a random function.

The entire preceding derivation may now be applied to the present case, giving

$$E[X(t) \mid \nu(r),\ -\infty < r < \infty] = \int_{-\infty}^{\infty} f(t-x)\, \nu(x)\, dx,$$

$$Cov[X(t_1)\, X(t_2) \mid \nu(r),\ -\infty < r < \infty] = \int_{-\infty}^{\infty} f(t_1-x)\, f(t_2-x)\, \nu(x)\, dx,$$

and, taking expectations

$$E\, X(t) = \int_{-\infty}^{\infty} f(t-x)\, \mu(x)\, dx,$$

$$Cov[X(t_1)\, X(t_2)] = \int_{-\infty}^{\infty} f(t_1-x)\, f(t_2-x)\, \mu(x)\, dx,$$

where $\mu(t) = E\nu(t)$

Thus first- and second-order statistics of $X(t)$ are determined by first-order statistics of $\nu(t)$. In particular, when $\nu(t)$ has a constant mean μ,

$$EX(t) = \mu \int_{-\infty}^{\infty} f(x)\, dx$$

$$Cov[\, X(t_1)\, X(t_2)\,] = \mu \int_{-\infty}^{\infty} f(x)\, f(x + t_2 - t_1)\, dx,$$

which are identical to the expressions for m an and covariance of shot noise produced by a stationary Poisson process, with constant mean rate μ; clearly, when $\nu(t)$ has a constant mean, X(t) is wide-sense stationary.

SYNTHESIS OF TIME-VARYING NETWORKS

JSEP Grant AF-AFOSR-139-64865
D. Layton (Prof. I.T. Frisch)

The problem under consideration is the following: given the differential equation $L_a \cdot y = L_b \cdot x$ . . .(*), where L_a and L_b are linear differential operators with variable coefficients, find a network consisting of both fixed and time varying resistors, inductors, and capacitors which when excited by an input x(t) produces a response y(t) which satisfies (*).

Synthesis techniques for time invariant linear networks have been developed almost entirely from a Laplace transformed s-domain point of view; it is thus natural to expect that integral transforms might also provide a means of approach to the synthesis of time-varying networks. A number of integral transforms have been developed which, when applied to a time-varying equation yield polynomials in the transform variable, for certain specific classes of operators. A particularly useful one is that developed by Wattenburg [1], wherein it is assumed that L_a and L_b are expressible as polynomial functions of some simpler operator L(say). That is, $L_a = \phi_a(L)$, $L_b = \phi_b(L)$. Then, (*) may be written as $\phi_a(L) \cdot y = \phi_b(L) \cdot x$. If the coefficients of the operator L are sufficiently well behaved, there exists an integral transform T such that $T\{\phi(L) \cdot y\} = \phi(K) \cdot Y(K)$, where $T\{y(t)\} = Y(K)$, K being the transform variable. Applying T to (*) yields:

$T\{\phi_a(L) \cdot y\} = T\{\phi_b(L) \cdot x\} \Rightarrow \phi_a(K) \cdot Y(K) = \phi_b(K) \cdot X(K)$, or,

$\frac{Y(K)}{X(K)} = \frac{\phi_b(K)}{\phi_a(K)}$ where ϕ_b and ϕ_a are polynomials in K. The K domain transfer function $\frac{Y}{X}$ may now be realized as if it were a time invariant network. The correspondence between K domain and time-varying

[1] W.H. Wattenberg, "Transform Methods and Time Varying Systems," ERL Report No. 321, Ser. 60.

elements is determined by the form of L.

A method of synthesis for a class of equations (*) has been developed by McMahon [2]. The class considered are those for which the operator is $L = \frac{d}{dt} \cdot a(t)$, where a(t) is piecewise continuously differentiable and satisfies

$$a < b \leq a(t) \leq B < \infty, \quad -\infty < t < \infty; \; b, B = \text{const.}$$

McMahon [2] shows that such equations can be realized by a network containing a finite number of fixed resistances and time varying reactances, with all reactance elements varying the same way.

McMahon's results [2] have been extended to include networks which also contain time varying resistances, which resistances need not (but may) vary in the same way as the reactances. The operator L has the form $L = \frac{d}{dt} a(t) + b(t)$, where b(t) satisfies restrictions similar to those on a(t). Although this introduces an additional degree of freedom and enlarges the class of operators L_a, L_b, which may be expressed as polynomial functions of L, this class is still quite small, there being very restrictive relations between allowable coefficients in L_a and L_b. Means of approximating a given operator by one which may be expressed a a polynomial function of L of the form state above are being investigated.

TUNNEL DIODE NETWORKS

JSEP Grants AF-AFOSR-139-64865 and NSF Grant GP-2684
Prof. I.T. Frisch

We have previously shown that a uniformly distorted Butterworth imbedding network can be used for a tunnel diode to stabilize the quilibrium point when the complete linear equivalent circuit has been used for the tunnel diode. Using the stability criteria of Brayton and Moser we have shown that is the condition

$$\frac{4}{C_{j\,min}} \left(\frac{L_i}{R_i} \right)_{max} \leq -\delta$$

is satisfied, then the origin is actually stable not only for the linear model but, in addition, if any nonlinearity in the first and third quadrants is added to the negative resistor, as long as the norm of the current through the nonlinear resistor approaches infinity as the norm of the state vector approaches infinity, C_j is the smallest capacitor in the

---

[2] E.L. McMahon, "Impulse Response Synthesis for Networks Characterized by Functions of a First Order Linear Operator"; Cooley Electronics Laboratory (University of Michigan) Tech. Rep. No. 135.

embedding network; $\left(\frac{L_i}{R_i}\right)_{max}$ is the maximum ratio of series inductance to series resistance for any section of the embedding ladder.

Using the Popov stability criterion we have shown that the tunnel diode with linearized negative conductance -G can be stabilized for any nonlinearity in a sector bounded by the line kV where $k \leq 2G$ as long as the angle of the reflector coefficient is in a specified range.

In general, the Popov criterion gives stronger conditions than the Brayton and Moses method. However, the Popov method is more difficult to apply to complicated networks. Attempts are to be made at unifying this two-stability method and at further synthesis of stabilizing networks for the nonlinear tunnel diode networks.

SYNTHESIS OF ORIENTED COMMUNICATION NETS

AROD Grant DA-ARO-D-31-124-G576
D.K. Sen (Prof. I. T. Frisch)

The problem of realizability of a square unsymmetric matrix as the terminal capacity matrix of an oriented communication net has been investigated. A necessary and sufficient condition for realizability has been found for a restricted class of matrices, named "maximally distinct." A simple algorithm, which directly reduces the given matrix to the branch capacity matrix of its realization, has been constructed for the maximally distinct matrices. A report of this work has been presented at the Symposium on Signal Transmission and Processing, at Columbia University, New York, May 13, 14, 1965.

Recently, we extended this approach to a more general case. The basic algorithm has been modified to a suitable form which is applicable to matrices that are not maximally distinct. This has led to a sufficient condition for realizability of general matrices.

COMMUNICATION NETS

AROD Grant DA-ARO-D-31-124-G576
T. C. Cisco (Prof. I.T. Frisch)

The previous period has been devoted to a study of literature concerning the multi-commodity networks flow problem. Work in this area will be discontinued during the summer and resumed in September.

PASSIVE AND ACTIVE NETWORK REALIZATIONS

JSEP Grants AF-AFOSR-139-64and 65
C.W. Ho (Prof. I.T. Frisch)

The unbalanced bridged-T network in Fig. 1 is now under investigation.

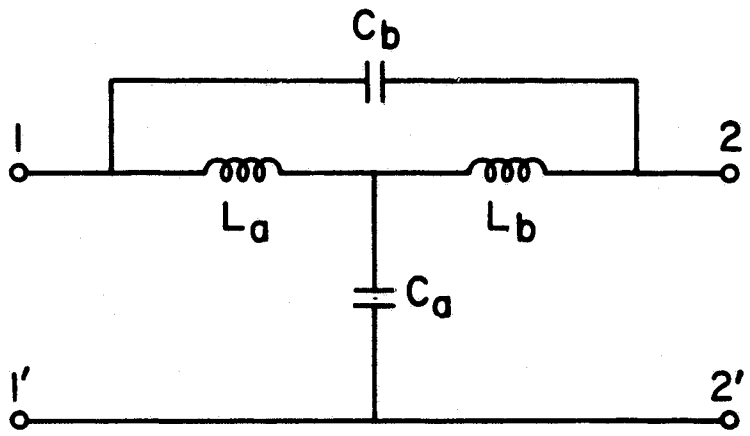

Fig. 1.

We have shown two cascaded Brune cycles of the form in Fig. 2, which is equivalent to the bridge-T network with respect to ports 1 and 2

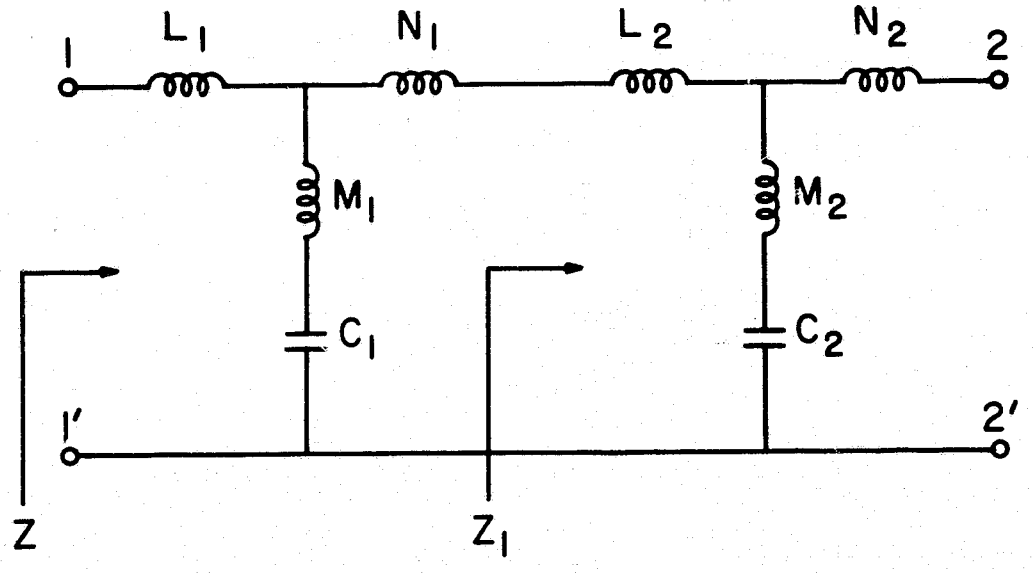

Fig. 2.

provided the following two conditions are satisfied:

$$\frac{L_1 + M_1}{N_1 + M_1} \cdot \frac{L_2 + M_2}{N_2 + M_2} = 1 \qquad \text{(a)}$$

$$\frac{C_1 C_2}{C_1 + C_2} \cdot \frac{M_1 + M_2}{M_1 C_1 + M_2 C_2} = \sqrt{\frac{L_1 + M_1}{N_1 + M_1}} \qquad \text{(b)}$$

These conditions are in terms of both Z and Z_1 (as well as Z', Z_1') which are not readily applicable for direct realization. An attempt to make these two conditions depend on Z and its derivatives is thus of considerable interest.

As a special, therefore simpler, case we first let $M_1C_1 = M_2C_2$, that is let the two Brune cycles have the same transmission zero. It is interesting to note that conditions (a), (b) can be reduced to a form where not only $Z(s)$, but also $Z''(s)$ and $Z'''(s)$ are involved. The results are:

$$X'(\omega_0) + 3\frac{X(\omega_0)}{\omega_0} = 0$$

$$\frac{11}{3} X'''(\omega_0) - 64\frac{X''(\omega_0)}{\omega_0} + 192\frac{X(\omega_0)}{\omega_0^3} = 0$$

where $X(\omega_0) = \dfrac{Z(j\omega_0)}{j}$ $\qquad$ $X'(\omega_0) = \left.\dfrac{dZ(s)}{ds}\right|_{s=j\omega_0}$

$$X''(\omega_0) = j\left.\frac{d^2Z(s)}{ds^2}\right|_{s=j\omega_0} \qquad X'''(\omega_0) = -\left.\frac{d^3Z(s)}{ds^3}\right|_{s=j\omega_0}$$

and ω_0 is the resonant frequency of M_1 and C_1.
For more general cases, similar conditions are unavailable.

DISTRIBUTED NETWORKS

JSEP Grants AF-AFOSR-139-64 and 65
C.C. Tung (Prof. I.T. Frisch)

The necessary and sufficient conditions for synthesizing an open or short circuit driving point function $Z_{in}(s)$ as a cascade of RC (γ, ℓ) line elements under the transformation $p = \tanh \gamma \ell$ is that $\sqrt{s}\, Z_{in}(p)$ be a positive, real, odd function of the complex frequency p. The extracted line element of (γ, ℓ) type will then have a characteristic impedance

$$Z_{10} = \frac{1}{\sqrt{s}} Z_{in}(p)\Big|_{p=1} = \frac{R_1}{\sqrt{SR_1C_1}} .$$

Richard's theorem will ensure that the remaining driving function is a positive real function in p multiplied by a factor s.

A voltage ratio can also by synthesized by assuming z_{21} and z_{11} have the same poles and synthesizing z_{11} as a driving point function.

Distributed equivalents for Darlington D-sections and Darlington C-sections for wider range than are presently available are under investigation.

Example:

$$\sqrt{s}\ \ Z_{in} = \frac{2p^3+18p}{17p^2+3} \qquad Z_{10} = \frac{1}{\sqrt{s}} \cdot 1$$

$$\sqrt{s}\ \ Z_2 = \frac{15p}{2p^3+3}$$

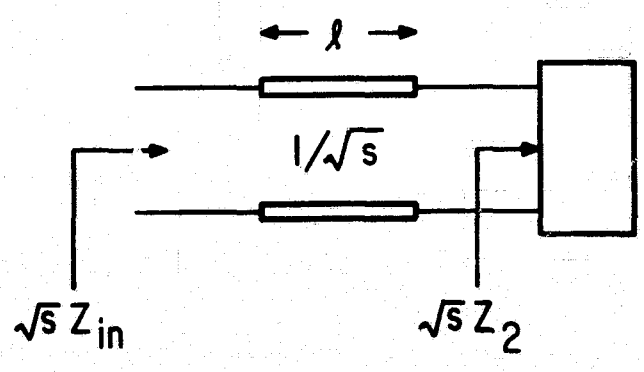

Repeating the same procedures we have the network below:

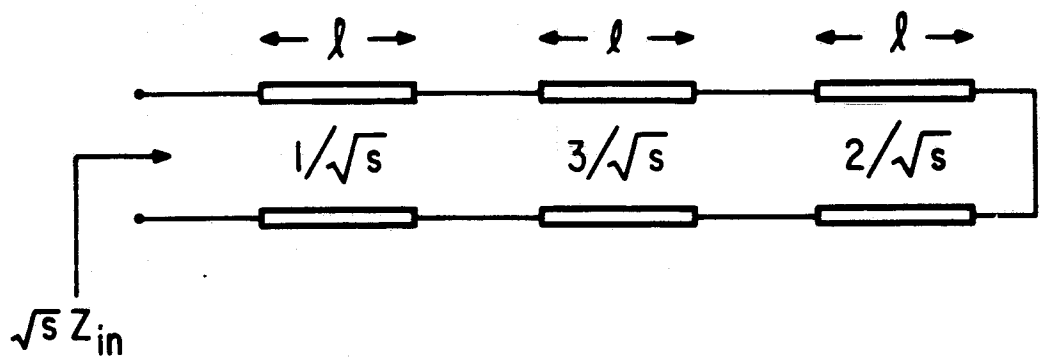

STATE-SPACE APPROACH TO LINEAR NETWORKS

NSF Grant GP-2684
J. Tow (Profs. E.S. Kuh and P.R. Bryant)

Linear, lumped, time-invariant, passive electrical networks which consist of R, L, C, and generalized ideal transformers T, have been studied. The order of complexity and the constraints on the topology for the network to possess unique solution of any RLCT network are derived. Simple necessary and sufficient conditions for a real matrix to be the state space characterization, (i.e., the A-matrix), of an RLCT network are also obtained.

A generalized ideal transformer, or simply "transformer", has its multiple windings wound on a magnetic material having infinite permeability. Associated with each transformer is a magnetic circuit or a magnetic graph [1]. A magnetic tree can be defined on this magnetic graph in the same manner as on an electric graph. Two simple examples are given in Fig. 1.

Any RLCT network defines an electric graph N (in the usual manner) and a magnetic graph M (M is the ensemble of the magnetic graphs for each transformer; the "connectivity" of M is equal to the number of transformers). In general, the subgraph of N corresponding to the transformer branches (windings) is not the same as M.

Definition 1 A proper tree for an RLCT network is any set of electric branches which forms a tree in N and such that the corresponding set of transformer magnetic branches also forms a tree (or forest) in M.

---

[1] P.R. Bryant, "Problems in Electrical Network Theory," PhD Dissertation, University of Cambridge, England, July 1959.

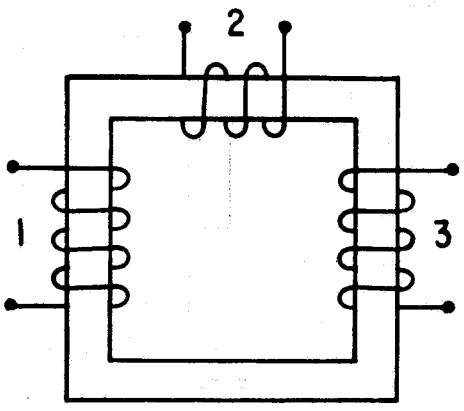

genealized ideal transformer

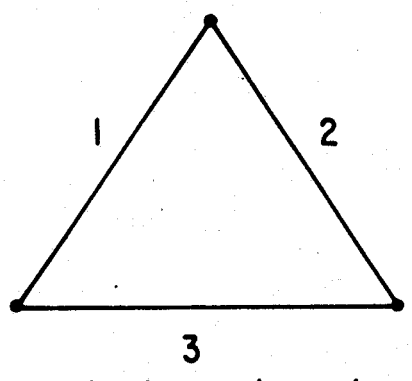

associated magnetic graph

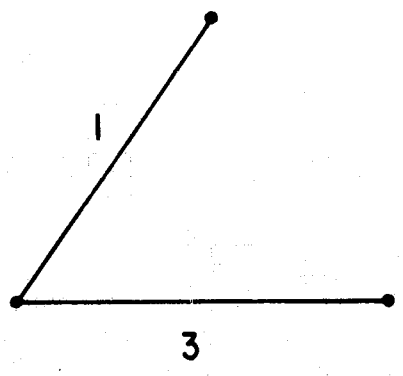

a magnetic tree

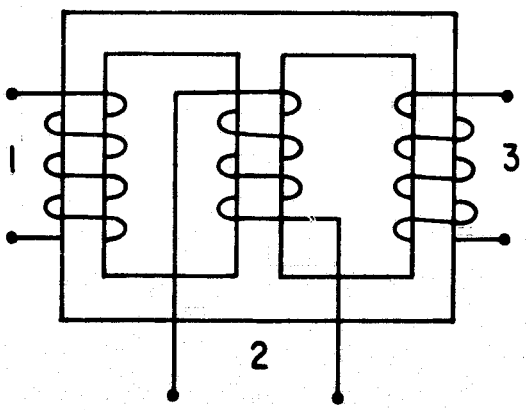

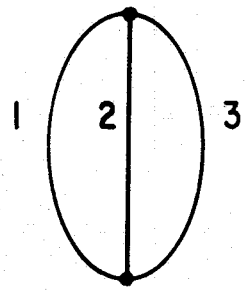

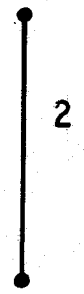

Fig. 1

Definition 2 A maximal proper tree is a proper tree and such that the sum of its tree capacitors and co-tree inductors is maximum among the set of proper trees.

Theorem 1 If an RLCT network has no proper tree, then it does not possess a unique solution.

Theorem 2 The order of complexity, defined as the total number of natural frequencies, σ, of an RLCT network is equal to the sum of tree capacitors and co-tree inductors of any of its maximal proper trees.

Proofs of theorems 1 and 2 are omitted here.

Remark It is possible that, for a particular set of transformer-turn-numbers, σ is reduced; however, the "measure" of such a set is zero.

Starting with a maximal proper trees, one can obtain the explicit form of the A-matrix for any RLCT network by using the voltages across the tree capacitors and the currents through the co-tree inductors as a set of state variables. The method is similar to Bryant's formulation for the RLC case [2].

Theorem 3 A real matrix A is the A-matrix of an RLCT network, i.e.,

$$\dot{x} = -Ax, \tag{1}$$

where x is the state vector corresponding to voltages across capacitors and currents through inductors, if and only if A admits a decomposition of the following form

$$A = \begin{pmatrix} C^{-1} & 0 \\ U & L^{-1} \end{pmatrix} \begin{pmatrix} A_{11} & A_{12} \\ -A_{12}^{t} & A_{22} \end{pmatrix}, \tag{2}$$

where C and L are positive definite;

A_{11} and A_{22} are positive semi-definite.

Remark

(i) This decomposition is necessary and well-known for any RLC network.

(ii) The realization of an A-matrix without transformers has not been solved yet.

---

[2] P.R. Bryant, "The Explicit Form of Bashkow's A-matrix," IRE Trans. CT, pp. 303-306, September 1962.

Proof The necessity comes directly from the explicit form of the A-matrix, which we have omitted here.

The sufficiency is proved by realization. Let

$$A = \begin{pmatrix} C^{-1} & 0 \\ 0 & L^{-1} \end{pmatrix} \begin{pmatrix} A_{11} & A_{12} \\ -A_{12}^t & A_{22} \end{pmatrix}, \tag{2}$$

where C, L are positive definite; A_{11}, A_{22} are positive semi-definite. By similarity transformations, we have

$$P_1^t \; C \; P_1 = \Lambda_C = \text{diag.}\ (C_1, \ldots, C_n)$$

$$P_2^t \; L \; P_2 = \Lambda L = \text{diag.}\ (L_1, \ldots, L_m)$$

If we made a transformation of variables in Eq. 2, i.e., letting

$$x = \begin{pmatrix} x_1 \\ x_2 \end{pmatrix} = \begin{pmatrix} P_1 & 0 \\ 0 & P_2 \end{pmatrix} \begin{pmatrix} e_C \\ i_L \end{pmatrix} \tag{3}$$

and premultipling both sides of Eq. 2 by $\begin{pmatrix} P_1^t & 0 \\ 0 & P_2^t \end{pmatrix}$, we obtain

$$\begin{pmatrix} \Lambda_C & 0 \\ 0 & \Lambda_L \end{pmatrix} \begin{pmatrix} \dot{e}_C \\ \dot{i}_L \end{pmatrix} = -\begin{pmatrix} P_1^t A_{11} P_1 & P_1^t A_{12} P_2 \\ -P_2^t A_{12}^t P_1 & P_2^t A_{22} P_2 \end{pmatrix} \begin{pmatrix} e_C \\ i_L \end{pmatrix} = -\begin{pmatrix} A'_{11} & A'_{12} \\ -A'^t_{12} & A'_{22} \end{pmatrix} \begin{pmatrix} e_C \\ i_L \end{pmatrix} \tag{4}$$

where A'_{11} and A'_{22} are again positive semi-definite.

Eq. 4 can be realized by an RLCT network as is shown in Fig. 2.

Since the transformation of variables, Eq. 3 can be realized by congruent transformers; therefore, Eq. 1 has a realization and the proof is completed.

There exist two problems in the decomposition of the given matrix into the form Eq. 2:

(i) Partition of the state variables into two groups, i.e., $x = \begin{pmatrix} x_1 \\ x_2 \end{pmatrix}$

(ii) The actual decomposition into the form Eq. 2.

There exists an algebraic method for accomplishing this decomposition. The failure of this method to produce at least one such form implies that the given A-matrix is not realizable as an RLCT network.

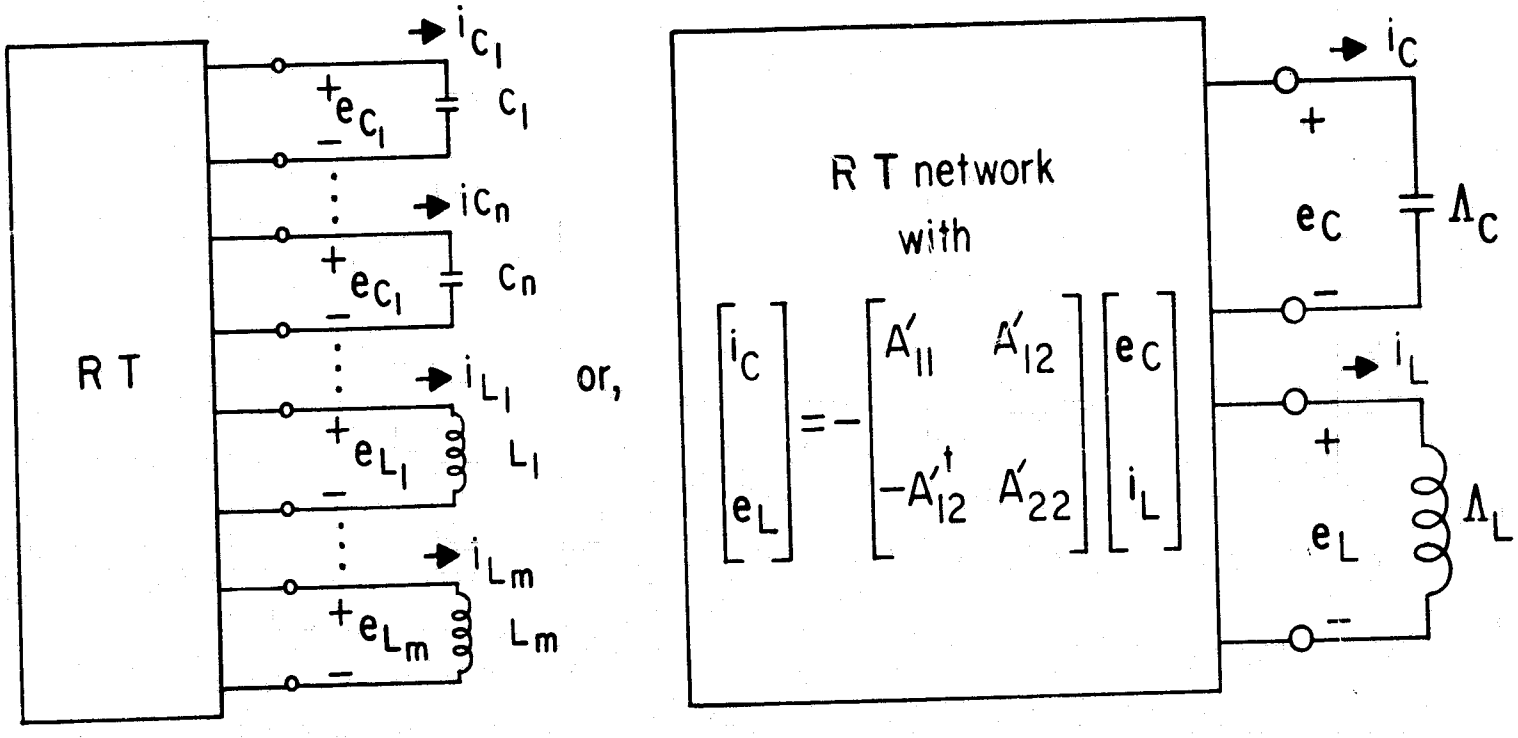
R T
i_{C_1}
$+e_{C_1}-$
C_1
ic_n
$+e_{C_1}-$
C_n
i_{L_1}
$+e_{L_1}-$
L_1
i_{Lm}
$+e_{L_m}-$
L_m
or,
R T network
with
$\begin{bmatrix} i_C \\ e_L \end{bmatrix} = -\begin{bmatrix} A'_{11} & A'_{12} \\ -A'^{t}_{12} & A'_{22} \end{bmatrix} \begin{bmatrix} e_C \\ i_L \end{bmatrix}$
i_C
+
e_C
−
Λ_C
i_L
+
e_L
−
Λ_L

Fig. 2.

STABILITY OF LINEAR TIME-VARYING NETWORKS

NSF Grant GP-2684
Y-L. Kuo (Prof. E.S. Kuh)

With the advent of parametric devices and the control problem encountered in the design of space vehicles, the need has arisen for stability criteria which can be applied easily in the design of linear and nonlinear time-varying networks (systems). To this end, the development of sufficient stability conditions has been, in the past few years, of great interest in the study of feedback systems containing nonlinear time-varying elements [1-4]. These stability conditions have been sought in terms of the real-frequency characteristics of the linear time-invariant part of the system and the bounds on the nonlinear time-varying elements, analogous to the Nyquist stability criterion for linear time-invariant feedback systems.

In the following the method of Sandberg [2-3] is employed to investigate the stability of general linear time-varying RLC networks. For simplicity we consider a network with a single time-varying resistance, capacitance, and inductance as shown in Fig. 1,

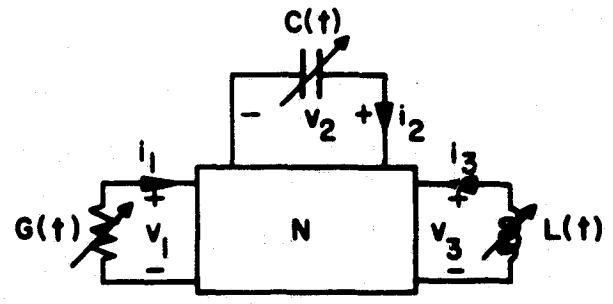

Fig. 1. N is a linear time-invariant network without independent sources.

[1] J.J. Bongiorno, "Real-Frequency Stability Criterion for Linear Time-Varying Systems," Proc. IEEE, Vol. 52, No. 7 pp. 832-841; July 1, 1964.

[2] I. W. Sandberg, "A Stability Criterion for Linear Networks Containing Time Varying Capacitors," IEEE Trans. on Circuit Theory, Vol. CT-12, No. 1, pp. 2-11; March, 1965.

[3] I.W. Sandberg, "Frequency-Domain Criterion for the Stability of Nonlinear Feedback Systems," Proc. National Electronics Conference 1964, pp. 737-741.

[4] G. Zames, "On the Stability of Nonlinear Time-Varying Feedback Systems," Proc. National Electronics Conference 1964, pp. 725-730.

where $\alpha_1 \leq G(t) \leq \beta_1$, $0 < \alpha_2 \leq C(t) \leq \beta_2$, $0 < \alpha_3 \leq L(t) \leq \beta_3$ for all t. Let

$$\gamma_1 = 1/2(\beta_1 - \alpha_1), \quad \gamma_2 = 1/2(\beta_2 - \alpha_2), \quad \gamma_3 = 1/2(\beta_3 - \alpha_3),$$

$$G_0 = 1/2(\beta_1 + \alpha_1), \quad C_0 = 1/2(\beta_2 + \alpha_2), \quad L_0 = 1/2(\beta_3 + \alpha_3).$$

Then Fig. 1 is equivalent to Fig. 2,

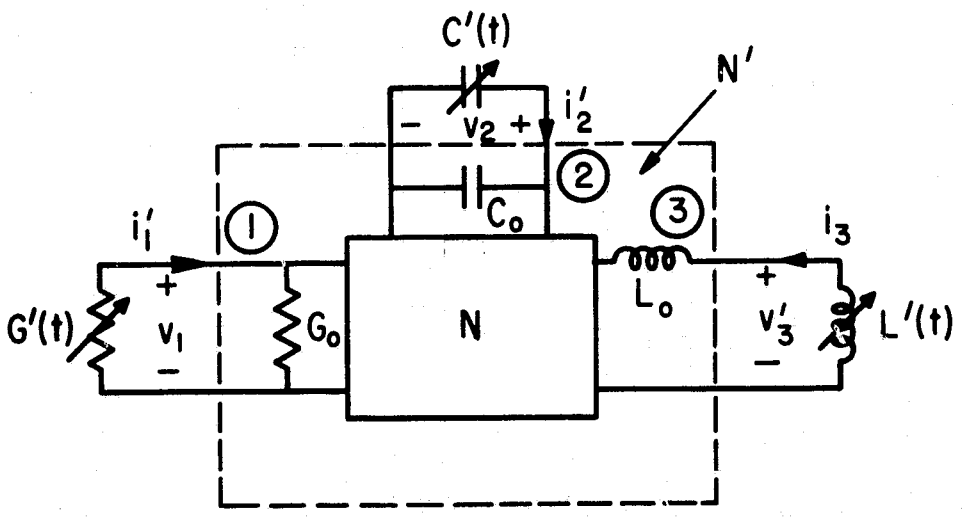

Fig. 2. N' is a linear time-invariant network without independent sources.

$$|G'(t)| \leq \gamma_1, \; |C'(t)| \leq \gamma_2, \; |L'(t)| \leq \gamma_3$$

Let $\underline{v} = \begin{pmatrix} v_1 \\ v_2 \\ i_3 \end{pmatrix}$ and $\underline{u} = \begin{pmatrix} i'_1 \\ i'_2 \\ v'_3 \end{pmatrix}$, with $i'_1(t) = -G'(t)\, v_1(t)$,

$i'_2(t) = -\frac{d}{dt}\,[\,C'(t)\, v_2(t)\,]$, and $v'_3(t) = -\frac{d}{dt}\,[\,L'(t)\, i_3(t)\,]$. Assume that the network is characterized by a Thevenin-type relation between $\underline{v}$ and $\underline{u}$ of the form:

$$\underline{v}(t) = \underline{v}_0(t) + \int_0^t \omega(t-\tau)\, \underline{u}(\tau)\, d\tau \quad \text{for } t \geq 0, \qquad (1)$$

where $\underline{v}_0(t) = \begin{pmatrix} v_{10}(t) \\ v_{20}(t) \\ i_{30}(t) \end{pmatrix}$ is the response due to initial conditions,

$\omega(t)$ is the unit impulse response of the linear, time-invariant part, N'. The Laplace transform of $\omega(t)$ is denoted by $W(s)$, where

$$w(t) = \begin{pmatrix} w_{11}(t) & w_{12}(t) & w_{13}(t) \\ w_{21}(t) & w_{22}(t) & w_{23}(t) \\ w_{31}(t) & w_{32}(t) & w_{33}(t) \end{pmatrix} \text{ and } W(s) = \begin{pmatrix} z_{11}(s) & a_{12}(s) & h_{13}(s) \\ z_{21}(s) & z_{22}(s) & h_{23}(s) \\ h_{31}(s) & h_{32}(s) & y_{33}(3) \end{pmatrix}$$

Notation:

$$\Lambda\{M\} = (\text{largest eigenvalue of } M^* M)^{1/2}.$$

$$L_2(0, \infty) = \{\underline{f} \mid \int_0^{\infty} \underline{f}'(t)\, \underline{f}(t)\, dt < \infty\}.$$

Assume that:

(i)

(a) $\int_0^{\infty} | w_{ij}(t) |^p dt < \infty$ for $p = 1, 2$ and $i, j = 1, 2, 3$.

(b) $\int_0^{\infty} | \frac{d}{dt} w_{ij}(t) |^p dt < \infty$ for $p = 1, 2, ; i = 1, 2, 3; j = 2, 3$.

(c) In addition, $w_{ij}(t) \longrightarrow 0$ as $t \longrightarrow \infty$ for $i = 1, 2, 3; j = 2, 3$.

(ii) $\underline{v}_0(t) \in L_2(0, \infty)$ and $\underline{v}_0(t) \longrightarrow 0$ as $t \longrightarrow \infty$.

(iii) $\underline{v}(t) \in L_2(0, T)$ for all $T < \infty$.

We also assume that the variations of G(t), C(t), and L(t) are sufficiently smooth that the network possesses a physically meaningful solution.

Definition The network of Fig. 2 is said to be stable if the following conditions are satisfied for all sets of initial conditions:

(i) $\underline{v}(t) \in L_2(0, \infty)$.

(ii) $\underline{v}(t) \longrightarrow 0$ as $t \longrightarrow \infty$.

The main result is stated in the following Theorem:

Let $\gamma = \max(\gamma_1, \gamma_2, \gamma_3)$,

and

$$W_1(s) = \begin{pmatrix} z_{11}(s) & sz_{12}(s) & sh_{13}(s) \\ z_{21}(s) & sz_{22}(s) & sh_{23}(s) \\ h_{31}(s) & sh_{32}(s) & sy_{33}(s) \end{pmatrix}$$

Under the assumptions (i) - (iii) and if

$$\gamma \sup_{-\infty<w<\infty} \Lambda\{W_1(iw)\} < 1 \qquad (2)$$

then the network is stable.

Remarks

1. The linear, time-invariant part of the network is described by a convolution integral as given in Eq. 1. No specific assumptions are made concerning the internal structure of the linear part. It may be a lumped or a distributed network.

2. By using Sandberg's argument [2], the stability criterion given in Eq. 2 still holds true if the following inequalities are satisfied:

$$\alpha_1 \leq \frac{i_1[v_2,t]}{v_1} \leq \beta_1 \text{ for } t \geq 0,\ v_1 \neq 0;\ i_1[0,t] = 0 \text{ for } t \geq 0,$$

$$0 < \alpha_2 \leq \frac{q_2[v_2,t]}{v_2} \leq \beta_2 \text{ for } t \geq 0,\ v_2 \neq 0;\ q_2[0,t] = 0 \text{ for } t \geq 0,$$

$$0 < \alpha_3 \leq \frac{q_3[i_3,t]}{i_3} \leq \beta_3 \text{ for } t \geq 0,\ i_3 \neq 0;\ q_3[0,t] = 0 \text{ for } t \geq 0.$$

3. The main result can also be extended to the network with multiple G(t)'s, C(t)'s, and L(t)'s with mutual coupling allowed). For n etworks with multiple time-varying capacitances, if appropriate constant parts of the varying capacitances are imbedded into the time-invariant network, it can be shown that the stability condition is sharper than the result obtained by Sandberg [2].

4. Since there are eight different characterizations of W(s) (in terms of impedance, admittance and hybrid parameters), we have eight different forms of stability criteria. The choice of the proper characterization depends on the frequency response of the time-invariant part.

The proof of the theorem and other details will be published in the near future as an ERL Report.

GENERAL MATCHING THEORY AND APPLICATIONS TO STABILITY AND SYNTHESIS OF TUNNEL DIODE AMPLIFIERS

JSEP Grants AF-AFOSR-139-64 and 65
Y.T. Chan (Prof. E.S. Kuh)

The classical problem of lossless broadband matching was initiated by Bode and solved by Fano. Recently, Youla [1] proposed an alternate theory, which simplified Fano's treatment for some more general passive load impedances. The present work represents a generalization of Youla's to include both passive and active impedences. The theory is applied to the tunnel diode problem, where the complete equivalent circuit including the series resistance and inductance is used. It is demonstrated that the necessary condition for potential stability of Smilen and Youla [2] is also sufficient. Furthermore, a straightforward synthesis procedure is developed, which is based on the general matching theory. A complete presentation will be published soon in an ERL report.

Consider the circuit shown in Fig. 1, where $z(s)$ is a given impedance which can be either passive or active, and $Z(s)$ is a passive impedance to be designed. Let us denote the complex reflection coefficient by

$$\rho(s) = \frac{Z(s) - z(-s)}{Z(s) + z(s)} \quad .$$

Thus, if $z(s)$ is passive and lossy, the conventional broadband matching can be summarized as follows: (1) to investigate the constraints imposed on $\rho(s)$ by z, (2) from these constraints, choose a realizable $\rho(s)$ so that $|\rho(j\omega)|$ approximates a constant over a given band which is also minimized, and (3) realize the lossless 2-port from $\rho(s)$.

In case $z(s)$ is active, the problem can be similarly stated in terms of the above three steps. However, in (1) we must consider the stability of the overall circuit, and in (2) we wish to maximize $|\rho(j\omega)|$ over a band. The restriction on $\rho(s)$ can be expressed in terms of the coefficients of the Laurent series expansions at the closed RHP poles of $z(s)$ and $z(-s)$ and the zeros of the even part of $z(s)$. It is proved that if $\rho(s)$ satisfied these constraints, a passive $Z(s)$ is obtained.

Integral constraints on $\rho(s)$ can also be derived. Based on the integral constraints, we obtained a set of curves which indicate the maximum realizable bandwidth for a tunnel diode amplifier with lossless 2-port coupling network. The plot is shown in Fig. 2. A typical amplifier along with its calculated performance is shown in Fig. 3.

---

[1] D.C. Youla, "A New Theory of Broadband Matching," Trans. IEEE CT-11, March 1964.

[2] L.I. Smilen and D.C. Youla, "Stability Criteria for Tunnel Diodes," Proc. IEEE Vol. 49 No. 7, July 1961.

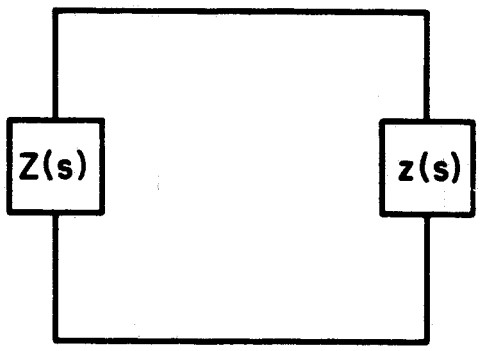

Fig. 1.

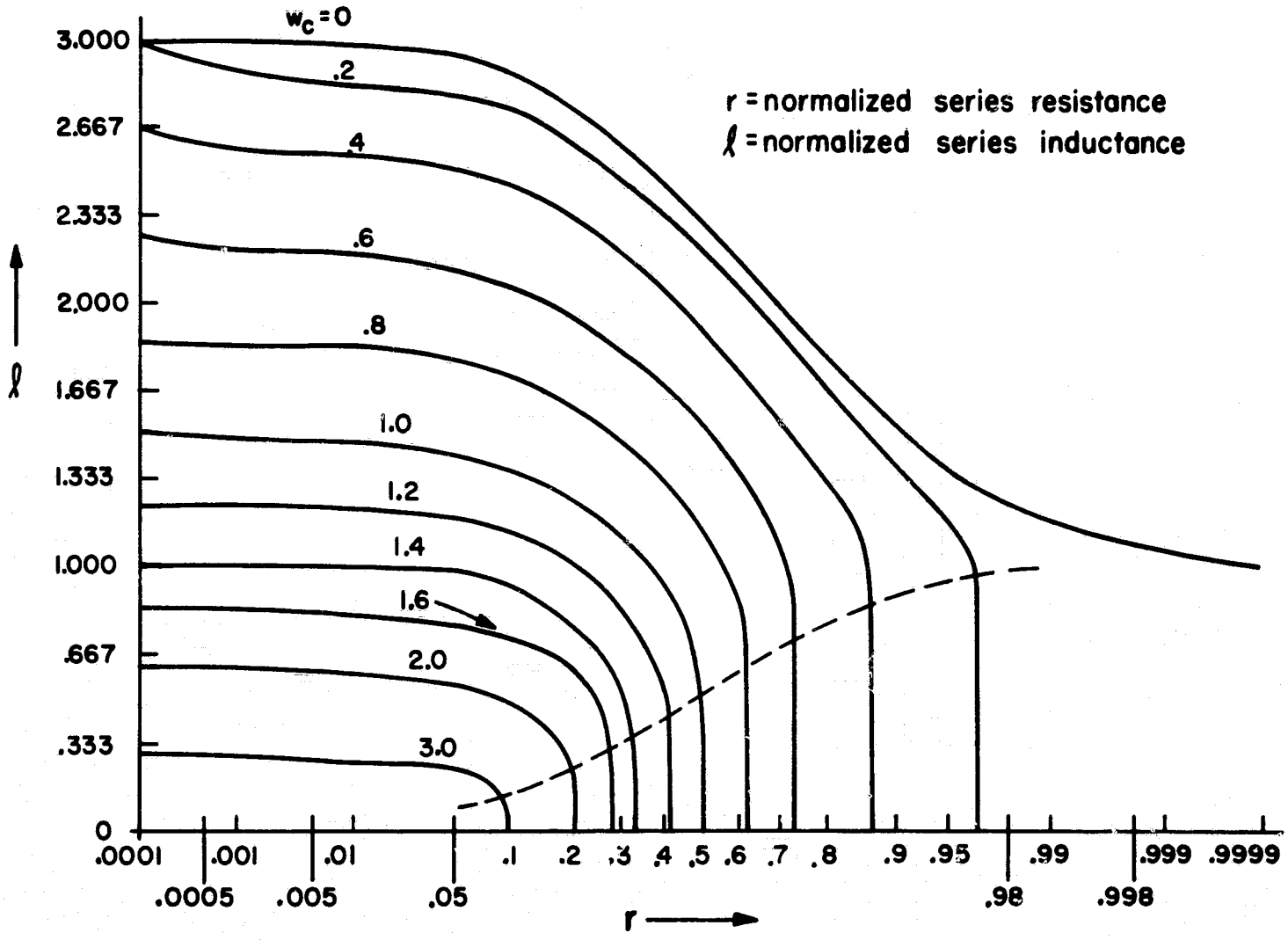

Fig. 2. Bandwidth limitation of tunnel diode.

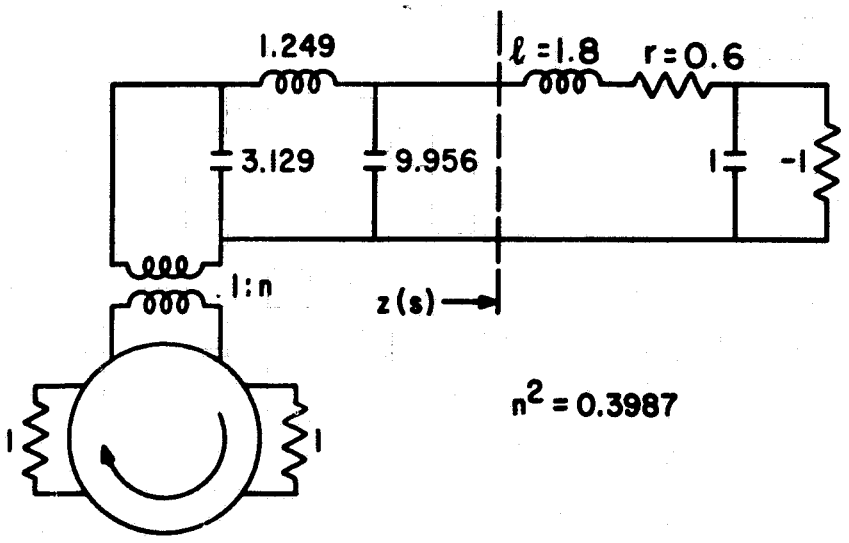

(a) A tunnel diode amplifier.

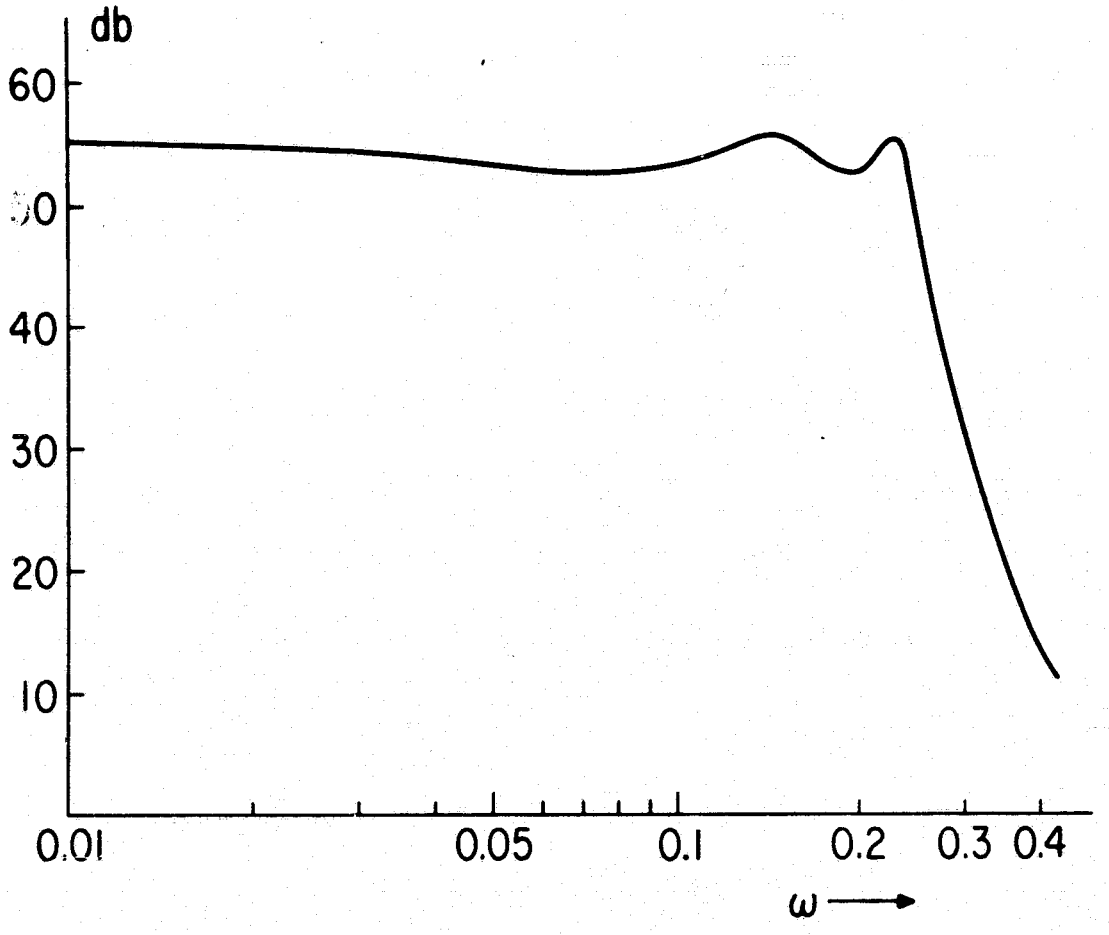

(b) Frequency response of the tunnel diode amplifier.

Fig. 3.

SENSITIVITY ANALYSIS FOR GENERAL SYSTEMS

University of California Support
R.N. Biswas (Prof. E.S. Kuh)

A new method for evaluating the sensitivity of any general system has been developed. In contrast with the conventional parameter sensitivity, where the effect of the variations of certain parameters on the system response is investigated, attention is focussed on the variation in the response due to the variations in the functions (which may in general be nonlinear as well as time-varying, scalar, or vector-valued), constituting the mathematical description of the system. The method is based on a simple vector flow graph representation, which is a direct generalization of the linear vector flow graph described previously [1].

Given any system, it can be shown by proper flow graph manipulation and augmentation that the following representation is always possible.

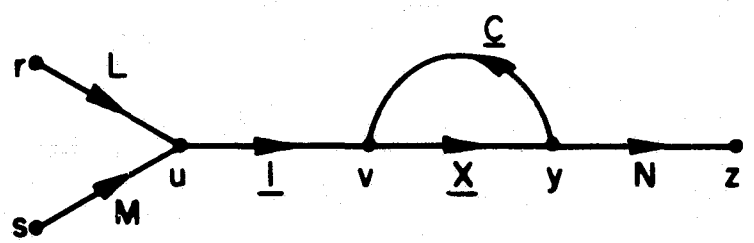

$\underline{X}$ is, in general, a non-linear operator consisting of the functions describing the system; $\underline{C}$ is a linear operator, containing the information about the topology of the system; and $\underline{1}$ is the identity operator. ($\underline{X}$, $\underline{C}$ and $\underline{1}$ are all mappings of a finite Euclidean space into itself.) L, M, and N are constant matrices. r is the system input vector, s is the initial state vector, and z is the system output vector. The system equations are then given by the following:

$$\begin{aligned} u &= Lr + Ms, \\ v &= u + \underline{C}y, \\ y &= \underline{X}v, \\ z &= Ny. \end{aligned} \qquad (1)$$

---

[1] R.N. Biswas and E.S. Kuh, "Multiparameter Sensitivity Analysis for Linear Systems," ERL Report 65-8, March 1965.

Now let us consider first-order perturbations in the system, which may be represented by a variation $\underline{\delta x}$ in the system operator $\underline{X}$. Since at any instant of time, $\delta u = 0$ for a given initial state and a given input, we have from Eq. 1:

$$\begin{aligned} \delta v &= \underline{C}\delta y, \\ \delta y &= \delta(\underline{X}v), \\ \delta z &= N\delta y. \end{aligned} \tag{2}$$

Now, $\delta(\underline{X}v) = \underline{\delta X}v + \underline{J}\delta y$, where the linear operator $\underline{J}$ is defined by the relation $\underline{J}\delta v = J\delta v$, J being the Jacobian matrix of the operator $\underline{X}$ for the given initial state and the given input at the instant of time under consideration. (The matrix elements are given by $j_{pq}(t) = \dfrac{\partial y_p(t)}{\partial v_q(t)}$.) Elimination of v and y from Eq. 2 then leads to:

$$\delta z = N(\underline{1} - \underline{JC})^{-1}\,\underline{\delta X}\;\; v. \tag{3}$$

The existence of the inverse follows from the assumption that first-order perturbations produce first-order variation in the output.

Clearly, $\underline{\delta X}v$ represents the variation in y due to the perturbations in the system functions alone ($\equiv$ "open loop error"), v remaining the same as in the unperturbed system. Let $\underline{\delta X}v = \hat{\delta y}$. We then have the following model for the net variation in the output.

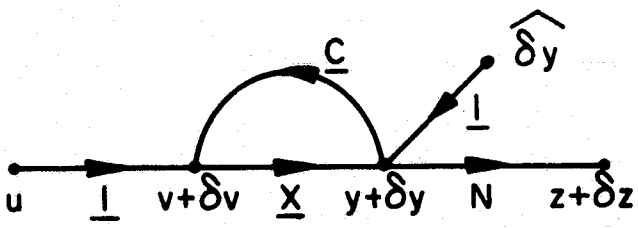

Actual system

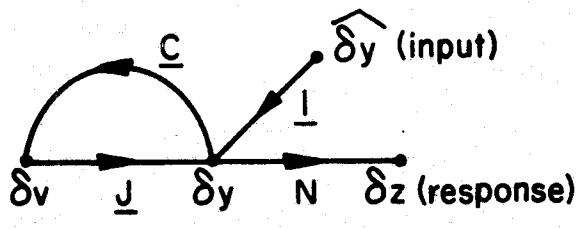

Linearized system

The sensitivity operator $\underline{S} \triangleq N(\underline{1} - \underline{JC})^{-1}$. Clearly, $\underline{S}$ maps the perturbation $\hat{\delta y}$ of the system functions into the variation δz in the output. It follows from the model of the linearized system, therefore, that $\underline{S}$ represents the input-output relation of a linear system, and hence, must be an integral operator, with the corresponding impulse response matrix $S(t, \tau)$ of the linearized system as its kernel. Eq. 3 may then be written in the integral form

$$\delta z(t) = \int_0^t S(t, \tau)\;\hat{\delta y}(\tau). \tag{4}$$

For obvious reasons, $S(t, \tau)$ is defined to be the sensitivity matrix. It is easy to see that for linear time-invariant systems, this definition corresponds exactly to the frequency-domain definition of the sensitivity matrix[1]

We now consider the special case where the system consists of n distinct blocks described by n scalar functions $x_1, \ldots, x_2, \ldots, x_n$. Then it can be shown that the operators $\underline{X}$, $\underline{\delta X}$ and $\underline{J}$ are given by the relations:

$$\underline{X}v = \text{col}\,(x_1[v_1(t),t]\,,\ x_2[v_2(t), t]\,, \ldots,\quad x_n[v_n(t), t]\ ),$$

$$\underline{\delta X}v = \text{col}\,(\delta x_1[v_1(t), t]\,, \delta x_2[v_2(t), t]\,, \ldots,\quad \delta x_n[v_n(t), t]\ ),$$

and $$J = \text{Diag.}\left(\frac{\partial x_1(\cdot\,, t)}{\partial(\cdot)}\,,\ \frac{\partial x_2(\cdot\,, t)}{\partial(\cdot)}\,, \ldots,\quad \frac{\partial x_n(\cdot\,, t)}{\partial(\cdot)}\right).$$

The elements of the sensitivity matrix then have the following significance.

$s_{ik}(t, \tau) \triangleq$ sensitivity coefficient of the ith output variable with respect to the kth block characteristic,

= response at the ith output node of the linearized system due to an impulse input $\delta(t-\tau)$ applied at the output node of the kth block.

The variation in the ith output variable may be expressed as

$$\delta y_i(t) = \sum_{k=1}^{n} \int_0^t s_{ik}(t, \tau)\ \widehat{\delta y}_k(\tau)\,,$$

where $\widehat{\delta y}_k(\tau)$ is the variation in the value of the kth function at the instant of time τ.

An important class of systems having this special property is the general R-L-C network with no mutual coupling. It can be shown that an R-L-C network satisfying the conditions for the existence of a unique continuous response may be represented by the following vector flow graph [2].

---

[2] E.S. Kuh, "Representation of Nonlinear Networks," Proc. Nat. Electronics Conf., 1965.

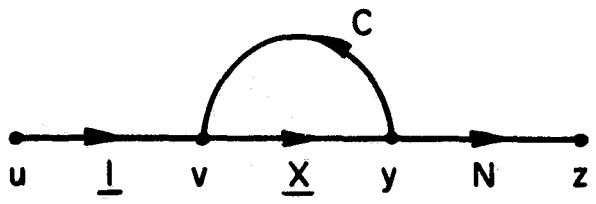

y = col. (link currents, tree-branch voltages)
v = col. (link voltages, tree-branch currents)
u = col. (fundamental loop voltage sources, fundamental cut-set current sources)

$$C = \begin{pmatrix} 0 & -F \\ F^t & 0 \end{pmatrix}$$, where F is a submatrix of the fundamental loop matrix B obtained by partitioning B as B = (1, F), 1 being the unit matrix.

It is a well-known result that for the same ordering of the branches, the fundamental cut-set matrix Q may be partitioned as $Q = (-F^t, 1)$.

Thus it is seen that for the R-L-C network, $\underline{\underline{X}}$ involves only the branch characteristics and $\underline{\underline{C}}$ involves only the topology of the system. Usually in a network problem, only one scalar output is of interest, so that z is one dimensional, and as a result N is a row vector. The sensitivity matrix is also a row vector in that case, its elements being the sensitivity coefficients with respect to the different network elements. It follows from the construction of the flow-graph model that the sensitivity coefficient with respect to a voltage- (or flux-) controlled element is given by the response to an impulse of current applied in parallel with the element; and similarly the sensitivity coefficient with respect to a current- (or charge-) controlled element is given by the response to an impulse of voltage applied in series with the element.

REPRESENTATION OF NONLINEAR NETWORKS

JSEP Grant AF-AFOSR-139-65
Prof. E.S. Kuh

Consider a general nonlinear, time-varying network which is lumped and finite. A straightforward method of writing the governing differential equation in the normal form $\dot{\underline{x}} = \underline{f}(\underline{x}, \underline{u}, t)$, in terms of network topology and nonlinear branch relations has been obtained.

The method is based on a simple signal flow graph representation of a general nonlinear network. Reduction of the signal flow graph leads immediately to the governing differential equation and sufficient conditions for the existence and uniqueness of the solution.

The signal flow graph representation is shown in Fig. 1. The three blocks describe the nonlinear capacitive, resistive, and inductive branch relations, while the interconnection specifies the topology of the network. A detailed explanation will be presented in the Proceedings of the National Electronics Conference, Chicago, Illinois, October, 1965.

EXPERIMENTAL DATA ACQUISITION AND DIGITAL DATA PROCESSING SYSTEMS

JSEP Grants AF-AFOSR-139-64 and 65
T. Fujita, P. Jackson (Professor W. H. Wattenburg)

The purpose of these systems is to provide fast reliable means of automatic data collection. Compatibility with several input and output devices, variable sample work length scans, code conversion, word counter, and AUTO or KEYBOARD mode of operation are basic features.

Either current or voltage mode signals are accepted. The system is capable of handling two to five digit samples, and by using the appropriate circuit card the input code is converted to the IBM 8-4-2-1 BCD code. The output signals drive either a paper tape punch unit or a magnetic tape unit.

Conversion of parallel input signals to serial output signals is accomplished with a control shift register. A separator code is automatically inserted after each sample. A word counter may be enabled when a certain number of samples are to be recorded, and after the preset number of samples (maximum of 127 samples) have been recorded the system inserts a termination code. If the work counter is not used, the termination code is manually generated.

The keyboard allows the operator to enter identification or error flagging information. A mode switch is provided for selecting either the automatic scanning mode or the keyboard mode for manual insertion of information. All control switches for the system are mounted on the keyboard for convenience.

Complete design, construction, and operation of the automatic data acquisition system are described in the following Masters' theses:

"System Design of an Automatic Data Acquisition Unit," by Ted Y. Fujita;

"Logical Design of an Automatic Data Acquisition Unit," by Prentiss W. Jackson; and

"Circuit Design of an Automatic Data Acquisition Unit," by Bit-Leung Seto.

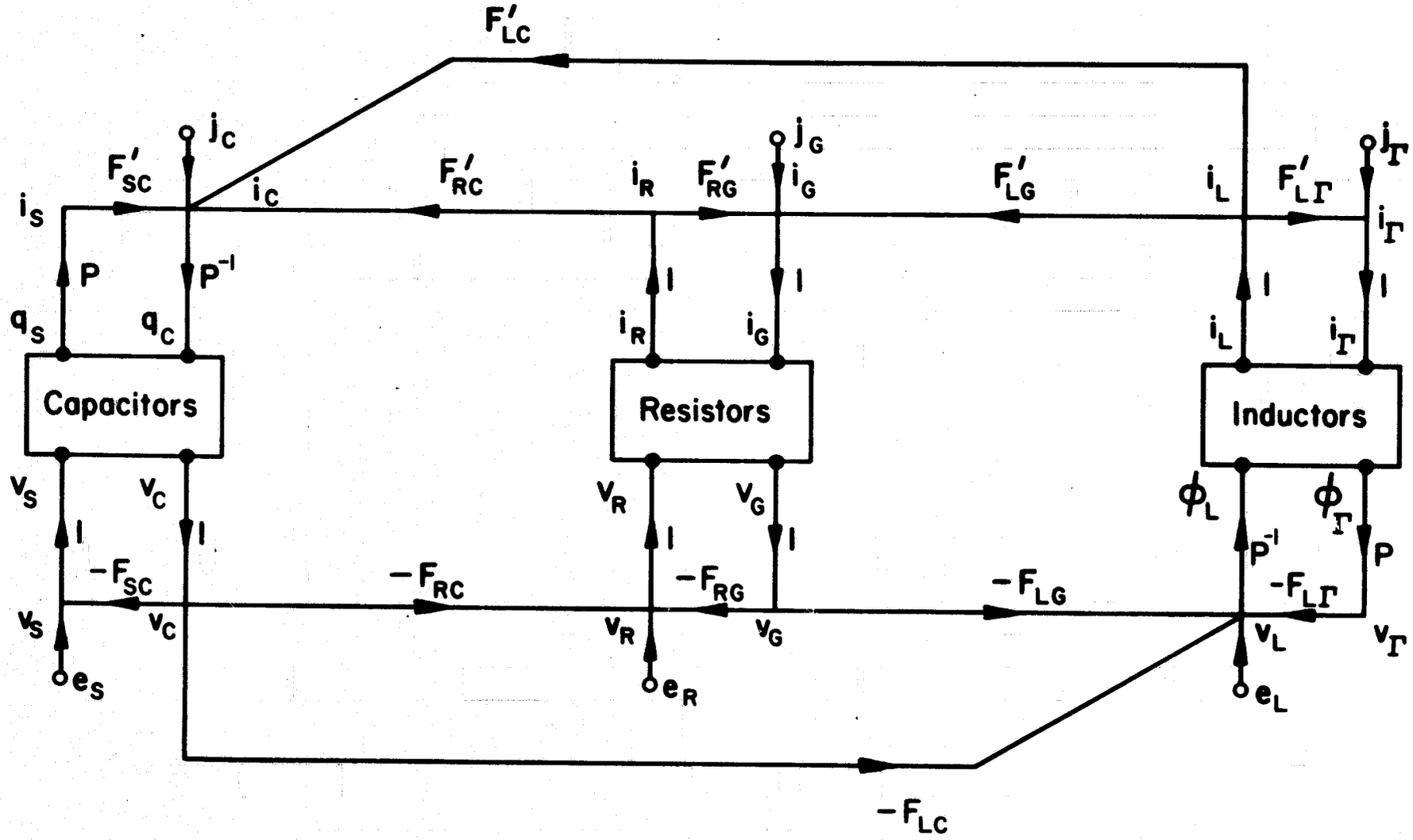
F'_{LC}
j_C
F'_{SC}
i_C
F'_{RC}
i_R
F'_{RG}
j_G
i_G
F'_{LG}
i_L
$F'_{L\Gamma}$
j_Γ
i_Γ
i_S
P
P^{-1}
I
q_S
q_C
i_R
i_G
i_L
i_Γ
Capacitors
Resistors
Inductors
v_S
v_C
v_R
v_G
ϕ_L
ϕ_Γ
$-F_{SC}$
$-F_{RC}$
$-F_{RG}$
$-F_{LG}$
$-F_{L\Gamma}$
v_L
v_Γ
e_S
e_R
e_L
$-F_{LC}$

Fig. 1.

A CIRCUIT MODEL FOR THE STEP-RECOVERY DIODE

JSEP Grants AF-AFOSR-139-64 and 65
D. Frohman (Professor D. C. Evans)

Research on this project has been completed and will be published in a forthcoming ERL technical report. An abstract follows.

A circuit model for the step-recovery diode, based on the lumped π Linvill model is proposed. The model is derived from the finite difference approximation of the continuity equation for minority carriers in a p-n junction with a built-in retarding field. A set of terminal parameters is given based on correspondence between the lumped approximation and the distributive analysis. The diode performance in digital circuit applications is analysed and the results are in excellent accord with experimental measurements performed on different diodes.

V. PUBLICATIONS

A. TECHNICAL REPORTS AND MEMORANDA

The following technical reports and memoranda were published by the Electronics Research Laboratory between 16 November 1964 and 30 June 1965.

ERL Report No.	
64-44	L. A. Zadeh, "Fuzzy sets," November 16, 1964.
64-45	W. H. Wattenburg, "Techniques for automating the construction of translators for programming languages," January 13, 1965.
65-1	A. Baghdasarian and D. J. Angelakos, "Solution of Circular loop antennas and scattering from conducting loops by numerical methods," January 8, 1965.
65-2	V. H. Rumsey, "Frequency independent antennas," January 12, 1965.
65-3	R. S. Muller and M. Bujatti, "Photovoltaic effects at rectifying junctions to deposited CdS films," January 14, 1965.
65-4	C. E. Frank, "The detection of weak magnetic fields using dipole resonance in thin-permalloy films," January 18, 1965.
65-5	E. Wong and M. Zakai, "On the convergence of the solutions of differential equations involving brownian motion," January 19, 1965.
65-6	D. L. Moorehead, "The analysis and synthesis of probability transformers," January 28, 1965.
65-7	A. J. Lichtenberg and A. W. Trivelpiece, "Annual report on research in high energy plasmas," February 18, 1965.
65-8	R. N. Biswas and E. S. Kuh, "Multiparameter sensitivity analysis for linear systems," March 9, 1965.
65-9	V. H. Rumsey, et al., "Annual report on research in frequency independent antennas," March 29, 1965.
65-10	M. Fukada, "Study of wide-band parametric amplifiers and converters," April 30, 1965.

65-11 P. Govindan, A. J. Lichtenberg and J. R. Woodyard, "Microwave loss in a reflex plasma discharge," May 3, 1965.

65-12 E. S. Kuh and R. A. Rohrer, "The state variable approach to network analysis," May 20, 1965.

65-13 D. J. Angelakos and J. R. Whinnery, "Joint services electronics program--final report," June 1, 1965.

65-14 Various, "Notes on system theory, Vol. VII," May 1965.

65-15 L. H. Lin, "Optical level population inversions in a sodium-mercury mixture discharge," June 4, 1965.

65-16 H. K. Forsen, "The two-stage magnetic mirror compression experiment with a rotating plasma source," June 7, 1965.

65-17 A. Gill and M. A. Harrison, "Switching and automata theory--final report," June 8, 1965.

65-18 L. J. Demeter, "Design and construction of high-field compression and transfer coil systems for a magnetic mirror machine," June 18, 1965.

ERL Memo No.

M-106 J. P. Jacob, "The design of circuits for performing operations and computing functions over finite fields," November 30, 1964.

M-107 M. A. Breuer, "Simplification of the integer programming formulation of the covering problem," November 30, 1964.

M-108 I. T. Frisch and C. W. Ho, "A unified theory of synthesis with unsymmetric four-element lossless lattices," December 11, 1964.

M-109 C. T. Chen, "On the stability of nonlinear sampled-data feedback systems," February 25, 1965.

M-110 D. J. Sakrison, "Efficient recursive estimation of the parameters of a radar or radio astronomy target," December 18, 1964.

M-112 A. Rault and E. I. Jury, "Nonlinear sampled-data systems and multidimensional z transform," February 11, 1965.

M-113 D. J. Sakrison, "Processing of telemetry data generated by sensors moving in a varying field," March 16, 1965.

M-114 A. G. Dewey and E. I. Jury, "A stability inequality for a class of nonlinear feedback systems," March 31, 1965.

M-115 A. G. Dewey and E. I. Jury, "A note on Aizerman's conjecture," May 20, 1965.

M-116 C. D. Cullum and E. Polak, "Equivalence relations for the classification and solution of optimal control problems," May 25, 1965.

M-117 A. Pine, "Optical photon--acoustic photon interactions: stimulated Brillouin scattering," May 26, 1965.

M-118 A. J. Lichtenberg and S. Sesnic, "Absolute radiation standard in the far infrared," May 27, 1965.

M-119 H. Halkin, B. W. Jordan, E. Polak and J. B. Rosen, "Theory of optimum discrete time systems," June 1, 1965.

M-120 T. I. Kamins, "Surface mobility of silicon MOS devices," June 3, 1965.

M-121 K. F. Lam, "Electrical properties of metal-doped polymer membranes," June 23, 1965.

B. TECHNICAL TALKS
November 16, 1964 to June 30, 1965

Everhart, T. E. "The scanning electron microscope--theory and applications," San Francisco Section of IEEE, Combined Meeting of Professional Technical Groups on Electron Devices and Circuit Theory on Integrated Circuit Evaluation using Electron-Beam Techniques; December 1964.

Frisch, I. T. "A unified theory of synthesis with four-element lossless unsymmetric lattices," IEEE Int'l Conf., New York; March 23-25, 1965.

"Synthesis of oriented communication nets," Symposium on Signal Transmission, Columbia Univ.; May 13-14. 1965. (with D. K. Sen)

Harrison, M. A. "A census of finite automata," Fifth Annual Symposium on Switching Circuit Theory and Logical Design, Princeton University, Princeton, N. J.; November 1964.

Jury, E. I. "On the absolute stability of multi-nonlinear systems," Automation and Remote Control Conf., Moscow, USSR; June 1965. (with B. W. Lee)

Kuh, E. S. "Sensitivity analysis and multiple loop feedback amplifiers," Fairchild Semiconductor Lab., Mountain View, Calif.; June 1, 1965.

Mouthaan, K. — "New statistical theory for the smooth-bore magnetron," Twenty-third Annual Conf. on Electron Device Research, Urbana, Ill.; June 23-25, 1965.

Muller, R.S. — "The deposited piezoelectric MOS device as an electromechanical transducer," IEEE-NASA-Navy Dept. Conf. on Thin Film Active Devices, Baltimore, Maryland; April 14-15, 1965.

Oldham, W.G. — "Vapor growth of Ge on Ge, Si, and GaAs substrates," Electrochemical Soc. Spring Meeting; Spring 1965.

Rao, R.A. — See T. Van Duzer

Sakrison, D.J. — "Processing telemetry data generated by sensors moving in a varying field," Sixth Int'l. Space Science Symposium, Buenos Aires, Argentina; May 11-19, 1965.

Sasaki, A. — "Invariant noise parameters and noise figure of crossed-field amplifiers," Twenty-third Annual Conf. on Electron Device Research, Urbana, Ill.; June 23-25, 1965.

Smith, O.J.M. — "Computer for writing an analytic differential equation for an unknown system," Anais do Primeiro Congresso Nacional de Engenharia Eletronica, Instituto Tecnologico de Aeronautica, S.J. dos Campos, S.P., Brazil; January 4, 1965.

"Synchronous machine stability enhancement with statespace switching," Anais do Primeiro Congresso Nacional de Engenharia Eletronica, Instituto Tecnologico de aeronautica, S.J. dos Campos, S.P., Brazil; January 4, 1965.

Susskind, C. — See K. Mouthaan.

Turin, G.L. — "Signal design for sequential detection systems," IEEE Los Angeles District Info. Theory Group Meeting; April 15, 1965.

Van Duzer, T. — "A method for synthesis of crossed-field guns," Twenty-third Annual Conf. on Electron Device Res., Urbana, Ill.; June 23-25, 1965. (with R.A. Rao)

Vogelhut, P.O. — "Structure of bound water in biological systems," Oak Ridge National Lab., Oak Ridge, Tenn.; and Michigan State Univ., Biophysics Dept., East Lansing, Mich., November 22-25, 1964.

Welch, W.J. — "Recent planetary observations at wavelengths near 1 cm," American Astronomical Soc. Meeting, Montreal Canada; December 28-31, 1964.

Zadeh, L. A. "Decision-making under uncertainty," Shell Development Co., Houston, Texas; November 30, 1964.

"Information theory and automatic pattern recognition," IEEE Session on System Theory, Montreal, Canada; December 30, 1964.

"A new view of system theory," Symposium of System Theory, Polytechnic Institute of Brooklyn; April 20, 1965.

"Fuzzy sets, abstractions, and pattern classification," Popov Society Meetin, Moscow, USSR, US IEEE Delegation; May 1965.

C. PUBLISHED PAPERS

July 1, 1964 to June 30, 1965

Berlekamp, E. R. "Note on recurrent codes," PGIT; July 1964.

"A polygon problem," Amer. Math. Monthly, Vol. 72, No. 3, pp. 233-241; March 1965.

Birdsall, C. K. "Sheet-current plasma model for ion-cyclotron waves," The Physics of Fluids, Vol. 7, No. 10, pp. 1590-1600; October 1964. (with A. Hasegawa)

"Laser-induced emission of electrons, ions and neutrals from Ti and TiD surfaces," Applied Physics Letters, Vol. 5, No. 9, pp. 171-172; November 1964. (with T. Y. Chang)

"Focusing of an electron stream with radio-frequency fields," J. Electronics and Control, Vol. 17, No. 6, pp. 601-622; December 1964. (with G. W. Rayfield)

"Limiting stable currents in bounded electron and ion streams," IEEE Trans. on Electron Devices; May 1965.

Chai, S. Y. See P. O. Vogelhut

Chang, A. "An optimal regulator problem," J. SIAM Control, Vol. 2, Ser. A, pp. 220-233; 1965.

Chang, T. Y. See C. K. Birdsall

Conragan, J. See R. S. Muller

Dalziel, C. F. "Electric shock hazards of fresh water swimming pools," IEEE Trans., 31, CP, 65-735; May 1965.

Desoer, C. A. "Nonlinear RLC networks," The Bell System Technical Journal, Vol. XLIV, No. 1, pp. 161-198; January 1965. (with J. Katzenelson)

"Linearity vs nonlinearity and asymptotic stability in the large," IEEE Trans. on Circuit Theory, Vol. CT-12, No. 1, pp. 117-118; March 1965. (with R. Liu and L. V. Auth, Jr.)

"An optimization problem in circuits," IEEE Trans. on Circuit Theory, Vol. CT -12, No. 1, pp. 28-31; March 1965.

"A generalization of the Popov criterion," IEEE Trans. on Automatic Control, Vol. AC-10, No. 2, pp. 182-185; April 1965.

"A stability criterion obtained by a method of comparison," IEEE Trans. on Automatic Control, Vol. AC-10, No. 2, pp. 185-186; April 1965.

"A general formulation of the Nyquist criterion," IEEE Trans. on Circuit Theory, Vol. CT-12, No. 2, pp. 230-234; June 1965.

Dewey, A. G. See E. I. Jury

Everhart, T. E. "Evaluation of passivated integrated circuits using the scanning electron microscope," J. Electrochem. Soc., Vol. III, No. 8, pp. 929-936; August 1964.

"A novel method of semiconductor device measurements," Proc. IEEE, Vol. 52, No. 12, pp. 1642-1647; December 1964. (with O. C. Wells and R. K. Matta)

Frey, J. See C. K. Birdsall

Frisch, I. T. "A stability criterion for tunnel diodes," Proc. IEEE, Vol. 52, No. 8, pp. 922-923; August 1964.

"A minimal representation of a cascade of lattices," Proc. Second Annual Elec. Conf. on Circuits, Univ. of Illinois, pp. 467-483; September 1964. (with D. Layton)

"A class of RLC networks with fewer nonreactive elements than the Brune realization," IEEE Trans. on Circuit Theory, Vol. CT; September 1964.

"A unified theory of synthesis with unsymmetric four element lossless lattice," IEEE Int'l. Convention Record Part 7, pp. 147-157; March 1965. (with C.W. Ho)

"Synthesis of oriented communication nets," Conf. Record of IEEE Symposium on Signal Transmission, pp. 90-101; May 1965. (with D.K. Sen)

Forsen, H.K. "Fast-acting valve which operates at temperatures up to 400°C," The Review of Scientific Instruments, Vol. 35, No. 10, pp. 1362-1363; October 1964.

Galindo, V. "Design of dual-reflector antennas with arbitrary phase and amplitude distributions," IEEE Trans. on Antennas and Propagation, Vol. AP-12, No. 4; July 1964.

Gans, M.J. "A general proof of Floquet's theorem," IEEE Trans. on Microwave Theory and Techniques, Vol. MTT-13, No. 3; May 1965.

"Frequency independent baluns," Proc. IEEE, Vol. 53, No. 6, pp. 647-648; June 1965. (with V.H. Rumsey and D. Kajfez)

See V.H. Rumsey

Gill, A. "Analysis and synthesis of singular modular circuits," Summaries of Papers, Int'l Conf. on Microwaves, Circuit Theory and Information Theory, Part 3, Paper I-14-6, pp. 159-160; September 1964.

"Analysis and synthesis of stable linear sequential circuits," J. Assoc. Comp. Machinery, Vol. 12, No. 1, pp. 141-149; January 1965.

"On the bound to the memory of a sequential machine," Electronics Computers; June 1965.

"The minimization of linear sequential circuits," IEEE Trans. on Circuit Theory; June 1965.

Hachtel, G.D. "Unijunction transistor oscillators," Technical Digest, Int'l. Solid State Circuits Conf., p. 54; 1965.

Harrison, M.A. "A remark on uniform distribution," IEEE Trans. on Electronic Computers, Vol. EC-13, No. 5; October 1964.

"Census of finite automata," Can. J. Math., Vol. 17, pp. 100-113; 1965.

Hasegawa, A. — See C.K. Birdsall

Ho, C.W. — See I.T. Frisch

Jayson, J.S. — See A.J. Lichtenberg

Jury, E.I. — "On the absolute stability of nonlinear sampled-data systems," IEEE Trans. on Automatic Control, Vol. AC-9, No. 4, pp. 551-554; October 1964. (with B.W. Lee)

"Supplement to 'A literature survey of biocontrol Systems,'" IEEE Trans. on Automatic Control, Vol. AC-10, No. 1, p. 117; January 1965. (with T. Pavlidis)

"A general formulation of the total square integrals for continuous systems," IEEE Trans. on Automatic Control, Vol. AC-10, No. 1, pp. 119-120; January 1965. (with A.G. Dewey)

"A note on the evaluation of the total square integral," IEEE Trans. on Automatic Control, Vol. AC-10, No. 1, pp. 110-111; January 1965.

"Analysis of a new class of pulse-frequency modulated feedback systems," IEEE Trans. on Automatic Control, Vol. AC-10, No. 1, pp. 35-43; January 1965. (with T. Pavlidis)

"A modified stability table for linear discrete systems," Proc. IEEE, Vol. 53, No. 2, pp. 184-185; February 1965.

"Remarks on the finite and infinite sums of the form $\sum \frac{p(x)}{Kx}$," Proc. IEEE, Vol. 53, No. 2, p. 173; February 1965.

"The use of transforms to sum array factors," IEEE Trans. on Antennas and Propagation, Vol. AP-13, No. 2, p. 318; March 1965.

"Discussion of 'analysis of a new class of pulse-frequency-modulated feedback systems,'" IEEE Trans. on Automatic Control, Vol. AC-10, No. 2, pp. 211-214; April 1965. (with T. Pavlidis)

"Comments on the statistical design of linear sampled-data feedback systems," IEEE Trans. on Automatic Control, Vol. AC-10, No. 2, pp. 215-217; April 1965.

"On the stability condition of non-linear sampled-data systems," IEEE Trans. on Automatic Control, Vol. AC-10, No. 2, pp. 217-218; April 1965. (with B. W. Lee)

Kajfez, D. — See M. J. Gans

See V. H. Rumsey

Kuh, E. S. — "Stability of linear time varying networks--the state apace approach," IEEE Trans. on Circuit Theory, Vol. CT-12, No. 2, pp. 180-187; June 1965.

Layton, D. — See I. T. Frisch

Lee, B. W. — See E. I. Jury

Lichtenberg, A. J. — "Synchrotron radiation measurements from a plasma in a magnetic mirror machine," The Physics of Fluids, Vol. 7, No. 9; September 1964. (with S. Sesnic and A. W. Trivelpiece)

"Synchrotron radiation from a self-consistent plasma," Bulletin APS; November 1964. (with D. Tuma)

"Propagation and instabilities of waves in bounded finite temperature plasmas," J. Applied Physics, Vol. 36, No. 2, pp. 449-455; February 1965. (with J. S. Jayson)

See A. W. Trivelpiece

Mantena, N. R. — See T. Van Duzer

Maxum, B. J. — See A. W. Trivelpiece

Mei, K. K. — "Solutions to spherical anisotropic antennas," IEEE Trans. on Antennas and Propagation, Vol. AP-12, pp. 459-463; July 1964.

"On the integral equations of thin wire antennas," IEEE Trans. on Antennas and Propagation, Vol. AP-13, No. 3, pp. 374-378; May 1965.

Mouthaan, K. — "Wave-mechanical approach to the non-linear theory of O-type travelling-wave tubes," Int'l. J. Electronics; May 1965.

Muller, R.S. "Theoretical admittance variation with frequency in insulators having traps subject to charge injection," Proc. Int'l. Conf. on Physics of Semiconductors, Paris 1964, pp. 631-638; November 1964.

"Transducer action in a metal-insulator piezoelectric semiconductor triode," Appl. Physics Letters, Vol. 6, No. 5, pp. 83-85; March 1965. (with J. Conragan)

Oldham, W.G. "Chemical polishing of GaP," Electrochemical Technology, Vol. 3, No. 1-2; January-February 1965.

Pavlidis, T. See E.I. Jury

Pease, R.F.W. "Scanning electron microscopy of the growth and subsequent sectioning by sputtering of iron oxide films," Proc. Third European Reg. Conf. on Electron Microscopy, Prague, Czechoslovakia, pp. 389-390; September 1964. (with A.N. Broers and R.A. Ploc)

"High resolution scanning electron microscopy," J. Scientific Inst., Vol. 42, pp. 81-85; February 1965. (with W.C. Nixon)

"The determination of the area of emission of electrons in a scanning electron microscope," J. Sci. Inst., Vol. 42, pp. 158-159; March 1965.

Polak, E. "Fundamentals of the theory of optimal control," Fizmatgiz Math. Revs., Moscow 1963, Vol. 29, No. 2; February 1965. (with A.A. Fel'dbaum)

"Optimal control of aperiodic discrete-time systems," SIAM; April 1965.

Rumsey, V.H. "Frequency independent baluns," Proc. IEEE; May 1965. (with M. Gans and D. Kajfez)

Sakrison, D.J. "A continuous Kiefer-Wolfowitz procedure for random processes," The Annals of Math. Stat., Vol. 35, No. 2; July 1964.

Sasaki, A. See T. Van Duzer

Scharer, J.E. See A.W. Trivelpiece

Schwarz, S.E. "Note on laser monitors," Proc. IEEE, Vol. 53, No. 4, pp. 414-415; April 1965.

Sen, D. K. — See I. T. Frisch

Sesnic, S. — See A. J. Lichtenberg

See A. W. Trivelpiece

Smith, O. J. M. — "Discussion of transient stability of a synchronous generator under conditions of bang-bang excitation scheduling," IEEE Trans. on Power Apparatus and Systems, Vol. PAS-84, No. 1; January 1965.

"Optimal transient removal in a power system," IEEE Trans. on Power Apparatus and Systems, Vol. PAS-84, No. 5, pp. 361-374; May 1965. Also Vol. PAS-84, No. 6, pp. 530-531.

"Discussion of stability studies and tests on a 532-MW ross-compound turbine-generator set," IEEE Trans. on Power Apparatus and Systems, Vol. PAS-84, No. 6, pp. 526-527; June 1965.

Spector, J. — See A. W. Trivelpiece

Susskind, C. — "Electronics and the blind," Adv. in Electronics and Electron Physics, Vol. 20, pp. 261-301; 1964. (with P. G. Shrager)

"Some observations of electromagnetic-wave radiation before Hertz," Actes du 10e Congres Int'l. d'Histoire des Sciences, Ithaca, New York, Paris: Hermann, pp. 785-788; 1964.

"Interactions in cold-cathode magnetrons," Comptes Rendus du 5e Congres Int'l. Tubes pour hyperfrequences, Paris: Dunod, pp. 311-313; 1964.

"Anode structures for cold-cathode high-power magnetrons," The Radio and Electronic Engineer, 29, pp. 93-99; 1965. (with Y. Ikeda)

"Scientific studies of the agricultural museum," (book review), Technology and Culture, 6, pp. 136-137; 1965.

"An introduction to engineering and engineering design," by E. V. Krick (book review), J. Eng. Ed., p. 55; 1965.

"Distortions in the history of radio," Proc. IEEE, Vol. 53, No. 2, pp. 162-164; February 1965.

Trivelpiece, A. W. — "Slow-waves in ferrites and their interactions with electron streams," J. Applied Physics, Vol. 35, No. 7, pp. 2030-2039; July 1964. (with J. Spector)

"Measurements of the synchrotron radiation spectrum from a hot plasma," Phys. Rev. Letters, Vol. 13, No. 13; January 1965. (with S. Sesnic and A. J. Lichtenberg)

"Quasistatic analysis of waves in a plasma-filled waveguide," J. Applied Physics, Vol. 36, No. 1, pp. 318-319; January 1965. (with J. E. Scharer)

"Two-stream cyclotron and plasma wave interactions," J. Applied Physics, Vol. 36, No. 2, pp. 481-494; February 1965. (with B. J. Maxum)

See A. J. Lichtenberg

Tuma, D. — See A. J. Lichtenberg

Van Duzer, T. — "Crossed-field backward-wave amplifier noise-figure studies," J. Electronics and Control, Vol. 17, pp. 497-611; November 1964. (with N. R. Mantena)

"Crossed-field noise studies: guns and transducers," Proc. of the Int'l. Conf. on the Physics of Semiconductors, Paris 1964, pp. 11-14; 1965. (with N. R. Mantena and A. Sasaki)

"A 3.5 db-noise-figure, S-band, medium-power, forward-wave, injected-beam, crossed-field amplifier," Proc. of Inst. of Electrical and Electronic Engrs., pp. 425-426; April 1965. (with R. P. Wadhwa)

Vogelhut, P. O. — "Use of microwave techniques for the determination of bound water," Nature, Vol. 203, No. 4950, pp. 1169-1170; September 1964.

"Activation energy of direct-current electrical conductivity of ice with HF and NH_3 added," Science, Vol. 148, No. 3677, pp. 1595-1598; June 1965. (with S. Y. Chai)

Welch, W. J. — "Recent planetary observations at wavelengths near 1 cm," Astronomical Journal, Vol. 70, p. 149; 1965. (with D. D. Thornton)

"Observations of Thurus A and the quasi-stellar object 3C273 at 1.53 cm," Pub. A. S. P. 77; June 1965. (with D. R. W. Williams and D. D. Thornton)

"Variation of the lunar radio brightness during an eclipse," J. G. R. 70; June 15, 1965. (with D. D. Thornton and S. Winter)

Whinnery, J.R. "Low-absorption measurements by means of thermal lens effect using an He-Ne laser," Applied Physics Letters, Vol. 5, No. 7, pp. 141-143; October 1964. (with R.C.C. Leite and R.S. Moore)

"Long transient effects in lasers with inserted liquid samples," J. Applied Physics, Vol. 36, No. 1, pp. 3-8; January 1965. (with J.P. Gordon, R.C.C. Leite, R.S. Moore and S.P.S. Porto)

"Focusing of a light beam of gaussian field distribution in continuous and periodic lens-like media," Proc. IEEE, Vol. 53, No. 2, pp. 129-136; February 1965. (with P.K. Tien and J.P. Gordon)

White, R.M. "Monochromatic illumination of cadmium-sulfide oscillator," Proc. IEEE; June 1965.

Wong, E. "The construction of a class of stationary Markoff processes," Proc. Symposia in Appl. Math., Vol. 16, pp. 264-276; 1965.

"On the relation between ordinary and stochastic differential equations," Int'l. J. Eng. Science; June 1965. (with M. Zakai)

"Iterative synthesis of threshold functions," J. Math. Analysis and Applications; June 1965.

Zadeh, L.A. "Electrical engineering at the crossroads," 1965 IEEE Int'l. Conv. Record, Part 13; pp. 47-50; 1965.

"Fuzzy sets," Information and Control, Vol. 8, No. 3; June 1965.

UNCLASSIFIED
Security Classification

DOCUMENT CONTROL DATA - R&D

(Security classification of title, body of abstract and indexing annotation must be entered when the overall report is classified)

1. ORIGINATING ACTIVITY *(Corporate author)*

Electronics Research Laboratory
University of California, Berkeley

2a. REPORT SECURITY CLASSIFICATION

UNCLASSIFIED

2b. GROUP

3. REPORT TITLE

SEMIANNUAL PROGRESS REPORT NO. I

4. DESCRIPTIVE NOTES *(Type of report and inclusive dates)*

Progress Report

5. AUTHOR(S) *(Last name, first name, initial)*

Faculty and Graduate Research Students, Electronics Research Laboratory

6. REPORT DATE	7a. TOTAL NO. OF PAGES	7b. NO. OF REFS
June 30, 1965	304	

8a. CONTRACT OR GRANT NO.	9a. ORIGINATOR'S REPORT NUMBER(S)
Various	
b. PROJECT NO.	No. 1
c.	9b. OTHER REPORT NO(S) *(Any other numbers that may be assigned this report)*
d.	

10. AVAILABILITY/LIMITATION NOTICES

Qualified requesters may obtain copies of this report from DDC.

11. SUPPLEMENTARY NOTES	12. SPONSORING MILITARY ACTIVITY

13. ABSTRACT

This report presents a summary of research conducted by the Electronics Research Laboratory, University of California, Berkeley, from 16 November 1964 through 30 June 1965.

DD FORM 1 JAN 64 1473

UNCLASSIFIED
Security Classification

14. KEY WORDS	LINK A		LINK B		LINK C	
	ROLE	WT	ROLE	WT	ROLE	WT
Bioelectronics Electron Streams and Interactions Plasmas Quantum and Optical Electronics Radiation and Propagation Solid-State Electronics Systems						

INSTRUCTIONS

1. ORIGINATING ACTIVITY: Enter the name and address of the contractor, subcontractor, grantee, Department of Defense activity or other organization *(corporate author)* issuing the report.

2a. REPORT SECURITY CLASSIFICATION: Enter the overall security classification of the report. Indicate whether "Restricted Data" is included. Marking is to be in accordance with appropriate security regulations.

2b. GROUP: Automatic downgrading is specified in DoD Directive 5200.10 and Armed Forces Industrial Manual. Enter the group number. Also, when applicable, show that optional markings have been used for Group 3 and Group 4 as authorized.

3. REPORT TITLE: Enter the complete report title in all capital letters. Titles in all cases should be unclassified. If a meaningful title cannot be selected without classification, show title classification in all capitals in parenthesis immediately following the title.

4. DESCRIPTIVE NOTES: If appropriate, enter the type of report, e.g., interim, progress, summary, annual, or final. Give the inclusive dates when a specific reporting period is covered.

5. AUTHOR(S): Enter the name(s) of author(s) as shown on or in the report. Enter last name, first name, middle initial. If military, show rank and branch of service. The name of the principal author is an absolute minimum requirement.

6. REPORT DATE: Enter the date of the report as day, month, year; or month, year. If more than one date appears on the report, use date of publication.

7a. TOTAL NUMBER OF PAGES: The total page count should follow normal pagination procedures, i.e., enter the number of pages containing information.

7b. NUMBER OF REFERENCES: Enter the total number of references cited in the report.

8a. CONTRACT OR GRANT NUMBER: If appropriate, enter the applicable number of the contract or grant under which the report was written.

8b, 8c, & 8d. PROJECT NUMBER: Enter the appropriate military department identification, such as project number, subproject number, system numbers, task number, etc.

9a. ORIGINATOR'S REPORT NUMBER(S): Enter the official report number by which the document will be identified and controlled by the originating activity. This number must be unique to this report.

9b. OTHER REPORT NUMBER(S): If the report has been assigned any other report numbers *(either by the originator or by the sponsor)*, also enter this number(s).

10. AVAILABILITY/LIMITATION NOTICES: Enter any limitations on further dissemination of the report, other than those imposed by security classification, using standard statements such as:

(1) "Qualified requesters may obtain copies of this report from DDC."

(2) "Foreign announcement and dissemination of this report by DDC is not authorized."

(3) "U. S. Government agencies may obtain copies of this report directly from DDC. Other qualified DDC users shall request through

_____."

(4) "U. S. military agencies may obtain copies of this report directly from DDC. Other qualified users shall request through

_____."

(5) "All distribution of this report is controlled. Qualified DDC users shall request through

_____."

If the report has been furnished to the Office of Technical Services, Department of Commerce, for sale to the public, indicate this fact and enter the price, if known.

11. SUPPLEMENTARY NOTES: Use for additional explanatory notes.

12. SPONSORING MILITARY ACTIVITY: Enter the name of the departmental project office or laboratory sponsoring *(paying for)* the research and development. Include address.

13. ABSTRACT: Enter an abstract giving a brief and factual summary of the document indicative of the report, even though it may also appear elsewhere in the body of the technical report. If additional space is required, a continuation sheet shall be attached.

It is highly desirable that the abstract of classified reports be unclassified. Each paragraph of the abstract shall end with an indication of the military security classification of the information in the paragraph, represented as *(TS), (S), (C), or (U)*.

There is no limitation on the length of the abstract. However, the suggested length is from 150 to 225 words.

14. KEY WORDS: Key words are technically meaningful terms or short phrases that characterize a report and may be used as index entries for cataloging the report. Key words must be selected so that no security classification is required. Identifiers, such as equipment model designation, trade name, military project code name, geographic location, may be used as key words but will be followed by an indication of technical context. The assignment of links, roles, and weights is optional.